THE UNIVERSITY OF NOTTINGHAM

PEMC Research Group

Department of Electrical and Electronic Engineering

Faculty of Engineering

On the damper cage of salient-pole synchronous generators

Stefano Nuzzo, Ph.D. Candidate

Submitted to the University Of Nottingham for the degree of Doctor of Philosophy, December 2017

TABLE OF CONTENTS

Tables of Figures ..... **x**

List of Tables ..... **xix**

List of Acronyms ..... **xx**

Glossary of Symbols ..... **xxii**

ABSTRACT ..... ***XXIX***

ACKNOWLEDGMENTS ..... ***XXXI***

CHAPTER 1 INTRODUCTION ***1***

1.1 Project description **4**

1.1.1 The DIG142 and its main design challenge 4

1.1.2 The HC4 and its main design challenge 5

1.1.3 Proposed solution(s) 7

1.2 Aims and objectives **9**

1.3 Thesis outline **12**

CHAPTER 2 LITERATURE REVIEW ***15***

2.1 Introduction **15**

2.2 The damper cage **17**

2.2.1 Conventional damper cage in synchronous generators 17

2.2.2 Benefits and drawbacks 18

2.2.3 Review of methods 20

2.2.4 Final considerations 21

2.3 Skewing and its effects and roles 22

2.3.1 Skewing in various machines 23

2.3.2 Skewing in synchronous generators 24

2.3.3 Review of methods 25

2.3.4 Final considerations 26

2.4 The considered platforms 27

2.4.1 The DIG142 27

2.4.2 The HC4 29

2.4.3 Summary 31

2.5 Conclusions 32

CHAPTER 3 THE HYBRID ANALYTICAL-NUMERICAL MODEL .. 33

3.1 Model introduction 34

3.2 Model assumptions 34

3.3 Problem definition 36

3.4 Model description 38

3.4.1 Introductory aspects 39

3.4.2 The windings 40

3.4.3 The geometrical quantities 40

3.4.4 The constitutive equation 41

3.5 The solution 42

3.6 The model adapted to SGs 46

3.6.1 The damper cage 46

3.6.2 The slot openings 52

3.6.3 Further considerations 53

3.7 The hybrid analytical-numerical approach 54

3.7.1 The equivalent functions 54

3.7.2 The inductances 58

3.7.3 The Matlab-Simulink model 61

3.8 Model validation against FE results 63

3.8.1 Comparison of results 63

3.9 Conclusions 67

3.10 Contributions to research 69

CHAPTER 4 DEVELOPMENT OF THE FE MODELS 71

4.1 The 2-D FE model of the considered SGs 72

4.1.1 General aspects 72

4.1.2 Geometry and materials 73

4.1.3 Coils and electrical circuits 75

4.1.4 Model structure 79

4.1.5 Solving 84

4.1.6 Final considerations 87

4.2 Modelling of surface rotor losses 88

4.2.1 Background 88

4.2.2 The proposed method 90

4.3 Modelling of skew 92

4.3.1 Objective 93

4.3.2 Conceptual considerations 94

4.3.3 The proposed model 98

4.3.4 Comparison with other FE techniques 100

4.4 Model validation against experimental results 107

4.4.1 No-load characteristic 107

4.4.2 Short-circuit characteristic 110

4.4.3 Full-load results 111

4.4.4 Power losses 113

4.4.5 Skew and its effects 116

4.5 Conclusions 120

4.6 Contributions to research 121

CHAPTER 5 DAMPER CAGE LOSS AND VOLTAGE THD SENSITIVITY ANALYSIS 123

5.1 Introduction 124

5.2 The general scheme for the sensitivity analysis 126

5.3 Sensitivity analysis – the DIG142 127

5.3.1 Key parameters 128

5.3.2 Influence of slot wedge permeability 128

5.3.3 Influence of bar pitch 131

5.3.4 Influence of tangential displacement 132

5.3.5 Influence of radial displacement 134

5.3.6 Intermediate conclusions 136

5.4 Sensitivity analysis – the HC4 137

5.4.1 Key parameters 138

5.4.2 Influence of the pole span 139

5.4.3 Influence of the pole tips shape 141

5.4.4 Influence of the tangential bar displacement 143

5.4.5 Intermediate conclusions 144

5.5 Conclusions 146

5.6 Contributions to research 147

CHAPTER 6 AN IMPROVED DAMPER CAGE FOR THE CONSIDERED SALIENT-POLE SYNCHRONOUS GENERATORS ... 149

6.1 Damper cage modulation 150

6.1.1 Perceived advantages 151

6.2 Investigation with modulation – the DIG142 157

6.2.1 Input parameters 157

6.2.2 Optimization strategy 159

6.2.3 Output variables 160

6.2.4 Optimization results 161

6.2.5 Final proposed solution 162

6.2.6 Considerations on the dynamic parameter 165

6.2.7 Intermediate conclusions 169

6.3 Investigation with modulation – the HC4 170

6.3.1 Methodology 171

6.3.2 Preliminary optimization results 173

6.3.3 Final optimization results 175

6.3.4 Final proposed solution 177

6.4 Conclusions 182

6.5 Contributions to research 183

CHAPTER 7 PROTOTYPE AND EXPERIMENTAL VALIDATION OF THE PROPOSED CONCEPT 185

7.1 Manufacturing of the rotor prototype 185

7.2 Experimental results 192

7.2.1 Waveform analysis 193

7.2.2 No-load characteristic 198

7.2.3 Short-circuit characteristic 200

7.2.4 Power losses and efficiency 203

7.2.5 Dynamic parameters 208

7.3 Conclusions 215

7.4 Contributions to research 216

CHAPTER 8 CONCLUSION 217

8.1 General conclusions 217

8.2 Contributions to research 220

8.2.1 The hybrid analytical-numerical model 223

8.2.2 The single-slice technique 225

8.2.3 The modulated damper cage 226

8.3 Future work 229

APPENDIX 1 – INTRODUCTION TO THE FE TECHNIQUE 231

Methodology 232

2-D modelling 233

Boundary conditions 234

APPENDIX 2 – INTRODUCTION TO GAS 236

General introduction 236

Multi-objective optimization problems 241

APPENDIX 3 – INTRODUCTION TO EDM 246

REFERENCES 249

Tables of Figures

Fig. 1 – The DIG142 alternator. 5

Fig. 2 – The HC4 alternator. 6

Fig. 3 – Modulated damper bar concept. 8

Fig. 4 – Damper winding with connected end rings between adjacent poles [27]. 18

Fig. 5 – Damper winding with non-connected end rings between adjacent poles [27]. 18

Fig. 6 – Open slot structure of the DIG142 stator lamination. 28

Fig. 7 – Rotor topology with damper cage displaced around the polar axis. 29

Fig. 8 – 2-D half view of the HC4 stator and rotor laminations. 30

Fig. 9 – Example of a generic machine with cores, magnets and coils [77]. 39

Fig. 10 – Equivalent circuit topology for a damper cage of complete (left) and incomplete type (right): example referred to the HC4 SG..... 48

Fig. 11 – Compound planar schematic of a generic rotor cage loop for symmetrical machines. 49

Fig. 12 – Typical winding function of a single damping cage loop. 51

Fig. 13 – Cage loop winding function for the compound representation. 51

Fig. 14 – Simplified representation of the equivalent inner stator profile. ... 53

Fig. 15 – Equivalent airgap thickness function of the considered generator, after the application of the tuning procedure against the FE model. 55

Fig. 16 – Equivalent airgap radius function of the considered generator, after the application of the tuning procedure against the FE model. 56

Fig. 17 – Equivalent permeability function of the considered generator, after the application of the tuning procedure against the FE model. 57

Fig. 18 – Winding function of the rotor field equivalent phase..... 58

Fig. 19 – Winding functions of the stator armature equivalent phases..... 58

Fig. 20 – Self- and mutual-inductances of the rotor circuits. 59

Fig. 21 – Stator self- and mutual-inductances. 60

Fig. 22 – Mutual-inductances between rotor and stator circuits..... 61

Fig. 23 – Linear model of the electrical aspects implemented in Simulink.. 62

Fig. 24 – Experimental no-load characteristic of the HC4. 65

Fig. 25 – No-load voltage waveforms: analytical vs. FE results at 7.5% of the base field current..... 65

Fig. 26 – No-load voltage waveforms: analytical vs. FE results at 29% of the base field current..... 66

Fig. 27 – No-load voltage waveforms: analytical vs. FE results at 53% of the base field current..... 66

Fig. 28 – No-load voltage waveforms: non-linear analytical vs. FE results at 29% of the base field current. 67

Fig. 29 – BH curve of the ferromagnetic material utilised for the stator and rotor cores of the DIG142 and the HC4 alternators..... 74

Fig. 30 – Electrical circuits relative to the DIG142 SG coupled with the FE model. 78

Fig. 31 – Electrical circuits relative to the HC4 SG coupled with the FE model. 78

Fig. 32 – Imposition of boundary conditions onto the DIG142 FE model... 80

Fig. 33 – Imposition of boundary conditions onto the HC4 FE model. 81

Fig. 34 – Mesh refinement relative to the DIG142 FE model. 83

Fig. 35 – Mesh refinement relative to the HC4 FE model. 84

Fig. 36 – Subdivision of the pole shoe (on the left) for loss calculations and averaging of the flux density waveforms (on the right). 91

Fig. 37 – Variable airgap thickness function ε_{AG} vs. angular displacement λ. 95

Fig. 38 – 2-D cross-section of the HC4, including the skewing angle α_{sk} and its submultiple δ. 96

Fig. 39 – Zoom on the variable airgap thickness function – comparison between an un-skewed (N_s=1) and a skewed stator (N_s=5 and N_s=9). 96

Fig. 40 – Stator winding function: comparison between an un-skewed and a skewed stator. 97

Fig. 41 – The multi-slice FE model, with 5 slices simultaneously evaluated. 101

Fig. 42 – No-load terminal voltage – Comparison amongst the three methods. 102

Fig. 43 – No-load currents induced in one damper bar: comparison amongst the three techniques. 104

Fig. 44 – No-load, RMS values of damper cage currents: comparison. 104

Fig. 45 – Full-load, RMS values of damper cage currents: comparison. ... 105

Fig. 46 – Stator phase currents: comparison. 106

Fig. 47 – No-load characteristics of the DIG142 – Comparison between FE and experimental results. 108

Fig. 48 – No-load characteristic of the HC4 – Comparison between FE and experimental results. 108
Fig. 49 – No-load field map of the DIG142. 109
Fig. 50 – No-load field map of the HC4. 109
Fig. 51 – Short-circuit characteristics of the DIG142: comparison between FE and experimental results. 110
Fig. 52 – Short-circuit characteristics of the HC4: comparison between FE and experimental results. 110
Fig. 53 – Full-load field map of the DIG142. 111
Fig. 54 – Full-load field map of the HC4. 112
Fig. 55 – Copper losses in the DIG142 at different load levels and power factors: comparison between FE and experimental results. 114
Fig. 56 - Copper losses in the HC4 at different load levels and power factors: comparison between FE and experimental results. 114
Fig. 57 – Iron losses in the DIG142, at different load levels and power factors. 115
Fig. 58 - Iron losses in the HC4, at different load levels and power factors. 116
Fig. 59 – Experimental test bench of the considered SG. 117
Fig. 60 – Phase voltage THD: comparison between FE and experimental results. 120
Fig. 61 – No-load, radial airgap flux density of the DIG142. 125
Fig. 62 – Skewed vs. skew-less HC4 stator: comparison between the no-load, line-to-line voltage waveforms. 126

Fig. 63 – High level flowchart of the sensitivity analysis. 127

Fig. 64 - Zoom on radial air-gap flux densities: comparison among machines with different slot wedge materials..... 129

Fig. 65 – No-load damper cage loss vs. bar pitch..... 131

Fig. 66 – Different damper cage positions shifted by: a) -1.68°, b) 0° (symmetrical case) and c) +1.68° with respect to the polar axis. 132

Fig. 67 – No-load damper cage loss vs. tangential position. 133

Fig. 68 – No-load voltage THD vs. tangential position..... 134

Fig. 69 - Parametrization of the damper cage position along radial and tangential directions..... 135

Fig. 70 – Damper cage losses versus radial and tangential positions. 135

Fig. 71 – Voltage THD versus radial and tangential positions..... 136

Fig. 72 – Effects of the angular span of the salient poles on the no-load line-to-line voltage THD. 140

Fig. 73 - Effects of the angular span of the salient poles on the no-load line-to-line output voltage. 140

Fig. 74 – Qualitative illustration of the pole tips modifications. 141

Fig. 75 - Effects of the g_{max}/g_{min} ratio on the no-load line-to-line voltage THD. 142

Fig. 76 – Effects of the g_{max}/g_{min} ratio on the no-load line-to-line output voltage..... 142

Fig. 77 – Effects of the tangential position of the damping bars on the no-load line-to-line voltage THD..... 144

Fig. 78 – Input parameters of the damper cage optimizations: a) α_{bi} with $i=1,\ldots,10$ and b) modulated damping bars concept ($\beta_i \neq \beta_{i+1}$)..... 151

Fig. 79 – Modulated damper winding function and its effect on harmonics. 156

Fig. 80 – Damper cage circuit coupled to the FE model, when odd periodic boundary conditions are used. 158

Fig. 81 – No-load damper cage losses vs. THD: optimization solutions.... 162

Fig. 82 – Optimal damper cage solution for reduced losses and THD. 162

Fig. 83 – Bar losses comparison between the actual and the improved designs at no-load operating condition. 163

Fig. 84 – Currents in bar 6: comparison existing and optimal damper cages at no-load operating condition. 163

Fig. 85 – Bar losses comparison between the actual and the improved designs at full-load operating condition..... 164

Fig. 86 – Setup for the sudden three-phase short-circuit test carried out on the original 4MVA SG..... 166

Fig. 87 – Circuits coupled to the FE model for the short-circuit test. 166

Fig. 88 – Envelope curves resulting from the sudden three-phase short-circuit test: FE results (in red) are relative to the existing and the optimal machine; experimental results (in blue) are relative to the existing machine. 168

Fig. 89 – No-load damper cage losses vs. THD: preliminary optimizations results (six input parameters). 174

Fig. 90 – Updated FE (half) model of the HC4 used for optimization purposes. 175

Fig. 91 - No-load damper cage losses vs. THD: optimization solutions with 12 input variables. 176
Fig. 92 - Optimal damper cage pattern for reduced losses and THD. 176
Fig. 93 – Effects of modulation on the voltage waveform: comparison between Machine A and Machine C. 178
Fig. 94 – No-load line-to-line voltage harmonic amplitude spectra: comparison between Machine A and Machine C. 179
Fig. 95 – No-load line-to-line voltage waveforms: comparison between Machine B and Machine C. 180
Fig. 96 – No-load line-to-line voltage harmonic amplitude spectra: comparison between Machine B and Machine C. 180
Fig. 97: Photo of the prototyped skew-less HC4 stator. 187
Fig. 98 – EDM machines used for the rotor lams manufacturing. 187
Fig. 99 – Rotor lamination with zoom on the modulated holes for the damper cage. 188
Fig. 100 – Rotor stack, after the insertion of damping bars inside the relative holes. 189
Fig. 101 – Rotor winding process: a) bead RTD, b) RTD terminal embedded into the winding layers and c) man at work. 189
Fig. 102 – Location of rotor winding RTDs. 189
Fig. 103 – Stator winding process: a) thin-film RTD, b) location of RTDs in slots. 190
Fig. 104 – Location of RTDs in the end windings: a) photo and b) schematic. 190

Fig. 105 - Location of RTDs on outer stator surface: a) photo and b) schematic. 191
Fig. 106 – Air temperature sensor in the airstream between a) stator and frame (outboard) and b) rotor and stator (inboard). 191
Fig. 107 – The whole HC4 gen-set prototype. 192
Fig. 108 – HC4 prototype test bench. 194
Fig. 109 – Voltage measurement: a) LeCroy probe and b) stator terminal box with leads. 195
Fig. 110 – Photo of the no-load voltage waveforms available at prototype's stator terminals. 195
Fig. 111 – No-load line-to-line voltage waveforms: comparison between FE and experimental results. 196
Fig. 112 - No-load line-to-line voltage waveforms: comparison between a) Machine A and Machine C and b) Machine B and Machine C. 197
Fig. 113 – Open-circuit characteristic test set-up. 199
Fig. 114 – Slip rings used for field voltage and current measurements. 199
Fig. 115 – No-load characteristic: experimental comparison between optimal and existing HC4. 200
Fig. 116 – Short-circuit characteristic: experimental comparison between optimal and existing HC4. 201
Fig. 117 – Short-circuit test set-up. 202
Fig. 118 – Short-circuit test: short-circuiting connections and CTs used for the current measurements. 202
Fig. 119 – Windage and friction loss evaluation. 204

Fig. 120 – Iron loss determination. 204

Fig. 121 – Decrement test set-up. 209

Fig. 122 – Decrement test: photo of a) the test cell set-up and b) the CTs. 210

Fig. 123 – Typical current oscillations after a sudden short-circuit. 210

Fig. 124 – Envelope curve for the phase A: numbering of the peaks. 211

Fig. 125 – Decrement test: curves for the dynamic parameters determination. 212

List of Tables

Table 1 – Technical datasheets of the considered generators. 31

Table 2 – THD and RMS values – Comparison amongst the three techniques. 103

Table 3 – Damper cage loss: comparison amongst the three techniques.... 106

Table 4 – Full-load results for the DIG142..... 112

Table 5 – Full-load results for the HC4. 113

Table 6 – Experimental and FE results: comparison at different loadings and power factors..... 119

Table 7 – DIG412 losses and THD vs. magnetic wedge permeability. 129

Table 8 – Summary of the improvements achieved by the optimal topology. 165

Table 9 – Reactances and time constants of the DIG142 generator. 168

Table 10 – Comparison amongst the three case studies. 181

Table 11 – Electrical load parameters registered during full-load, steady-state operation of the generator prototype..... 205

Table 12 – Efficiency calculation by loss summation method. 207

Table 13 – Dynamic parameters: experimental comparison between optimal and existing topologies. 214

Table 14 – Major advantages of the proposed model with respect to the classical literature. 224

Table 15 – Harmonic mitigation topologies and applications. 228

List of Acronyms

2-D	Two-dimensional
3-D	Three-dimensional
AS	Averaged-slice
AVR	Automatic voltage regulator
BNC	Bayonet Neill Concelman
CGT	Cummins Generator Technologies
CIC	Cummins Innovation Centre
CL	Cage loop
CT	Current transformer
DC	Direct current
DoE	Design of experiment
EDM	Electrical discharge machining
FE	Finite-element
FW	Field winding
GA	Genetic algorithm
Gen-set	Generating set
ICEMS	International conference on electrical machines and systems
IEMDC	International electric machines & drives conference
IET	Institution of engineering and technology
IM	Induction machine
mmf	Magneto-motive force
MOGA	Multi-objective genetic algorithm
MS	Multi-slice

PEMD	Power electronics, machines and drives
PEMC	Power electronics, machines and control
PM	Permanent magnet
RMS	Root mean square
SG	Synchronous generator
SRM	Synchronous reluctance machine
RTD	Resistance temperature detector
SC	Short-circuit
THD	Total harmonic distortion
UoN	University of Nottingham
WEMDCD	Workshop on electrical machine design, control and diagnosis
WF	Winding function

Glossary of Symbols

A, B, C, D	Coefficients relative to the exponential trend of the curves extracted for the dynamic parameters determination.
a, b	Parameters utilised for the determination of the $t=0$ line in the current oscillation graph typical of a sudden short-circuit test.
a_1, b_1, c_1	Slot opening parameters utilised for the tuning procedure of the analytical model with the FE one.
B_i	Flux density values in the rotor and stator.
$\hat{B}$	Peak flux density.
B_{AG}	Air-gap flux density function.
c, d, e	Coefficients used in the modified Steinmetz formula for the hysteresis loss component.
F_I	Magneto-motive force linked with a generic loop.
F_{RS}	Magnetic voltage drop between rotor and stator.
f	Frequency.
g_{max}, g_{min}	Air-gap thicknesses evaluated in correspondence of the pole tips (g_{max}) and of the polar axis (g_{min}).
H_{AG}	Air-gap field strength function.
h	Harmonic order relative to the Fourier expansion of the equivalent magnetic permeability function.
h_s	Slot opening height.
k	Ratio between g_{max} and g_{min}.

k_e, k_{ex}, k_h	Eddy current (k_e), extra (k_{ex}) and hysteresis (k_h) loss coefficients.
I_{bi}	Value of the current flowing into the generic damper bar i.
I_R	Field current value used in the circuit coupled to the FE model.
I_{rated}	Armature rated current.
I_{SS}	Field current required to produce I_{rated} for a sustained symmetrical short circuit at the generator terminals.
I_{ss}	Steady state current after the fault.
$i_{t=0}$, $i'_{t=0}$	Short-circuit current readings on the curves extracted for the dynamic parameters determination.
L_a, L_b, L_c	Lumped inductances used in the FE model to represent the stator armature windings.
L_{ij}	Generic element of the inductance matrix: self- (if $i=j$) or mutual-inductance (if $i \neq j$).
L_{bibj}	Self- (if $i=j$) or mutual-inductance (if $i \neq j$) between the rotor cage loops.
L_{bisj}	Mutual-inductance between the rotor cage loop i and the stator phase j.
L_{bir}	Mutual-inductance between the rotor cage loop i and the field winding.
L_f	Lumped inductance used in the FE model to represent the rotor field winding.
l	Machine axial length.

m	Number of stator phases.
N_{Ej}	Equivalent winding function of the generic phase j.
${}^{r}N_i$	Fourier amplitude coefficient of harmonic order r relative to the generic equivalent winding function of the phase i.
N_j	Winding function of the generic phase j.
N_{kh}	Number of conductors of the generic group (i.e. the active side) h of the phase k.
N_p	Number of harmonics considered for the iron loss calculation.
N_s	Number of 2-D, FE slices.
n	Steinmetz coefficient.
n_b	Total number of damping bars.
n_E	Total number of machine phases.
n_h	Number of harmonics used to evaluate the Fourier series decomposition of the no-load line-to-line voltage.
n_k	Total number of groups of active conductors.
P_{eddy}, P_{hyst}	Eddy current (P_{eddy}) and hysteresis (P_{hyst}) iron loss contributors.
P_{iron}	Total iron losses.
P_{losses}	Sum of the overall losses in the machine.
P_{out}	Output real power of the machine.
p	Number of pole pairs.
R_a, R_b, R_c	Lumped resistances used in the FE model to represent the stator armature windings.

R_{bb}	Lumped resistance used in the FE model to represent the bar-to-bar end connection.
R_{bi}	Resistance of the generic damper bar *i*.
R_f	Lumped inductance used in the FE model to represent the rotor field winding.
R_{vd}	Lumped resistance used in the FE model to represent the active sides of the windings present in correspondence of the ventilation ducts.
R_{Rew}, R_{Sew}	Lumped resistance used in the FE model to represent the rotor (R_{Rew}) and the stator (R_{Sew}) end windings.
r, *s*	Harmonic orders relative to the Fourier expansions of the equivalent winding function and its transposed.
r_{AG}	Equivalent air-gap radius function.
r_r, r_s	Equivalent outer rotor (r_r) and inner stator (r_s) radii functions.
T_d', T_d''	Transient (T_d') and sub-transient (T_d'') short-circuit time constants.
t	Time variable.
V_1	Fundamental component of the no-load, line-to-line voltage.
V_i	Fourier amplitude coefficient of harmonic orders *i* relative to the no-load, line-to-line voltage.
V_f	Field winding voltage value used in the circuit coupled to the FE model.
X_d	Direct-axis synchronous reactance.

$X_d^{'}, X_d^{''}$	Transient ($X_d^{'}$) and sub-transient ($X_d^{''}$) synchronous reactances.
x	Generic scalar quantity.
α	Mechanical state variable: rotor angular position.
α_{bi}	Variable angular distance of the generic damper bar *i* from the polar axis.
α_{sk}	Stator skewing angle.
β	Angular frame locked to the rotor.
β_i	Variable damper bar pitch.
γ	Angular frame locked to the stator.
γ_{kh}	Position of the conductors of the generic group (i.e. the active side) *h* of the phase *k*.
δ	Simulation angle step used in the FE model.
ε_{AG}	Equivalent air-gap thickness function.
η	Machine efficiency.
θ	Generic phase variable.
λ	Normalised rotor coordinates.
${}^{h}\lambda_E$	Fourier phase coefficient of harmonic orders *h* relative to the equivalent permeability function.
${}^{r}\lambda_i$	Fourier phase coefficient of harmonic orders *r* relative to the generic equivalent winding function of the phase *i*.
μ_0	Permeability of the air.
μ_E	Equivalent air-gap permeability function.

μ_r	Relative permeability.
${}^h\mu_E$	Fourier amplitude coefficient of harmonic order *h* relative to the equivalent permeability function.
ν	Equivalent saliency function.
τ_d	Damper bar pitch.
τ_s	Stator slot pitch.
φ	Generic phase of a generic scalar quantity.
ψ_{Mk}	Flux linkage of the phase *k*, i.e. an element of the vector of the fluxes linked with the machine phases.
Ω_{AG}	Air-gap magnetically potential surface
$\bar{\imath}$	Electrical state variable: vector of currents.
$\bar{v}$	Vector of the phase voltages.
$\overline{v_E}$	Vector of the electromagnetic component of the phase voltage.
$\overline{v_{EL}}$	Vector of the inductive component of the electromagnetic voltage.
$\overline{v_{EM}}$	Vector of the motional component of the electromagnetic voltage.
$\overline{v_E}$	Vector of the electromagnetic voltage.
$\overline{v_R}$	Vector of the resistive component of the phase voltage.
D[·]	Diagonal matrix operator.
L	Main inductance matrix.
L_L	Leakage inductance matrix.
$\bar{N}$	Vector of the winding functions.

$\overline{N_E}$	Vector of the equivalent winding functions.
R	Resistance matrix.
R_{add}	Additional resistance matrix used to simulate the load conditions in the Matlab-Simulink model.
$\overline{\Psi}$	Vector of the fluxes linking with the machine phases.
$\overline{\Psi_M}$	Vector of the main fluxes (i.e. not leakage) linking with the phases.
$\overline{\Psi_L}$	Vector of the leakage fluxes.
$Coil_{1_20}$	Coil used in the circuits coupled with the FE model: it represents the series of 20 coils.
$Coil_{1_8//1_8}$	Coil used in the circuits coupled with the FE model: it represents the parallel of two groups of 8 coils in series.
$Coil_R$	Coil used in the circuits coupled with the FE model: it represents the series of the field winding coils.
$Coil_{b_i}$	Coil used in the circuits coupled with the FE model: it represents a single (solid) damper bar.

Abstract

In the field of power generation, the wound-field synchronous generator has a well consolidated history of utilisation, mainly due to its proven and excellent performance. Nevertheless, due to the ever-increasing requirements in terms of power quality, efficiency, grid compliance and manufacturing costs, there is interest in renewing the design of this electrical machine, also allowed by the recent advancements in the computational resources.

In this thesis, an unconventional, modulated damper cage topology for salient-pole synchronous generators is proposed in order to address the requirements inherent to the power quality (by improving the total harmonic distortion of the output voltage), the efficiency (by reducing the damper cage associated losses) and the manufacturing costs and times (by achieving an un-skewed stator core structure). In order to achieve these objectives, a suite of innovative modelling techniques are proposed and validated in this work, including hybrid numerical/analytical models, a new methodology to model skewing in an accurate and fast manner and specific optimisation methodologies for synchronous generators.

In this work, these tools are then used to propose improvements to synchronous generators through new configurations of the damper winding. The thesis focuses on two main platforms, namely 1) a 4*MVA* generator, where the modulated damper bars are shown to improve the losses and the THD of the system and 2) a 400*kVA* generator, where it is shown how

through a new damper winding configuration, the traditional skewing of the stator can be removed without compromising the machine performance in any way.

Acknowledgments

My thanks go to all those who helped and contributed in realising and completing the Ph.D. project discussed in this work.

Special gratitude goes to my friend and supervisor Dr. Michael Galea for his constant help, guidance and support, as well as to Prof. Chris Gerada for his intervention whenever required.

Heartfelt thanks go to Prof. Paolo Bolognesi for the continuous collaboration and the "transfer of knowledge" provided during my MSc years, which allowed for overcoming challenging steps along the PhD experience.

Many thanks to all my colleagues and friends that were part of the difficult but fantastic journey towards the completion of the objectives outlined in this thesis.

My warmest thankfulness goes to my parents, my whole family and my extended "family of friends" from Stornara and Pisa, always present in both the pleasant and difficult times of my life.

Finally, thanks to Carmela who made my life simply better.

Chapter 1
Introduction

The Cummins Innovation Centre (CIC) is a £5M research framework, funded by the power generation company Cummins Generator Technologies (CGT) and hosted within the Power Electronics, Machines and Control (PEMC) Research Group at the University of Nottingham (UoN). This framework is aimed at achieving seamless and efficient academic/industrial interaction with main focus on research related to one of the most important market products for Cummins, namely the power generating set (gen-set).

The main component of the gen-set is arguably the main alternator. In Cummins gen-sets, this usually takes the form of a classical, wound-field, salient-pole synchronous generator (SG). In recent years, the CIC has invested significant research effort aimed at improving the performance, reducing the cost and simplifying the manufacturing processes of this consolidated machine technology, in order to achieve more efficient, effective and flexible products. This is also due to the ever-increasing grid compliance requirements in terms of power quality and efficiency.

The energy sector has long implemented and utilized the SG as a main source for power generation. In earlier times, when power generation and usage was implemented only at local levels, the sector was mainly dominated by the dynamo (direct-current machine). However, starting from the late 19^{th} century, as long distance power transmission and distribution developed (in

parallel to improvements in insulation systems permitting higher voltage levels and thus improved long distance transmission capability), the importance of the SG as the optimal power generation device came to the fore [1].

The year 1891 saw a major milestone in terms of SG technology, when for the first time three-phase AC power was generated and then transmitted for $175km$. This was achieved by a $210kW$ hydro-generator designed to provide $95V$ line-to-line, which was stepped up by a three-phase transformer to $15kV$ for transmission purposes. The overall efficiency of the system was 96.5% and consisted of a salient pole SG [1].

As more advanced systems evolved, including the advent of the steam turbine, a new class of SGs surfaced. In particular, the high centrifugal forces caused by high speed rotation made the salient-pole rotors unsuitable for such purposes and this led to the development of the cylindrical rotor. Nevertheless, for low-to-medium speed applications, salient-pole SGs still represented the predominant choice in power generation and, nowadays, they are almost exclusively used for such purposes.

The social and economic growth of the 20^{th} century forced the sector to enter a new age in terms of power generation and machine design in general. More stringent regulations and the need for efficient and economic systems set the scene for improvements in the design of SGs, especially in terms of loss reduction, more efficient cooling, new insulation materials, better mechanical design and application specific steels, leading to the modern machines we use

and know today. However it is very important to note that all the advances in power generation technologies, including the SG development of the last century, have always been strictly incremental, with no significant disruptive, game-changing advancements being made in the last 50 years or so. In fact, most SG design and development philosophies still in use today are mainly based on techniques and processes developed in the 1950s and 60s. The turn of the 21st century with its push towards greener and more efficient systems (resulting from the economic and ecological requirements), has accelerated the need for new, advanced design philosophies.

In fact, today, as power quality standards, efficiency and grid compliance [2-6] become so demanding and constraining, there is an enormous interest in revamping the design and development of such classical machines. This industry pull towards 'better and improved' SGs is also enabled by the technology push resulting from recent advances in materials, manufacturing techniques and better system level integration processes. Also, significant improvements in computational resources and capabilities are allowing the utilisation of modern techniques and tools such as finite element (FE), analysis platforms, multi-physics modelling [7] and virtual prototyping [8]. The use of these advanced, modern design and development techniques enables the achievement of today's stringent requirements.

1.1 Project description

Its long history and proven performance capability makes the wound-field, salient-pole SG, the natural choice when an efficient and reliable electrical machine is required for generation applications. Being such a consolidated technology, a wealth of literature exists stemming from the long years of utilisation of these machines. However, it is also true that in terms of design and analysis, the wound-field SG remains one of the more academically interesting and complex electrical machines, with lots of opportunities for challenging and stimulating research.

This work will therefore focus on improved designs aimed at enhancing the electromagnetic performance, the thermal management and the manufacturing process of SGs. Two products from CGT's current product range, known as the DIG142 and the HC4 will be considered and these and their respective main challenges are introduced below. Although focus will be given to these specific platforms, the concepts, the models and the methodologies proposed in this thesis can be broadly exploited for various applications and electrical machines.

1.1.1 The DIG142 and its main design challenge

The DIG142 is a 4*MVA* machine and a general picture of the frame enclosing the whole gen-set is shown in Fig. 1 below.



Fig. 1 – The DIG142 alternator.

More detailed technical data, specifications and operation parameters will be given later in the thesis, but it is important to mention that an identified design improvement opportunity is related to the machine's thermal behaviour and limitations, more specifically on its rotor. From relevant studies, it has been identified that a major contributing factor to this challenge is the loss generated in the bars of the damper cage, which is located on the rotor. Thus, innovative techniques aimed at addressing this design challenge for this machine will be proposed and investigated in this thesis.

1.1.2 The HC4 and its main design challenge

The HC4 is a 400*kVA* machine and a general picture of the frame enclosing the whole gen-set is shown in Fig. 2 below. This is a very important machine from a CGT business perspective with sales amounting to $368M over the last decade.

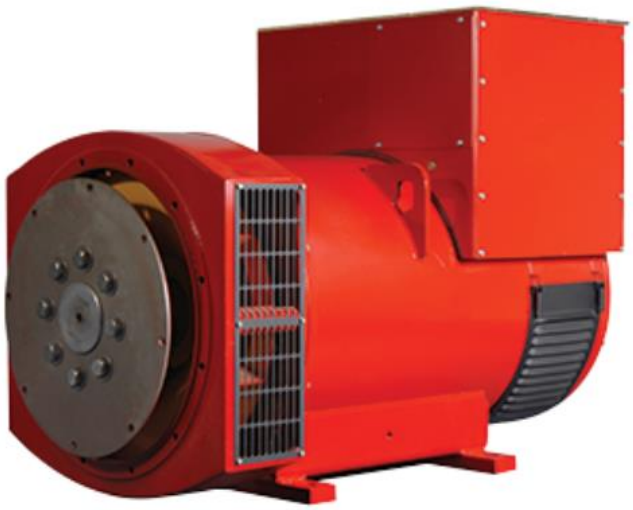


Fig. 2 – The HC4 alternator.

As for many other SGs and various electrical machines, this product employs an operation-enhancing technique known as skewing of the core(s). Skewing of the cores in general means that the stator and/or the rotor are assembled with an appropriate angular offset along the axial length. The main purpose of such a design feature is that it can significantly reduce the air-gap flux density oscillations due to the tooth harmonics. This in turn results in notable improvements in the quality of current, voltage and torque waveforms. However, it is also well-known that skewing may result in a deterioration of the general performance of an electrical machine, such as the reduction in the output voltage available at its armature terminals as well as the torque available at its shaft [9]. Skewing can also negatively affect the manufacturing process, resulting in more time consuming and expensive procedures. Thus, reduction or elimination of skewing is a highly desirable factor for such market-oriented systems, where cost and performance are of critical importance. In-depth analyses of these aspects are included in this

thesis. New methodologies to address these design challenges are proposed and validated.

1.1.3 Proposed solution(s)

Considering the identified issues highlighted above for the DIG142 and the HC4 generators, it is clear that there is a lot of potential for efficiency and power quality improvements as well as for cost reduction. In particular,

1) The DIG142 study aims at reducing the losses associated with the damper cage, allowing for potential improvements of the overall efficiency of the machine and at the same time reducing the resulting rotor temperature. This needs to be done without compromising the power quality constraints of the machine and/or the generator's performance in dynamic conditions.
2) The HC4 analysis is aimed at achieving an un-skewed stator topology, allowing for a significant simplification of the manufacturing industrial processes which in turn leads to reductions in manufacturing cost and production time. This needs to be done without compromising the quality of the SG operation and waveforms (i.e. meeting standard power quality constraints).

From all the above observations, it can then be perceived that this work is very much dedicated and focused on a critical component of wound-field SGs, namely the damper winding (or damper cage) located on the rotor. A detailed introduction and overview of the nature, role and performance of damper windings is given in Chapter 2. It is the aim of this project to address

the design challenges of the machines described above through new and innovative techniques and methodologies associated with the design of this additional winding.

Traditionally, for salient pole SGs, the bars of the damper winding are symmetrically distributed around the rotor poles. This thesis proposes a ‘departure’ from this conventional topology and is built around the innovation spawned from a customised positioning of the bars, which can be named as the concept of employing a modulated bar pitch [10]. This concept is illustrated in Fig. 3, where an example of a customised modulation of the bars can be easily observed.

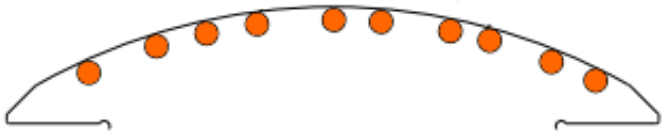


Fig. 3 – Modulated damper bar concept.

For the DIG142 machine case study, it is postulated that a carefully-chosen, irregular bar pitch can interact with the stator open slot structure in such a way that the air-gap parasitic harmonics are attenuated, allowing to significantly reduce the losses in the damper winding, whilst maintaining the voltage total harmonic distortion (THD) at an acceptable limit.

The same concept of attenuating the “slot harmonics” through customised modulation of the damping bars can also be applied to the HC4 machine in order to address the challenge of achieving a ‘skew-less’ design that still complies with the set THD values of the machine.

Considering the different power rating of the two considered CGT's alternators and the dissimilar nature of the relevant challenges, it is clear that the modulated damper bar concept can be applied to any SG equipped with such rotor winding.

It is important to note that the concept of having asymmetrical or modulated windings is not a completely new philosophy. Some efforts (albeit quite limited) have been recorded, mainly focusing on the design of the stator windings in induction machines [11]. However, to the author's knowledge, no such methodology has ever been applied to address losses and THD improvements in salient-pole SGs. The application, the design space and the overall system being proposed and investigated in this thesis comes with a completely different context, solutions and required analyses than for an induction machine (IM) situation.

1.2 Aims and objectives

As outlined in the above introductory sections, this thesis is focused on achieving a marked performance improvement in SGs, even though this is a family of machines which is very well-known and established. This is achieved through the development of advanced analytical, numerical and hybrid tools for electromagnetic analysis and the implementation of GA-based optimisation approaches aimed at obtaining optimal solutions. As platforms for investigating the accuracy and validity of these tools, two alternators are considered, namely the DIG142 and the HC4, which are in the 4*MVA* and 400*kVA* power range, respectively.

A major part of this work is thus focused on the analysis, modelling and testing of the DIG142 SG, whose performance will be improved by achieving an optimal damper winding design consisting in modulating (i.e. repositioning) the damper bars. Innovative analytical and numerical tools, based on virtual prototyping and optimization techniques, will be described, implemented and used to reduce the losses associated with the damper winding, while keeping the THD of the output voltage and the dynamic parameters of the generator within acceptable limits. These tools, once validated, will be then used to achieve another challenging target, i.e. a skew-less SG, which will make up the most significant part of this thesis. For this purpose, the skewed HC4 machine will be considered, its performance will be analysed and validated against experimental measurements and, finally, a skew-less solution will be proposed by applying the same modulating technique to the damper cage of the SG. To this end, the performance of a prototype built on-purpose will be compared with the baseline machine, showing the feasibility of an un-skewed stator for SGs without significantly compromising its power quality.

The main novelty proposed in this thesis consists in the concept itself of unconventionally displacing the bars of the damper windings of SGs. This is perceived as having significant effects of a multi-disciplinary nature, including electromagnetic (i.e. improving the power quality), thermal (i.e. reducing rotor losses and temperatures) and manufacturing (i.e. simplifying the relevant processes) aspects. In particular, the implementation of a modulated damper cage can allow to meet the power quality requirements

without resorting to the skewing, potentially leading to game-changing opportunities in the field of such classical machines. This is especially true in relatively low-to-medium rated alternators, where historically skew of the cores has always been implemented to meet such stringent requirements. Additional novelties of this work are represented by the analytical, numerical and genetic algorithm (GA) based modelling techniques developed and implemented to achieve optimal solutions, aimed at improving SGs' performance and the overall efficiency of the whole gen-set.

In summary, the main aim of this project is to investigate the proposed damper bar modulation technique and consolidate the improvements in terms of performance, power quality, cost and manufacturing that it can potentially result in, when implemented in SGs. In order to achieve this aim, a number of objectives and deliverables were identified at the start of the project and these include

1) Build a comprehensive understanding of wound-field SGs, with particular focus on
    a. the damper winding and its effects on losses and THD;
    b. the stator skewing and its effects on THD and overall performance.
2) Propose and develop a new modelling approach based around combining analytical-numerical techniques that will allow for accurate but time-efficient modelling of the machines (DIG142 and HC4) in question.

3) Validate these models against experimental results carried out on the current version of the considered platforms.
4) Propose and investigate new ways, based around improved damper cage configurations relative to the modulated bar technique that will allow
    a. improvements in the damper bar losses and the no-load voltage THD for the DIG142 SG;
    b. the removal of the stator skew, without compromising the power quality and efficiency compliances for the HC4 alternator.
5) Confirm the validity of the proposed technique by building and testing a skew-less HC4, that even without skew would have at least the same performance as the original, skewed HC4. This will then prove the validity of the proposed modulated bars concept and confirm the feasibility of a skew-less, power quality compliant, 400*kVA* SG.

1.3 Thesis outline

The thesis structure is organised in such a way to report all the logical passages and steps of the methodology followed towards the completion of the objectives of this project.

Chapter 1 introduces the project by highlighting the required applications, providing relevant background and outlining aims and objectives of the project. In Chapter 2, these concepts are strengthened through a review of

existing methods in terms of design, modelling and analysis of SGs, with special focus on the damper cage loss reduction and the skewing as a method to improve the power quality. An in-detail description of the features of the considered alternators concludes this chapter and this first part of the thesis.

The knowledge gained from the literature review is used in Chapter 3 and Chapter 4 to develop and implement fast and accurate analytical and FE models of the studied platforms. The models are then validated against available experimental measurements.

Having validated these modelling techniques, then the thesis goes into the 'heart' of the whole work, which is represented by Chapter 5 and Chapter 6. In Chapter 5, the validated models are used to achieve a full understanding of the roles and effects of the damper cage for both SGs by performing accurate sensitivity analyses on a number of parameters. The knowledge gained here is then applied in the most important chapter of all, namely Chapter 6, where the new designs of the damper windings for both SGs relative to their respective needs/aims are presented. These designs follow a detailed optimisation procedure in light of achieving the afore-mentioned objectives of

1) significantly reducing the damper cage losses in the DIG142, while keeping the voltage THD within the requirements;
2) achieving a voltage THD lower than 3% [12] in the HC4 even without resorting to the skewing, with no deterioration of the machine performance.

Experimental validation is then performed on the HC4 prototype. A prototype equipped with a skew-less stator and a modulated damper cage rotor is manufactured. The manufacturing aspects of this prototype are discussed and the results from the experimental testing are then presented and compared with the predicted results in Chapter 7. It is worth noting that it was not possible to manufacture a new 4*MVA* DIG142 prototype due to the costs and time-lines involved.

Chapter 8 concludes this thesis, by presenting overall discussions and further work to be done in the related applications.

Chapter 2

Literature review

This chapter deals with the literature review carried out for preliminary investigation of the challenges related to this project which were introduced in Chapter 1. In particular, focus is given to the review of the methods aimed at improving efficiency and power quality in SGs, which have been the matter of research in recent literature.

However, given the aims and objectives of this work listed in Section 1.2, the literature survey does focus on the damper cage and on skewing techniques, when implemented onto SGs in order to comply with the efficiency and power quality requirements mentioned above.

2.1 Introduction

As higher power density and efficiency levels are being required, many improvements options have been proposed over the last century or so. In this context, several aspects such as the thermal management, different winding configurations, the rotor pole shape and the damper cage topology have been widely considered.

It is well known that the thermal performance of an electric machine has a great effect on the insulation material's lifetime [13]. In fact, reduced temperatures usually result in improved efficiencies and increased machine

lifetimes [14]. Improved cooling systems can allow to push the temperatures to the highest limits, resulting in augmented power densities [15, 16]. Also, strategies relative to the stator winding configuration are known to be of significant impact on the general performance of these machines, in particular on the output voltage waveform [17-21]. The geometry of the stator slots and rotor poles can also affect the performance of electrical machines in terms of power quality and efficiency. In [22], the geometry of the stator slots has been optimized in order to achieve the optimum torque production while minimising the total amount of loss in the machine. In addition, the geometry of the rotor poles plays a very important role on the airgap flux density [23] when specific space harmonics need to be eliminated, although this comes at the cost of an increased leakage flux [17]. A review of all these methods utilised as options to increase power density, efficiency and power quality in SGs is given in [24].

Finally, the damper winding design and the rotor and/or stator skew has been extensively shown to be of a great effect on the overall performance of SGs. As these techniques represent the main aspects investigated in this work, the related literature surveys are treated separately in the following sections. The relevant background is described below, with the aim of highlighting features, benefits and drawbacks of such aspects.

2.2 The damper cage

Most synchronous motors and generators are provided with a damper winding. Although this damper cage winding, also called amortisseur winding, is usually designed for guaranteeing the power system stability [25, 26], it also affects the machine behaviour under different operating conditions, including the steady-state operation. Due to its proven role in classical SGs, this section focuses on the description of various damper cage topologies conventionally used in alternators and on the purposes of this additional winding, highlighting benefits and drawbacks. Finally, recent advancements in this field are also given.

2.2.1 Conventional damper cage in synchronous generators

The damper cage in wound-field, salient-pole, SGs consists of longitudinal bars placed in slots in the pole faces and connected together at each end. The end conductors in a "complete" damper winding (Fig. 4) are usually represented by relatively low-resistance rings connecting the bars of all the poles, while in an "incomplete" damper winding (Fig. 5) each group of bars embedded into the same pole is electrically insulated (i.e. not connected or realised through high-resistance paths) from each other. Complete damper windings are similar to the squirrel cage of an IM. Although it is preferable to equip generators with incomplete dampers in applications where the peripheral speeds are high, a complete configuration is usually implemented for its superior electrical performance. Besides this structural-based differentiation, the damper cage can be classified also according to its

resistance and inductance, whose values are chosen depending on the applications the synchronous machine is designed for.

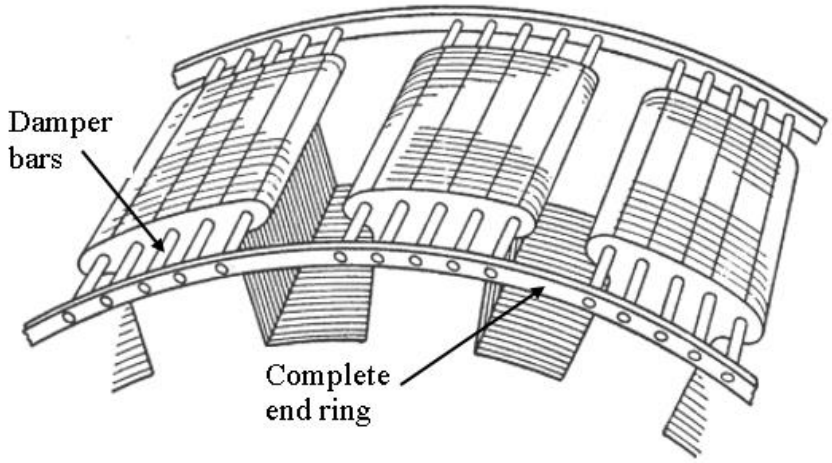


Fig. 4 – Damper winding with connected end rings between adjacent poles [27].

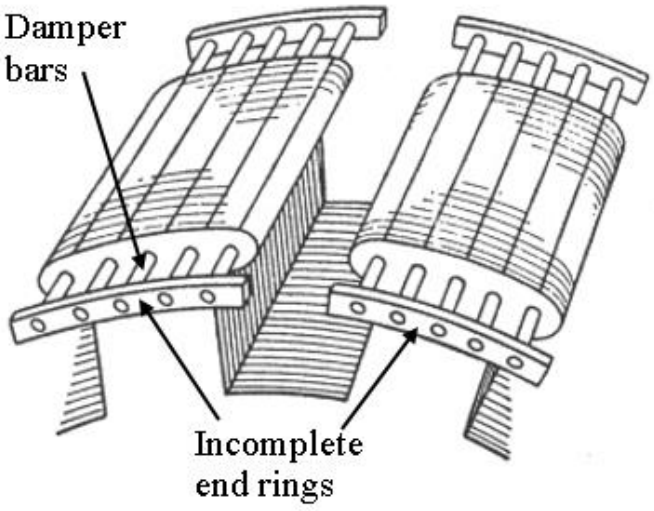


Fig. 5 – Damper winding with non-connected end rings between adjacent poles [27].

2.2.2 Benefits and drawbacks

The main reasons for providing a damper cage on salient-pole SGs, as summarized in [27], are

- providing starting torque for synchronous motors, condensers and converters;
- suppress “forced” hunting due to the pulsating torque of the driving engines or particular loads;
- suppress “spontaneous” hunting that occurs when synchronous machines are connected together by circuits having a high resistance/inductance ratio;
- damping oscillations caused by unforeseen and/or irregular events and shocks, such as short-circuits or switching;
- damping oscillations due to speed response inequalities of excitation systems of generators of the same power station;
- balancing terminal voltages of the machine phases during unbalanced loading by decreasing the negative-sequence voltage;
- preventing overheating of the pole tips of single-phase generators from eddy currents induced by sustained negative-sequence armature currents;
- providing braking torque on a generator during an asymmetrical fault, i.e. reducing the accelerating torque during the fault;
- providing additional torque for synchronizing generators;
- reducing the stress on the insulation of the field winding during current surges in the armature windings;
- preventing distortion of voltage waveform; in other words, to suppress harmonics.

The above features of the damper winding, presented as beneficial for the generator performance, usually incur the cost of induced voltages and thus currents in the bars themselves. This in turn produces additional losses in this winding, mainly due to the presence of parasitic harmonics in the air-gap flux density. As stated in [28], these harmonics are generated by the following:

- Tooth-ripple, due to the open slot structure typical of high-voltage machines.
- Armature reaction magneto-motive force (*mmf*), which causes parasitic harmonics on the rotor surface when currents flow in the stator windings.
- Unbalanced air-gap, which can induce high bar currents.

All the above confirms the worth of investigating into the design, analysis and modelling of this amortisseur winding, with the aim of finding improved designs which potentially allow, for the particular purposes of this project, for a minimisation of the induced ohmic losses, while still maintaining or even improving the winding capability of suppressing harmonics.

2.2.3 Review of methods

Traditionally, the design of damper windings has been done by means of conventional methods which combine theoretical and empirical techniques. Early works focused on the prediction of the damper-bar currents with the classical *dq* equivalent circuit approach [29, 30]. With the same purpose, permeance models based on Fourier expansion techniques are used in [31] and [32]. In [28] an innovative numerical integration method is proposed and

also compared with the traditional *dq*-axis approach with very positive results. Although the worth of these traditional techniques is well known and consolidated, with the recent advancements in computational capabilities, a significant shift towards numerical methods, such as FE and computational fluid dynamics [14, 15], allows for improved accuracy and extra degrees of freedom in the design process. Due to this, today there is an increasing interest in the damper winding designs (and SGs in general [19]), as this can be very beneficial to the overall SG performance. This is very important especially when considering the possibility to investigate the machine operation both in steady-state and in transient conditions. In particular, complete and incomplete damper windings are analysed in [33] and [34], showing that complete end connections lead to higher slot ripple harmonic amplitudes. In [35-37], FE analyses are used to predict and optimize the no-load voltage waveform. For example, [16] shows how improvements in the voltage output shape are achieved by inducing additional currents in the bars of the damper winding at the cost of increased losses and thermal issues. In [38], a sensitivity analysis on how the damper cage parameters affect associated losses and voltage THD is carried out, showing that these can be improved by increasing the distance of the damping bars from the airgap (i.e. moving the bars along the radial direction) and by shifting the cage around the polar axes (i.e. moving the bars along the tangential direction).

2.2.4 Final considerations

Although a number of techniques to improve the overall SGs performance has been widely presented in literature, the main objective of this work is to

provide an alternative solution to the state-of-the-art. In this context, an innovative damper cage topology is proposed to reduce the power loss associated with this winding at steady-state operation while keeping the no-load voltage THD under permissible limits. The proposed techniques are first considered on an existing machine platform in the form of a 4*MVA* SG (i.e. the DIG142). The SG in question is presented in Section 2.4.1, where it will be seen how this machine is an ideal vessel for the proposed work.

2.3 Skewing and its effects and roles

The positive effects of implementing various methods of skewing in electrical machines (to improve the general quality of operation) are well-known throughout the machines and drive community. Providing the stator and/or the rotor of an electrical machine with an appropriate angular offset along the axial length can significantly reduce the air-gap flux density oscillations due to the tooth harmonics. This in turn results in notable improvements into the quality of current, voltage and torque waveforms.

However, as mentioned above in Section 1.1.2, it is also well-known that skewing does produce some drawbacks, from both an electromagnetic and manufacturing points of view. In the next sections, an overview of how skewing is implemented in various electrical machines and how this is typically modelled is presented.

2.3.1 Skewing in various machines

The influence of axial skewing in IMs has been widely investigated [39-42]. In general, IMs usually employ skew in the rotor bars rather the stator slots in order to simplify the manufacturing processes. On-going research related to IMs includes investigations on the magnetic noise and the electromagnetic forces caused by skewing, as described in [43] and [44], where novel rotor structures are proposed at the cost of increasing manufacturing times and costs. The non-uniformity of the flux density axial distribution and the loss behaviour of a high-rated IM are investigated in [45].

In the field of permanent magnet (PM) machines, the analysis of skewing and its effects has also been widely dealt with, in particular for low speed applications, where high torque quality is often required. In such cases, skewing the stator slots or the PMs themselves [46, 47] can result in a significant reduction of the cogging torque component [48-52], which in turn produces improvements in the quality of the on-load torque. The challenge of minimising the torque pulsations has been dealt with in different types of PM machines in recent works. For example, [53] has shown that skewing in regular steps does not achieve significant improvements in the torque ripple of surface-mounted PM machines. An improved skewing method is presented in [54], where a spoke-type interior PM machine is optimised for torque ripple minimization without compromising the available average torque. An asymmetrical, bidirectional magnet skewing technique is instead proposed in [55], for a modular multi-stage axial-flux PM machine. An authoritative

review of magnet skewing techniques for double-rotor axial-flux disk motors is provided in [56].

In recent years, significant effort related to improving the torque quality in the field of synchronous reluctance motors (SRMs) has also been registered [57, 58]. In particular, the benefits of skewing the rotor, in combination with an appropriate stator winding design, are highlighted in [59]. In [60], it is highlighted how the torque ripple of a SRM can be further reduced if the skew is applied to an optimal asymmetric rotor structure. The three-dimensional (3-D) effects associated with skewing are examined in [61], where it is shown how end-effects and axial interactions between skewed steps can considerably deteriorate the torque ripple effects in SRMs.

2.3.2 Skewing in synchronous generators

A very important field which for historic reasons has never fully considered the importance of skewing is that related to the area of salient-pole SGs. As mentioned above, special focus is today being given to the THD of the output voltage of such electrical machines. For example, while [10], [24] and [38] show how the THD can be improved and optimised without resorting to skewing techniques, the work in [31] investigates how the choice of an optimal skew angle, combined with an increased air-gap thickness, can reduce the noise level within the standards and improve the THD in a hydro-generator. The study performed in [31] also aims to achieve an understanding of how the field distribution, the damper cage currents and the rotor pole face losses are affected by stator skewing and provides a wide range of

experimental data at no-load and full-load operations. In [62], a detailed analysis of a tubular SG is carried out in order to investigate the effects of stator skewing on the voltage waveform and the damper cage loss. For the same aspects, large SGs with an axial skew are analysed in [63] and [64]. Considering all the above, it is clear that skewing in SGs is rapidly becoming an important design aspect. While traditionally it has been very roughly implemented, today skewing and its effects need to be considered from a very early design stage and to an appropriate level of detail.

2.3.3 Review of methods

In this context, predicting the skewing's effects in a fast and accurate way is thus very important in the design routine of an electrical machine, in particular when heavy design iterations are required. Classical approaches for modelling skewing consist in 3-D calculations of air-gap permeances which also include axial field variations [65]. Fully analytical models (that consider skew and its effects) have also been proposed by implementing the winding function method [66] and the subdomain modelling technique [67, 68]. With recent improvements in computational capabilities and modelling accuracy allowed by numerical methods, a number of hybrid analytical/FE techniques have been proposed [63, 69, 70] as well as purely FE models [71]. A common approach is to use the multi-slice (MS) technique [39-41, 72, 73], which comprises the creation of a number of cross-sections of the machine along its axial length and the simultaneous simulation of these slices. The MS approach has been proposed in [73] in order to overcome inaccuracies resulting from averaging processes in machines with short-circuited cages,

i.e. IMs and SGs. Such a study also shows how averaging processes can be used for SGs if the magnetic field does not significantly change along the axial direction. In [74], the MS method has been extended to a magnetic equivalent circuit model and a constraint is imposed to ensure that axial currents are equal in each slide. Although all these techniques are very accurate, they come at the cost of high computational resources which are not suited for iteration-heavy designs.

2.3.4 Final considerations

Considering all the above, it can be clearly deduced that

- predicting skewing effects in a fast and accurate way is very important in the design routine of an electrical machine;
- removing the skewing allows for improvements in the overall SG performance and leads to more economical design solutions.

An improved damper cage topology is proposed not only for the DIG142 but also for the HC4 alternator, with the aim of eliminating the stator skewing of such machine. While for the DIG142, 4*MVA* SG, the voltage THD represents a secondary objective, here the proposed techniques aim at achieving a power quality compliant machine, thus resulting in this critical parameter being considered as the main goal for the study relative to the HC4.

The considered DIG142 and HC4 alternators are described in detail in the next section in order to provide all the relevant features necessary for the implementation of the analytical, hybrid analytical-numerical and fully

numerical (i.e. FE) models of electromagnetic analysis which will be focus of the next chapters.

2.4 The considered platforms

In this section, a detailed description of the DIG142 and the HC4 generators under study is given. All the features related to the geometry, the windings' structure and the ferromagnetic materials of these machines are listed to provide all the information necessary for modelling and analysis purposes.

2.4.1 The DIG142

The DIG142 is an alternator utilised in several applications (e.g. power plant, oil & gas, continuous power and standby). The machine has a rated apparent power of 4*MVA* at 0.8 power factor. The generator is designed to provide a three-phase output voltage of 11*kV* at 50*Hz*, achieved with Y-connections of the armature phases. Some of the major features of this SG are as follows:

- the stator is laminated and has an open-slot structure;
- the number of slots-per-pole-per-phase is 5 with a double-layer winding structure;
- the stator coils are grouped in 2 parts, having different number of turns to reach a certain desired magneto-motive force;
- there are no parallel circuits on the stator windings;
- the stator core is equipped with radial ventilating ducts along the axial direction; these reduce the active material of the machine but improve cooling and airflow;

- the rotor is laminated and made from the same electromagnetic steel as the stator laminations;
- the number of rotor pole pairs is equal to 2;
- the ratio between the rotor diameter (in correspondence of the minimum airgap) and the axial length is 0.5;
- the damper cage on the rotor is displaced around the polar axis in alternating directions on each pole, in order to improve the harmonic content of the output voltage waveform in the absence of rotor or stator skewing;
- the number of damper bars per pole is equal to 10;
- the damper cage end connections are created by press plates made out of aluminium, i.e. laminations thicker than the rotor ones.

The two-dimensional (2-D) cross-section of the stator and rotor of the DIG142 are respectively shown in Fig. 6 and Fig. 7, where most of the features described above can be observed.

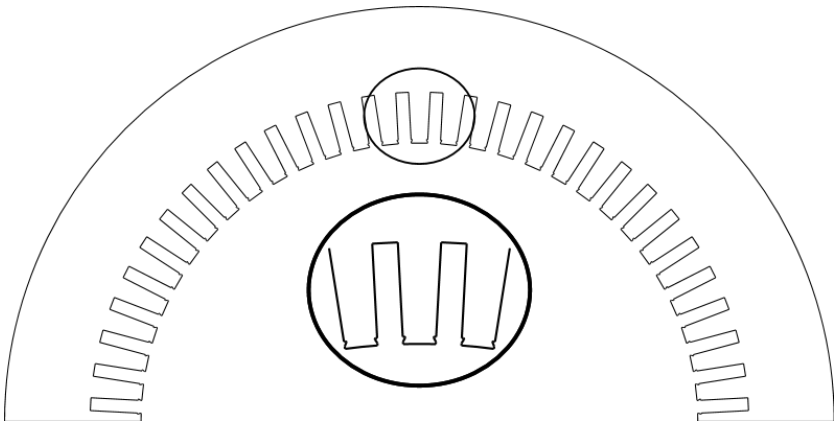


Fig. 6 – Open slot structure of the DIG142 stator lamination.

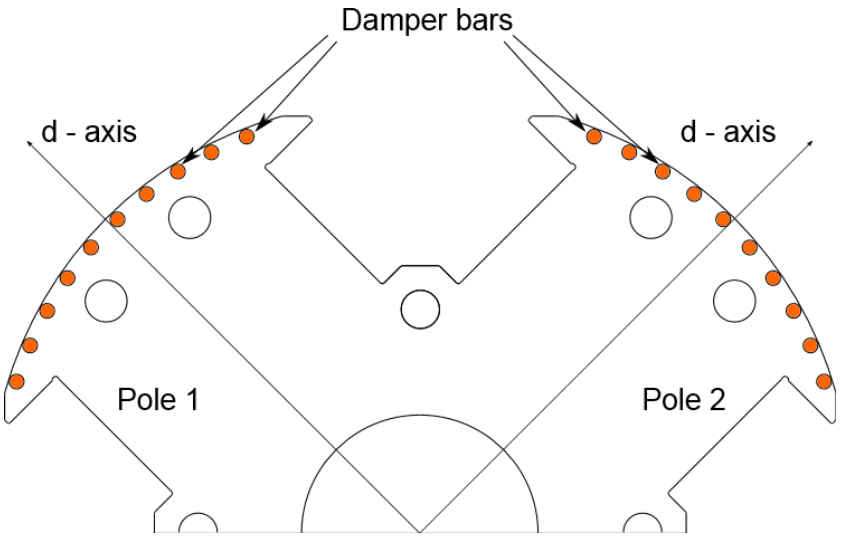


Fig. 7 – Rotor topology with damper cage displaced around the polar axis.

2.4.2 The HC4

The HC4 is a salient-pole SG with a rated apparent power of 400*kVA* and a rated voltage of 400*V*, at 50*Hz* and at 0.8 power factor, achieved with Y-connection of the armature phases. Some of the features of the considered SG are as follows:

- the stator and the rotor have a laminated core and are made of the same electromagnetic steel;
- the stator is skewed by one slot pitch allowing to mitigate the slot harmonics on the output voltage waveform;
- the number of slots-per-pole-per-phase is 4 with a double-layer winding structure;
- the stator winding is short-pitched by 4 slots, to eliminate the third harmonic on the phase-to-neutral voltage, as the generator is also designed to operate under single-phase conditions;
- the number of parallel circuits on the stator windings is 2;

- the stator slot opening has an angular span which is about half of that of the slot pitch;
- the rotor is such that the airgap is constant along the entire angular span of the pole shoes;
- the angular pole span covers the 75% of the whole pole pitch;
- the number of rotor poles is equal to 4;
- the ratio between the stator outer diameter and the axial length is 1;
- the rotor is equipped with a damper cage symmetrically displaced around the polar axes;
- the number of bars per pole is 6;
- the damper cage end connections are created by press plates made out of aluminium, i.e. laminations thicker than the rotor ones.

The 2-D cross-section of the HC4 is shown in Fig. 8, where some of the features described above can be observed.

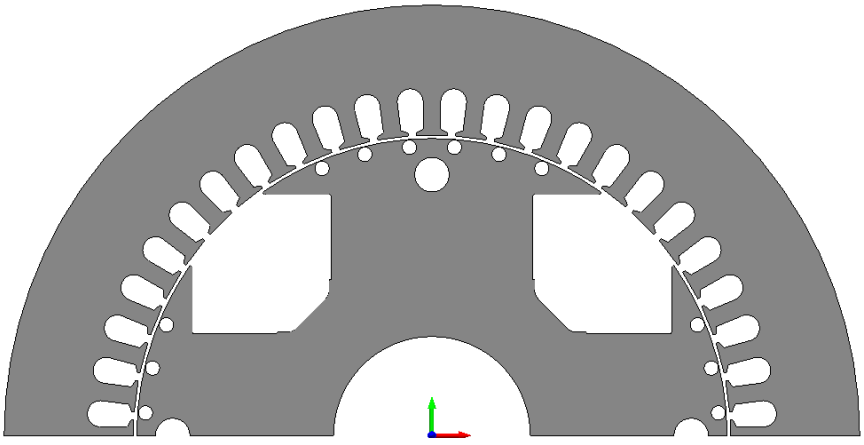


Fig. 8 – 2-D half view of the HC4 stator and rotor laminations.

2.4.3 Summary

Section 2.4 presented the major design features of the generators used as vessels to investigate the challenges related to this Ph.D. project. Due to confidentiality agreements with the industrial partner, the geometrical dimensions cannot be published "directly". However, the bulleted lists of sections 2.4.1 and 2.4.2, relative to the DIG142 and the HC4 respectively, comprehensively describe the considered platforms, whose main nameplate characteristics are summarised in Table 1.

Table 1 – Technical datasheets of the considered generators.

Generator name	DIG142	HC4
Main application	Stationary power plant	Industrial and marine
Rated power	4450*kVA*	400*kVA*
Power factor	0.8	0.8
Rated voltage	11k*V*	400*V*
Speed	1500*rpm*	1500*rpm*
Frequency	50*Hz*	50*Hz*
Rated current	233.6*A*	577.4*A*
Winding pitch	5/6	2/3
Insulation class	F	H
Cooling	Open-circuit ventilation	Open-circuit ventilation

2.5 Conclusions

This chapter presented a literature survey on SGs, with special focus on the methods used for improving the efficiency and power quality of such machines, stemming from those that for historical reasons have been most commonly utilised for such purposes. Given however the objectives of this work, this chapter focused on the effects and roles that the damper cage and the skewing have on the performance of SGs, highlighting the recent advancements and the state-of-the-art in the field. To conclude the chapter, an in-detail description of the DIG142 and the HC4 is provided. A summary of their characteristics is given in Table 1.

The challenges related to this project as identified in Chapter 1 as well as all the aspects investigated in Chapter 2 in the form of literature review, are utilised in the next two chapters to develop, implement and validate accurate models for the analysis of classical, wound-field, SGs.

Chapter 3
The hybrid analytical-numerical model

The equivalent circuit methodology has been widely exploited for the theoretical analysis of electromagnetic devices and is considered a classical approach for modelling the phenomena internally occurring in electrical machines. In the field of classical wound-field SGs, the presence of the damper cage complicates the analysis of such devices and the accurate prediction of the inherent induced currents is still a matter of ongoing research.

In this chapter, an advanced and generalised theoretical model for the analysis of electromagnetic devices is proposed and then properly adapted to the considered machines. Special focus is given to the damper cage modelling, where inherent assumptions allow for intermediate conclusions and simplifications, resulting in a reduced system of electromagnetic equations to be considered. However, due to the induced nature of the currents in the damper bars, a numerical solution is also required, resulting in a hybrid analytical-numerical approach being implemented. In order to validate the model, a 2-D corresponding FE model (whose details will be given in the Chapter 4) is built, also to take into account the complex electromagnetic phenomena that are not inherently considered in the generalised, analytical model.

3.1 Model introduction

Rather than focusing on a specific machine configuration, i.e. assuming for example symmetrical and full-pitched windings (eventually with a sinusoidal distribution [75]), symmetrical structure of cores [76] and PMs (when present), a general model valid for any class of machine topology is proposed. The basic structure of the proposed analytical model is first introduced and presented in [77]. In this thesis, this basic framework is updated and customised to the requirements of this project.

3.2 Model assumptions

To set the context of the scheme, the main introductory assumptions are defined in this section. The proposed theoretical approach concerns the class of rotating electrical machines identified by the following features:

- a "drum-type" arrangement with coaxial rotor and stator cores separated by a reasonably narrow main airgap;
- stator and rotor magnetic cores featuring an equal axial length *l*;
- an axially extruded geometry with approximately cylindrical envelope profiles of the surfaces facing the main airgap;
- belt-shaped yokes encircling the active parts of the machine respectively on the external and internal sides;
- salient poles with approximately cylindrical main head surfaces;

- phase windings composed of thin wire, each one featuring a geometrically closed shape with active sides laying parallel to the machine axis either inside the slots or around the salient poles;
- PMs, when present, located for instance only on the external side of the rotor core and featuring a rather small thickness and a planar grossly radial magnetization;
- main airgap interposed between the permanent magnets layer and the internal stator surface;
- negligible secondary phenomena, such as hysteresis and parasitic currents inside the magnetic cores.

From the basic, generic features listed above, the following considerations can be drawn, as shown in [78]:

- A main region, corresponding to the axial portion of the machine delimited by the magnetic cores, can be defined and differentiated from a secondary region, mainly involving the phenomena occurring in the end parts of the windings.
- Assuming that the shape of the magnetic cores and of the windings can be generated by straight extrusion along the machine axis, a 2-D approximation of the field map can be considered to derive the general model.
- It is assumed that the ferromagnetic materials feature a sufficiently high permeability to permit neglecting the *mmf* drop inside the cores with respect to the *mmf* across the airgap.

- The mutual influence between the main field lines and the secondary lines (representing the flux leakage) can be neglected, permitting to separately analyse such phenomena.
- The shape of the main flux lines in the airgap is assumed to be mainly determined by the profiles of the magnetic cores and by the rotor position, meaning that the dependency on the currents is neglected.
- The variation of the magnetic field intensity along the portions of the field lines in the main airgap is considered to be small, permitting to focus on the average value and on its variation along the tangential direction.

Given the above hypotheses, assumptions and considerations, it becomes then possible to derive the equations correlating flux linkages, phase currents and the position variables associated with the mechanical degrees of freedom of the device under analysis. It is important to mention that in classical SGs there is only one mechanical state variable, which is associated with the position of the rotor vs. stator.

3.3 Problem definition

The basic quantities used in the analysis are the vector $\bar{\imath}$ composed by the currents flowing into the machine phases and the vector $\bar{\psi}$ of the fluxes linking with the phases. The voltage at the phases' terminals of any device is made up of two main components, due to the resistive (Ohm's law) and

electromagnetic (Lenz-Faraday's law) phenomena respectively. While the resistive component $\bar{v}_R(t)$ is equal to $R\,\bar{\imath}(t)$, where R is the matrix of the phase resistances, the electromagnetic portion $\bar{v}_E(t)$ is given by the derivative $\frac{d\bar{\psi}(t)}{dt}$ of the vector $\bar{\psi}$ respect to the time. Considering the elements of the current vector $\bar{\imath}$ and the rotor position α as state variables, the electromagnetic voltage can be further exploited as in (1).

$$\bar{v}_E(t) = \frac{d\bar{\psi}(\alpha(t), \bar{\imath}(t))}{dt} = \left(\frac{\delta\bar{\psi}(\alpha,\bar{\imath})}{\delta\alpha}\bigg|_{\alpha(t),\bar{\imath}(t)}\right)\frac{d\alpha(t)}{dt} + \left(\frac{\delta\bar{\psi}(\alpha,\bar{\imath})}{\delta\bar{\imath}^T}\bigg|_{\alpha(t),\bar{\imath}(t)}\right)\frac{d\bar{\imath}(t)}{dt} \quad (1)$$

In (1), the further separation of the electromagnetic voltage in two more terms can be observed and these are

- the motional component $\bar{v}_{EM}(t) = \left(\frac{\delta\bar{\psi}(\alpha,\bar{\imath})}{\delta\alpha}\Big|_{\alpha(t),\bar{\imath}(t)}\right)\frac{d\alpha(t)}{dt}$, due to the variation of the position, when the currents are fixed;
- the inductive components $\bar{v}_{EL}(t) = \left(\frac{\delta\bar{\psi}(\alpha,\bar{\imath})}{\delta\bar{\imath}^T}\Big|_{\alpha(t),\bar{\imath}(t)}\right)\frac{d\bar{\imath}(t)}{dt}$, due to the variation of the currents, when the position is fixed.

By further developing (1) and by adding the voltage drop across the winding resistance, the expression for the total voltage linked with the phases can be written as shown in (2), where L contains all the inductances characterising the considered machine and $D[\bar{\imath}(t)]$ is a diagonal matrix, whose each not-null element is composed by $\bar{\imath}$. However, the assumption introduced in Section 3.2 relative to the magnetic linearity, allows for the consideration of the matrix L

as being only dependant on α. Thus (2) can be simplified and re-written as shown in (3).

$$\bar{v}(t) = R\bar{\imath}(t) + \left(\frac{\delta L(\alpha, \bar{\imath})}{\delta \alpha}\bigg|_{\alpha(t),\bar{\imath}(t)} \bar{\imath}(t) \right) \frac{d\alpha(t)}{dt} + \left(\frac{\delta L(\alpha, \bar{\imath})}{\delta \bar{\imath}^T}\bigg|_{\alpha(t),\bar{\imath}(t)} D[\bar{\imath}(t)] \right) + L(\alpha, \bar{\imath}) \frac{d\bar{\imath}(t)}{dt} \quad (2)$$

$$\bar{v}(t) = R\bar{\imath}(t) + \left(\frac{\delta L(\alpha)}{\delta \alpha}\bigg|_{\alpha(t)} \bar{\imath}(t) \right) \frac{d\alpha(t)}{dt} + L(\alpha) \frac{d\bar{\imath}(t)}{dt} \quad (3)$$

It can be clearly observed that the inductance matrix $L(\alpha)$ plays a key role in (3) and thus on the internal electromagnetic behaviour of the device under analysis. Considering the above, the following sections are aimed at finding an expression for $L(\alpha)$, by introducing geometrical functions and elaborating the constitutive equations needed for the solution of the electromagnetic problem.

3.4 Model description

Having introduced the analytical model and the relevant assumptions, the next step consists in defining the reference frame, the windings' features, the geometrical quantities and the constitutive equations needed to obtain a final, accurate expression of $L(\alpha)$. All these aspects are presented below in this section.

3.4.1 Introductory aspects

The description of the features and of the physical quantities of a generic device can be referred to two angular reference frames related to the cross-section of the machine. These two angular reference frames are respectively locked to stator and rotor and their coordinates are indicated with γ and β. Employing the zero position of the rotor frame with respect to the stator frame as the rotor angular position variable α, the simple relationship $\gamma=\alpha+\beta$ then correlates the above variables. This concept is illustrated in Fig. 9.

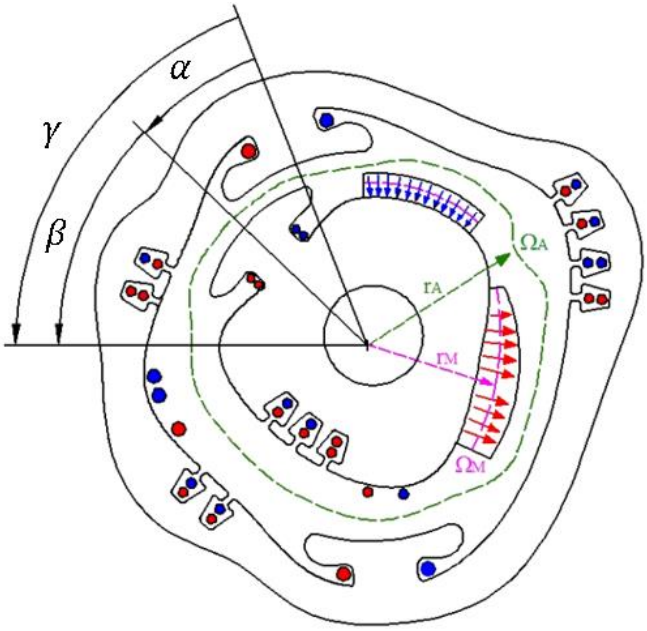


Fig. 9 – Example of a generic machine with cores, magnets and coils [77].

The proposed analytical model can be developed referring to either stator or rotor coordinates. Nevertheless, due to the convenience of using the coordinates of the machine component which shows significant anisotropies, β is used for the application at hand, as SGs present an evident saliency on the rotor structure (i.e. salient poles). In order to simplify the treatment, a

normalised coordinate is also defined by $\lambda=\beta/(2\pi)$, allowing to map the whole airgap along the tangential direction by spanning in the interval [0,1).

3.4.2 The windings

Considering the winding as made up of n_E phases each one including n_k groups of active conductors, the position and the number of conductors in each group are respectively given by the quantities $\gamma_{kh}(\lambda)$ and N_{kh} ($k=1,\ldots,n_E$ and $h=1,\ldots,n_k$), where the sign of N_{kh} depends on the conventional direction of the current flow in the conductors and it is again an arbitrary choice. The position γ_{kh} can be assumed to correspond to the location of the slot openings or to the position of the pole tip of the salient pole. The information related to how the several active conductors of each phase are connected through the end windings is not contained in any of the above-mentioned quantities. In fact, this is not necessary for the 2-D nature of the electromagnetic problem described in Section 3.2.

3.4.3 The geometrical quantities

Although the model has been presented in its general framework, for the sake of this project it is irrelevant to introduce all the functions related to the potential presence of PMs in the considered machines. However, it is worth to keep in mind that this approach can be easily generalised and used to analyse different machines, as for example shown in [79]. Considering this, the layer in which most of the electromagnetic energy is stored during the normal operation of the machine is represented by the airgap, whose geometrical description is provided by

- its radial thickness function $\varepsilon_{AG}(\lambda,\alpha)$;
- a magnetically potential surface $\Omega_{AG}(\lambda,\alpha)$, which crosses the airgap and is point by point orthogonal to the flux lines along the tangential direction, thus exhibiting a shape which follows the profiles of the outer rotor and inner stator surfaces;
- the radial distance of $\Omega_{AG}(\lambda,\alpha)$ from the axis, which is given by the function $r_{AG}(\lambda,\alpha)$.

3.4.4 The constitutive equation

The assumption related to the smooth variation of fields along the radial direction into the airgap implies that only the average values of the flux density and field strength along $\Omega_{AG}(\lambda,\alpha)$ need to be considered. The state functions corresponding to the above defined field components are named $\mathrm{B}_{AG}(\lambda,\alpha,\vec{\imath})$ and $\mathrm{H}_{AG}(\lambda,\alpha,\vec{\imath})$, respectively. These are assumed to be correlated by the well-known linear, constitutive equation of the airgap layer as given in (4), where μ_0 is the permeability of air. Conceptually, in a generalised scenario, the quantity linking the two state functions is the permeability $\mu_{AG}(\lambda,\alpha)$ of the material filling the airgap [77]. However, for the application at hand where no insulating sleeves are present between the rotor and the stator, μ_0 can be used.

$$\mathrm{B}_{AG}(\lambda,\alpha,\vec{\imath}) = \mu_0\,\mathrm{H}_{AG}(\lambda,\alpha,\vec{\imath}) \tag{4}$$

3.5 The solution

Given all the conditions to solve the electromagnetic problem presented above, the last step towards the completion of this process consists of determining the analytical expression of $\bar{\psi}(\alpha, \vec{\imath})$, thus depending on the position and the currents. Referring to the assumption related to the absence of mutual influence between principal and secondary phenomena (see Section 3.2), this state function can be considered as composed by two terms, i.e. the main flux $\overline{\psi_M}(\alpha, \vec{\imath})$ and the leakage component $\overline{\psi_L}(\vec{\imath})$, represented by a linear relationship independent by the rotor position, where the proportionality constant is the leakage inductance L_L. The determination of $\overline{\psi_L}(\vec{\imath})$ can be carried out by a detailed knowledge of some features of the machine, such as the slot geometry, the end windings layout, etc. In practical applications, simple considerations about the physical symmetry of the machine lead to corresponding expressions for the inductances related to the leakage phenomena, as shown for example in [80-85]. Standard expressions for deriving L_L are then used, which are not included here.

Therefore the main focus is the determination of $\overline{\psi_M}(\alpha, \vec{\imath})$, which is solved by applying the conventional laws of electromagnetism. Ampere's law can be verified for every possible simple loop that crosses the main airgap, passing through the stator and rotor yokes. One of the branches of these loops is at an arbitrary fixed reference position. Assuming that this position corresponds to the origin of the rotor reference frame, as shown in Fig. 9, then Ampere's law can be expressed by (5), where $F_{RS}(\lambda, \alpha, \vec{\imath})$ is the magnetic voltage drop

between the rotor (*R*) and stator (*S*) cores given by the product shown in (6), while $F_I(\lambda, \alpha, \bar{\imath})$ is the *mmf* linked with the considered loop according to the positive direction assumed for the currents. By introducing the concept of a winding function (WF) [86], this *mmf* can be written as shown in (7), where $\bar{N}(\lambda, \alpha)$ is the vector grouping the WFs of all of the machine phases. This vector contains the information related to the distribution of the conductors of the corresponding phase among the different groups (slots), their location along the tangential direction and their orientation according to the reference direction assumed for the current flowing inside each phase.

$$F_{RS}(\lambda, \alpha, \bar{\imath}) - F_{RS}(0, \alpha, \bar{\imath}) = F_I(\lambda, \alpha, \bar{\imath}) \tag{5}$$

$$F_{RS}(\lambda, \alpha, \bar{\imath}) = H_{AG}(\lambda, \alpha, \bar{\imath})\, \varepsilon_{AG}(\lambda, \alpha) \tag{6}$$

$$F_I(\lambda, \alpha, \bar{\imath}) = \bar{N}(\lambda, \alpha)^T\, \bar{\imath} \tag{7}$$

Having applied Ampere's law as described above, then Gauss' law is used to define the additional quantities required for the final expression of the matrix $L(\alpha)$. In particular, the application of this law to the generalised cylinder whose lateral surface is represented by $\Omega_{AG}(\lambda,\alpha)$, leads to the integral constraint shown in (8). The use of the relationships (4) and (6) in (8) leads to the definition of an equivalent function, whose dimensions are those of a permeability. Thus, the new quantity $\mu_E(\lambda,\alpha)$ is named as the equivalent permeability function and its expression is given in (9). The constraint (8) can then be re-written as in (10) and, by using (5) for the magnetic voltage $F_{RS}(\lambda, \alpha, \bar{\imath})$, the unknown function $F_{RS}(0, \alpha, \bar{\imath})$ calculated in $\lambda=0$ can be determined. The latter is easily deduced by (11), where another function

$\nu(\lambda,\alpha)$ can be defined as shown in (12). This further exploitation leads to express (5) in the form shown in (13), which in turn provides the definition of an equivalent WF vector $\overline{N_E}(\lambda,\alpha)$, whose expression is given by (14).

$$\int_0^1 B_{AG}(\lambda,\alpha,\bar{\imath})\, r_{AG}(\lambda,\alpha)\, d\lambda = 0 \tag{8}$$

$$\mu_E(\lambda,\alpha) = \mu_0 \frac{2\,\pi\, r_{AG}(\lambda,\alpha)}{\varepsilon_{AG}(\lambda,\alpha)} \tag{9}$$

$$\int_0^1 \mu_E(\lambda,\alpha)\, F_{RS}(\lambda,\alpha,\bar{\imath})\, d\lambda = 0 \tag{10}$$

$$F_{RS}(0,\alpha,\bar{\imath}) = -\frac{\int_0^1 \mu_E(\lambda,\alpha)\, F_I(\lambda,\alpha,\bar{\imath})\, d\lambda}{\int_0^1 \mu_E(\lambda,\alpha)\, d\lambda} \tag{11}$$

$$\nu(\lambda,\alpha) = \frac{\mu_E(\lambda,\alpha)}{\int_0^1 \mu_E(\lambda,\alpha)\, d\lambda} \tag{12}$$

$$F_{RS}(\lambda,\alpha,\bar{\imath}) = \bar{N}(\lambda,\alpha)^T\, \bar{\imath} - \int_0^1 \nu(\lambda,\alpha)\, \bar{N}(\lambda,\alpha)^T\, \bar{\imath}\, d\lambda \tag{13}$$

$$\overline{N_E}(\lambda,\alpha) = \bar{N}(\lambda,\alpha) - \int_0^1 \nu(\lambda,\alpha)\, \bar{N}(\lambda,\alpha)\, d\lambda \tag{14}$$

All the equations given above can be further commented as follows:

- (9) shows that all the information regarding the anisotropies characterising the machine are contained in $\mu_E(\lambda,\alpha)$;

- (10) allows for achieving the final expression of the unknown quantity $F_{RS}(0, \alpha, \vec{\imath})$, provided by (11);
- (11) shows that $F_{RS}(0, \alpha, \vec{\imath})$ corresponds to the weighted average value of the *mmf* $F_I(\lambda, \alpha, \vec{\imath})$ with respect to $\mu_E(\lambda,\alpha)$;
- The function $\nu(\lambda,\alpha)$ defined in (12) represents an indicator of the saliency level presented by the machine (e.g. in a fully isotropic device $\nu(\lambda,\alpha) = 1$);
- (13) shows the compact form of the Ampere's law evaluated on any generic loop previously mentioned;
- finally, (14) shows that the vector $\overline{N_E}(\lambda, \alpha)$ is defined by the difference between the vector $\bar{N}(\lambda, \alpha)$ and its weighted average value with respect to $\nu(\lambda,\alpha)$.

Having defined all the quantities necessary for the determination of the fluxes linked with the phases, the single element $\psi_{M_k}(\alpha, \vec{\imath})$ of the vector $\overline{\psi_M}(\alpha, \vec{\imath})$ can be resolved as given in (15), while the compact form is provided in (16). Finally, by using (4)-(7), $B_{AG}(\lambda, \alpha, \vec{\imath})$ can be further exploited in (16), leading to the final equation for the inductance matrix shown in (17).

$$\psi_{M_k}(\alpha, \vec{\imath}) = \sum_{h=1}^{n_k} N_{kh}\, l \int_{\lambda_{kh}}^{1} B_{AG}(\lambda, \alpha, \vec{\imath})\, r_{AG}(\lambda, \alpha)\, d\lambda \tag{15}$$

$$\overline{\psi_M}(\alpha, \vec{\imath}) = l \int_{0}^{1} \overline{N_E}(\lambda, \alpha)\, B_{AG}(\lambda, \alpha, \vec{\imath})\, r_{AG}(\lambda, \alpha)\, d\lambda \tag{16}$$

$$L(\alpha) = l \int_0^1 \mu_E(\lambda, \alpha)\, \overline{N_E}(\lambda, \alpha)\, \overline{N_E}(\lambda, \alpha)^T \, d\lambda \tag{17}$$

It can be therefore concluded that *L(α)* depends only on two functions, namely the equivalent permeability and the equivalent WF, meaning that these quantities play the most important role for the machine performance prediction.

3.6 The model adapted to SGs

Having proposed a generalised mathematical model for the analysis of electrical machines, it is now possible to limit the scenarios to the relevant applications dealt with in this thesis, i.e. salient-pole SGs. In this section, special focus is given to damper cage modelling, by proposing an alternative equivalent circuit which leads to obtain intermediate and simplifying results allowing for reducing the number of equations to be considered.

3.6.1 The damper cage

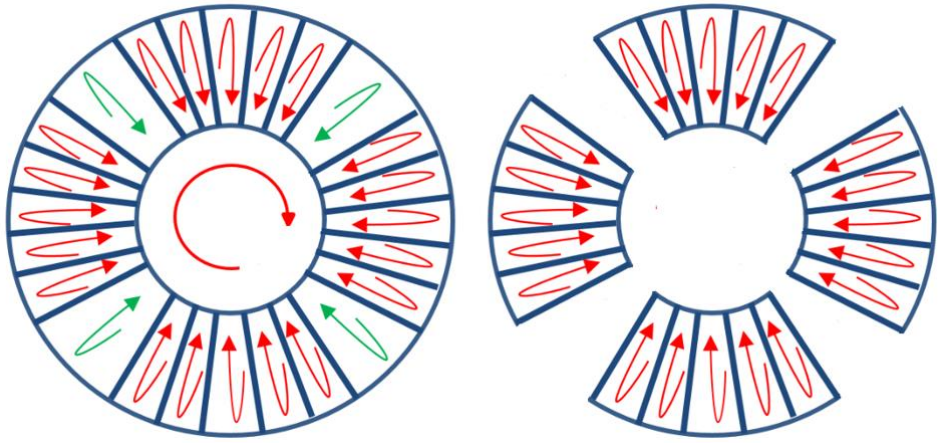
From a structural point of view, damper windings of salient-pole SGs can be classified according to their electrical connection at the end sides of the machine, as mentioned in Section 2.2.1. For modelling purposes, it is worth to recall and expand the concepts which are behind this differentiation, thus highlighting the major aspects of complete and incomplete damper cages.

Typically, the bars located inside each pole are connected through effectively low-resistance end paths consisting in ring sectors or press-plates. This is true for the considered DIG142 and HC4 case studies. Such groups of

interconnected bars can be connected to each other through equally effective low-resistance paths, for example when a complete ring exists at each side. Alternatively, the different pole bar groups may be purposely left insulated, for example when the end rings are segmented and the bars are not in contact with, or may be connected by means of paths featuring a much higher resistance than the inter-bar connections. The cage type is labelled "complete" in the first case and "incomplete" in the second one.

When a complete cage is implemented as a set of n_b straight parallel bars connected by two circular end rings, its equivalent topology can be obtained by enlarging the front end ring and shifting it to the same plane of the rear end ring, in such a way to obtain a planar net as shown in Fig. 10a. Such a topology indicates that the currents flowing in each side can be expressed as functions of the loop currents flowing in the natural loops of this planar representation, i.e. the n_b loops delimited by any couple of adjacent bars plus the inner loop corresponding to the rear end ring. With respect to the electromagnetic phenomena, the whole cage can be then modelled using the classical approach where each loop is considered as an equivalent short-circuited phase, meaning that the cage itself can be conceptually replaced with a set of closed conductive loops inside which the loop currents flow. Nevertheless, the resistive phenomena need to be taken into account, i.e. for any bar or rear ring arc, the related voltage drop depends from both of the loop currents flowing in the two adjacent loops, meaning that a non-diagonal form of the resistance matrix has to be considered in the electric model.

For the case of an incomplete cage as in Fig. 10b, the same approach above described may be used, but the number of natural loops is reduced to n_b-*2*p*, since the *2*p+1* loops connecting the facing bars located in adjacent pole groups are suppressed, as well as the rear end loop.



a) b)

Fig. 10 – Equivalent circuit topology for a damper cage of complete (left) and incomplete type (right): example referred to the HC4 SG.

In any common SG, typically the rotor poles are identical also with respect to the deployment of the bars, usually featuring a symmetrical distribution with respect to the pole axis. Therefore, the physical symmetry related to the number of pole pairs *p* of the machine can be extended to the cage and also to the set of currents flowing in it, unless very unusual operating conditions are considered. This means that, at any given operative condition, the pattern of the currents flowing in the bars and end-rings inside any pole pair sector can be assumed to be identical in all of the other sectors, thus resulting in a reduced number of actually independent loop currents: n_b*/p+1* for complete cages, n_b*/p-2* for incomplete cages. Additionally, if a full physical odd symmetry (with respect to the pole pitch) also stands for the electromagnetic

aspects, the current patterns related to the bars located in the two homologous sequences of poles may be assumed to be just opposite: the number of independent cage loop currents is then further reduced to $n_b/(2*p)+1$ for complete cages and to $n_b/(2*p)-1$ for incomplete cages.

These relationships indicate that the correlated loop current patterns can be embedded into the model of the machine by assuming that the equivalent loop phases are properly connected in series/anti-series throughout the $2*p$ poles of the machine, as shown in Fig. 11 for an incomplete cage. Such an elegant connection also has the advantage of imposing the null voltage constraint to each short-circuited loop phase, since it is equivalently achieved by simply zeroing the total voltage across such compound phases thanks to the assumption of identical behaviour.

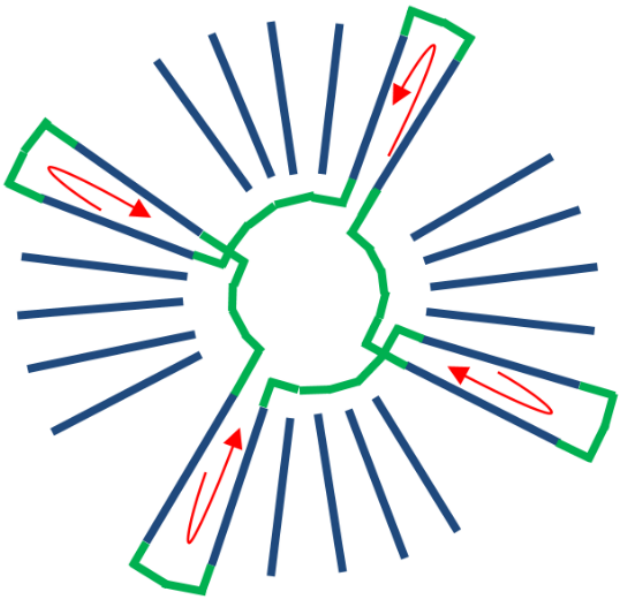


Fig. 11 – Compound planar schematic of a generic rotor cage loop for symmetrical machines.

For the considered machines, all of the hypotheses assumed above about the symmetry properties are verified, whereas the electrical connections between bar groups actually exist thanks to paths along the press plates. However, these paths are much longer than the distance between adjacent bars. This justifies the consideration that such a damper cage can be termed as “incomplete”. Given the validity of such hypotheses for both the platforms, all the numerical quantities and graphical examples reported in this chapter will be referred to only one of those SGs, namely the HC4.

Considering the HC4 damper cage, consisting of 6 bars-per-pole, it can be observed that the number of compound phases used to represent this winding may be then reduced to 5, as shown in Fig. 11, whereas the total number of phases in the machine is then 1+3+5=9. This is therefore the dimension of the vector differential equation shown in (3) that has to be solved in order to estimate the voltage waveforms.

A comparison between the WFs related to a single cage loop and to the compound phase incorporating the four cage loops located in corresponding positions along the rotor periphery can be seen in Fig. 12 and Fig. 13. In general, any loop phase WF has to be single-signed, meaning that the corresponding equivalent WF calculated according to (14) will be a positive-negative square waveform (as shown in Fig. 12), usually asymmetric, whatever is the trend of the equivalent permeability function. This in turn implies that the different loop phases will be magnetically coupled to each other, besides being coupled to the field and armature windings.

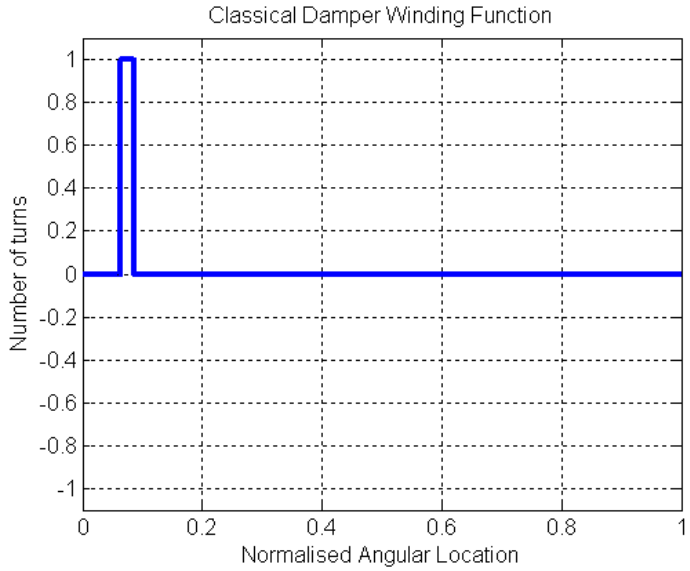


Fig. 12 – Typical winding function of a single damping cage loop.

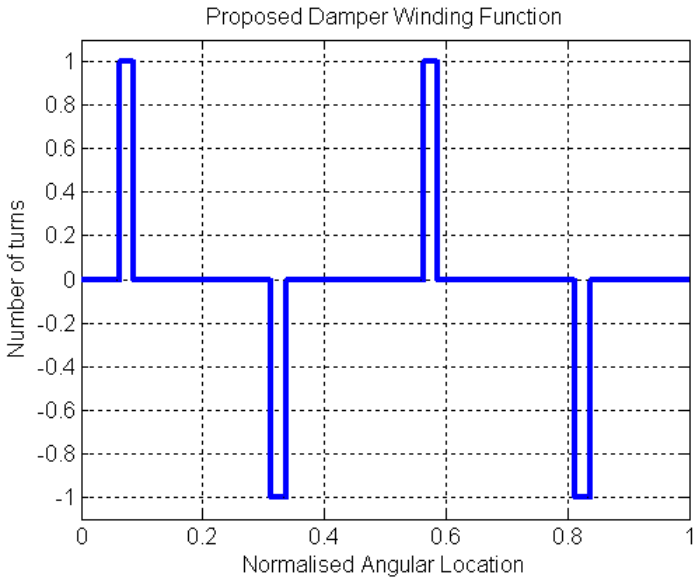


Fig. 13 – Cage loop winding function for the compound representation.

On the other hand, in general the WF of the compound phase representing any set of corresponding loops features inherently an odd symmetry periodicity with respect to one pole pitch. Considering that the equivalent permeability function of any normal symmetric machine is either constant or features a period just equal to one pole pitch, it can be easily concluded that

the equivalent WF will result just equal to the WF. This means that the equivalent WFs related to any couple of compound phases will not share any interval where both are non-zero, which implies that they are not magnetically coupled for what concerns the main flux tubes. Therefore, one can conclude that by using the compound phases not only the size of the system (3) is minimised, but also the complexity of the inductance matrix is reduced, thus reducing the computational burden.

3.6.2 The slot openings

Although the basic, general framework of the model proposed in [77] is maintained for the analysis of the considered machine, it is clear that some adaptions and more assumptions need to be introduced for the sake of this study. In particular, as the main aim of this chapter is to estimate the no-load voltage waveform, it is necessary to introduce in the model the effects of the stator slot openings. In fact, the related harmonics can play a very important role in determining the actual waveform of the output voltage. In other words, the stator slot openings cannot be neglected as in [77]. As a first approximation, their equivalent profile is represented by a trapezoidal variation of the inner radius of the stator core vs. angular location, assuming the same slot opening width c_1 of the real laminations and considering as characteristic parameters only the depth a_1 and the width b_1 of the ramp. Referring for example to the considered case study, in Fig. 14 the trapezoidal approximation and a schematic representation of the original profile are sketched, highlighting the characteristic parameters being considered.

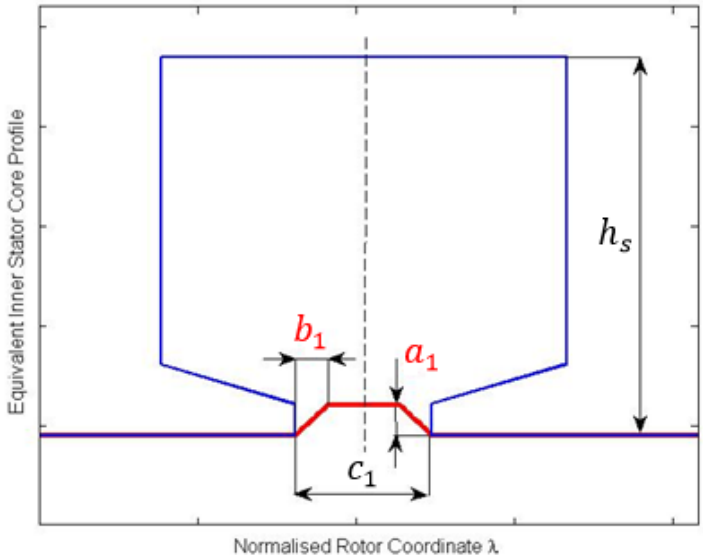


Fig. 14 – Simplified representation of the equivalent inner stator profile.

The values of the equivalent parameters characterizing the slots are intended to be determined by means of a tuning procedure, carried out by comparing the results from the simplified model to the ones obtained by a corresponding 2-D electromagnetic FE model of the machine, as discussed in-depth in the next sections.

3.6.3 Further considerations

The first sections of Chapter 3 recall the introductory aspects and the main functions of the generalized analytical model proposed by [77], valid for any electromagnetic device and properly adapted for the analysis of SGs. Updates regarding the effects of the stator slot openings (see Fig. 14) and an alternative way of modelling the damper cage (see Fig. 11 and Fig. 13) are proposed. All the assumptions above highlighted stand for machines provided with a symmetrical damper winding and when normal operating conditions are considered. In fact, the hypothesis on the currents featuring opposite

waveforms in corresponding bars of adjacent poles is always verified, unless any type of event resulting in an anomalous operation of the generator occurs. These include potential unbalances, single-phase operations, faults, etc. which basically produce an 'asymmetrical' response of the damping bars, thus not allowing to model the relevant winding as previously illustrated. On the other hand, all these events are not taken into consideration in this thesis, as the main goal is that of evaluating the no-load voltage waveform under normal 3-phase, symmetrical operation. To conclude, the not-null elements of $L(\alpha)$ involving the rotor cage loops will be then evaluated by using the equivalent WFs of the type shown in Fig. 13.

3.7 The hybrid analytical-numerical approach

Having set all the context necessary to implement the quantities defined and presented in the previous sections, it becomes possible to determine the inductance matrix $L(\alpha)$. In this section, the equivalent functions and the ensuing inductances of the HC4 generator will be first shown and, in a second instance, the development of a hybrid analytical-numerical model will be proposed. The related results will be finally presented.

3.7.1 The equivalent functions

In order to determine the inductance matrix, it is necessary to implement all the equivalent functions involved in the integral (17), i.e. $\mu_E(\lambda,\alpha)$ and $\overline{N_E}(\lambda,\alpha)$. The geometrical quantities involved in (9) have been defined in Section 3.4.3 and, for the application at hand, they are calculated as in (18)

and (19), where $r_s(\lambda,\alpha)$ and $r_r(\lambda,\alpha)$ are the equivalent inner stator and outer rotor radii respectively. In other words, these two equivalent functions retrace the inner stator and outer rotor profiles, resulting in the inherent inclusion of the slot openings and the salient poles in the relevant functions.

$$\varepsilon_{AG}(\lambda,\alpha) = r_s(\lambda,\alpha) - r_r(\lambda,\alpha) \tag{18}$$

$$r_{AG}(\lambda,\alpha) = \frac{r_s(\lambda,\alpha) + r_r(\lambda,\alpha)}{2} \tag{19}$$

As salient-pole SGs exhibit an intrinsic symmetry that turns into a repetitive trend with period equal to *1/(2*p)* for all the quantities involved in (18) and (19), $\varepsilon_{AG}(\lambda,\alpha)$ and $r_{AG}(\lambda,\alpha)$ are plotted vs. λ inside one repetition period in Fig. 15 and Fig. 16, respectively.

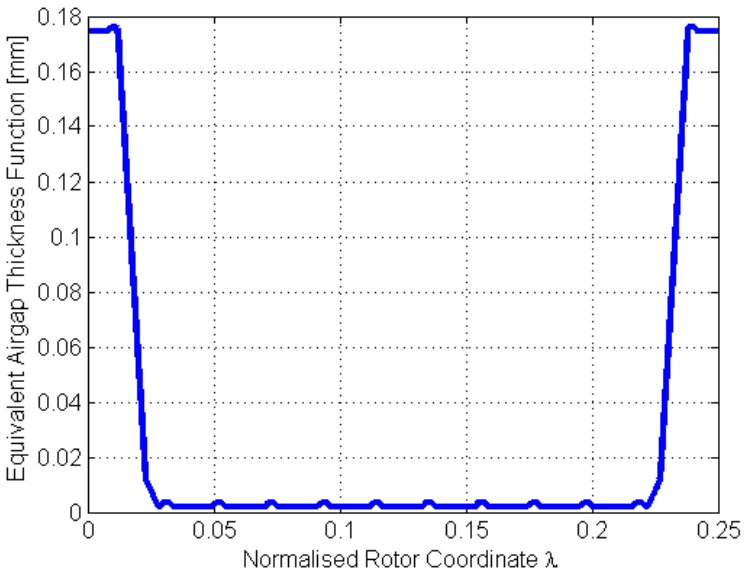


Fig. 15 – Equivalent airgap thickness function of the considered generator, after the application of the tuning procedure against the FE model.

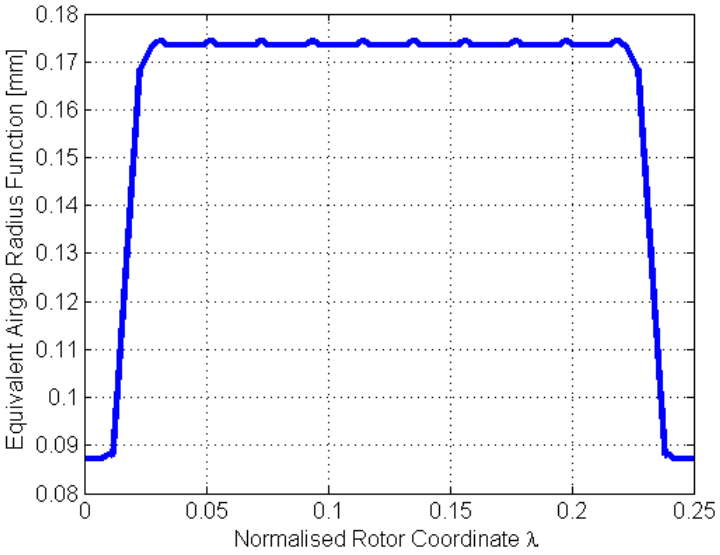


Fig. 16 – Equivalent airgap radius function of the considered generator, after the application of the tuning procedure against the FE model.

Having implemented these equivalent geometrical quantities, it becomes possible to develop (9) for the considered generator and this is shown in Fig. 17, at a specific, fixed rotor position. Fig. 17 also highlights the effects of the slot openings and the rotor poles profile on the equivalent permeability function. The width and the depth of the dips that can be observed on such functions are determined by a tuning procedure that is compared to results obtained through the FE analysis of the SG being studied. In particular, the values of the characteristic parameters a_1 and b_1 (defined in 3.6.2 and shown in Fig. 14) of the slot opening are achieved by minimising the error, at any instant in time, between the no-load voltage waveform obtained by means of the proposed hybrid approach and that one determined through the corresponding FE model.

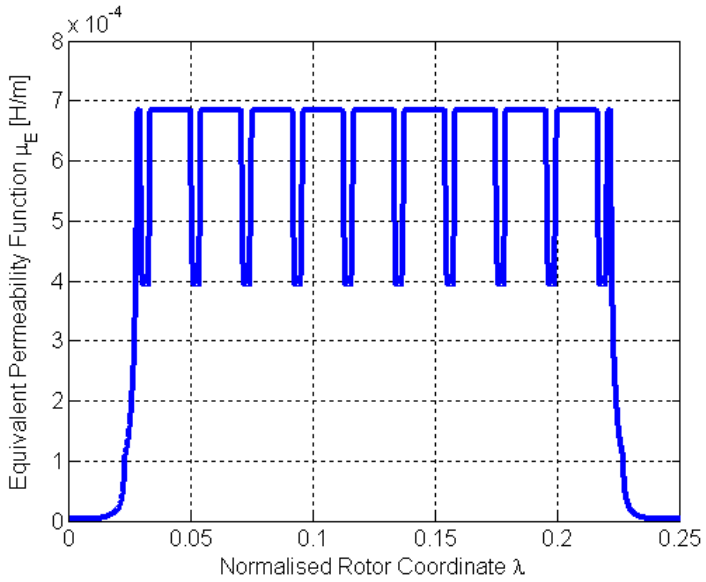


Fig. 17 – Equivalent permeability function of the considered generator, after the application of the tuning procedure against the FE model.

Before going into the details of such models, it is of worth to show the WFs contained in $\overline{N_E}(\lambda, \alpha)$ and associated to the considered 400*kVA* alternator. While those related to the damper cage loops were reported in Section 3.6.1, those related to the rotor field and the 3-phase stator windings are plotted vs. λ below in Fig. 18 and Fig. 19, where some of the relevant features listed in Section 2.4.2 can be observed. As well as the geometrical quantities shown above, the equivalent WFs of the machine phases present an intrinsic symmetry that turns into a repetitive trend with period equal to *1/p*, which is double of the characteristic period of the functions shown in Figures 15-17.

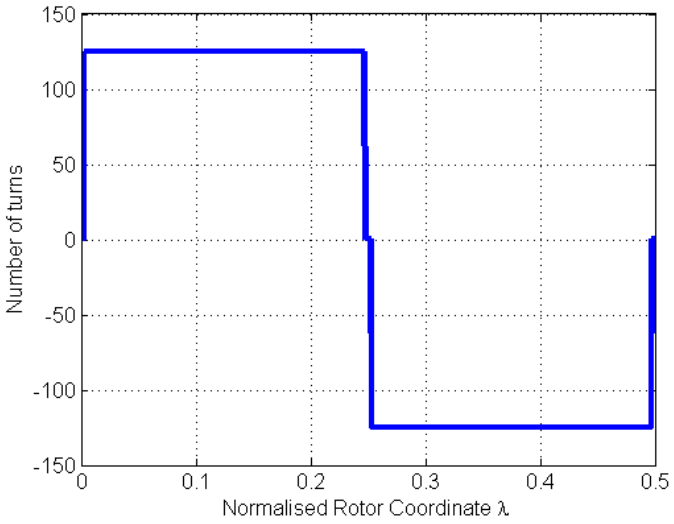


Fig. 18 – Winding function of the rotor field equivalent phase.

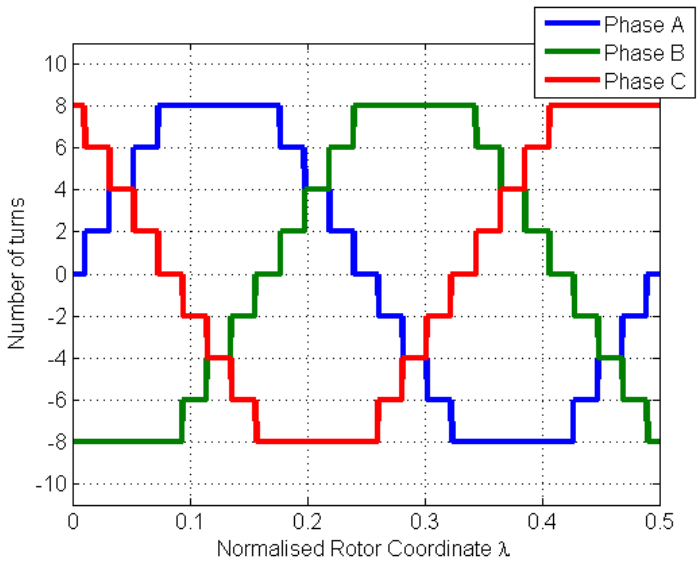


Fig. 19 – Winding functions of the stator armature equivalent phases.

3.7.2 The inductances

The implementation of the geometrical quantities shown in (9) and of the equivalent WFs provided by (14) allows for the calculation of the machine's inductances through the use of (17). The inductances are calculated off-line as well as the approximated values of their derivatives with respect to the rotor position α. Having adopted the rotor coordinate λ for the definition of

any function depending on the tangential location, it is worth highlighting that:

- The dependence on the position α of the self- and mutual-inductances related to the rotor circuits is exclusively due to the stator slot openings; this feature can be observed in Fig. 20, where the self-inductance of the field winding (first subplot), the mutual-inductance between the field winding and one of the rotor cage loop (second subplot) and the self-inductance of one cage loop (third subplot) are plotted against α.

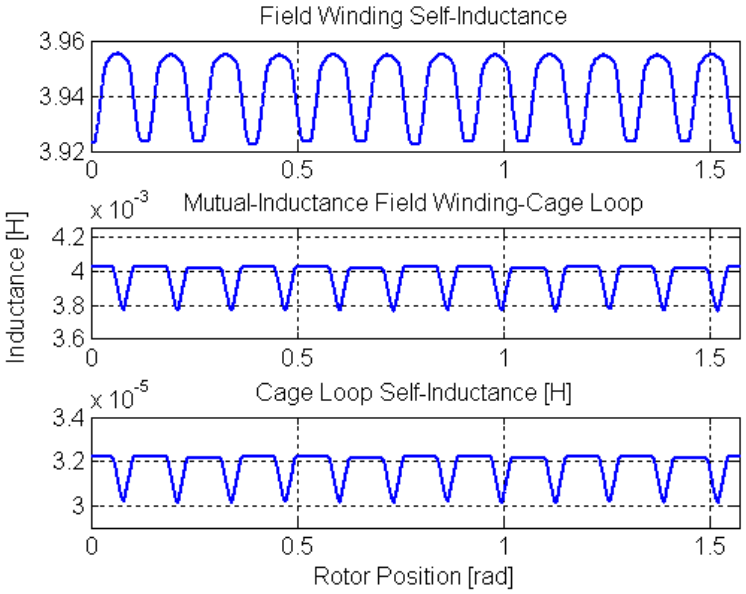


Fig. 20 – Self- and mutual-inductances of the rotor circuits.

- The dependence on the rotor position α of the stator self- and mutual-inductances, is due to the anisotropies featured by both the stator and rotor structures (slot openings and salient poles profile). This concept is shown in Fig. 21 and Fig. 22. In particular, the stator self- and

mutual-inductances are shown in Fig. 21. In Fig. 22, the mutual-inductances between the field winding (indicated as FW in the legend) and the three stator phases can be observed in the top subplot, while in the bottom one the mutual-inductances between one cage loop (indicated as CL in the legend) and the three stator windings are shown.

When the inductance matrix $L(\alpha)$ is determined as well as the matrices $\partial L(\alpha)/\partial\alpha$ and R, it becomes possible to solve the system (3). Because of the induced nature of the damper cage currents, a numerical solution is needed to estimate such quantities. A Matlab-Simulink model is therefore implemented for such purposes and its features are described in the next section.

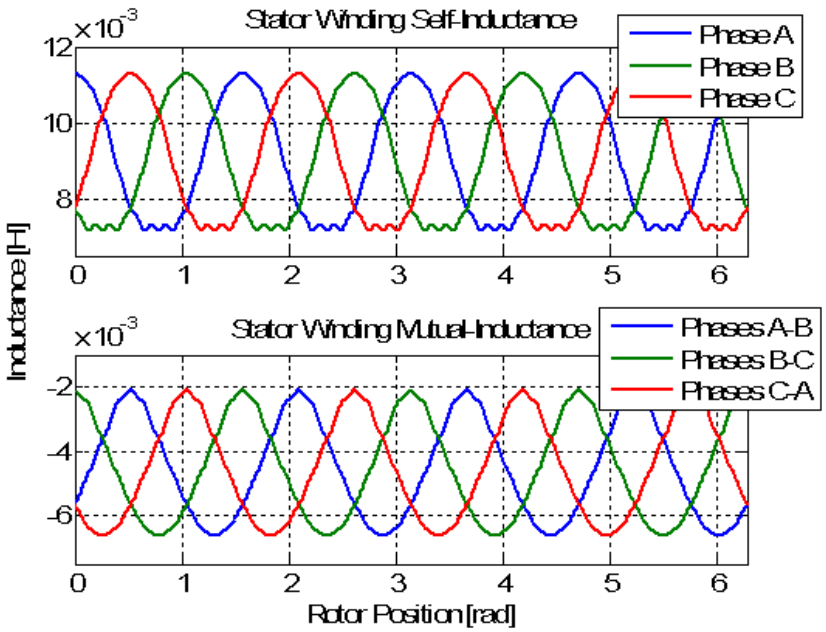


Fig. 21 – Stator self- and mutual-inductances.

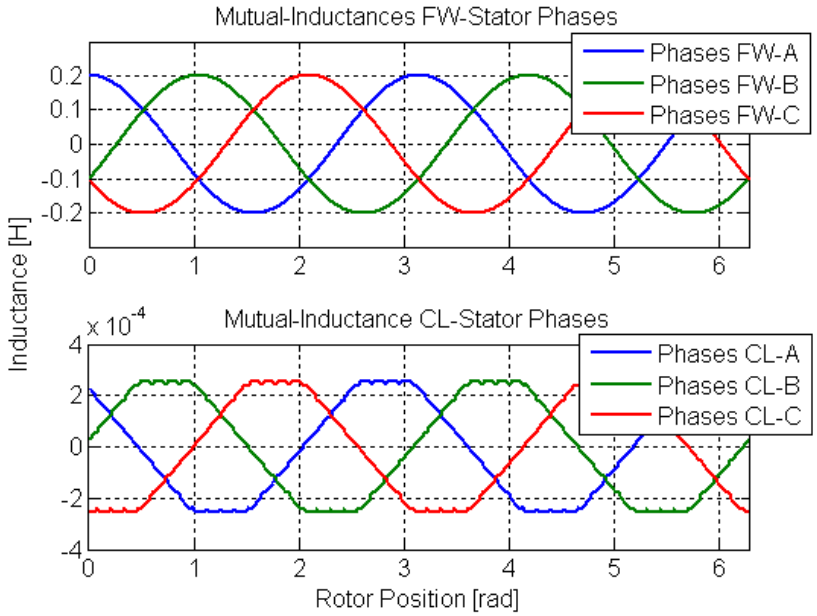


Fig. 22 – Mutual-inductances between rotor and stator circuits.

3.7.3 The Matlab-Simulink model

By manipulating the system of differential equations (3), it can be re-written as in (20) in the space-state representation, where $\bar{\imath}$ is the state vector.

$$\frac{d\bar{\imath}(t)}{dt} = (L(\alpha))^{-1} * \left(\bar{v}(t) - R\bar{\imath}(t) - \left(\frac{\delta L(\alpha)}{\delta \alpha}\bigg|_{\alpha(t)} \bar{\imath}(t) \right) \frac{d\alpha(t)}{dt} \right) \qquad (20)$$

Therefore the system (20), updated with an additional equivalent resistive voltage drop (represented by R_{add}), can be implemented in a Matlab-Simulink environment as shown in Fig. 23.

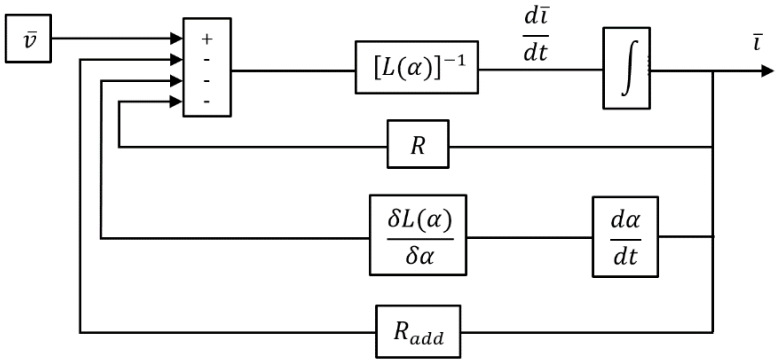


Fig. 23 – Linear model of the electrical aspects implemented in Simulink.

In the schematic of Fig. 23, it can be observed that the voltage vector $\bar{v}(t)$ is used as input for the solution of the system. The additional term R_{add} is a diagonal resistance matrix which gives flexibility to the model as it allows to simulate different load conditions. For example, in order to simulate the no-load operation, all the terms contained in $\bar{v}(t)$ are set to zero except for the term related to the field winding, while the terms in R_{add} relative to the stator phases are set to a very large value practically ensuring that the stator currents will be almost null.

It becomes now possible to solve the system of differential equations. The method used for such purpose is the Dormand-Prince solver, which is a member of the Runge-Kutta family of ODE solvers [87]. It uses six function evaluations to calculate fourth- and fifth-order accurate solutions. The difference between these solutions is then taken to be the error of the fourth-order solution. This error estimation is very convenient for adaptive step-size integration algorithms. In fact, a variable-step type simulation was performed to obtain the no-load voltage waveform of the considered SG. The relevant results are shown in the next section (Figures 25-27) in comparison with a

corresponding FE evaluation, for validation purposes, where the output voltage related to specific values of the excitation current are reported as examples.

3.8 Model validation against FE results

This section validates the results relevant to the hybrid model described above. For such purposes, a 2-D FE electromagnetic analysis of the HC4 alternator considered in this work was carried out. A full and in-detail description of the FE model is provided in Chapter 4. It is however important to note here, that in order to be consistent with the assumptions inherent to the linear behaviour of the ferromagnetic materials used for the stator and rotor cores, a high permeability magnetic steel is employed. A transient with motion evaluation is performed at no-load operation, with the field winding voltage imposed, the three-phase stator winding open-circuited (i.e. connected to a circuital resistance of a practical infinite value) and the damper bars connected in parallel.

3.8.1 Comparison of results

A comparison between the no-load waveforms provided by the analytical and FE methods is shown in Figures 25-27, for three different values of the excitation current. Those values are taken on the linear portion of the no-load characteristic of the considered generator, as the proposed hybrid model assumes linear behaviour of the ferromagnetic materials. An experimental evaluation of the no-load curve for the considered case study is shown in Fig.

24, where the airgap line of the machine (in blue) can be observed. In this figure, it can be noted that no saturation occurs until the excitation current is below 53% of the base field current, having defined the latter as that current value which provides the rated voltage when the armature phases are open-circuited. An excellent similarity between the no-load phase voltage waveforms can be observed in all the cases, proving the validity of the mixed analytical-numerical approach. An important aspect to clarify is the need for a FE tuning procedure to achieve such minimum prediction errors. Although this is a limitation of the hybrid model, a single FE evaluation is sufficient to tune the slot opening parameters (see Section 3.6.2), proving that the proposed approach is however valid and turns out much faster than the FE method.

Although the proposed model is based on the assumption of linear behaviour of the ferromagnetic materials, it is interesting to observe the deviations of the waveforms obtained through the implemented model from those evaluated by a FE analysis, when in the relevant model non-linear materials are employed. Fig. 28 shows this additional comparative exercise, where a value equal to 29% of the base field current is used (as for the evaluation of the waveforms of Fig. 26). Although a good match can still be observed between the no-load waveforms of Fig. 28, small discrepancies can be observed due to additional peaks introduced by the non-linear materials, when these are implemented in the FE model for the stator and rotor cores of the considered machine.

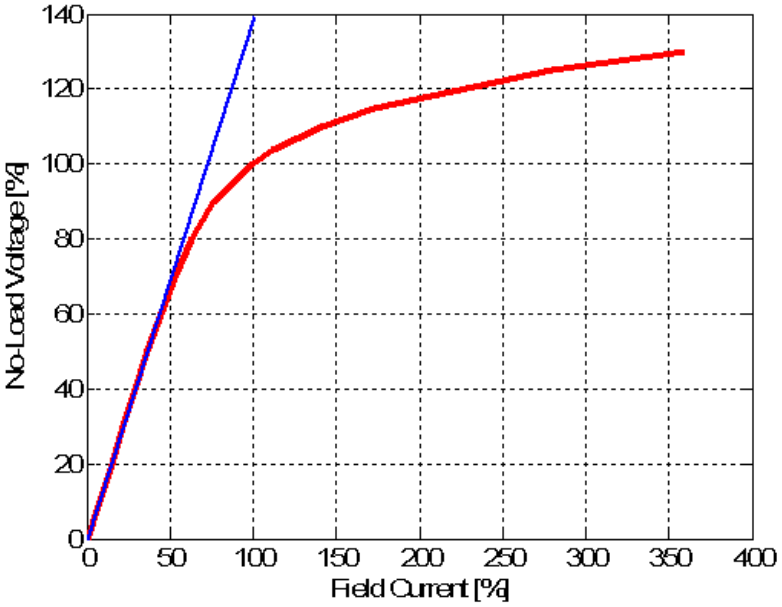


Fig. 24 – Experimental no-load characteristic of the HC4.

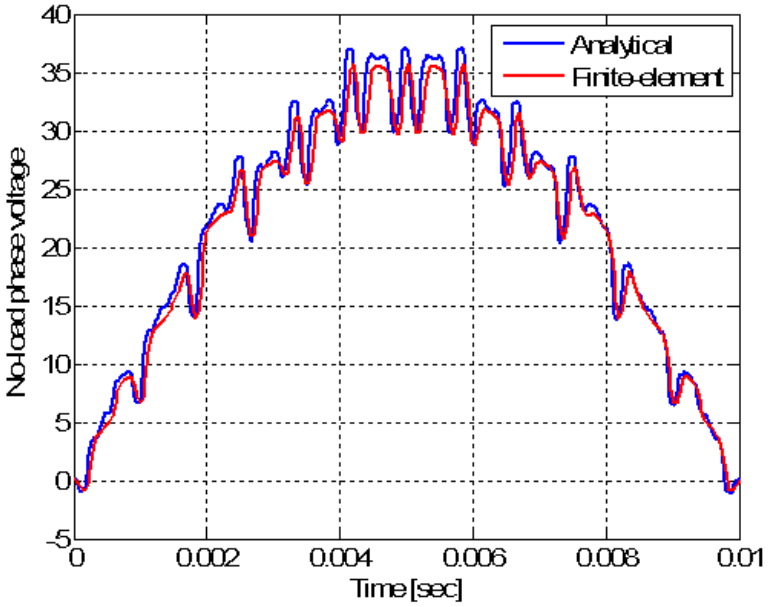


Fig. 25 – No-load voltage waveforms: analytical vs. FE results at 7.5% of the base field current.

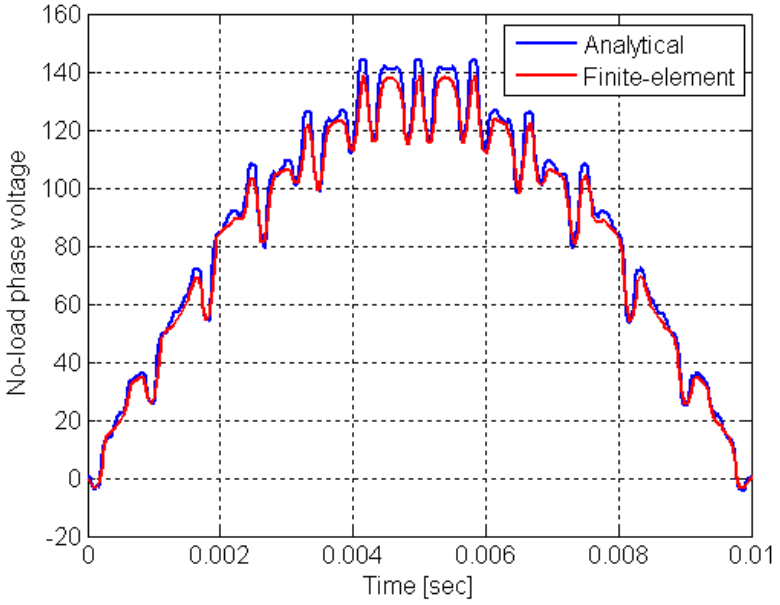


Fig. 26 – No-load voltage waveforms: analytical vs. FE results at 29% of the base field current.

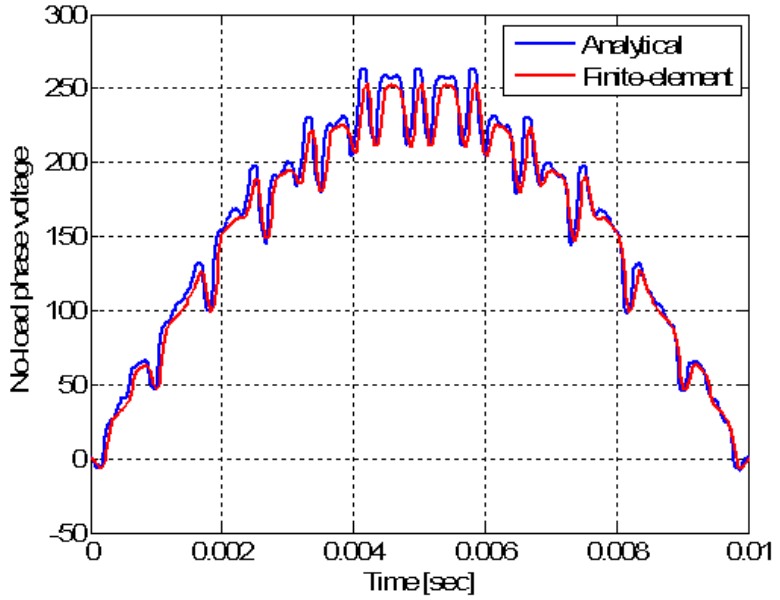


Fig. 27 – No-load voltage waveforms: analytical vs. FE results at 53% of the base field current.

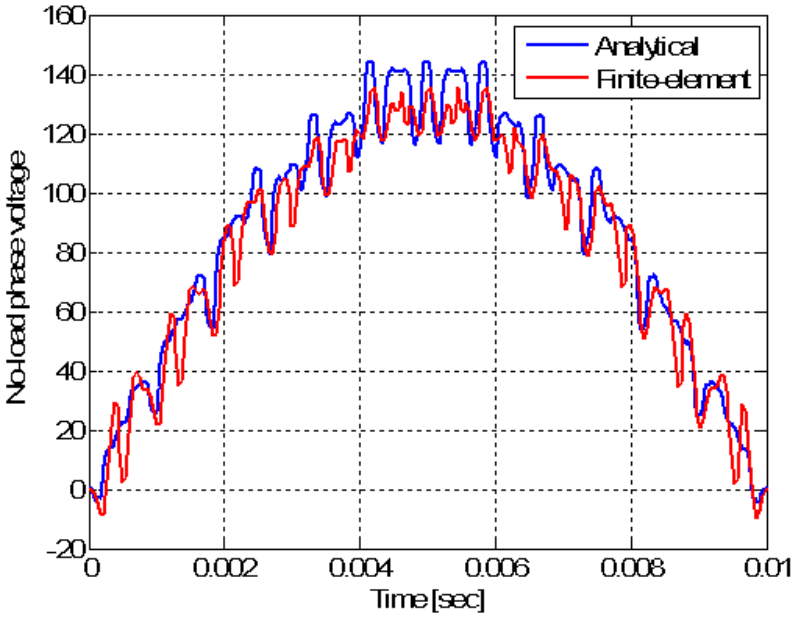


Fig. 28 – No-load voltage waveforms: non-linear analytical vs. FE results at 29% of the base field current.

3.9 Conclusions

In this chapter, the development and the implementation of a hybrid, analytical-numerical model for the accurate estimation of the voltage waveforms in SGs was discussed. The first part of the chapter presents all the introductory aspects and assumptions necessary for the definition of the electromagnetic problem and of the quantities involved in the analysis tool. After having derived the solution in the form of an integral for the inductance matrix determination, it was shown how this matrix plays the most important role in the system of differential equations given by (3). Focus was then given to the damper cage analysis, whose modelling was carried out in an alternative way compared to the classical literature. This allowed to

drastically reduce the number of equations to be solved. A very important step for the adaption of the proposed, generalized model to the analysis of SGs was that of including the slot opening effect by opportunely implementing an equivalent inner stator radius function. Finally, a mixed analytical-numerical model that turns out much faster than the classic FE method was proposed. As case study, the HC4 SG was considered. When operating in linear conditions, promising results were achieved at different no-load operating points, showing the validity of the proposed hybrid methodology. The analytical results have been compared to the FE ones, also when a non-linear material is employed for the corresponding analysis. This showed some limitations of the proposed approach, although the similarity between results was still very good.

Considering the above, further work would be that of including in the model the most representative non-linear parts of the machine, in order to better simulate the machine operation also on-load. With respect to this latter point, however, it is worth to highlight the significant flexibility the Simulink model was built with. In fact, the inclusion of an additional resistance/inductance matrix branch allows to simulate different loadings and power factors.

The main aim of the hybrid model was therefore that of proposing a general and fast approach for the electromagnetic analysis of classical, wound-field SGs. However, due to the complexity of the phenomena under investigation in this thesis (e.g. the damper cage loss) and to the assumptions inherently related to the symmetric distribution of the damping bars, the proposed

approach will not be used for future optimization purposes. Therefore, while the analytical expressions derived in this chapter will be used to study the skewing effects (see Section 4.3.2) and to understand the rationale behind the modulated damper cage concept (see Section 6.1.1), the hybrid model is put aside and the FE method is used as a means to investigate the improved design solutions presented in Chapter 5 and Chapter 6. The next chapter aims at describing the features of such very important analysis tool and then at validating it against experimental results.

3.10 Contributions to research

The model proposed and presented in this chapter represents a significant contribution to the machine and electro-magnetism community. The model originally implemented in a general way in [77], has been successfully modified in this thesis for the detailed analysis of SGs. Its main advantages include the followings:

- The model is *general*, ideal for (almost) the analysis of any type of electrical machine.
- The model is *fast*, also due the proposed, innovative way of modelling the damper cage.
- The model is *flexible*, ideal for the analysis of different loadings.

The results of this chapter are reported in one academic publication in a high profile machines conference. The publication name is listed below.

- S. Nuzzo, P. Bolognesi, M. Galea, C. Gerada and N. Brown, "A hybrid analytical-numerical approach for the analysis of salient-pole synchronous generators with a symmetrical damper cage", *IEEE International Electrical Machines and Drives Conference (IEMDC)*, Miami, 2017.

To confirm its "generality", the model described in this chapter has been applied also to the exciter of the considered HC4 SG. The relevant results are reported in two academic publications, one in the "Transactions on Industrial Electronics" and one in a conference. The publication names are the following:

- S. Nuzzo, M. Galea, C. Gerada and N. Brown, "Analysis, modelling and design considerations for the excitation systems of synchronous generators", *IEEE Transactions on Industrial Electronics*, 2017.
- S. Nuzzo, M. Galea, C. Gerada and N. Brown, "Prediction of the voltage drop due to the diode commutation process in the excitations system of salient-pole synchronous generators", *IEEE 19th International Conference on Electrical Machines and Systems (ICEMS)*, 2017.

Finally, additional work is ongoing to circumvent the model limitations highlighted in the chapter, mainly those related to the assumptions of magnetic linearity and symmetry of the damper cage.

Chapter 4
Development of the FE models

Nowadays, the FE method represents the most accurate tool for the modelling, analysis and design refinement of electrical machines. Although analytical methods are still in common use, the accuracy offered by this numerical tool makes it a mandatory passage during the design process of electrical machines, especially when complex phenomena such as saturation and eddy currents have to be taken into account. Also, the complexity of the electromagnetic phenomena associated to the achievement of an optimal damper cage topology and a skew-less stator structure (for efficiency and power quality improvements) needs a high level of detail only ensured by the FE methodology.

This chapter therefore deals with the description of a 2-D FE model, purposely built for the analysis of the alternators considered in this work. The corresponding results are then shown in a comparative exercise against experimental measurements, performed on both the benchmark DIG142 and the HC4 SGs for validation purposes. Once validated, the developed tools will be then used for proposing innovative design solutions on both the platforms. These studies are presented in Chapter 5 and Chapter 6. A brief introduction of the concepts which are behind the FE technique is given in Appendix 1, with special focus on the applications of such a tool to the field

of electrical machines. A comprehensive understanding of this methodology is provided by a number of existing works [88-93].

4.1 The 2-D FE model of the considered SGs

In general terms, the skewing, the presence of ventilating ducts along the axial length, the damper winding, the rotor laminations support bars and their related stacking issues make the classical SG a very complex machine to model and analyse. Other critical aspects are the leakage fluxes due to the end-windings and the presence of the aluminium end plates needed to give electrical continuity to the damper cage. It is clear then that a 3-D FE model would be ideal for the analysis of the SGs considered in this work. Ventilation ducts (implemented onto the DIG142) and stator skewing (implemented onto the HC4) are inherently 3-D features. However, a full 3-D analysis is very time consuming, thus a 2-D FE model of the 4*MVA* and 400*kVA* generators is built. In order to take into account all the aspects highlighted above, a number of compensation factors are included in the model. The relevant details are given below in the next sections.

4.1.1 General aspects

The FE analyses and the relative results which will be shown in the next sections of this thesis have been performed by using the software *Infolytica MagNet* [94]. The main reason for this choice is due to the flexibility of the software in terms of "interoperability" with any other *ActiveX*-compliant applications. Due to the simplicity of its programming code, *Matlab* is used

as an interface software, allowing for automation of any repetitive tasks, from pre-processing (such as modelling variations, solving a given model with options different from the default ones, etc.) to post-processing (specific global quantity calculations, graphing, data analysis, etc.). In other words, this direct link between these environments allows for an easy "scripting". Considering all this, the models developed for the FE analyses of the generator platforms are built upon this philosophy to facilitate the design optimization processes which will be used in Chapter 5 and Chapter 6 for efficiency and power quality improvements purposes.

4.1.2 Geometry and materials

The first phase of a simulation process is the geometrical modelling, that is concerned with the representation of the shape and dimensions of the various parts of the device under analysis. Depending on the device, the desired output quantities and accuracy level, more or less details will have to be included in the geometrical representation. Once created (or imported) the geometry of the machine, materials have to be assigned to the built components of the machine. MagNet is provided with a large library of materials and also allows the user to create new ones. This latter capability increases the model accuracy, especially for the considered case studies, due to the fact that a) the ferromagnetic materials used in the considered SGs were previously characterised through the well-known Epstein frame test [95] and b) the stator and rotor windings' temperatures were previously measured during the machine normal operation. Considering the above, the following materials were purposely created:

- A ferromagnetic material, employed for the stator and rotor cores, whose magnetisation curve is shown in Fig. 29. Besides the BH curve, also the loss density values are used as input for the creation of the material, as well as the electric conductivity and the mass density. While all the data and results relative to the iron loss prediction will be dealt with in Section 4.2, it is worth to mention here that a null value is assigned to the electric conductivity, meaning that the eddy currents loss component is neglected at this stage. This is acceptable at least as a first approximation, due to the small value of the lamination thickness (0.35*mm*) relative to the application at hand (i.e. SGs rotating at a steady state speed of 1500*rpm*).

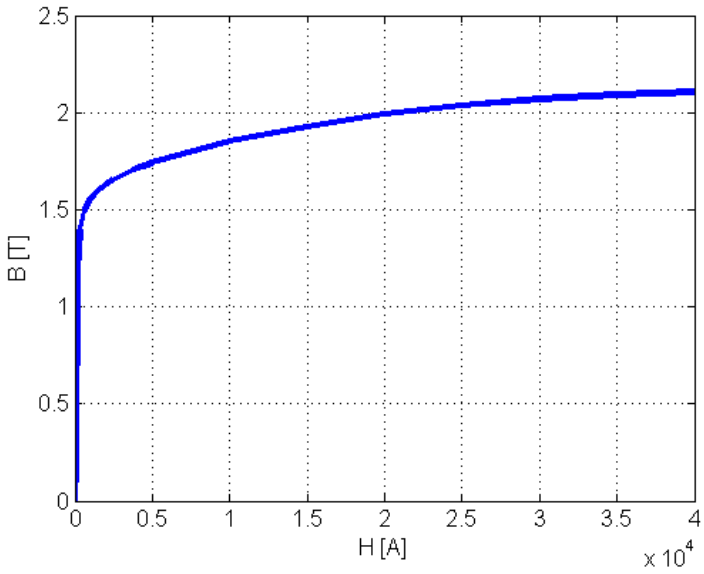


Fig. 29 – BH curve of the ferromagnetic material utilised for the stator and rotor cores of the DIG142 and the HC4 alternators.

- A number of copper materials, in order to take into account the effects of the temperature on the rotor and stator windings during

operation at different loadings. In other terms, these copper materials exhibit different values of electric conductivity from each other. As well as for the magnetic materials, other quantities can be used for creating materials typically used for the windings of electrical machines: these include the thermal conductivity, the thermal heat capacity and the mass density.

4.1.3 Coils and electrical circuits

The next step of the pre-processing phase consists in creating the coils, to be then used in electrical circuits of arbitrary complexity. Once created, it is possible to specify the terminals, the number of turns and the coil types. In MagNet, there are two types of coil, namely stranded and solid, whose features are described below:

- Stranded coils are typically used to represent windings of insulated wires, made up of a certain number of turns. These turns are assumed a) to be uniformly distributed over the coil's cross-section, b) to be electrically insulated from one another, c) to be connected in series and d) to be carrying a uniform current density over their own cross-section. In time-varying situations, the stranded coil is typically used when the skin effects can be neglected [96]. It is easy to demonstrate that this assumption is well-founded for the rotor field and the stator armature windings, at the frequency of interest (i.e. $50Hz$) for the analysis of the considered SGs. Therefore, these windings are set as “stranded” in the FE model.

- Solid coils, on the other hand, represent a solid piece of conductor, in which the current is free to flow where it wants. When the skin depth of penetration is smaller than the radius of the individual wire strands, the current density is not constant over the coil's cross section and the coil must be modelled as an actual solid conductor. In MagNet, solid coils are treated as a current flow problem, allowing for cross-sectional current density redistribution (from uniform profile) according to Maxwell's equations. Thus, time-harmonic or time-transient induced (eddy) currents, as well as DC currents redistributions are taken into account in solid coils. Thus, considering that the main investigation of this thesis focuses on the damper windings, it is considered essential in the name of accuracy to model the amortisseur bars as solid conductors in order to take into account the potential skin effect resulting from the higher order slot harmonics [97, 98].

In actual devices, the voltage and current at the coils' terminals are not known directly, rather the way they are connected to external driving or load circuits. In MagNet, it is possible to couple the internal electromagnetic field quantities to the external electric circuit quantities by defining a circuit. According to the features of the rotor and stator windings described in Sections 2.4.1 and 2.4.2, respectively for the DIG142 and the HC4, the relevant circuits coupled to the FE model are shown in Fig. 30 and Fig. 31. The circuits representing the two machines' windings are very similar to each other: the main differences include 1) the number of stator coils-per-phase

(20 in the DIG142 and 16 in the HC4), 2) the number of phase connections in parallel (no parallel circuits in the DIG142 and two parallel circuits in the HC4), 3) the number of damping bars (40 in the DIG142 and 24 in the HC4) and 4) the nature of some of the additional resistances. With respect to the latter point, in fact, it has to be mentioned that a number of lumped resistances are considered in the model to account for the inherently 3-D features of the generators. In particular, while any contact between bars and laminations is assumed to be negligible for the sake of this study, the following compensation factors are instead considered:

- The bar-to-bar end connections – these are calculated by taking into account the shape and thickness of the end laminations. The lumped resistances included in the model in order to consider these connections are indicated as R_{bb} in Fig. 30 and Fig. 31.
- The ventilating ducts - the DIG142 alternator comprises the presence of ventilating ducts on the stator. Thus, in order to consider the parts of the windings which are present along these ducts, the lumped resistances R_{vd} are added to the model.
- The rotor field and stator armature end windings – the resistances of the field winding and the stator phases were directly measured with an ohmmeter at the machines' terminals and, consequently, relevant lumped circuital resistance values are included in the FE model by tuning with the experimental measurements. These are indicated as $R_{R,ew}$ and $R_{S,ew}$ in the respective schematics of Fig. 30 and Fig. 31.

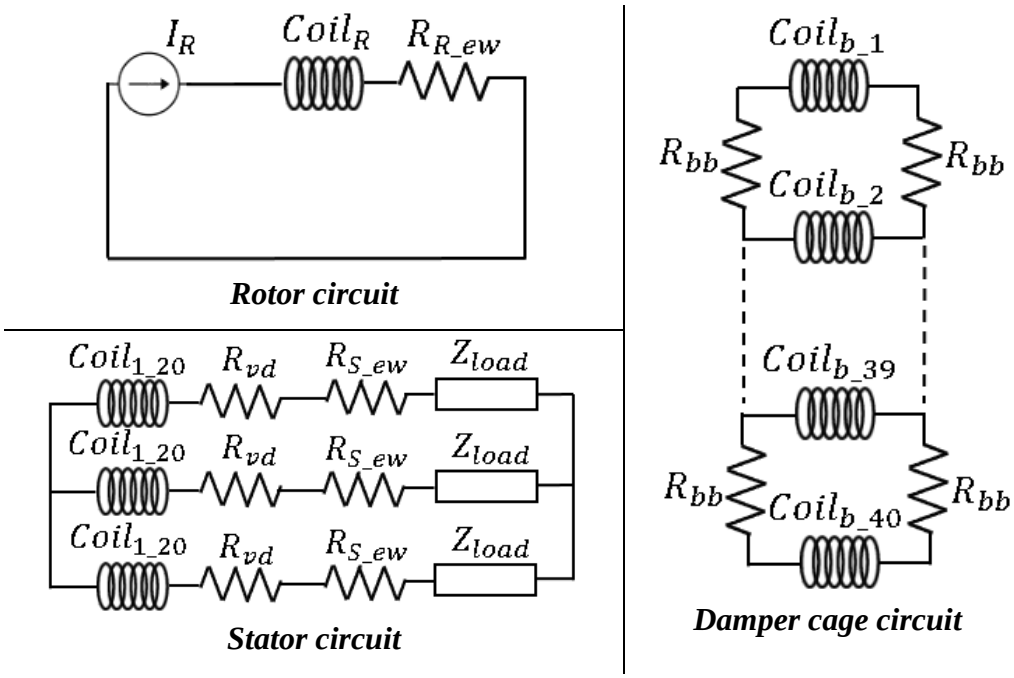


Fig. 30 – Electrical circuits relative to the DIG142 SG coupled with the FE model.

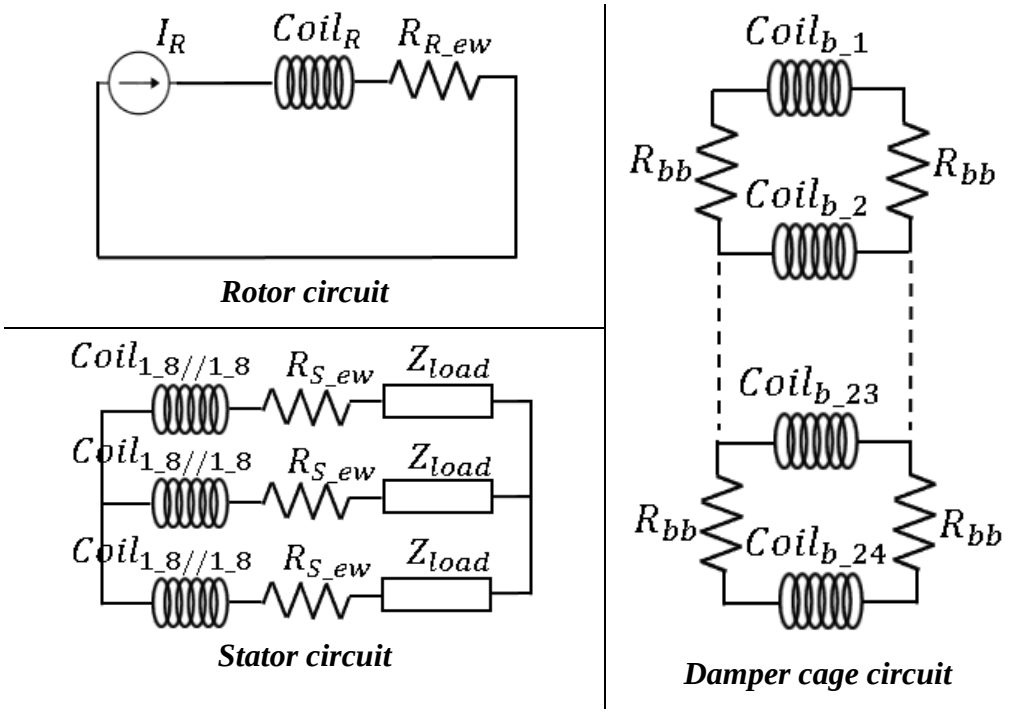


Fig. 31 – Electrical circuits relative to the HC4 SG coupled with the FE model.

For the sake of completeness, in Fig. 30, $Coil_{1_20}$ is the series of the 20 coils-per-phase which are representative of the DIG142 stator winding, while in

Fig. 31 $Coil_{1_8//1_8}$ is the parallel of two coils' groups, both representing the series of 8 coils of one stator phase of the HC4. Always referring to the same figures, for both the generators, $Coil_R$ is the series of the 4 rotor coils, while the circuit representative of the damper cage consists of n_b bars in parallel and the relevant (solid) coils are named $Coil_{b_i}$, where $i=1,\ldots,n_b$.

All the observations described above lead to consider that a 2-D, transient with motion evaluation can be used for accurately taking into account the most critical aspects related to the end effects without resorting to the 3-D modelling. Before going into the details of the solver options, the most critical aspects of the pre-processing are those relative to the imposition of the boundary conditions and to the properties of the mesh, as they affect in a significant way the accuracy and the computation time of the FE model. These criticalities are discussed in the next section.

4.1.4 Model structure

All the features and concepts behind the imposition of boundary conditions in a FE model are in general terms reported in Appendix 1. In this section, the application of these conditions to the SGs under analysis is discussed.

The first consideration to highlight is that the magnetic field in electrical machines is enclosed within the space delimited by the core yokes. Thus, in theory, a homogeneous Dirichlet's boundary condition must be applied to these delimiting surfaces in order to model this aspect. However, in reality, some flux does leak from the back iron and a realistic FE analysis requires the imposition of this boundary condition to an external circumference

outside the stator. These spaces external to the machine, where the field is weak, do not need to be modelled in great detail because they do not have a substantial effect on the solution. This concept is applied to both the machines' models as shown in Fig. 32 and Fig. 33, relative to the DIG142 and the HC4 respectively. It can be noticed that while for the 4*MVA* SG only an external air box surrounds the machine parts being modelled, for the 400*kVA* HC4 a hollow cylinder encloses the machine sector being analysed. This discrepancy between the models is due to the fact that the material used for the DIG142 shaft is a paramagnetic one (whose *BH* curve was available) this allows to analyse how the shaft affects the flux lines distribution, the field map and, in turn, the overall performance. On the other hand, the material used for the shaft of the HC4 is diamagnetic, meaning that its effect is negligible and the computational burden can be reduced.

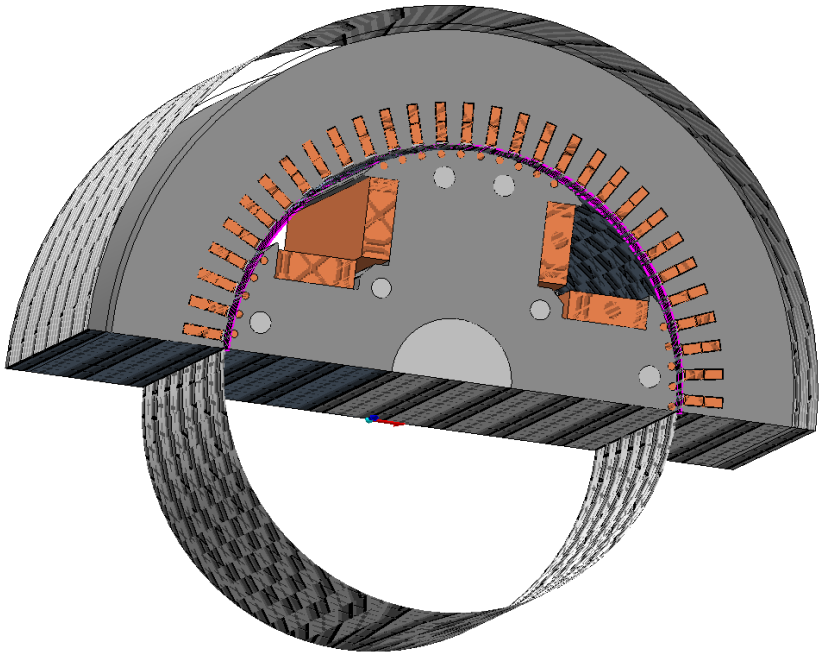


Fig. 32 – Imposition of boundary conditions onto the DIG142 FE model.

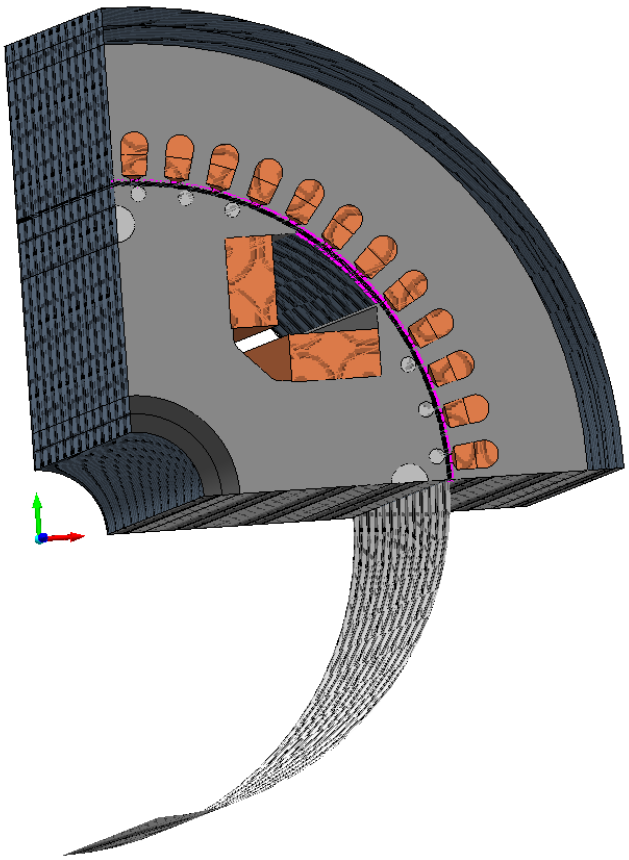


Fig. 33 – Imposition of boundary conditions onto the HC4 FE model.

The second step of this exercise aimed at limiting the domain of analysis, concerns the exploitation of the symmetries and the periodicities of the machine. Taking into account the damper winding topologies of the DIG142 and the HC4, different periodic conditions are used for the relevant models. In fact, as the damper cage of the DIG142 is displaced around the polar axis in alternating directions on each pole (see Fig. 7, in Section 2.4.1), it can be noted in Fig. 32 that the smallest machine sector that can be simulated for the full analysis of the considered SG corresponds to a one pole pair sector. This implies the use of even periodic boundary conditions along the tangential direction. On the other hand, the damper cage of the HC4 is symmetric, making the FE analysis simpler and faster, as the smaller machine sector that

can be simulated corresponds to a one pole sector. Therefore, odd periodic boundary conditions are imposed along the tangential direction, as can be seen in Fig. 33.

The last pre-processing step before solving a FE model consists in defining the mesh of the elements. As mentioned above, this represents a critical aspect of the modelling stage, as the elements' size and dimensions have to be chosen to satisfy the accuracy requirements, while keeping a relatively low computational time. MagNet allows for manual control of the mesh and, therefore, it is possible to define it according to the user objectives. For the applications at hand, it is clear that particular attention has to be given to the damper cage, considering that the prediction of the inherent induced currents (and associated losses) and of its effects on the output voltage THD represent the main goals of this work. In general, also the prediction of other loss contributors are important for the analysis of the considered SGs and, therefore, the mesh of elements of the relevant parts (i.e. cores and windings) have to be defined accordingly. Finally, special focus has to be given to the airgap, as in electrical machines with no magnets it represents the "component" where the majority of the electromagnetic energy is stored. Considering this, the airgap is divided in four layers along the radial direction in order to obtain a detailed field map; the two outer layers are marked "virtual air" with the purpose of improving the accuracy of the torque calculation via the Maxwell stress tensor method [17, 93], by shifting the integration surface inside a homogeneous region. Also, the software has the capability of enabling a "mesh edge subdivision" control tool, which allows

to control the mesh density along a component edge to be modified by specifying “seeds”. All the features described above regarding the mesh of elements in the various parts of the machine can be observed in Fig. 34 and Fig. 35, where it is also shown an in-zoom of the airgap area, highlighting the four layers subdivision concept as well as the “mesh edge subdivision” effects on the mesh. The mesh represented in the figures below and used for the FE analyses of the considered machines was achieved by adopting the “insensitivity of the solved quantity to further model refinement” philosophy. This was ensured by performing an iterative accuracy improvement process associated with a numerical sensitivity analysis. It is interesting to notice that, due to the higher complexity of the DIG142 than the HC4 (mainly due to the not-constant airgap along the salient pole tangential development), this iterative process led to consider smaller elements for the former SG. This discrepancy can be observed in the two figures below.

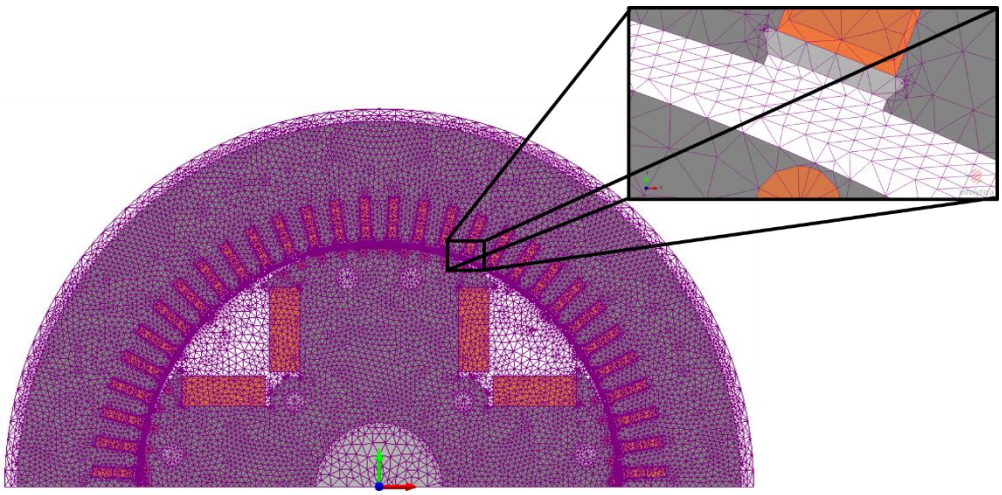


Fig. 34 – Mesh refinement relative to the DIG142 FE model.

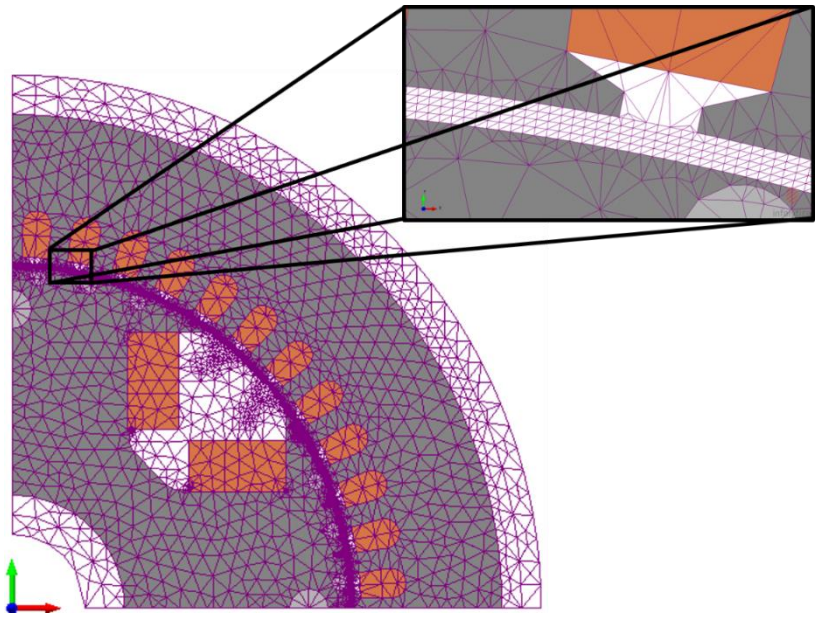


Fig. 35 – Mesh refinement relative to the HC4 FE model.

Having set-up the structure of the model as presented above, the next steps consist in selecting opportunely the solving options and finally performing the FE analysis, as described in the next section.

4.1.5 Solving

Before solving the developed FE model, a number of solver options has to be set according to the application at hand. The particular software utilised for the analysis provides the solver options detailed below:

a) Material type: this section allows to specify if materials are to be treated as linear or non-linear. Most of the analyses carried out in this thesis treats non-linear materials and, if not otherwise specified, the results shown in the next chapters will be referred taking this choice into consideration.

b) Method: the linearization method option allows to specify how non-linear model systems are to be linearized. The Newton-Raphson method [99] is used to linearize non-linear problems. It converges quadratically in the sense that the error at any given iteration is proportional to the square of the error at the previous iteration.

c) Newton tolerance and maximum Newton iterations: in non-linear models, an iteration loop is initiated at solving in order to linearize the system of equations to be solved. This iterative process will terminate either when the relative change in the solution x from one iteration to the next is smaller than the specified *Newton* tolerance or the maximum Newton iterations reaches the specified value. The maximum number of iterations is set at 20, as 5 or 6 steps are sufficient to reach convergence. Decreasing the Newton tolerance so as to cause an increase in the number of nonlinear iterations results in a more accurate solution.

d) CG tolerance: this option is used to determine when the iterative matrix system solution algorithm should be considered to have converged to the solution of the linearized matrix system resulting from the discretization of the model. The lower the CG tolerance, the more accurate and uniform the solution of the linearized matrix system.

e) Polynomial order: it controls the order of the base functions used to represent the solution. The higher the polynomial order of the base functions used to represent the solution, the greater the accuracy.

As well as for the mesh refinement, the same "insensitivity of the solved quantity to further model refinement" philosophy has been applied for the choice of the solver options listed above. Once selected and opportunely set in the model, a solver must be selected according to the analysis to be performed. In particular, MagNet distinguishes the "no-motion" solvers from the "transient with motion" solvers and the main features of both are described below:

a) The "no-motion" solvers can analyse devices with a moving component without taking into account the effects of motion. Basically, the device is solved with the moving component in different positions, meaning that the phenomena related to the eddy currents are neglected in the analysis.
b) The "transient with motion" solvers can solve models in which a) it is necessary to model the induce currents due to motional effects and b) it is necessary to couple with mechanical components. The analysis
    - can include any number of rigid components;
    - involves time-stepping from one instant to the next over the time frame of interest; since a second order time integration scheme is used, there are two calculations for each time step;
    - is quasi-static, i.e. displacement currents and wave effects are neglected.

Considering that the eddy currents' effects play an important role in the analysis of the damper winding and, in general, of the SGs under study, the

FE results reported in the next sections will be obtained through transient with motion simulations. Nevertheless, parametrised static simulations will be also used where fast solutions are necessary and when the eddy currents phenomena can be neglected.

4.1.6 Final considerations

In Section 4.1, an in-detail description of the FE model built and developed for the achievement of the objectives outlined in this work has been carried out. The product MagNet of Infolytica has been used for such purposes. The developed tool will be first used for an accurate performance prediction of the SGs considered in this thesis. The corresponding results of these analyses will be then validated against experimental measurements. Before going into the details of this comparative exercise, there are two critical aspects for the analysis of the considered alternators that need a dedicated treatment. These include 1) the iron loss, with special focus on the pole face loss, as it was an identified issue for the applications at hand (especially for the DIG142) and 2) the skewing, as this design feature is implemented on the stator of the HC4. As the relevant modelling of such aspects is not directly correlated to the FE model features described above, it will be the focus of the next sections.

4.2 Modelling of surface rotor losses

In general, power losses in electrical machines are composed of the following terms:

- resistive losses in stator and rotor conductors;
- iron losses in ferromagnetic materials;
- mechanical losses, i.e. windage and friction.

The way how the ohmic-resistive aspects have been taken into account in the developed FE model of the SGs being considered in this thesis have been discussed in Section 4.1.3. Considering this, no further details are discussed in this section and the validation exercise of such a loss contributor will be shown in the relevant section (i.e. Section 4.4.4). On the other hand, a more in-detail treatment is necessary for the iron loss modelling and this is discussed in the next sections.

4.2.1 Background

Due to a number of reasons, including manufacturing aspects that can have an impact on the magnetic properties of ferromagnetic materials, the estimation of this loss contributor represents a very difficult task for electromagnetic designers. Hence, as a first step, it was necessary to perform a literature survey to understand how core models have been traditionally developed. Regarding core losses with sinusoidal excitations, Steinmetz did much of the earlier work [100, 101]. The original model was aimed at representing core losses per unit volume in a single equation. Steinmetz

showed a separation into two components, as given in (21), namely the hysteresis and the eddy currents losses.

$$P_{iron} = k_h f \hat{B}^n + k_e (f\hat{B})^2 \tag{21}$$

The parameters in this equation were found empirically, i.e. n is the Steinmetz constant (usually fixed at 1.6), k_h and k_e are known as the hysteresis and eddy current loss coefficients, f is the excitation frequency and $\hat{B}$ is the peak flux density. In recent years, it has been shown that there exists a third loss component [102, 103]. This additional contributor is termed extra losses, originating from eddy currents induced around domain walls as they move under the influence of an alternating magnetic field. A new model was proposed and the relevant equation is provided below in (22).

$$P_{iron} = k_h f \hat{B}^n + k_e (f\hat{B})^2 + k_{ex} (f\hat{B})^{1.5} \tag{22}$$

In (22), n is not fixed and is material dependent. Ultimately, research focused on the explanation of the physical meaning of n, k_h and k_{ex}, which are often obtained through curve fitting techniques, and on the development of a core loss model that incorporates all the dynamics related to frequency and flux density [104]. The hysteresis component was recently modified by [105] as shown in (23), to reflect the frequency dependence of the hysteresis loss coefficient and the dependence of the Steinmetz's constant on the peak flux density. This model, combined with classical models, showed good performance. All the coefficients are obtainable through curve fitting.

$$P_{hyst} = k_h(f)\, f\, \hat{B}^{c+d\hat{B}+e\hat{B}^2} \tag{23}$$

In this thesis, the choice of the most accurate method for the loss estimation in the SGs under study was dictated by the following reasons:

a) Experimental measurements carried out on the considered alternators have shown high rotor temperatures (relatively to their insulation class) even during normal operation; this was an identified issue particularly for the DIG142. A detailed analysis of the loss contributors is then necessary to identify which losses are most sensitive to the high rotor temperatures.
b) The classical Steinmetz equation (21) is used in MagNet to determine iron losses. This may lead to obtain very inaccurate results, in particular when high flux density harmonics and minor loops are present.

Having provided the above introductory aspects behind the iron loss modelling, next section focuses on the methodology proposed in this work for the estimation of such significant loss contributor.

4.2.2 The proposed method

The method proposed and implemented for the estimation of the iron loss in the SGs under study consists in an algorithm based on Steinmetz equations but extended to all the harmonics [106]. In this way, surface losses due to the slot harmonics are properly considered over the whole amount of iron loss.

The computation algorithm of the iron losses can be summarized in the following:

1) A transient with motion 2-D finite-element analysis is performed.
2) From the magnetic field solution, the flux-density waveform corresponding to an electric cycle is extracted from the nodes of a grid built-on-purpose inside the iron regions, i.e. the stator and rotor steel for each element. On the left-hand side of Fig. 36, it is shown how the rotor pole shoe has been subdivided for such purposes. The use of a customised grid (rather than using the nodes of the mesh elements) gives more flexibility to the model, as it can be properly modified according to the objectives at hand.
3) The flux density in the middle of each element is calculated by averaging the flux density waveforms extracted in 2), as shown on the right-hand side of Fig. 36.

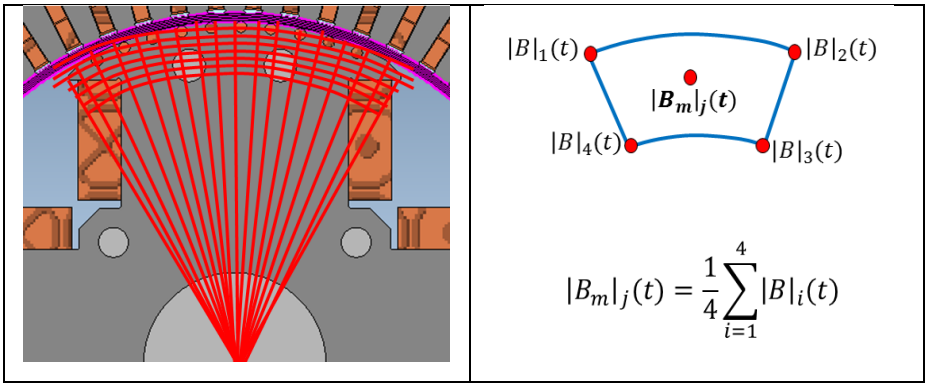


Fig. 36 – Subdivision of the pole shoe (on the left) for loss calculations and averaging of the flux density waveforms (on the right).

4) The Fourier-series decomposition is applied for all the flux density waveforms. The first 100 harmonics are considered, in order to account for the slotting effect on the loss computation.

5) The following equations are then used to compute the hysteresis and eddy current components in each element of the iron regions:

$$P_{iron} = P_{hyst} + P_{eddy} \tag{24}$$

$$P_{hyst} = k_h \sum_{i=1}^{N} (i\ f) B_i^n \tag{25}$$

$$P_{eddy} = k_e \sum_{i=1}^{N_p} (i\ f)^2\ B_i^2 \tag{26}$$

where f is the frequency, B is the peak flux density, k_h and k_e are the hysteresis and the eddy current loss coefficients, respectively, and n is the Steinmetz constant. These coefficients are determined through curve fitting techniques, by using the data available from the test previously carried out on an Epstein frame for obtaining the loss contribution separation.

6) The summation of all the losses per element gives the total iron loss.

As well as for the ohmic loss component, the validation exercise of the model proposed and described above will be provided in Section 4.4.4.

4.3 Modelling of skew

The second critical modelling aspect which needs a dedicated treatment in this chapter is that related to the skewing, as this is implemented onto the HC4 stator. The literature review relevant to the skewing has been discussed in Section 2.3, where it was highlighted how this 3-D feature can be

modelled with very accurate techniques (even in 2-D), although these come at the cost of high computational resources which are not suited for iteration-heavy designs. Considering this, a fast FE-based method is proposed in this section, able to accurately predict the effects of skew in SGs in a relatively shorter time than the traditional methods.

4.3.1 Objective

In this work, a technique for the modelling and the analysis of skew effects in electrical machines (with a focus on the platforms at hand, i.e. SGs) is proposed and investigated. A similar approach is presented in [107], where the analysis is focused on PM machines. However, in machines with short-circuited windings, where currents are induced by a number of phenomena of different nature, further investigations are required. Therefore, updates on the approach presented in [107] are implemented onto the 400*kVA* HC4 SG in order to predict the no-load and on-load THD of the machine's output voltage. Using the proposed modelling technique, then a theoretical explanation of the benefits due to the stator skew in the generator under analysis are carried out and presented. The technique and its results are then compared to the two more common approaches (for modelling of skew), via a purposely-built 2-D, SS FE model. The mentioned 'common' techniques are

1) the averaged-slice (AS) technique, where a set of 2-D slices with appropriate shift between rotor and stator are created and then post-processed by using averaging processes;

2) the MS technique, where a number of 2-D slices with appropriate shift between rotor and stator are created and then simultaneously solved.

The above-proposed method is thus used for the analysis of voltage waveforms, damper cage induced currents and associated losses in SGs. As shown below in the thesis, excellent results in terms of modelling, accuracy and time consumption are achieved. Experimental tests are performed to prove the validity of the fast, proposed SS technique.

4.3.2 Conceptual considerations

This section deals with some analytical considerations aiming at understanding the effects that skewing has on the overall performance of electrical machines. To do this, it is worth to recall the variable airgap thickness $\varepsilon_{AG}(\lambda,\alpha)$, defined in (18) as the difference between $r_s(\lambda,\alpha)$ and $r_r(\lambda,\alpha)$, which represent the stator and rotor radii respectively, evaluated along the tangential direction. In Section 3.5 and in particular in (8)-(17), it was highlighted the important role that this function plays in the solution of the electromagnetic problem. It was also presented in Section 3.6.2 how the slot opening effects can be implemented in the function $r_s(\lambda,\alpha)$. For the sake of this study, step functions are sufficient to describe the slot opening. This concept is shown in Fig. 37, where the slot harmonic can be easily observed in the function $\varepsilon_{AG}(\lambda,\alpha)$. It is clear that this slot harmonic will be present in the permeability function $\mu_E(\lambda,\alpha)$ and thus in the inductance matrix $L(\alpha)$, defined in (9) and (17) respectively. As expected, one possible solution to

mitigate the effects of the slot harmonics on the quantities recalled above (and consequently on the output voltage) is to axially skew the stator of SGs.

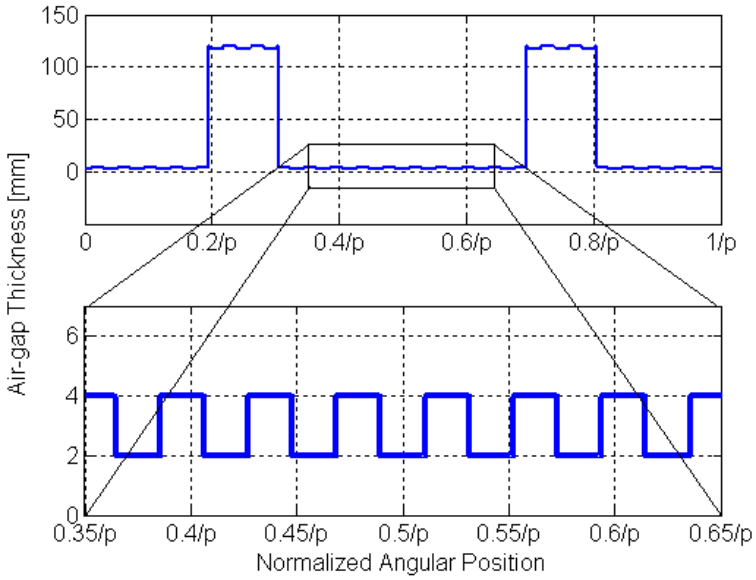


Fig. 37 – Variable airgap thickness function ε_{AG} vs. angular displacement λ.

To implement the skewing in $\varepsilon_{AG}(\lambda,\alpha)$, one can consider a number N_s of 2-D cross sections of the machine along the axial direction. Each slice is shifted from each other by a submultiple δ of the skewing angle α_{sk}, as shown in Fig. 38. In practice, this corresponds to a shift of $r_s(\lambda,\alpha)$ and this is recalculated by averaging each waveform over the number N_s of slices considered. In order to show this concept, the waveform obtained in Fig. 37 (where the skewing is not considered and thus N_s=1) is compared with the waveforms obtained when N_s=5 and N_s=9. This is shown in Fig. 39, where it can be observed how the slotting effect is reduced when considering an increasing number of slices. In the case of the HC4 SG analysed in this work, where a continuous (i.e. not stepped) skewing is applied to the stator, it is obvious that an accurate implementation of this machine's feature in the airgap thickness

function implies the choice of a theoretically infinite number of slices (N_s=∞). This results in the interesting result given in (27) where ${}^{6q\pm1}\varepsilon_{AG}$ is the first slot harmonic, evaluated under one pole pair.

$$\lim_{N_s\to\infty} {}^{6q\pm1}\varepsilon_{AG} = 0 \tag{27}$$

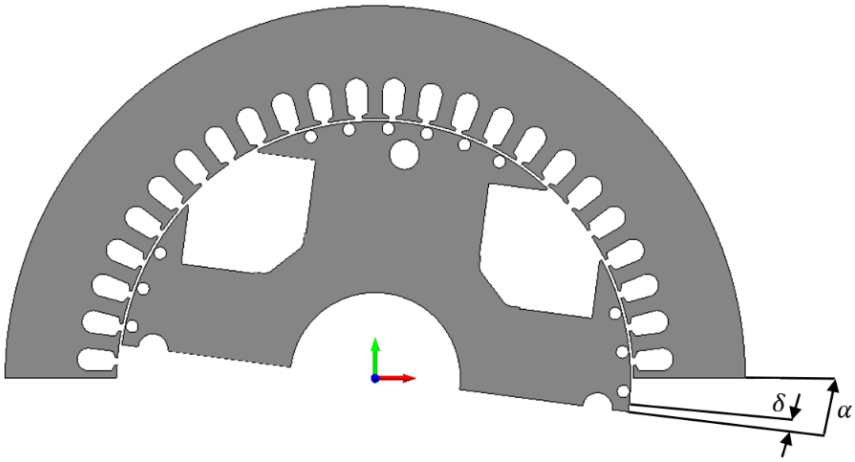


Fig. 38 – 2-D cross-section of the HC4, including the skewing angle α_{sk} and its submultiple δ.

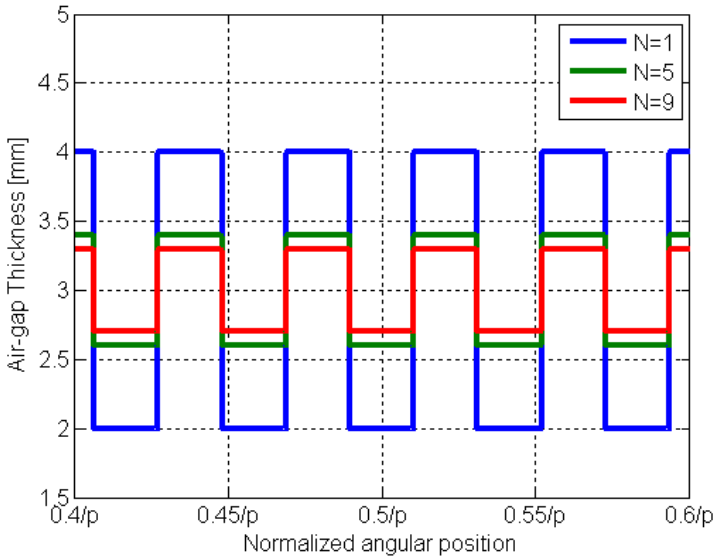


Fig. 39 – Zoom on the variable airgap thickness function – comparison between an un-skewed (N_s=1) and a skewed stator (N_s=5 and N_s=9).

Considering the above, it can be concluded that, although simplified shapes of $r_s(\lambda,\alpha)$ and $r_r(\lambda,\alpha)$ have been considered, some important results can be observed. In particular, it has been shown how skewing can mitigate the harmonics due to the stator slot openings (Fig. 39) and, in the case of a continuous stator axial skewing, a theoretical, complete elimination of these harmonics can be achieved (see (27)), allowing for improvements in the output voltage waveform.

It is also important to observe that, by applying the same concept of averaging the waveforms obtained by considering N_s axial slices of the machine, it is possible to 'improve' also the winding functions which describes the machine's phases. This concept is shown in Fig. 40, where the number of slices used is 5.

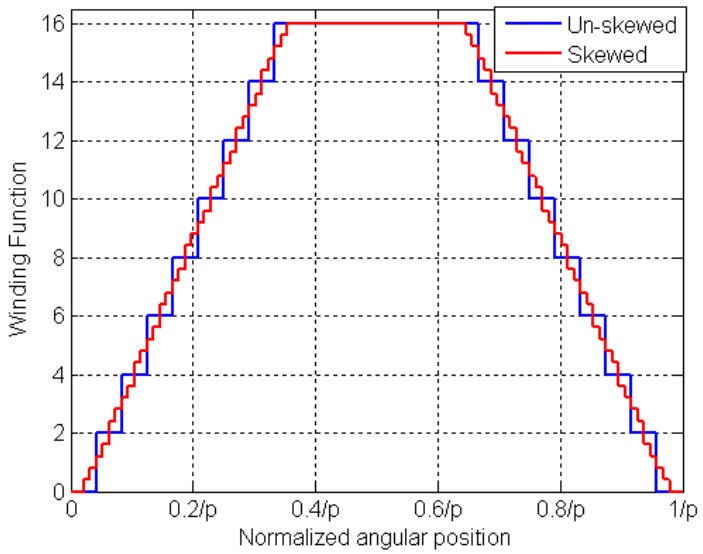


Fig. 40 – Stator winding function: comparison between an un-skewed and a skewed stator.

It can be observed that the skewed winding function (in red) is much more sinusoidal-distributed of that of the un-skewed one (in blue). The main effect is therefore that of producing a better winding distribution. However, this comes at the cost of reducing the winding factor (by 0.3% in the case of Fig. 40, where N_s=5) which in turn propagates a reduction of the performance of the machine. It is also clear that, when an increased number of slices is used for averaging the blue waveform, a further reduction of the winding factor can be observed, again highlighting that skewing is an optimizable feature in all the design stages of electrical machines.

All the above highlights that the effects due to the skewing can significantly affect the internal electromagnetic phenomena occurring in electrical machines. Therefore, it is of paramount importance to model it in a fast and accurate way, especially for iterative design purposes. Therefore, in the next sections, a single-slice (SS), 2-D FE modelling technique [108] is proposed and compared with the most known 2-D FE approaches. The validation process against experimental measurements will be presented in Section 4.4.5, for the sake of consistency with the other modelling aspects previously highlighted.

4.3.3 The proposed model

Considering the FE model described in Section 4.1, a SS method is proposed for the analysis of the skewing. A transient with motion evaluation of an un-skewed machine is undertaken, which comprises flexibility in terms of simulating different operating conditions according to the type of load

considered in the circuit coupled to the FE model. In other words, the no-load condition is simulated by setting a resistance equal to a practical infinite value, while the on-load operation is analysed by setting the circuital lumped parameters (resistance, inductance and capacitance) according to the given apparent power and power factor.

The key point of the proposed method is choosing a simulation angle step δ equal to a submultiple of the skewing angle α_{sk}. The smaller the simulation angle step, the more accurate the post-processed electromagnetic quantities, without significantly compromising the computational times. These quantities (i.e. fluxes linkages, voltages, currents, etc.) are phase shifted by the selected angle δ and averaged over the skewing angle, as given in (28) for the generic scalar quantity $x(\theta)$. For the sake of clarification, it is worth to point out that this process is also applied for the evaluation of the damper cage currents and losses.

$$x(\theta) = \frac{\delta}{\alpha_{sk}} \sum_{-\alpha_{sk}/2\delta}^{+\alpha_{sk}/2\delta} x(\theta + \varphi) \tag{28}$$

The averaging process shown in (28) assumes that there are no variations of the magnetic state of the skewed machine along the axial direction. It is also true that averaging processes can lead to inaccuracies in machines equipped with short-circuited rotor cages [71]. However, the main objectives of this exercise are

1) to propose a very fast technique for modelling the skewing in everyday, company-based design of SGs;

2) to prove that this method can be very accurate for estimating some critical standard grid requirements, such us the THD of the no-load and on-load voltages;
3) to highlight that the limitations of the proposed method for the estimation of more complex quantities, such as the currents induced in the damper cage, are not significantly critical.

The next section therefore deals with the analysis of the results obtained with the SS technique, at no-load and at full-load operations. The results are not presented on their own, but are illustrated directly in the validation comparisons with the results from the AS and the MS models. These are shown in Figures 42-46, Table 2 and Table 3.

4.3.4 Comparison with other FE techniques

This section is aimed at comparing the proposed SS method described above with the two most common ways used to model the skewing in electrical machines, namely the AS and the MS techniques. The major features of these methods are highlighted below:

1) The AS technique: it consists in creating a set of 2-D FE models, different from each other only for the initial phase shift between rotor and stator positions. Each model is then solved separately and the results are post-processed by averaging processes. The higher the number of models being used, the more accurate the field solution, but the required computational time is also compromised. This

technique is perfectly suitable for modelling stepped-based skewing, which for example is very common in PM machines.

2) The MS technique: it consists in creating a number of 2-D slices with a specific phase shift between rotor and stator positions, according to the skew angle (see Fig. 41). These slices are then solved simultaneously. This forces the currents flowing in skewed windings to be the same along the axial direction, thus allowing for much more accuracy than with an averaging procedure. This technique is the most accurate amongst 2-D FE methods for modelling the skewing. On the other hand, it requires significant computational resources.

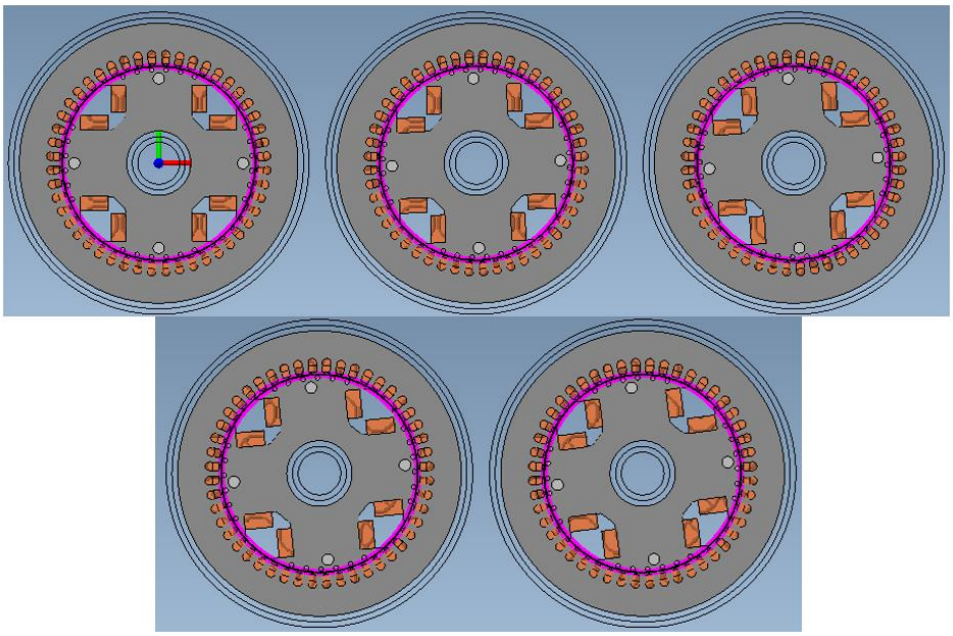


Fig. 41 – The multi-slice FE model, with 5 slices simultaneously evaluated.

An accurate, preliminary sensitivity analysis has been performed aiming to select the most appropriate number of slice N_s to be used for comparison purposes. The results of such analysis have led to consider a scheme with 5

slices. This number is chosen based on the results of a sensitivity analysis that indicated that no significant modifications on the electromagnetic quantities are observed when values of N_s bigger than five are used. The three techniques are thus compared with N_s=5 being used for all of them. All the results at no-load and full-load operations are shown in the following sections.

4.3.4.1 No-load

The results obtained with the proposed SS method at no-load operation are given in this section. Fig. 42 shows a comparison amongst the no-load output voltages obtained with the three different techniques. The terminal voltages obtained are not shown over-lapping to each other because of the excellent similarity being achieved. This is also confirmed by the results observed in Table 2, where the THD and the total RMS values of the open-circuit voltages are compared.

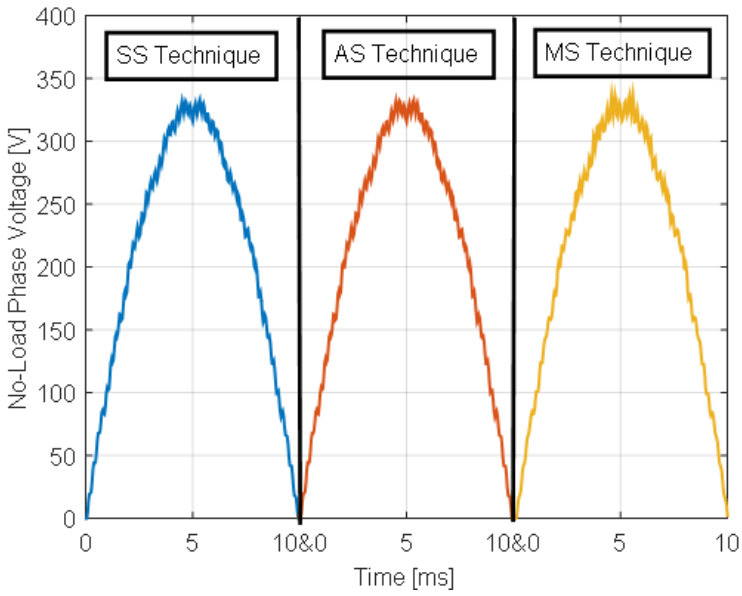


Fig. 42 – No-load terminal voltage – Comparison amongst the three methods.

Table 2 – THD and RMS values – Comparison amongst the three techniques.

---------- ----------	**No-load Phase Voltage**			
	SS	***AS***	***MS***	***Skew-less***
THD	2.193*%*	2.183*%*	2.221*%*	5.58*%*
Total RMS	230.01*V*	230.05*V*	230.25*V*	231.96*V*

It is important to note that in Table 2, the main aim is to compare the three techniques. However, the values of the voltage THD and total RMS for the skew-less machine are also shown to emphasize the advantages that skewing can achieve.

In Fig. 43 and Fig. 44, the comparison is carried out in terms of damper cage induced currents. In particular, Fig. 43 shows a comparison amongst the current's waveforms induced in one damper bar (e.g. the bar on the pole tip) evaluated with the three different methods. Fig. 44 compares the RMS values (y-axis) of such currents induced on the damper bars (x-axis) of one salient-pole. In this case, a good match amongst the results obtained with the three techniques can be seen, highlighting the validity of the proposed method at no-load operation. On the other hand, some differences can be observed amongst the currents in bars 3 and 4, especially when evaluated with the MS technique. This is due to the fact that the currents are constrained to be the same in each bar of this winding, and are not evaluated according to the same averaging concepts as the SS and the AS techniques do.

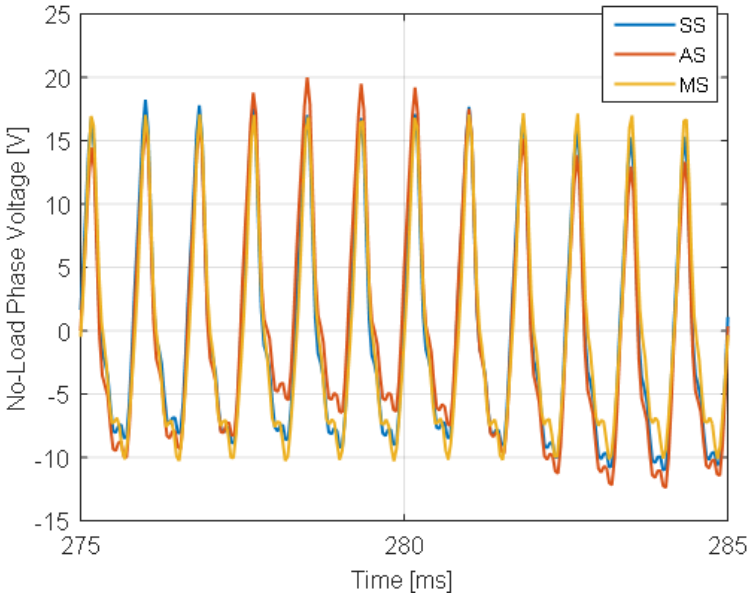


Fig. 43 – No-load currents induced in one damper bar: comparison amongst the three techniques.

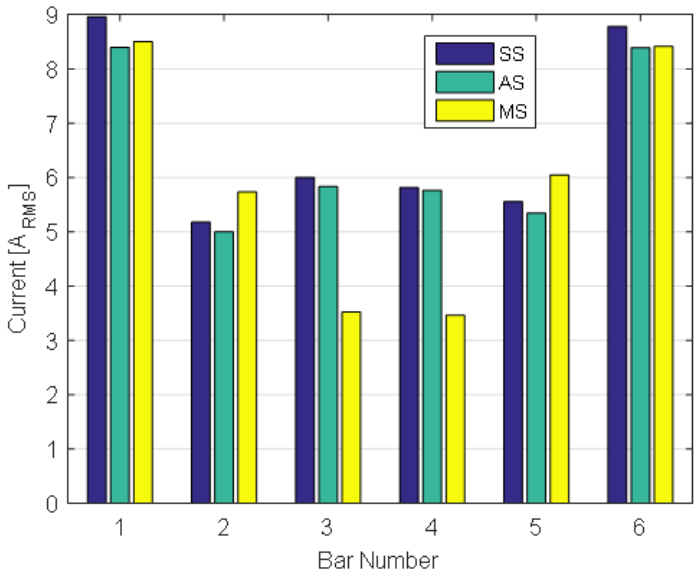


Fig. 44 – No-load, RMS values of damper cage currents: comparison.

4.3.4.2 Full-load

Classical averaging processes used to model skewed electrical machines can lead to inaccuracies in predicting the performance, especially when these are equipped with short-circuited windings. At full-load operation, besides the

effects due to the slot harmonics, additional damper cage currents are induced by the armature reaction [38]. As well as for the no-load operation, in order to validate the SS method, the damper cage currents are evaluated with the proposed technique and then compared with the well consolidated AS and MS simulations. An excellent similarity amongst the results of Fig. 45 can be observed, where the RMS values of the damper cage currents induced into the bars placed on one pole are shown. Also at full-load operation the damper cage currents predicted with the SS technique are very similar to those evaluated with the AS and the MS methods and the percentage error is very low. When considering the advantages in terms of computational times, then this relative accuracy is of course an added advantage for the proposed technique. The full-load stator currents are compared in Fig. 46, showing again a very good similarity amongst the results.

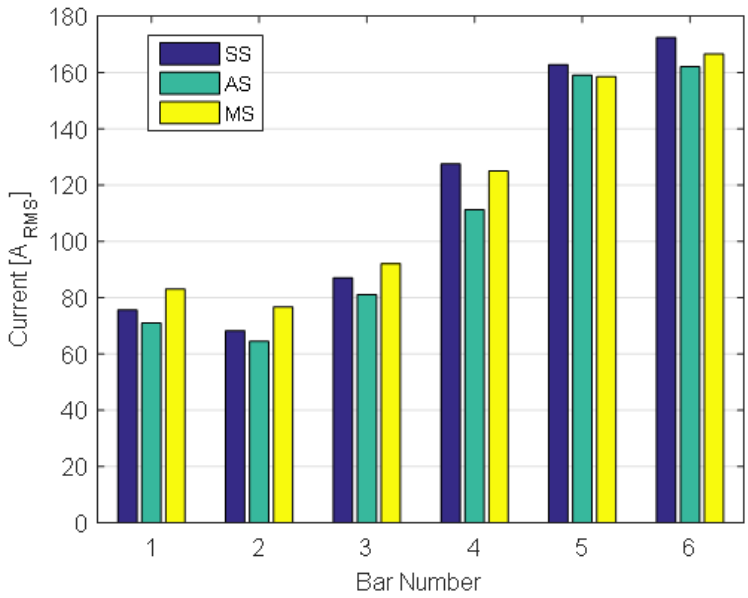


Fig. 45 – Full-load, RMS values of damper cage currents: comparison.

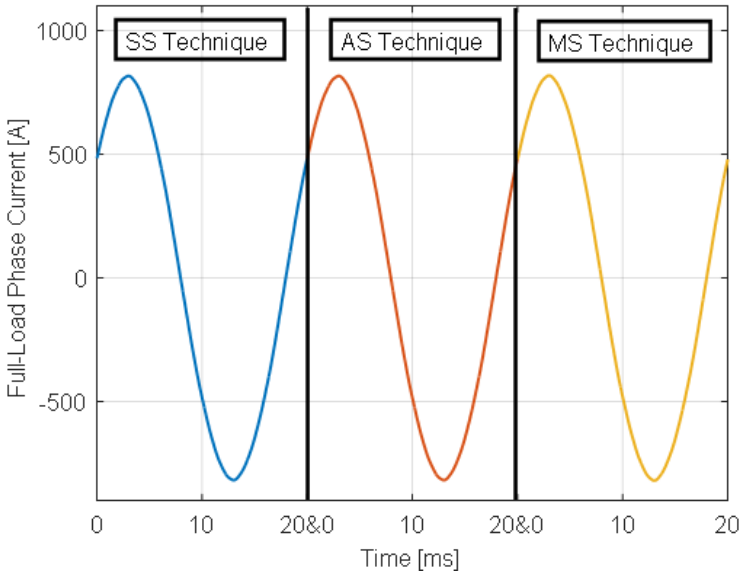


Fig. 46 – Stator phase currents: comparison.

For the sake of completeness, the damper cage losses are computed with the 3 different techniques and compared relative to each other but also to the case of a skew-less configuration. In Table 3, it can be observed that losses are reduced by 2.2% when skewing is applied, as the slot harmonic effect is attenuated. Although skewing can affect other loss components [64], such as the pole face losses, and can lead to an increased field current to compensate for the ensuing output voltage drop (see Table 2), it can be concluded that this stator feature does not significantly affect the overall efficiency of the considered platform.

Table 3 – Damper cage loss: comparison amongst the three techniques.

Damper Cage Loss			
SS	***AS***	***MS***	***Skew-less***
1136*W*	1131*W*	1126*W*	1155*W*

4.4 Model validation against experimental results

This section is aimed at confirming the validity of the models proposed above. The validation process is crucial for the further development of the project and for the achievement of the relevant objectives, as the validated tools will be then used for power quality and efficiency improvements through advanced optimization methodologies.

More specifically, besides the basic performance at no-load and full-operations of both the DIG142 and the HC4 SGs, the comparative exercise between FE and experimental results will focus on proving the accuracy of the power loss and the skewing models, respectively proposed in Sections 4.2 and 4.3. The experimental measurements were performed in the Tech Centre of CGT at this stage for both the alternators. In the next sections, only the general aspects of the tests will be presented, while the detailed setups and procedures will be provided in Chapter 7, where the experimental results carried out on a new prototype will be discussed.

4.4.1 No-load characteristic

The open-circuit characteristic is found by measuring the no-load terminal voltage at different levels of field current. For comparison purposes, first static FE simulations (phase A axis and d-axis parallel) were carried out as suggested in [93], in order to reduce the required computational resources. However, in order to fully consider the harmonic content of the no-load voltage, transient with motion simulations were also used. Fig. 47 and Fig. 48 compare these different FE approaches with the experimental measurements,

respectively carried out on the DIG142 and HC4 prototypes. It can be noticed that, although the static simulation curves are quite accurate, the transient simulation curves are almost exactly matching the experimental results.

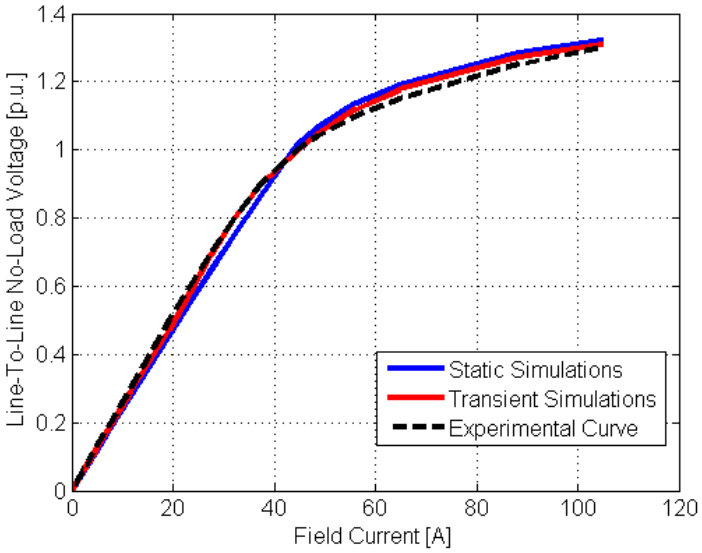


Fig. 47 – No-load characteristics of the DIG142 – Comparison between FE and experimental results.

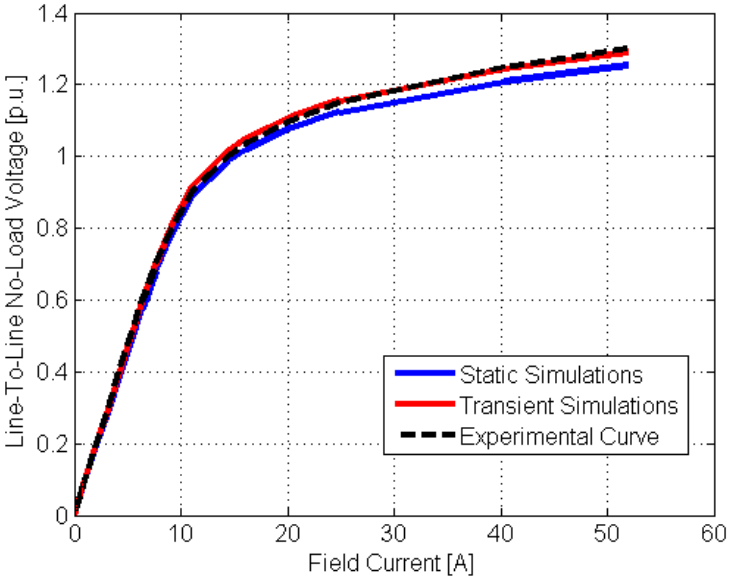


Fig. 48 – No-load characteristic of the HC4 – Comparison between FE and experimental results.

For the sake of completeness, the field maps at no-load for the DIG142 and for the HC4 are reported in Fig. 49 and Fig. 50, respectively. These are illustrated with the phase A-axis (highlighted in the figures) and d-axis (i.e. the polar axis) parallel.

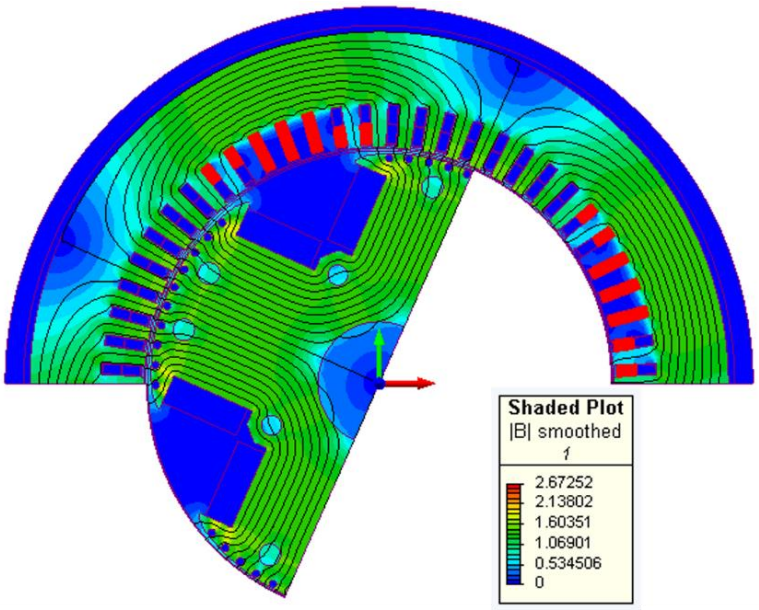


Fig. 49 – No-load field map of the DIG142.

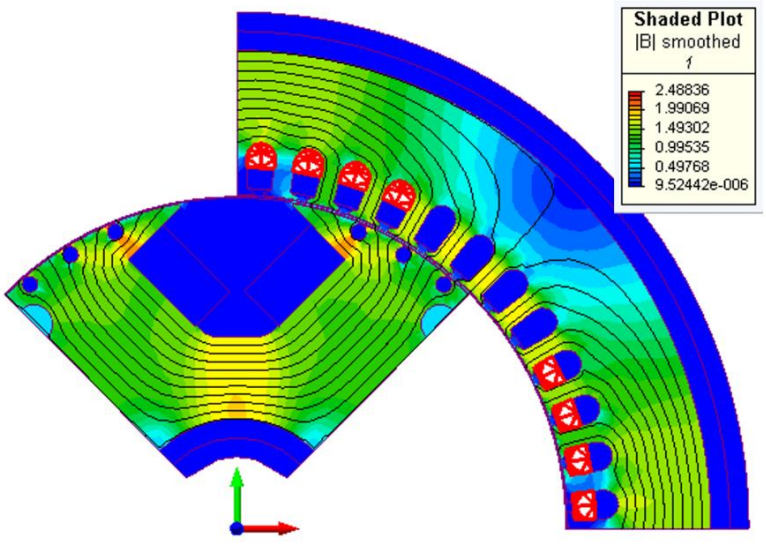


Fig. 50 – No-load field map of the HC4.

4.4.2 Short-circuit characteristic

The short-circuit characteristic is determined by measuring the armature stator currents at different levels of field current, when the generator terminals are short-circuited.

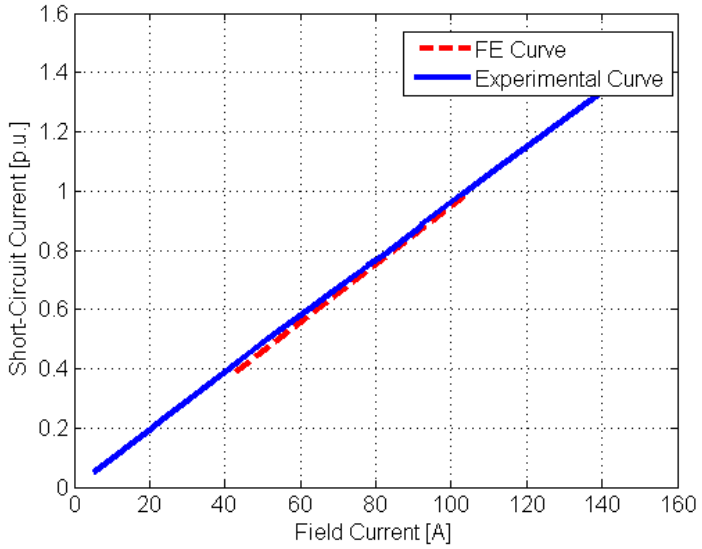


Fig. 51 – Short-circuit characteristics of the DIG142: comparison between FE and experimental results.

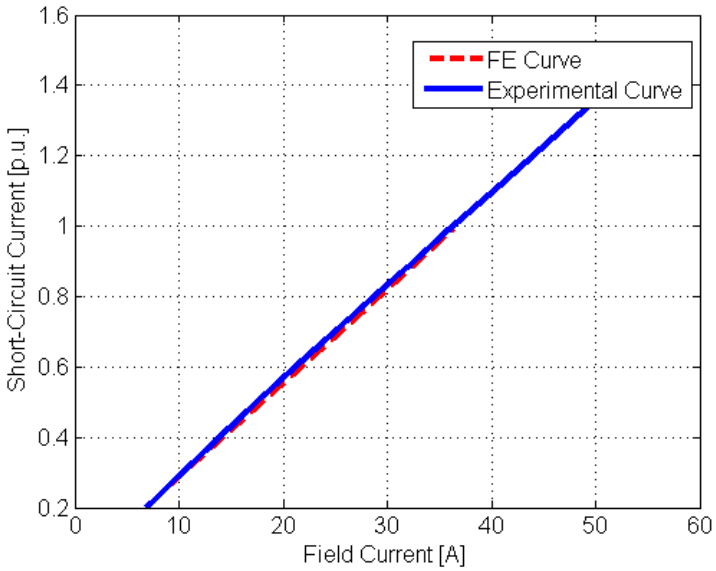


Fig. 52 – Short-circuit characteristics of the HC4: comparison between FE and experimental results.

The relevant test set-up is replicated through FE, transient with motion simulations for comparison and validation purposes. Fig. 51 and Fig. 52 show a good agreement between FE and experimental results, respectively for the DIG142 and the HC4 generators.

4.4.3 Full-load results

In Fig. 53 and Fig. 54, the field maps of the SGs under analysis at full-load rated conditions are shown. The effect of the transversal armature field component on the excitation field can be observed. This is due to the ohmic-inductive nature of the rated load, being the rated power factor equal to 0.8. In the FE model, depending on the required loading and power factor, the rotor currents and the passive components values can be set to run a transient simulation, until the steady-state condition is reached.

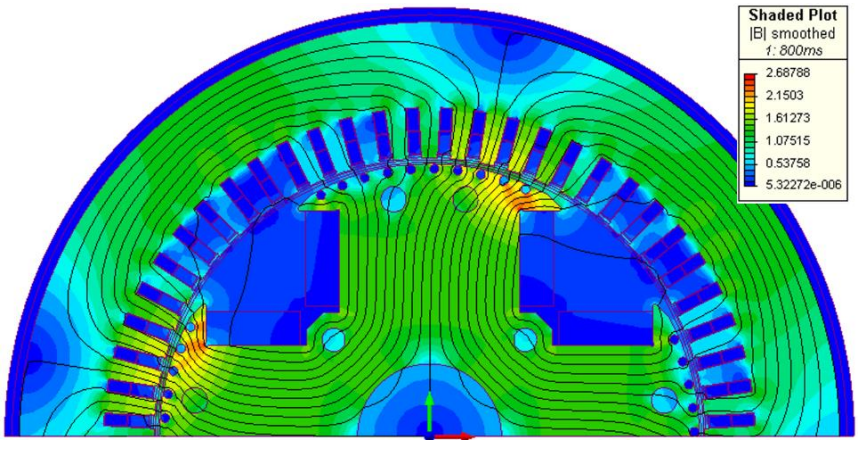


Fig. 53 – Full-load field map of the DIG142.

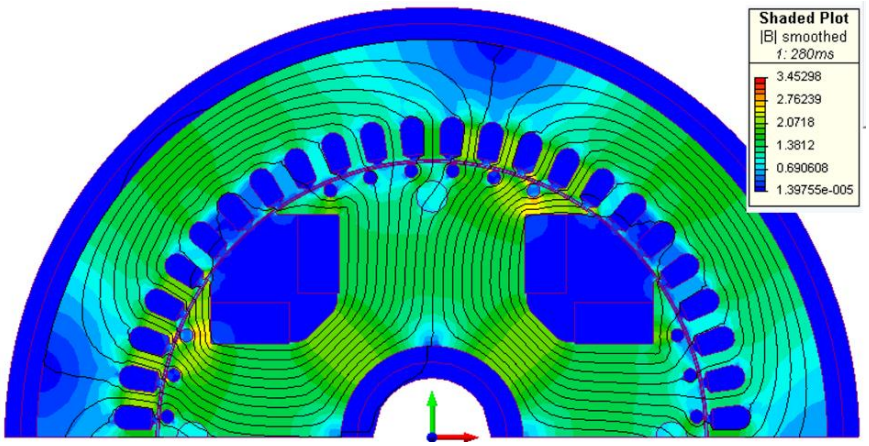


Fig. 54 – Full-load field map of the HC4.

From an experimental point of view, the electrical load parameters are registered during normal, full-load operation of the two SGs and the results therefore compared with the FE values for validation purposes. Table 4 summarises this comparative exercise for the DIG142 and Table 5 for the HC4, with the rated field current being used in the 2-D FE model and an excellent similarity being achieved.

Table 4 – Full-load results for the DIG142.

Electromagnetic Quantities	**FE Results**	**Experimental Results**	**Percentage Error**
Field Current	143.7*A*	143.7*A*	0%
Load Voltage	10998*V*	11000*V*	0.02%
Phase Current	230.2*V*	233.6*A*	1.46%
Power Factor	0.802	0.8	0.25%
Real Power	3.51*kW*	3.56*kW*	1.46%

Table 5 – Full-load results for the HC4.

Electromagnetic Quantities	**FE Results**	**Experimental Results**	**Percentage Error**
Field Current	50.3*A*	50.3*A*	0%
Load Voltage	400.2*A*	400*V*	0.05%
Phase Current	575.7*A*	577.4*A*	0.3%
Power Factor	0.783	0.8	2.13%
Real Power	313*kW*	320*kW*	2.19%

4.4.4 Power losses

This section deals with a comparison between the FE and the experimentally evaluated copper and iron losses of the generators being considered. In Section 4.1.3, it was described how to include the resistive effects not inherently modelled in the 2-D models of the SGs. These include the ventilating ducts, the end-windings and temperature effects on the copper conductivity. Based on this, it can be inferred that the resistances considered in the FE model are very close to the experimental ones. Therefore, while very small differences are detected for the field winding losses, the discrepancy between FE and experimentally determined currents reflects on the stator resistive loss. Fig. 55 shows a comparison between FE and experimental copper losses for the DIG142, at different loadings and power factors, where the percentage error at rated full-load condition is 5.46% for the stator loss.

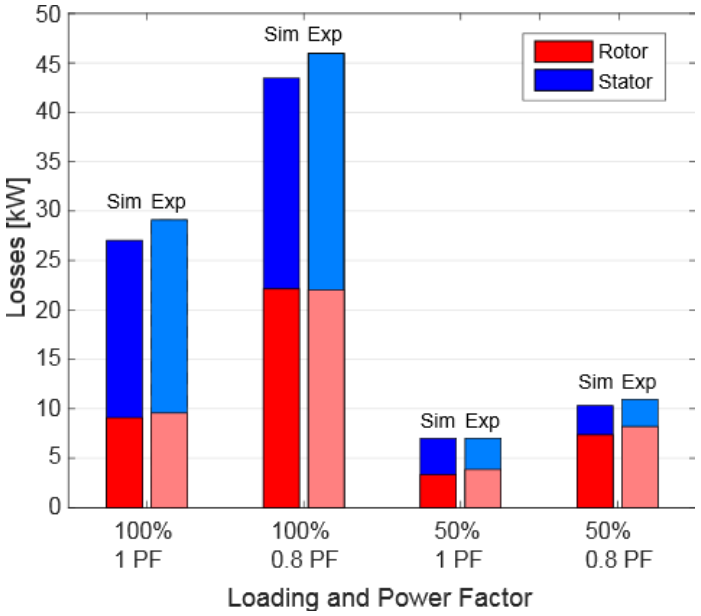


Fig. 55 – Copper losses in the DIG142 at different load levels and power factors: comparison between FE and experimental results.

The same comparison is carried out for the HC4 platform and illustrated in Fig. 56, where the percentage error at full-load operation is even smaller than the previous machine and results equal to 0.5%.

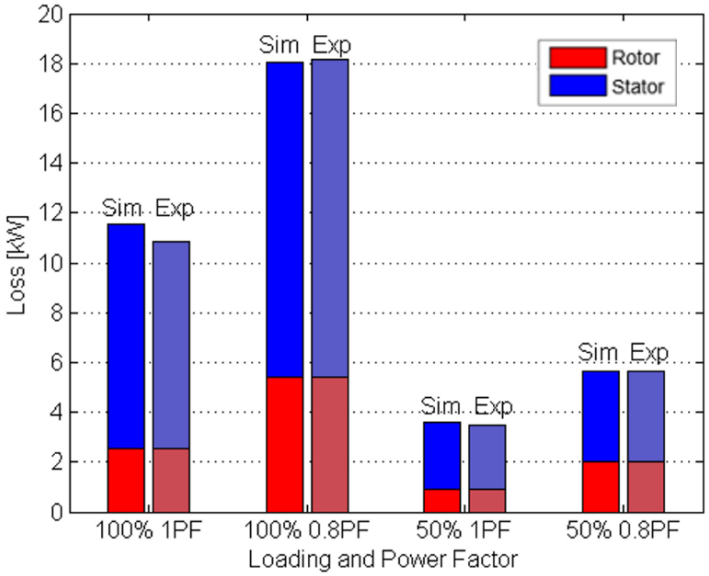


Fig. 56 - Copper losses in the HC4 at different load levels and power factors: comparison between FE and experimental results.

Core losses are experimentally measured at no-load and then assumed to be approximately constant for all load levels and power factors. Traditionally, only the total core loss is determined as any localization exercise to determine where the loss actually is (rotor or stator or damper), is very difficult to do. Therefore, although damper winding losses are of ohmic-resistive nature, they are included in the experimentally evaluated iron loss value. In Fig. 57, the DIG142 generator losses computed through the algorithm described in Section 4.2 can be observed at various loadings and power factors. It can be seen that iron losses are essentially constant in relation to loading and power factor, while damper cage loss significantly varies with respect to the same aspects. The same considerations can be drawn for the HC4 alternator, whose relative losses at different loadings and power factors are reported in Fig. 58.

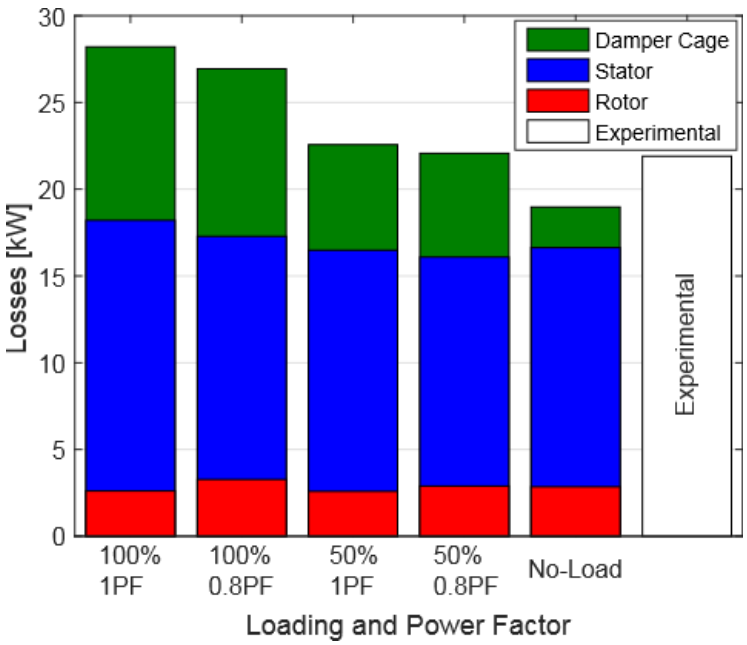


Fig. 57 – Iron losses in the DIG142, at different load levels and power factors.

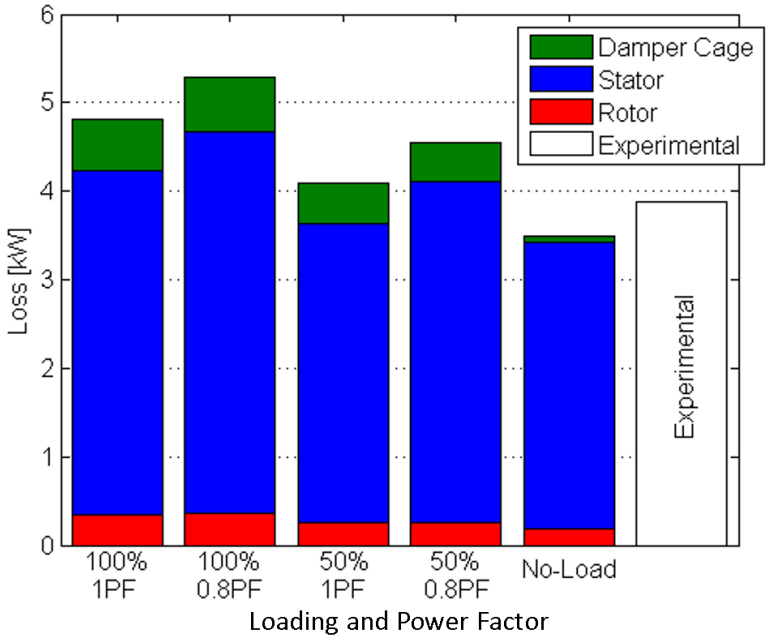


Fig. 58 - Iron losses in the HC4, at different load levels and power factors.

In order to be coherent with the experimental loss determination, the measured and predicted losses are compared only for the no-load condition. A very good similarity between FE and experimental results is observed, with percentage errors of ≈13% and ≈10% being achieved, for the DIG142 and the HC4 respectively.

4.4.5 Skew and its effects

In Section 4.3, the validity of the fast SS FE technique, proposed for the modelling of skewing and its effects in the considered 400*kVA* HC4 SG was proven and validated against the well-known and consolidated AS and MS techniques. Nevertheless, further validation is necessary because of the 3-D nature of the skewing. Hence, experimental measurements have been performed on the HC4 platform. This is briefly described in the next section and tests at several load conditions are then used to compare and validate the

proposed technique. In order to reach a certain level of accuracy, the simulation angle step δ is chosen in such a way that the number of slices used to extrapolate the current and voltage waveforms is equal to 21.

4.4.5.1 Description of the set-up

The experimental platform for the validation of the skewing modelling proposed above consists of an IM drive, acting as the prime mover, whose speed loop controls the frequency of the SG, which is mounted on the same shaft of the motor. A photo of the experimental bench can be observed in Fig. 59.



Fig. 59 – Experimental test bench of the considered SG.

A combination of testing methods including a load bank and the classical back-to-back (slave machine) method were used. For up to half load ratings, the machine terminals are connected to a resistive load bank, consisting of variable resistances whose power can be remotely varied up to $200kW$, thus giving the opportunity of more discretization in the testing samples. The

classical back-to-back method was used to perform measurements at full-load rated operation. All the experimental tests have been carried out with the machine's automatic voltage regulator (AVR) connected in order to maintain the output voltage at its rated value while changing the load.

4.4.5.2 No-load test

The no-load test is performed with the stator terminals open-circuited. The voltage waveforms and harmonics are recorded during the test through a typical power analyser. The voltage THD is evaluated and compared with the calculated value determined through the proposed technique. The results are shown in Table 6 (first row), with an excellent match being achieved at no-load operation.

4.4.5.3 Test at 50*kVA*, 100*kVA* and 200*kVA*, at unity power factor

These tests are performed with the resistive load bank (Y-connected) set at 50*kW*, 100*kW* and 200*kW*, respectively. The voltage waveforms and harmonics are registered during the measurements through a power analyser. The voltage THD is determined and then compared with that evaluated through the SS technique. Table 6 also shows the comparison at different loading levels (referring to the unity power factor rows), where a very good similarity can be observed.

4.4.5.4 Test at 400*kVA*, at 0.8 power factor

This test is carried out with the considered platform's terminals connected to those of the 'slave' machine. The relevant details of this test setup will be shown in Chapter 7. The rated full-load condition has been evaluated, in order to compare the voltage THD between the FE and experimental

evaluations. The last row of Table 6 shows an excellent similarity between the above-mentioned results.

Table 6 – Experimental and FE results: comparison at different loadings and power factors.

Loading – power factor	**Voltage THD**	
	FE	**Experimental**
No-Load	1.26%	1.34%
$50kVA - 1pf$	1.13%	1.19%
$100kVA - 1pf$	1.39%	1.26%
$200kVA - 1pf$	2.44%	2.01%
$400kVA - 0.8pf$	2.17%	1.76%

4.4.5.5 Summary

Experimental tests have been carried out to prove the validity of the SS technique. The results in terms of voltage THD have been compared to the proposed method, resulting in an excellent similarity, which is clearly observable in Fig. 60. In this figure, an important aspect to note is the increasing discrepancy between FE and experimental results, relative to the increasing of the loading level. This is mainly due to the effects of the machine's armature reaction. An important factor to consider is the inaccuracies intrinsically included in the averaging process, inherent to the proposed SS, FE technique. While it is acknowledged that averaging the current induced in the armature windings (and in the damper cage) is conceptually incorrect, it has however been shown to be a reliable approximation. In fact, as shown in Section 4.3, even more complex and

more time-consuming techniques (such as the MS method) produce similar results. Potential improvements can be achieved by increasing the number of slices utilized for modelling the stator skew, i.e. reducing the simulation time step in the SS technique. On the other hand, this would come at the cost of more computational time and resources.

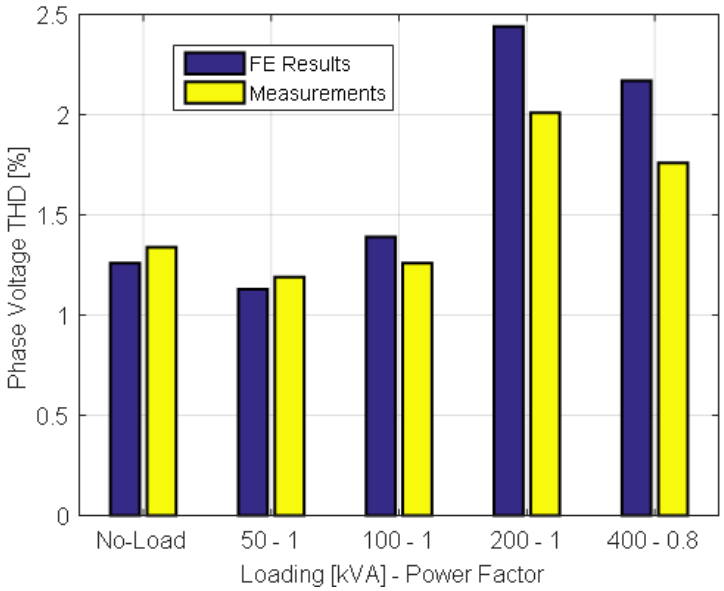


Fig. 60 – Phase voltage THD: comparison between FE and experimental results.

4.5 Conclusions

This chapter dealt with the description, the development and the validation of the FE model built for the electromagnetic analysis of the platforms being considered in this Ph.D. project.

Although it is clear that a 3-D model [109, 110] would be ideal for the electromagnetic analysis of the alternators analysed in this chapter, all the above confirms the validity of the built 2-D FE models of the 4*MVA* and 400*kVA* salient-pole SGs. It can be observed, in fact, that the obtained FE

results, when compared to the experimental ones, give an accurate match at several load conditions and for different power factors.

Figures 47-48 and Figures 51-52 show a comparison in terms of no-load and short-circuit characteristics. From Table 4 and Table 5, a very good agreement can be observed in terms of full-load results. The FE and experimental copper and iron losses are also compared and successfully validated for different loadings and power factors, as reported in Figures 55-58. Finally, the skewing effects on the output voltage THD of the HC4 are evaluated via an innovative technique, whose accuracy and validity can be observed in Table 6 and Fig. 60.

Having fully validated the developed FE tools, these will be used in the next, final stage of this thesis to propose solutions for the reduction of losses, as it was an identified issue for the applications at hand (especially for the DIG142), and for limiting the voltage THD without resorting to the skewing (implemented onto the HC4), as this is an expensive manufacturing technique. Hence, after performing a sensitivity analysis on both the SGs (Chapter 5), a novel damper cage design technique is identified and applied to the platforms being considered in this work (Chapter 6).

4.6 Contributions to research

In this chapter, the main contributions to research are related to

- a comprehensive review and implementation of 2-D FE modelling in salient-pole SGs;

- a fast method to model skew and its effects in SGs featuring such design characteristic.

The validity of the built FE model, confirmed by the excellent match with the experimental tests, has led to investigate specific machine's operating conditions which are different from those described in this chapter. For example, results relative to the single-phase operation of SGs are reported in the following conference publication:

- C. Spagnolo, S. Nuzzo, G. Serra, C. Gerada and M. Galea, "Analysis of salient-pole synchronous generators operating in single-phase condition", *IEEE Workshop on Electrical Machines Design, Control and Diagnosis (WEMDCD)*, 2017.

Referring to the fast model for the analysis of skewing and its effects described in this chapter, the results shown above are also reported in one academic publication in a high impact factor journal. The publication name is given below:

- S. Nuzzo, M. Galea, C. Gerada and N. Brown, "A fast method for modelling skew and its effects in salient-pole synchronous generators", *IEEE Transactions on Industrial Electronics,* 2017.

Chapter 5
Damper cage loss and voltage THD sensitivity analysis

In the previous chapter, a FE model of the 4*MVA* and the 400*kVA* SGs used as case studies to achieve the objectives of this Ph.D. project were built and then validated against experimental results on existing prototypes. The validated tools can now therefore be used to propose a number of design improvement solutions, aimed at addressing the damper cage loss and the voltage THD in both the generators under analysis. This study is carried out in the form of a detailed sensitivity analysis, whose objective is that of capturing the machine parameters that mostly affect the quantities mentioned above.

The first part of this chapter focuses on the DIG142 alternator, with special attention to the damper cage loss reduction, as it was observed that this component plays a significant role on the overall power losses and thus on the machine efficiency. The second part of the chapter describes the sensitivity study carried out on the HC4 machine, where the principal variable investigated is the no-load voltage THD, as the main target here is that of keeping it below the standard value of 3% without resorting to the skewing of the stator.

Considering the above, it is clear how these studies are fundamental for limiting the design space which will be investigated for future, optimization purposes. In fact, the results of this sensitivity analysis will allow to discard a priori the machine design parameters that are less effective on the variables under investigation. On the other hand, the most sensitive parameters will be then kept for the optimization procedure described in Chapter 6.

5.1 Introduction

Having validated the FE model of the considered generators in Section 4.4 of the previous chapter, the next step is to start focusing more in detail on the damper cage loss and the voltage THD in the generators being considered in this work.

Regarding the DIG142, from Fig. 57 (Section 4.4.4), it can be observed how the damper cage loss is a very important contributor to the DIG142 total loss. In particular, almost 30% of the total amount of rotor loss at no-load condition is due to the damper winding and about 27% at full-load rated condition. One of the main reasons for these elevated values of losses is the open slot geometry of the stator of the particular SG (see Fig. 6, in Section 2.4.1). As can be observed in Fig. 61 such a design indicates large variations in the air-gap flux (under the slot openings). The damper cage reaction to these variations results in excessive induced current flows in its bars; thus, a considerable resistive loss is always present in the damper cage, even during the steady state. Having identified the elevated value of losses as an issue for the studied 4*MVA* machine, also confirmed by the high temperatures

(≈180°C) reached by the rotor during normal operation, the next step is that of proposing solutions aimed at reducing the inherent losses. Section 5.3 focuses on these topics, developed in the form of a detailed sensitivity analysis performed for such purposes.

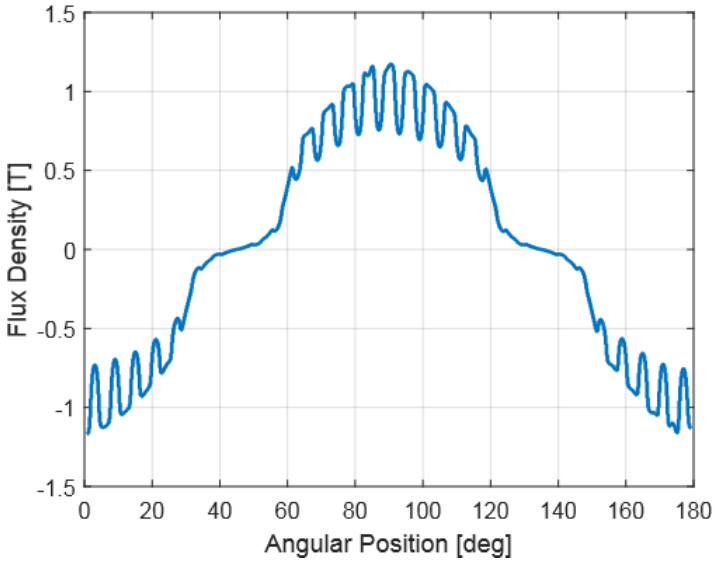


Fig. 61 – No-load, radial airgap flux density of the DIG142.

On the other hand, considering the HC4 SG, Table 6 (Section 4.4.5) shows that the no-load voltage THD is equal to 1.36% when the machine is equipped with a skewed stator, while a skew-less configuration features a THD of 5.58%. This is due to the fact that the slotting harmonics are much attenuated and almost absent in the voltage waveform when skewing is applied, allowing for the THD to be below the standard limit of 3%. This concept is also shown in Fig. 62, where a comparison between the no-load, line-to-line, rated voltages achieved with and without skew can be observed. On the other hand, it can be observed in Fig. 58 and Table 3 (see Section 4.4.4) that the damper cage loss does not significantly affect the overall loss

and efficiency of the machine, in both cases. However, the issues inherently related to the manufacturing aspects of skewing lead to consider possible solutions to overcome the limitations due the THD requirements. Considering this, as well as for the DIG142, a sensitivity analysis is also performed for the HC4 and this is discussed in Section 5.4.

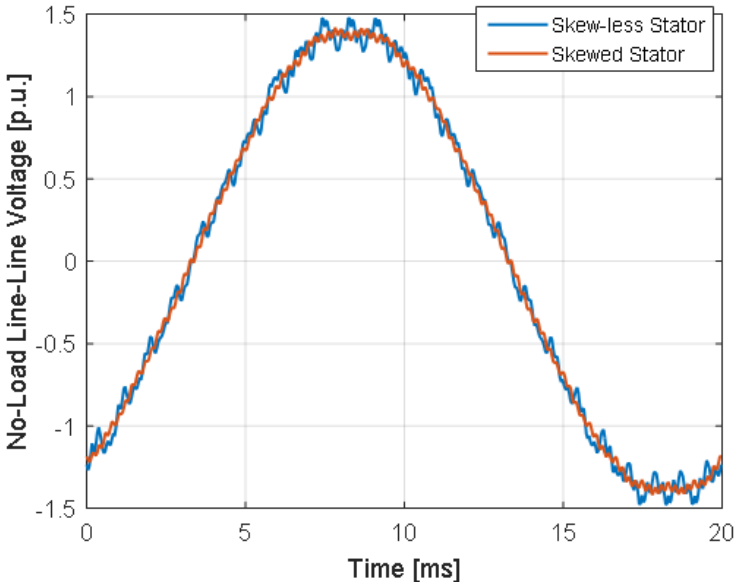


Fig. 62 – Skewed vs. skew-less HC4 stator: comparison between the no-load, line-to-line voltage waveforms.

5.2 The general scheme for the sensitivity analysis

A general scheme of this sensitivity analysis that is performed in this chapter is shown below in Fig. 63, where the interactions between the various inputs, outputs and the design parameters can be observed.

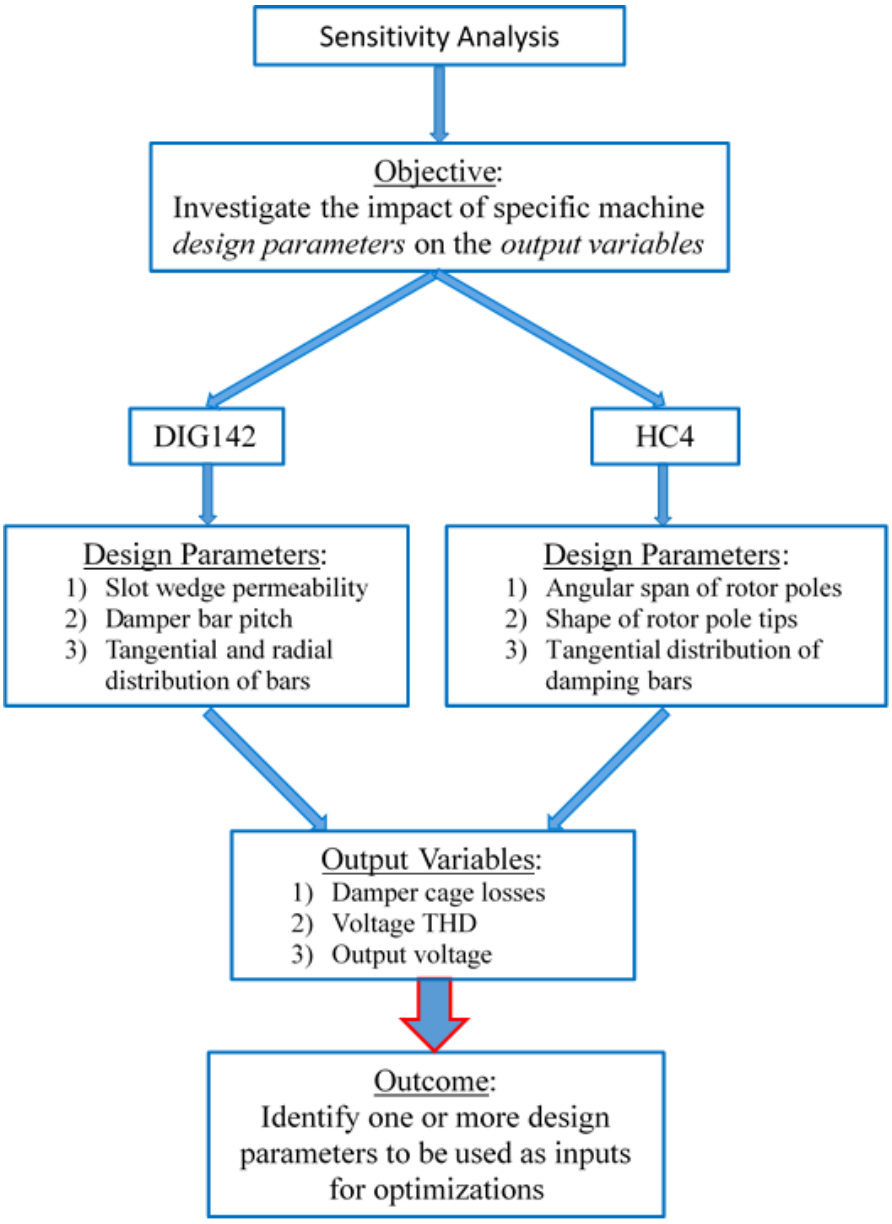


Fig. 63 – High level flowchart of the sensitivity analysis.

5.3 Sensitivity analysis – the DIG142

This section shows the results relative to some proposed design solutions aimed at reducing the losses associated to the damper cage of the DIG142, in the form of a sensitivity analysis. This is essential to identify the parameters that are most sensitive to damper cage loss and voltage THD variations. The

results shown in this section are therefore introductory to setup the optimization procedure which will be described in Chapter 6.

5.3.1 Key parameters

The main key parameters, whose effects on the damper cage losses and on the no-load voltage THD are investigated, are the following:

1) The *magnetic permeability* of the stator slot wedge.
2) The damper *bar pitch*.
3) The *asymmetric displacement* of the damping bars along the tangential direction.
4) The *radial position* of the damper cage

The relevant results are reported in the next sections.

5.3.2 Influence of slot wedge permeability

One way to reduce the heavy "slotting" effect on the air-gap flux density is by using a different material for the slot wedge [111]. In the actual machine, the material employed as the stator slot wedge is Magnoval Fe70, with a relative magnetic permeability μ_r=2.5. By increasing the magnetic permeability of the slot wedge material, the slotting effect considerably decreases [112] on both the rotor surface and the damper bars. Indeed the higher the permeability, the more isotropic is the stator surface which faces the main air-gap. This determines a reduction of damper cage losses. The overall effect of this aspect was investigated by testing the FE model of the 4*MVA* SG for a number of different slot wedge materials, each with its own

permeability value. Fig. 64 shows the reduced slotting effect on the airgap flux density, while the overall results are summarized in Table 7, reporting the damper cage losses calculated at no-load and full-load conditions, respectively. For each case, the no-load line-to-line voltage THD has been also computed, as shown in the fourth column.

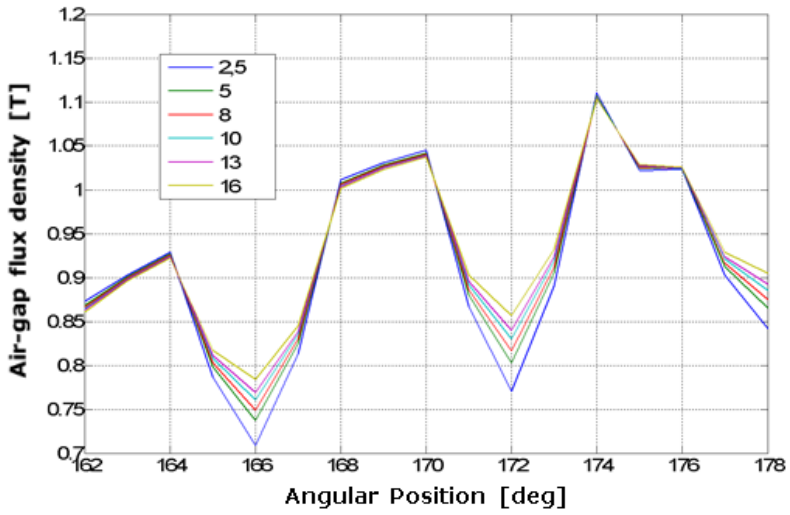


Fig. 64 - Zoom on radial air-gap flux densities: comparison among machines with different slot wedge materials.

Table 7 – DIG412 losses and THD vs. magnetic wedge permeability.

Permeability	**Damper cage loss**		**No-load voltage**
μ_r	**No-load [W]**	**Full-load [W]**	**THD [%]**
2.5	2351	9653	2.57
5	1832	6431	2.05
8	1521	5601	1.83
10	1398	5362	1.75
13	1274	5096	1.68
16	1191	4978	1.63

The relative magnetic permeability ranges from 2.5 to 16, all corresponding to Magnoval-based materials but with a different material composition. For the no-load condition, the cage losses decrease as the magnetic permeability of the slot wedge material increases. It can be noted that the major relative improvement is given by using a magnetic wedge with a relative permeability of 5, leading to a damper cage loss reduction of 23%. A further improvement could be achieved by using a magnetic wedge with μ_r=10, with a reduction of the losses by 40%. Similar considerations can be made for the full-load condition, where the damper cage losses are reduced almost by 33% if μ_r=5 and by about 42% if a material with a relative permeability of 8 or 10 is used. In both cases, a further increase in μ_r does not relate to any significant reduction of losses. A THD reduction of the no-load, line-to-line voltage can also be observed in Table 7. The main drawback of increasing the permeability is the increase of slot flux leakage especially at the full-load operating condition. This results in a less useful flux crossing the air-gap and consequently a higher voltage drop and a torque reduction. Comparing the results of the simulations performed with μ_r=2.5 and μ_r=16 materials, a voltage drop of 5% is found. This can be compensated by an increase of the excitation current at the cost of extra copper losses, which in turn can potentially negate the positive effect of having a higher permeability slot wedge material.

All the above confirms that significant advantages can be achieved by choosing an appropriate material for the slot wedges, where it is advised to

design for a good balance between the quality of the air-gap flux density and the resulting slot flux leakage.

5.3.3 Influence of bar pitch

Another important player in terms of damper cage losses is the effect due to the pitch of the damper bars τ_d, which strongly relates to the stator slot pitch τ_s. Traditionally, this is chosen by applying well-known empirical rules, e.g., it can be varied from $0.8\tau_s$ to $1.2\tau_s$. However, with detailed modern numerical techniques, this can also be analysed in more detail and potentially improved by a considerable margin. Thus, in order to fully understand this aspect, the FE model of the DIG142 SG is modified by varying the bar pitch with the damper cage being kept symmetric with respect to the polar axis. The results show no significant improvements with respect to the case where the original bar pitch is used. On the contrary, the current bar pitch (i.e., 5.7°) is the most appropriate in terms of the loss reduction, as one may note in Fig. 65.

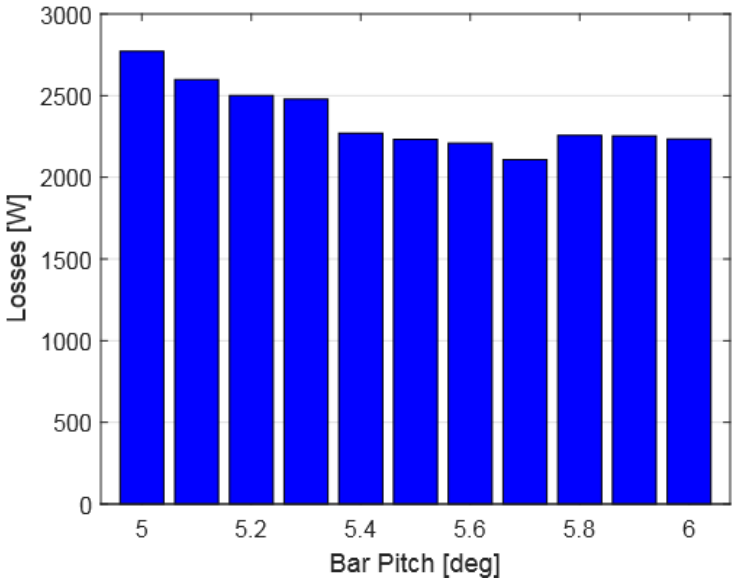


Fig. 65 – No-load damper cage loss vs. bar pitch.

5.3.4 Influence of tangential displacement

In order to improve the voltage THD, the damper cage can be displaced by a particular angle, usually chosen as a fraction of the stator slot pitch, with respect to the polar axis. Some considerations on improved design and analysis of this aspect are presented in [113], with the main focus on the improvement of the machine voltage THD, with no consideration for reducing losses. This geometrical feature can be seen in Fig. 66, where the damper bars are displaced in an asymmetric form over the rotor poles. In the case of the generator being studied in this section, the actual configuration is the one shown in Fig. 66a.

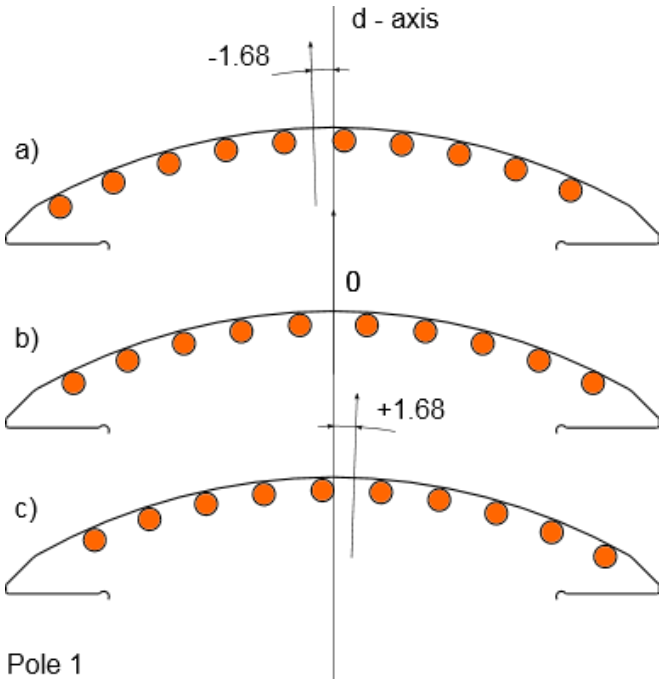


Fig. 66 – Different damper cage positions shifted by: a) -1.68°, b) 0° (symmetrical case) and c) +1.68° with respect to the polar axis.

In order to investigate the effects that this asymmetry has on both the total amount of losses in the damper cage and the voltage THD, a number of tests

by using different positions along the azimuthal direction are performed. In particular, the damper cage angles are varied from 1.68° (corresponding to the original displacement) to +1.68°, (corresponding to the position shown in Fig. 66c). From Fig. 67 and Fig. 68, it can be observed that a symmetrical configuration (position 0°, as shown in Fig. 66b) presents the lowest cage loss with respect to the other tangential positions, but at the same time results in a THD of about 7%, which for the application at hand is not acceptable. On the other side, the original damper winding position is the only one that achieves a THD lower than 3%. Even considering the importance of having a low THD for this application, this is still not an optimal solution because, as shown in Fig. 67, it also presents considerable damper winding ohmic losses, resulting in more heat generation and consequently a deterioration of the total machine efficiency. In particular, with respect to the symmetrical case, losses are increased by 15%.

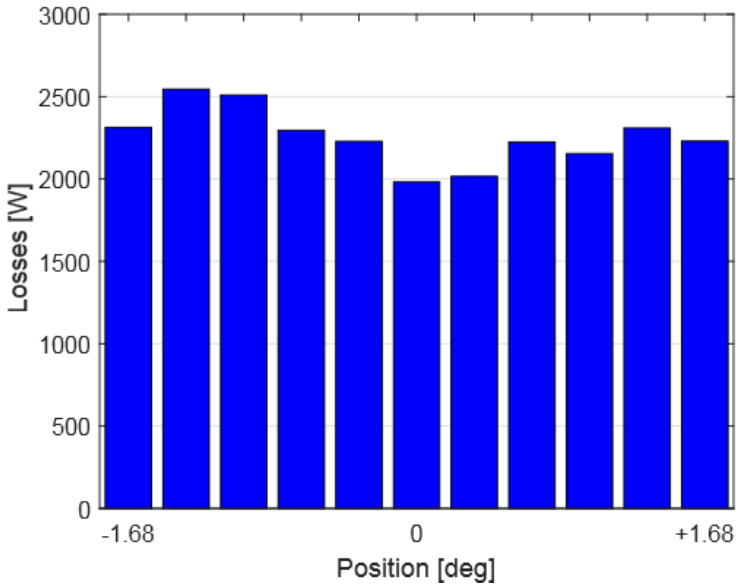


Fig. 67 – No-load damper cage loss vs. tangential position.

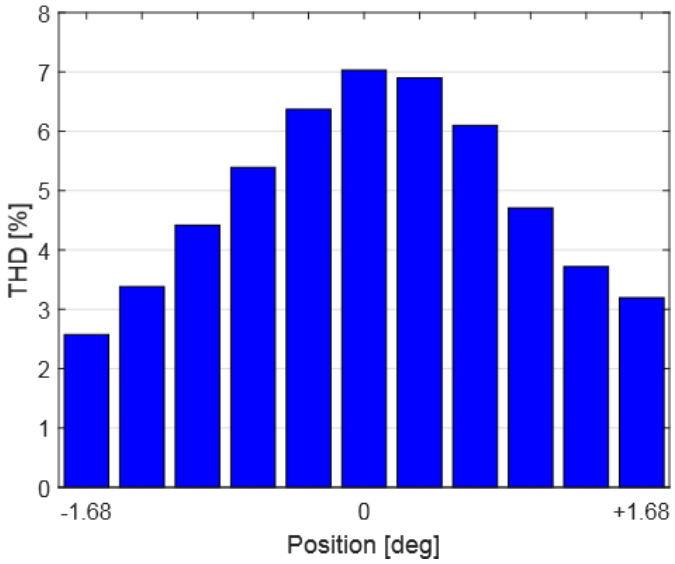


Fig. 68 – No-load voltage THD vs. tangential position.

Considering all the above, it is clear that while the original design of the damper cage meets some of the requirements (THD<3%), significant margins of improvement (mainly in terms of reducing losses) can be achieved.

5.3.5 Influence of radial displacement

While the previous section investigated the effects of moving the damping bars in the tangential direction, considerable variations on the machine performance can also be achieved by increasing the distance of the damper bars from the air-gap, which means that the effects of the open slot configuration would be significantly reduced. With all the above in mind, a sensitivity analysis of the damper winding position along the radial and the tangential directions, as shown by the red rows in Fig. 69, is carried out at the no-load condition.



Fig. 69 - Parametrization of the damper cage position along radial and tangential directions.

As can be observed in Fig. 70, the losses in the damping bars are heavily affected by the radial distance from the air-gap. Fig. 71 shows the resulting total THD for the implemented variations of the radial and tangential position of the bars. It can be concluded that moving the bars further away from the airgap by 1*mm* for an optimal tangential position, the no-load output voltage THD can be improved by 17%, resulting in a damper winding loss reduction of 92.3% at no-load and 43.8% at full-load.

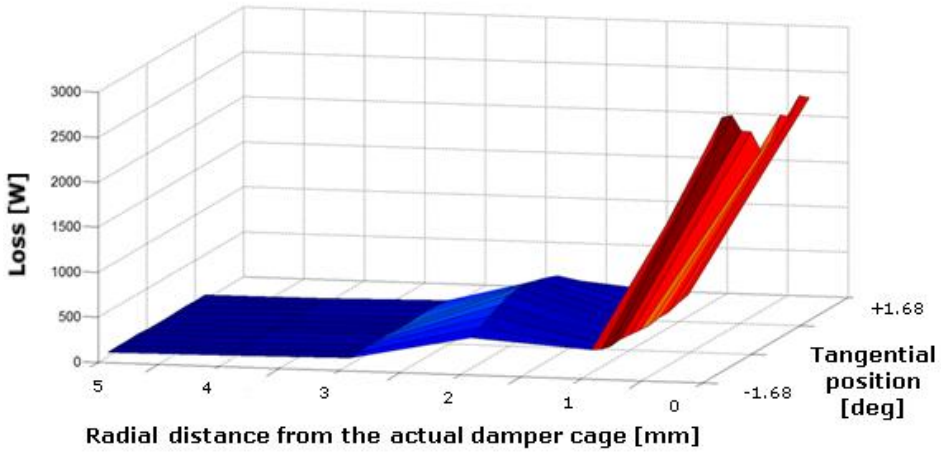


Fig. 70 – Damper cage losses versus radial and tangential positions.

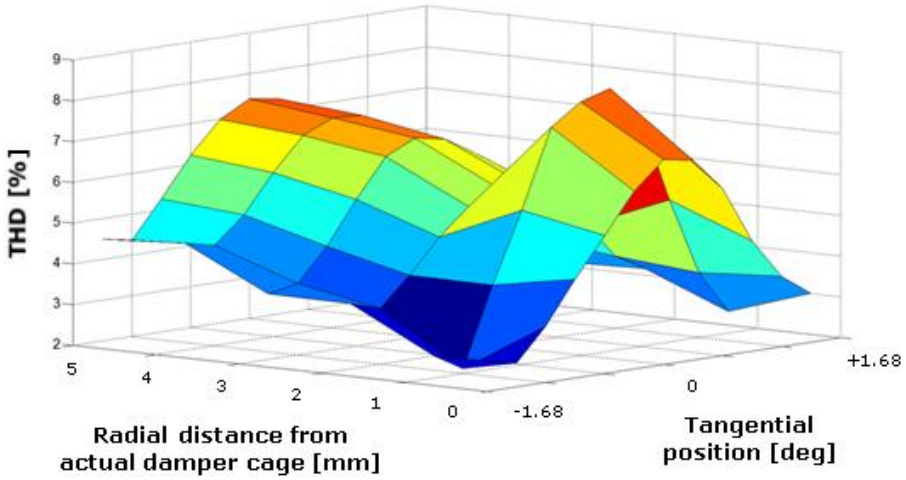


Fig. 71 – Voltage THD versus radial and tangential positions.

5.3.6 Intermediate conclusions

This section investigated possible methods on how to reduce the damper cage losses and improve the output voltage THD in salient-pole SGs. The DIG142 was used as vessel to test these improvement solutions.

- The damper cage loss can be significantly decreased by using a stator slot wedge with an appropriate magnetic permeability. This however comes at the cost of a higher slot flux leakage (especially at full-load operating condition), which in turn propagates other negative effects such as torque reduction.
- The damper bar pitch affects the damper cage loss. For the 4*MVA* SG, it was concluded that the original damper pitch of 5.7° can be considered as the optimal value in terms of loss minimisation.
- There is a very close relationship between the voltage THD and the tangential position of the damper cage. This does produce improvements on the voltage shape, but it also results in higher losses and produces overheating issues.

- Moving the bars along the radial direction (i.e. increasing the distance of the damper cage from the airgap) and placing them in an appropriate tangential position produce benefits in terms of damper cage loss as well as voltage THD. On the other hand, this can lead to a significant modification of the generator behaviour during transient operation, as the relevant inductances are different from those of the original machine.

Considering all the above, it is clear that improvements on the overall performance of the generator can be achieved by optimising the design of this sensitive rotor winding. However, usually this comes at the cost of compromising other machine parameters.

5.4 Sensitivity analysis – the HC4

As well as for the DIG142, a number of design solutions are proposed for the HC4. This section therefore describes the results of a sensitivity analysis aimed at reducing the THD of the no-load voltage waveform of the HC4 generator, without resorting to the skewing of the stator core. The relevant results are essential to work out the design parameters that are most sensitive to voltage THD variations and therefore introductory to setup the optimization procedure which will be described in Chapter 6.

5.4.1 Key parameters

The main key parameters, whose effects on the no-load voltage THD are investigated, are the following:

1) The *angular span* of the rotor poles.
2) The *shape* of the rotor pole tips.
3) The *asymmetric displacement* of the damping bars along the tangential direction.

The relevant results are reported in the next sections. It is worth to mention that, contrarily to what being done for the DIG142 in Section 5.3, the damper cage loss sensitivity analysis is not performed for the 400*kVA* machine for the following reasons:

1) In sections 4.3 and 4.4, it was observed that the damper cage loss in the HC4 is not an important contributor to the overall loss and therefore to the machine efficiency. It was also shown how this loss contributor is not significantly affected by the skewing.
2) While the damper cage loss reduction is the main target for the 4*MVA* SG, the main objective for the HC4 platform is to achieve a THD lower than 3% when a skew-less stator topology is implemented onto it.
3) No significant variations of bar losses were registered by performing the sensitivity analysis of the key parameters listed above.

On the other hand, these design parameter variations may lead to an ensuing output voltage drop, which in turn would deteriorate the overall machine

performance. Considering the above, these aspects are monitored during the sensitivity analysis described in the next sections.

5.4.2 Influence of the pole span

The first parameter considered for the voltage THD sensitivity analysis is the angular span of the rotor poles. From a conceptual point of view, a modification of the rotor angular span results in the variation of the equivalent permeability function $\mu_E(\lambda,\alpha)$ introduced in (9) and shown in Fig. 17 of Section 3.7.1. Here, the actual angular span (i.e. 70°) of the salient poles was investigated and used to define and plot the above mentioned electromagnetic quantity. It can be easily deduced that, if the angular span was to be modified, also the harmonic content of the function $\mu_E(\lambda,\alpha)$ would be significantly altered, resulting in a variation of the inductance matrix $L(\alpha)$ (see (17) in Section 3.5) and thus of the voltage harmonic content, including its fundamental and slotting components. Considering this, it is clear that there is potential for investigating these aspects and, therefore, the angular span of the rotor poles is varied from 65° to 75° in order to evaluate the performance via a FE analysis. Fig. 72 and Fig. 73 show how the THD and the total RMS value of the no-load rated voltage vary with the angular span. The evaluations are carried out considering that no stator skewing is applied to the SG at hand. It can be observed how a span of 73° presents the minimum voltage THD (see Fig. 72), while the maximum RMS value (given in *p.u.* in Fig. 73) is obtained with an angular span equal to 70°, which corresponds to the one of the actual machine. This explains this specific design choice. In fact, although the above study has proven that there is room

for THD improvements by changing the pole angular span, however the THD requirements are achieved by skewing the stator of the considered generator, meaning that the output voltage maximization objective was prioritised at the design stage of the 400*kVA* SG.

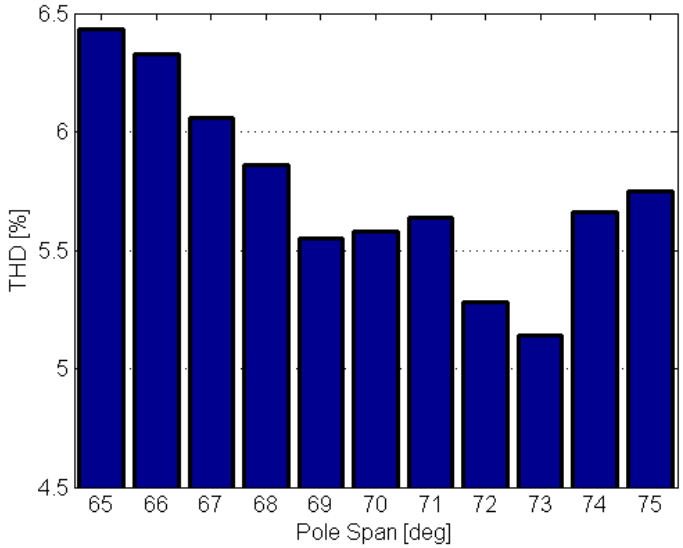


Fig. 72 – Effects of the angular span of the salient poles on the no-load line-to-line voltage THD.

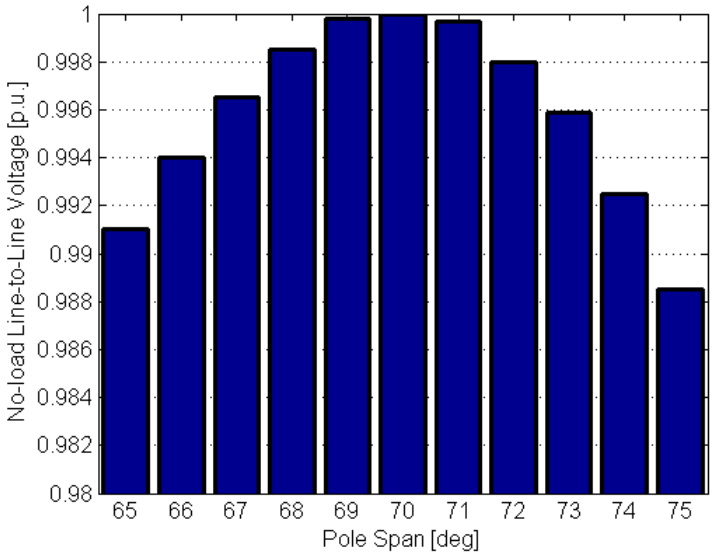


Fig. 73 - Effects of the angular span of the salient poles on the no-load line-to-line output voltage.

5.4.3 Influence of the pole tips shape

The equivalent airgap thickness represents the main machine parameter used by SG's designers to optimise the flux density harmonic content in the airgap. Conceptual observations similar to those outlined in the previous section can be carried out on the effects that this parameter has on the equivalent airgap thickness $\varepsilon_{AG}(\lambda,\alpha)$ defined in Section 3.7.1 (see (18)), which heavily affects the shape of the function $\mu_E(\lambda,\alpha)$. Therefore, the effects on the voltage THD and total RMS of a non-uniform airgap along the salient poles is investigated in this section. The ratio k, defined as the ratio between the airgap thickness g_{max}, evaluated in correspondence of the pole tips, and the airgap thickness g_{min}, evaluated in correspondence of the polar axis, is varied from 1 (i.e. the actual, uniform airgap configuration in the considered machine) to 2. This concept is illustrated in Fig. 74, where these two cases are shown.

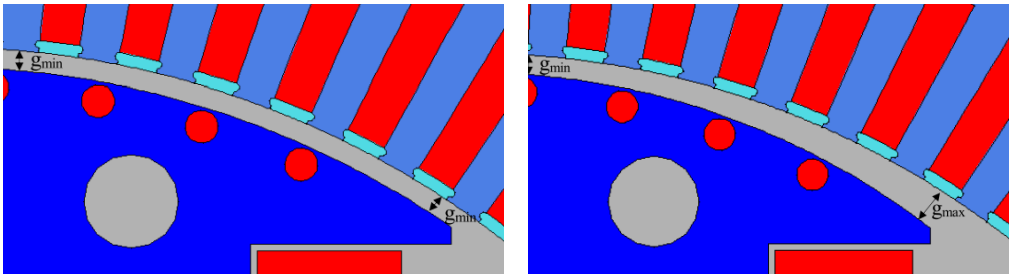


Fig. 74 – Qualitative illustration of the pole tips modifications.

An increased equivalent airgap results in a lower harmonic content of the no-load voltage, as shown in Fig. 75. This is mainly due to the 3rd harmonic reduction in the airgap flux density harmonic amplitude spectrum [24]. On the other hand, the overall THD reduction comes at the cost of a decrease of

the available output voltage at the open-circuited terminals of stator windings. This concept is shown in Fig. 76, where an overall voltage drop of 4% can be observed from the actual configuration (at *k=1*) to the maximum considered ratio value (i.e. *k=2*) analysed in this sensitivity study.

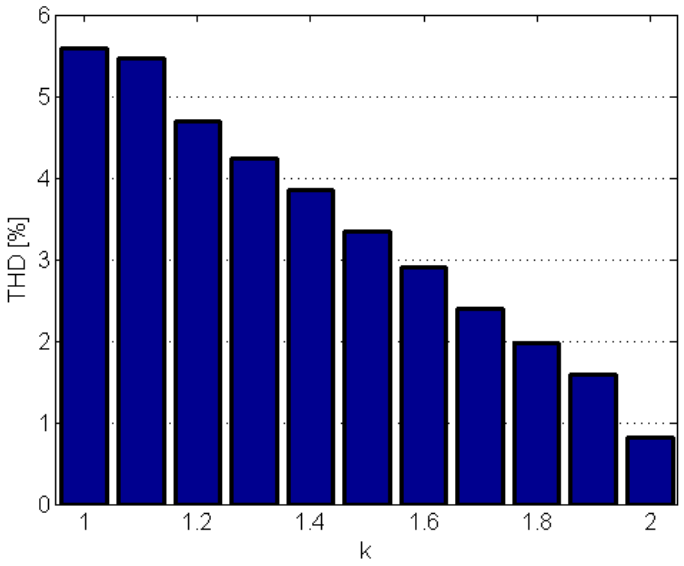


Fig. 75 - Effects of the g_{max}/g_{min} ratio on the no-load line-to-line voltage THD.

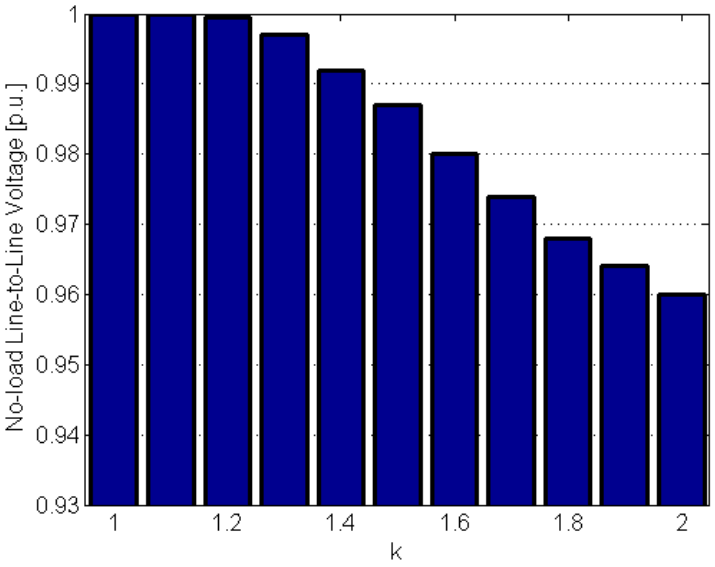


Fig. 76 – Effects of the g_{max}/g_{min} ratio on the no-load line-to-line output voltage.

It can be therefore concluded that the equivalent airgap thickness, although very effective from a THD reduction perspective, is disruptive from the point of view of maximising the available output voltage at the generators' terminals.

5.4.4 Influence of the tangential bar displacement

The HC4 alternator is equipped with a symmetrical damper cage embedded in the rotor poles (see Fig. 8, in Section 2.4.2). In Section 5.3.4, the influence of displacing the damping bars asymmetrically with respect to the polar axis was investigated for the DIG142 SG. It was shown that moving the bars along the tangential direction can be beneficial for the no-load voltage waveform, however at the cost of increasing the damper cage losses. A very similar analysis is performed for the HC4 SG in this section, where the effects of tangentially displacing the bars on the voltage THD, the total RMS and the bar losses are studied. All the bars have then been moved in a uniform direction from -6° to +6° with respect to the original position, according to the concept shown in Fig. 66 and relative to the DIG412 alternator (see Section 5.3.4). Fig. 77 indicates that the line-to-line voltage THD can be reduced by 1.5% by moving the bars tangentially to both sides by 3.3 degrees, confirming that this technique can be powerful in applications where THD requirements have to be met. Also, in opposition to the results shown in Section 5.3.4 for the DIG142, no significant variations of the damper cage loss as well as of the total RMS values are registered (and thus the relative results are not shown in this section) during this investigation for the HC4 generator. This is due to the fact that this machine presents a

constant airgap thickness along the whole tangential length of the polar shoes, making the bars less sensitive to the field variations than they are in the DIG142 generator.

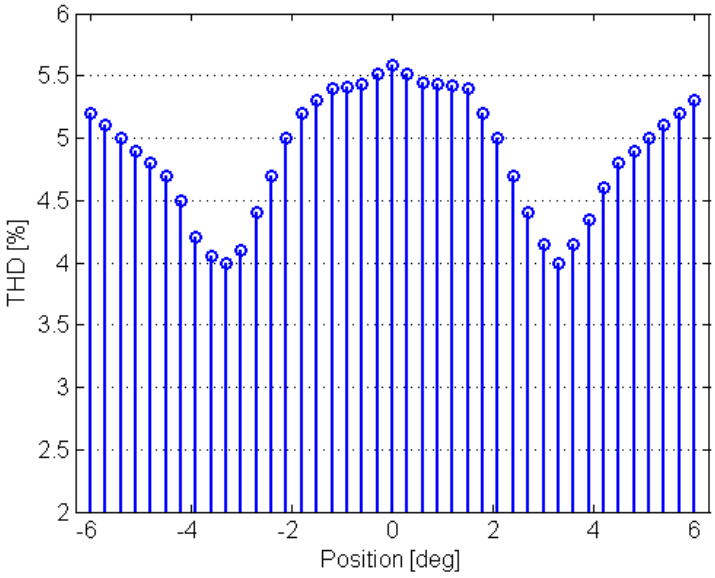


Fig. 77 – Effects of the tangential position of the damping bars on the no-load line-to-line voltage THD.

5.4.5 Intermediate conclusions

The objective of Section 5.4 was that of investigating methods potentially beneficial for THD reduction purposes in salient-pole SGs. In particular, as vehicle to carry out this study in the form of a sensitivity analysis, the HC4 was considered. The main results of this investigation are the followings:

- By varying the span of the rotor poles, an optimal angle does exist which minimises the no-load voltage THD. However, this optimal solution does produce a voltage drop at generators' terminal of ≈1% with respect to the original angular span (i.e. 70°), which instead is an optimum in terms of output voltage maximisation.

- By applying a non-uniform airgap for this machine, i.e. modifying the shape of the rotor pole tips, a significant reduction of the THD is observed, but at the cost of significantly deteriorating the terminal voltage. An important benefit of this technique is the reduction of the 3rd harmonic of the airgap flux density, which may allow one to consider a different stator winding configuration for the application at hand.
- By altering the tangential position of the damper bars by 3.3° with respect to the original position gives a 1.5% reduction of the voltage THD. Also, for the application at hand, no significant variations in the available output voltage is observed. This confirms that there is a very close relationship between the voltage THD and the tangential position of the damper cage.

The above study, performed on the HC4 generator, has confirmed that improvements on the overall performance of the machine can be achieved by optimising the design of such a sensitive rotor damper winding. The study has also confirmed that usually this comes at the cost of compromising some other machine parameters, such as the output voltage. The overall aspects that led to consider the modulated damper as a means to overcome these challenges are highlighted in the next, conclusive section of this chapter.

5.5 Conclusions

Chapter 5 proposes a methodology for a comprehensive sensitivity analysis of SGs and reports the results performed through FE evaluations of the considered platforms. The aim of this study was that of investigating the machine design parameters (mainly those related to the damper cage of such alternators) which mostly affect the damper cage loss and the THD of the no-load output voltage, that are the aspects identified as challenges in this work.

Some intermediate, conclusive considerations were highlighted in sections 5.3.6 and 5.4.5, relevant to the investigations carried out on the DIG142 and the HC4, respectively. However, a few aspects need further attention. These include the following:

1) Amongst all the investigated variables, the relocation of the bars along the tangential direction is the most effective method for THD reduction. On the other hand,
    a. for the DIG142, this comes at the cost of inducing more elevated currents in the damping bars, which in turn produce losses associated with this sensitive rotor winding;
    b. for the HC4, although the bar losses and the output voltage are not compromised, the 1.5% THD improvement is not sufficient to avoid the resorting to the skewing, as the 3% requirement is still not achieved.
2) Although some of the investigated variables (such as the slot wedge permeability, the radial bar position, the pole span and the pole tips

shape) have shown potential for addressing damper cage loss and THD requirements,

a. they either come at cost of unacceptable voltage drops at the generators' terminals or produce a different dynamic response of the damper cage during transients;
b. they would cause a significant change in the manufacturing process of such machines, which is against the goal of this project as well as the company's requirements and objectives.

Considering all the above, in order to meet the loss and the THD requirements for both the generators (while keeping the same dynamic performance and an unchanged manufacturing procedure), it is proposed to apply the modulated damper cage concept identified as "the proposed solution" in Section 1.1.3. In order to achieve an optimal solution, a GA-based optimization tool is built with the purpose of minimising the bar losses and the voltage THD, by giving more weight to the former for the DIG142 SG and to the latter for the HC4 SG. All these aspects will be presented in the next chapter.

5.6 Contributions to research

In this chapter, the main contributions to research are related to a comprehensive review and implementation of methods to improve efficiency and power quality in SGs. A methodology for executing a comprehensive sensitivity analysis for SGs was introduced and used to address some challenges on the considered platforms. The results shown in this chapter are

also reported in two academic publications, both in high profile conferences. These works are relative to the DIG142 (Section 5.3) and to the HC4 (Section 5.4) sensitivity analyses, respectively. The publication names are listed below:

- S. Nuzzo, M. Galea, C. Gerada, D. Gerada, A. Mebarki and N. Brown, "Damper cage loss reduction and no-load voltage THD improvements in salient-pole synchronous generators", *IET 8th International Conference on Power Electronics, Machines and Drives (PEMD)*, 2016.
- Y. Wang, G. Vakil, S. Nuzzo, M. Degano, M. Galea, C. Gerada, H. Zhang and N. Brown, "Sensitivity analysis for performance and power density improvements in salient-pole synchronous generators", *IEEE Workshop on Electrical Machine Design, Control and Diagnosis (WEMDCD)*, 2017.

Chapter 6

An improved damper cage for the considered salient-pole synchronous generators

In order to meet modern power quality requirements and to improve the overall efficiency and performance of such "classical" machines, an improved amortisseur winding topology for SGs is proposed and investigated in this chapter.

In the previous chapters, FE models of the 4*MVA* and the 400*kVA* SGs used as vessel to study the proposed concepts were first built and then validated against experimental results. The validated models were then used to propose a number of improved design solutions and to perform a sensitivity analysis aimed at reducing the design space for the investigation of the proposed concept. The results confirmed that there is room for efficiency and power quality improvements by optimising the design of the damper windings. In order to achieve an optimal solution, a GA-based optimization tool is implemented in this chapter.

First, the modulated damper cage concept is described in detail and its perceived advantages on bar losses and voltage THD are presented through preliminary analytical considerations. The DIG142 alternator is then firstly studied. A new, modulated topology which addresses the requirements for

lower loss components is found, without compromising the acceptable values of the output voltage THD. The performance of the optimised machine is compared to the original design both at a steady state and transient operating conditions. Due to the dimensions of the 4*MVA* generator and the ensuing economic effort necessary to implement the new damper cage topology onto it, the proposed concept is then applied to the 400*kVA*, HC4 generator. The optimal topology achieves a no-load voltage THD lower than 3% even with a skew-less stator structure. These aspects are all discussed in this chapter, while the manufacturing of the rotor prototype for the skew-less HC4 and the relevant experimental results will be shown and discussed in Chapter 7.

6.1 Damper cage modulation

All the studies shown in the previous chapters show that for certain aspects, there is a significant room for improvement by modifying the design of the damper cage windings. To reduce the losses in this winding, while maintaining the voltage THD at an acceptable limit, it is proposed to modify the positioning of the bars in the context of having a modulated bar pitch. This concept consists of having unconventionally displaced damper bars along the salient pole. In other words, when the bar pitch β_i is constant and equal to β_{i+1}, with $i=0,\ldots,9$, the damper cage is equally distributed. When the bar pitch is variable, with $\beta_i \neq \beta_{i+1}$, the winding can be called "modulated damper cage" and looks like the scheme illustrated in Fig. 78b. By applying this solution to the particular SG analysed, the irregular damper bar pitch

interacts with the stator open slot structure in such a way that the air-gap parasitic harmonics are reduced.

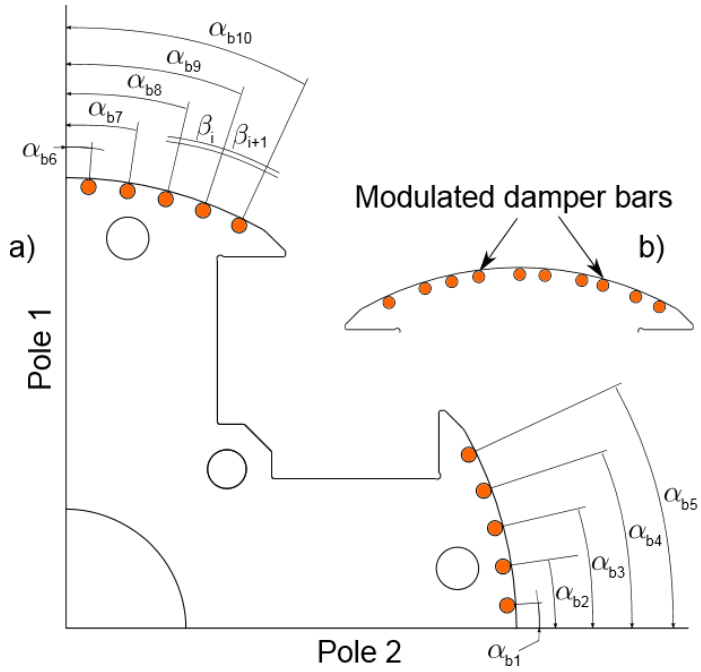


Fig. 78 – Input parameters of the damper cage optimizations: a) α_{bi} with $i=1,\ldots,10$ and b) modulated damping bars concept ($\beta_i \neq \beta_{i+1}$).

The next section describes some preliminary analytical considerations aimed at studying the perceived advantages of repositioning the bars along the salient poles of SGs. For such purposes, the equivalent-circuit-based approach described and implemented in Chapter 3 is used and further developed in this section to show how damper cage losses and voltage THD can be affected by a customised, modulated damper bar distribution.

6.1.1 Perceived advantages

An innovative way of modelling symmetrical damper windings in SGs was presented in Section 3.6.1. As the main aim of this section is that of investigating the perceived advantages of modulating the damping bars, the

symmetric properties are not a priori verified. Thus, the classical approach of modelling SGs as "$m+1+(n_b+1)$" (where m and n_b are the number of stator phases and rotor bars, respectively) circuits magnetically coupled to each other is used for the purposes of this section. In particular, it is common to model the damper cage as "n_b+1" loops [114]. This allows the voltage equations to be derived in the matrix form as given in (29). Neglecting the saturation effects in the soft magnetic parts of the machine, the analysis can then be dealt with as magnetically linear and (29) can be developed and described by (30).

$$\bar{v}(t) = R\bar{\imath}(t) + \frac{d\bar{\psi}(t)}{dt} \tag{29}$$

$$\bar{v}(t) = R\bar{\imath}(t) + \left(\frac{\delta L(\alpha)}{\delta \alpha}\bar{\imath}(t)\right)\frac{d\alpha}{dt} + L(\alpha)\frac{d\bar{\imath}(t)}{dt} \tag{30}$$

In (30), α is the mechanical variable associated with the rotor position, and R and L are $(m+n_b+1)\times(m+n_b+1)$ matrices containing all the resistances, and the self- and mutual-inductances that characterise the machine. It can be observed that, if the phase resistances and the state variables (i.e. currents and position) are known, then the machine performance is directly related to the inductance matrix. An expression for the inductance was derived in Section 3.5 and, for the sake of clarity, it is recalled in (31), where l is the axial length of the machine, λ the angular reference frame locked to the rotor and normalised over the electrical period and $\bar{N}_E(\lambda,\alpha)$ is the vector of the equivalent WFs of the phases. The equivalent WF $N_{Ej}(\lambda,\alpha)$ of the generic phase j was defined in (14) by the difference between the WF $Nj(\lambda,\alpha)$ and its

mean value weighted over the equivalent permeability function $\mu_E(\lambda,\alpha)$, which is re-given in (32).

$$L(\alpha) = l \int_0^1 \mu_E\,(\lambda,\alpha)\; \bar{N}_E(\lambda,\alpha)\; \bar{N}_E^T(\lambda,\alpha)\; d\lambda \tag{31}$$

$$\mu_E(\lambda,\alpha) = \mu_0\; \frac{2\,\pi\, r_G(\lambda,\alpha)}{\varepsilon_G(\lambda,\alpha)} \tag{32}$$

In (32), μ_0 is the permeability of the free space, and $r_G(\lambda,\alpha)$ and $\varepsilon_G(\lambda,\alpha)$, defined in Section 3.4.3, represent the air-gap radius and thickness, respectively evaluated along the tangential direction. In order to investigate the slot ripple harmonics and their associated effects on the performance of SGs, (31) needs to be further elaborated. As most electrical machines, including SGs, exhibit an intrinsic symmetry that turns into a periodical trend of *1/p* of all the quantities involved in (31), these can be developed into a Fourier series with respect to λ. The geometrical quantities involved in the (32) also have a periodicity which is half of that of the WFs of the vector $\bar{N}_E(\lambda,\alpha)$. Hence, considering one generic element of the inductance matrix, (31) can be written as shown in (33).

$$\begin{aligned} L_{ij}(\alpha) = l \int_0^1 & \left(\sum_{h=0}^{+\infty} {}^{h}\mu_E(\alpha) \cos\left(2\pi p h \left(\lambda - {}^{h}\lambda_E(\alpha)\right)\right)\right) \\ & * \left(\sum_{r=1}^{+\infty} {}^{r}N_i(\alpha) \cos\left(2\pi p r \left(\lambda - {}^{r}\lambda_i(\alpha)\right)\right)\right) \\ & * \left(\sum_{s=1}^{+\infty} {}^{s}N_j(\alpha) \cos\left(2\pi p s \left(\lambda - {}^{s}\lambda_j(\alpha)\right)\right)\right) \end{aligned} \tag{33}$$

Considering that the amplitudes of the Fourier components shown in (33) do not depend on the rotor position, then the final expression for the inductances can be written as given in (34).

$$
\begin{aligned}
L_{ij}(\alpha) = l \left(\sum_{h=1}^{+\infty} \frac{{}^{0}\mu_E \, {}^{h}N_i \, {}^{h}N_j}{2} \cos\left(2\pi p h \left({}^{h}\lambda_i(\alpha) - {}^{h}\lambda_j(\alpha) \right) \right) \right) \\
+ \sum_{\substack{h,r,s=1 \\ h=s-r}}^{+\infty} \frac{{}^{0}\mu_E \, {}^{r}N_i \, {}^{s}N_j}{4} \cos\Big(2\pi p \Big(h \, {}^{h}\lambda_E(\alpha) + r \, {}^{r}\lambda_i(\alpha) \\
- s \, {}^{s}\lambda_j(\alpha)\Big)\Big) \\
+ \sum_{\substack{h,r,s=1 \\ h=r-s}}^{+\infty} \frac{{}^{0}\mu_E \, {}^{r}N_i \, {}^{s}N_j}{4} \cos\Big(2\pi p \Big(h \, {}^{h}\lambda_E(\alpha) - r \, {}^{r}\lambda_i(\alpha) \\
+ s \, {}^{s}\lambda_j(\alpha)\Big)\Big) \\
+ \sum_{\substack{h,r,s=1 \\ h=r+s}}^{+\infty} \frac{{}^{0}\mu_E \, {}^{r}N_i \, {}^{s}N_j}{4} \cos\Big(2\pi p \Big(h \, {}^{h}\lambda_E(\alpha) - r \, {}^{r}\lambda_i(\alpha) \\
- s \, {}^{s}\lambda_j(\alpha)\Big)\Big)
\end{aligned}
\tag{34}
$$

The last three summations in (34) show that only the harmonics that comply with the relationship $h \pm r \pm s = 0$ contribute to the machine's inductances. For the sake of this study, slot ripple harmonics are of critical importance. Considering all the above, it is clear that in order to reduce these slotting effects, one may act on any of the quantities involved in (34). One possible option may be the repositioning of each damper bar along the salient poles of the machine, as this results in a modification of the following quantities:

- self- and mutual-inductances of the rotor damper windings $L_{b_i b_j}$;
- mutual-inductances between the damper windings and the stator circuits $L_{b_i s_j}$;
- mutual-inductances between the damper circuits and the field winding $L_{b_i r}$.

If (29) was to be written in its full form, it can then be observed that only the terms $L_{b_i s_j}$can affect the stator voltages. However, all of these terms, i.e. $L_{b_i b_j}$, $L_{b_i s_j}$ and $L_{b_i r}$ can have an impact on the damper cage currents. If the amplitudes ${}^{r}N_i$, ${}^{s}N_j$ and the phases ${}^{r}\lambda_i$, ${}^{s}\lambda_j$ involved in (34) are modified, then this can potentially result in improvements of

- the stator voltage waveforms, by minimising the harmonic components whose order comply with the relationship $h \pm r \pm s = 0$,
- the damper cage currents, by minimising the term $\frac{d\psi(t)}{dt}$ present in (29) and developed in (30).

An example of how one damper WF can be modified by repositioning two bars is shown in Fig. 79. The effects of this modification on the amplitude and phase spectra of the WF can also be observed.

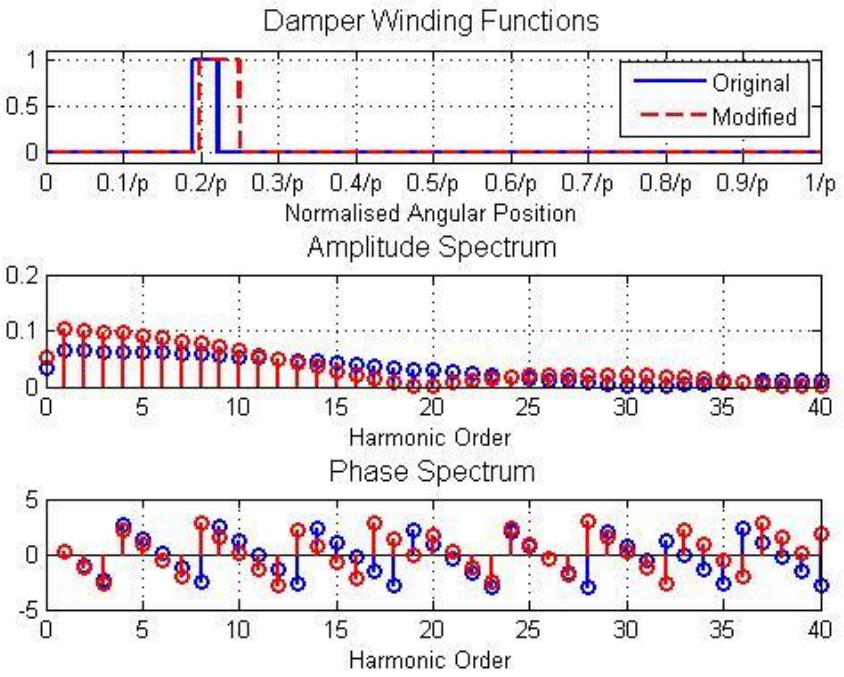


Fig. 79 – Modulated damper winding function and its effect on harmonics.

Considering the above preliminary analysis, it is clear that there is room for performance improvements by modulating the damper bar pitch of SGs. It can also be noticed that, due to the high number of bars-per-pole in both the considered generators, there is a significant amount of combinations that can potentially result in THD and damper cage losses improvements. In order to achieve more accurate and reliable solutions, FE-based analysis is used to investigate all the possible configurations that the damper winding can assume. The optimal solutions are achieved by carrying out GA-based optimisations, according to the procedure described in the next section.

6.2 Investigation with modulation – the DIG142

In Section 6.1, it was shown how the implementation of a modulated damper cage onto salient-pole SGs can be significantly beneficial for addressing losses and THD requirements in such classical machines. As vehicle to confirm such perceived advantages, the proposed technique is firstly investigated onto the DIG142 alternator. This section thus presents the FE-GA-based optimization procedure and the results relative to this 4*MVA* machine. The obtained optimal solution is finally compared to the existing generator, showing excellent achievements in terms of loss and THD improvements.

For the sake of completeness, it is worth to mention that the GA-based, commercial software *modeFRONTIER* of *ESTECO* is utilised for the optimizations. Main reason of this choice is due to the flexibility of the software in terms of "interoperability" with any other application. In particular, from this GA-based environment, it is possible to run Matlab scripts, which in turn generate in MagNet (through its *ActiveX* features described in Section 4.1.1) the geometries representing the individuals of the GA.

6.2.1 Input parameters

In order to take advantage of the geometrical periodicities of the synchronous machine under analysis (i.e., to reduce computational times), odd periodic boundary conditions are used in the model and coupled to the damper winding circuit, in order to be consistent with the fact that the fields and

signals should reverse when going from the modelled part of the device to one of its neighbouring un-modelled parts. In other words, an additional short-circuiting branch (shown in red in Fig. 80) is included in the electrical circuit associated to the damper cage winding. Only *1/4-th* of the machine is therefore considered in the FE model. This results in only ten design variables (i.e. the bars embedded in one salient pole) being considered and used as input parameters. The design variables are shown in Fig. 78a, in Section 6.1.1. They are constrained in such a way that two consecutive bars never interfere with each other.

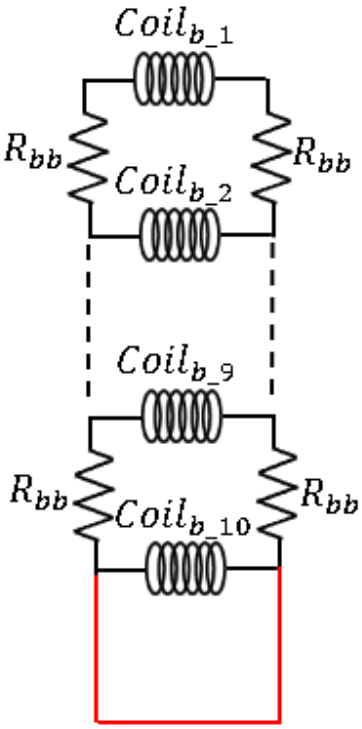


Fig. 80 – Damper cage circuit coupled to the FE model, when odd periodic boundary conditions are used.

6.2.2 Optimization strategy

A general introduction to GAs is reported in Appendix 2, whereas in this section only the optimization strategy relative to the application at hand is presented. The optimization process is initialized by a preliminary exploration of the design space. This phase is performed by using design of experiments (DoE) techniques [115, 116]. DoE is a methodology that maximizes the knowledge gained from experimental data. It provides a strong tool to design and analyse experiments, it eliminates redundant observations and reduces the time and resources to make the experiments. Hence, DoE techniques allow the user to try to extract as much information as possible from a limited number of test runs. Although this methodology is used in many applications, in this work DoE provides to the optimization algorithm an initial population of 50 designs. In particular, a DoE based on a random sequence is used to find an assignment to each input variable in such a way that all constraints are satisfied.

The second phase of the procedure consists in performing a preliminary optimization by using a Multi-Objective Genetic-Algorithm (MOGA). The algorithm is based on a scheduler designed for fast Pareto convergence, whose main features are

1) support geographical selection and directional crossover;
2) implements elitism for multi-objective search, allowing to preserve some excellent solutions without bringing the premature convergence to local-optimal frontiers;
3) enforces user defined constraints by objective function penalisation;

4) allows generational evolution;
5) allows concurrent evaluation of independent individuals.

Also, MOGA [117] requires only very few user-provided parameters, several other parameters are internally settled in order to provide robustness and efficiency to the optimizer.

In the end, a refinement is performed by using the best solutions of the previous iteration. In other words, the best 50 solutions of the first, preliminary optimization are used as initial population for this second iteration by implementing a user-defined DoE. Results have shown that only two iterations are sufficient to find an optimal solution.

6.2.3 Output variables

As highlighted in the previous section, a multi-objective GA is used for investigating possible design solutions aimed at reducing the total amount of the damper cage loss and, at the same time, maintaining the THD of the no-load voltage the same as the original machine. Therefore, these two output variables (i.e. the objectives of the GA) are investigated and the objective type was set to “minimise”, as this is the goal of the optimisation process for the application at hand. All the FE-based tests were performed at no-load operating condition and the best solutions analysed at full-load in a successive step. Both the objectives are constrained by the following expressions:

$$\sum_{i=1}^{n_b} R_{b_i} I_{b_i}^2 < 2000W \tag{35}$$

$$100 \frac{\sqrt{\sum_{i=2}^{n_h} V_i^2}}{V_1} < 3\% \tag{36}$$

The left-hand sides of (35) and (36) represent the damper cage loss and the THD calculations, respectively. The right-hand sides represent the imposed threshold values. In particular, in (35), R_{bi} is the resistance of the *i*-bar that takes into account the skin effect due to parasitic harmonics and I_{bi} is the value of the current flowing into the *i*-bar once the steady state is reached. In (36), n_h is the number of harmonics used to evaluate the Fourier series decomposition of the no-load line-to-line voltage, whose fundamental is indicated as V_1 and higher harmonic components as V_i. Priority has been given to the loss minimization for which a threshold value lower than the actual no-load cage loss was assigned. On the other side, it is sufficient that the THD is kept under the permissible limit of 3%.

6.2.4 Optimization results

The results obtained from the modulated damper cage optimization are shown in Fig. 81. Few designs satisfy the objective constraints (35) and (36), as highlighted in the target area. Most of them have a damper cage design with a similar geometry and therefore THD and losses are very close to each other. Among the best solutions, the one presenting the minimum amount of losses, while maintaining the same THD as in the current generator, has been selected for the comparison with the actual design. The rotor topology of the

best machine obtained is highlighted in the red square (Fig. 81) and shown in Fig. 82, where the particular pattern of the bar pitch modulation can be observed.

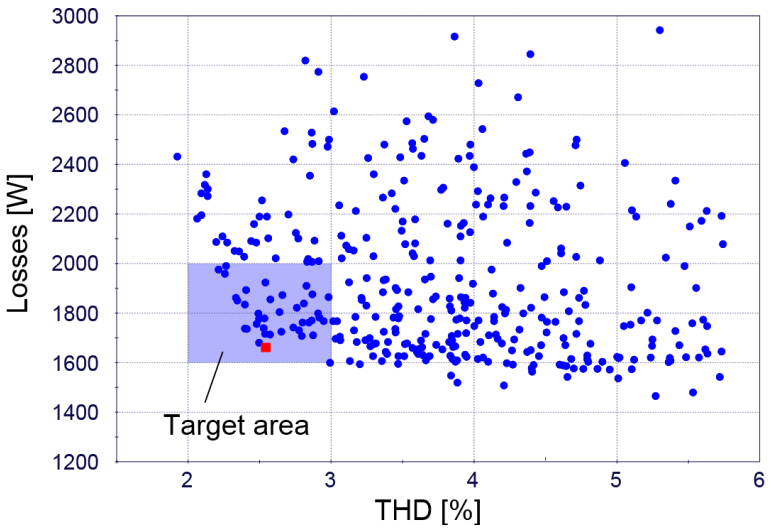


Fig. 81 – No-load damper cage losses vs. THD: optimization solutions.

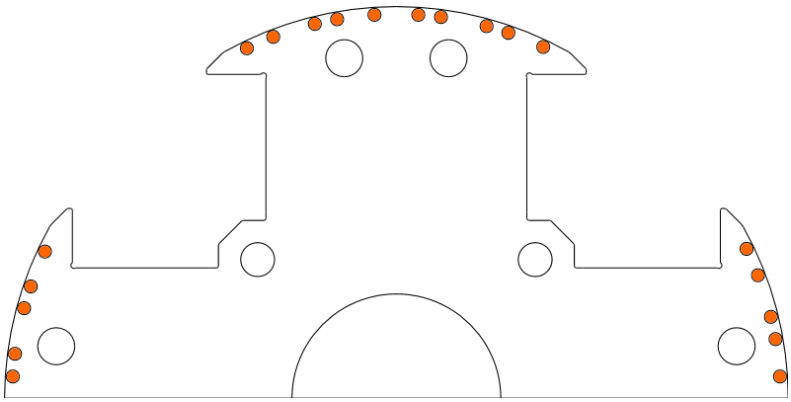


Fig. 82 – Optimal damper cage solution for reduced losses and THD.

6.2.5 Final proposed solution

A comparison between the actual and optimized damper bar losses in one salient pole is shown in Fig. 83. The bar numbering goes counter clockwise looking at the investigated salient pole. One may observe a considerable ohmic loss reduction in bars 3, 6, and 7. While losses have not been reduced

in all the bars (i.e., 4 and 5), the total amount of losses has been strongly attenuated. Fig. 84 shows a comparison between the currents in bar 6 of the original and the improved damper windings, where it can be observed that a strong current reduction has been achieved with the optimal solution.

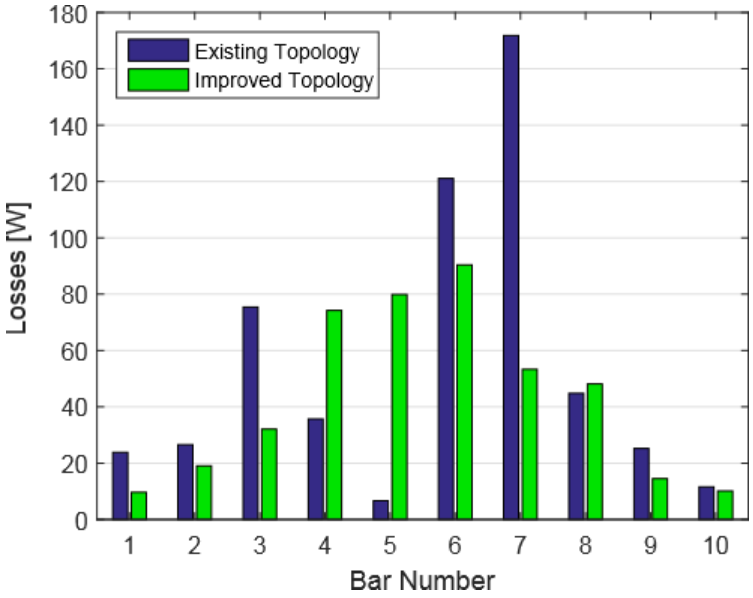


Fig. 83 – Bar losses comparison between the actual and the improved designs at no-load operating condition.

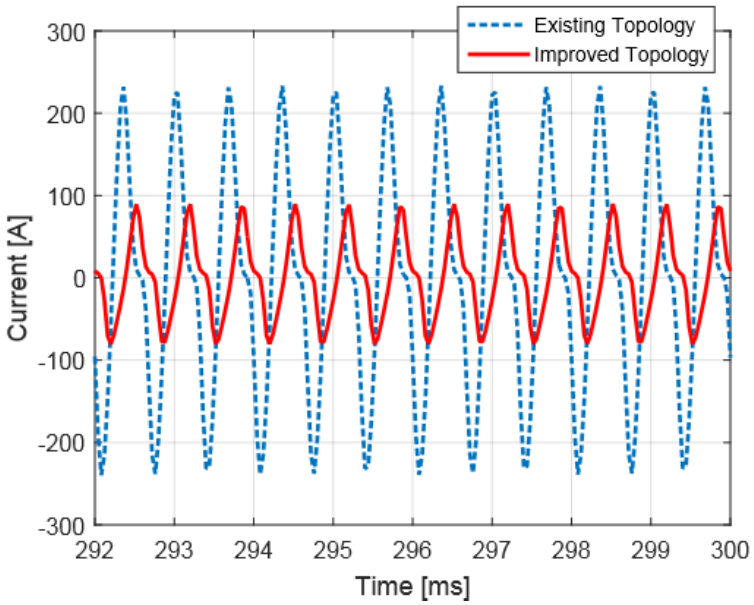


Fig. 84 – Currents in bar 6: comparison existing and optimal damper cages at no-load operating condition.

The same qualitative results are obtained at the full-load operation. In Fig. 85, ohmic losses in each bar are compared for the existing and the optimal topologies. At the no-load condition, there are few bars in the new cage with higher losses than in the existing design, i.e., bars 4 and 5, but the total loss in the whole damper cage has been reduced. Also, it can be noticed that the most loaded bars are the ones on the right-hand pole tip, due to the armature reaction.

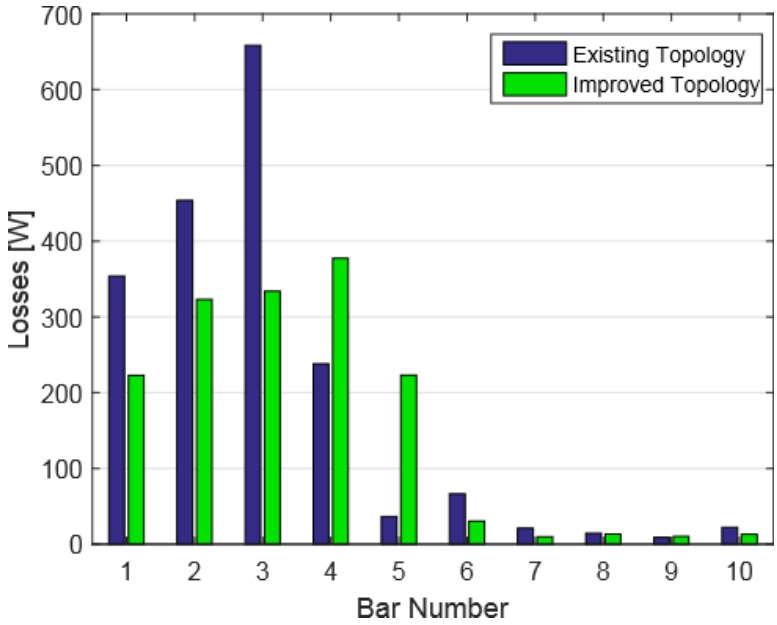


Fig. 85 – Bar losses comparison between the actual and the improved designs at full-load operating condition.

A summary of the comparison between the two topologies is shown in Table 8. The selected solution achieves a loss reduction of about 30% at the no-load condition and 35% at full-load condition. By analysing the optimal pattern of Fig. 82 and the results shown in Fig. 83 and Fig. 85, it can be concluded that losses are minimised because the presence of a graded airgap (not constant along the tangential direction) makes the bars positioned on the pole tips less

sensitive to the slot openings. For example, bars 1, 2, and 3 present an increased distance from the stator slots in the proposed design, with respect to the same bars of the existing machine. This has advantages at both no-load and full-load operations, where the same bars are less affected by the armature reaction field, as they link reduced flux due to their new repositioning.

Table 8 – Summary of the improvements achieved by the optimal topology.

Machine Topology	**No-load loss**	**Full-load loss**	**THD**
Current	2.331kW	9.653kW	2.573%
Improved	1.642kW	6.224kW	2.552%

6.2.6 Considerations on the dynamic parameter

In Section 6.2.4, it was shown that a significant loss reduction can be achieved by designing the damper cage in such a way that the bars are not uniformly spaced over the rotor surface (see Fig. 82). With this technique, the voltage THD can also be maintained approximately the same as the current SG, without reverting to disruptive techniques such as rotor and/or stator skewing. However, for a comprehensive design of the damper cage, the dynamic performance of the machine also needs to be studied and analysed. This is required in order to keep the characteristic values (transient and sub-transient time constants and reactances) within an acceptable range and thus, to avoid intolerable mechanical stresses resulting from excessive currents that occur during electrical disturbances at or near the SG stator terminals.

In order to determine the parameters that describe the dynamic behaviour of the machine, a sudden three-phase short-circuit test was performed (see Fig. 86) and the dynamic parameters were evaluated according to the procedure described in [36] and discussed in detail in the last chapter of this thesis. The prototype generator studied in this paper was tested at a rated output voltage.

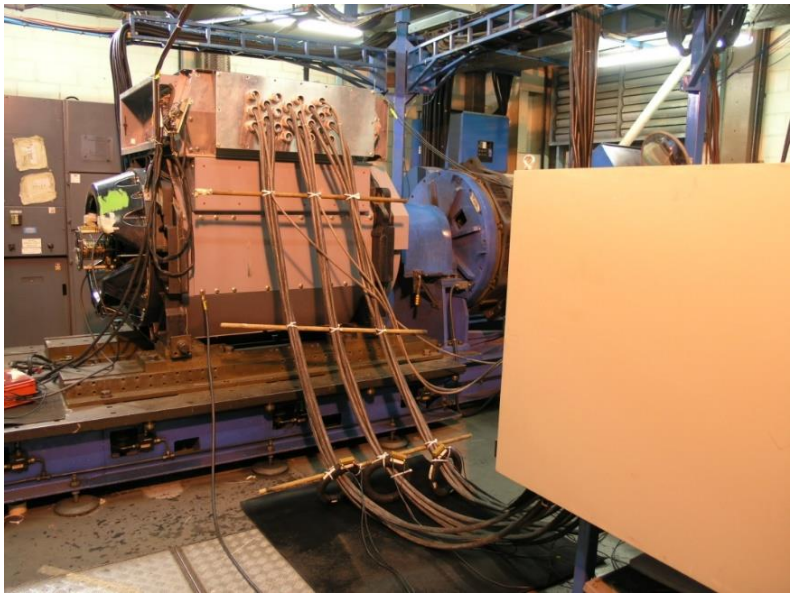


Fig. 86 – Setup for the sudden three-phase short-circuit test carried out on the original 4MVA SG.

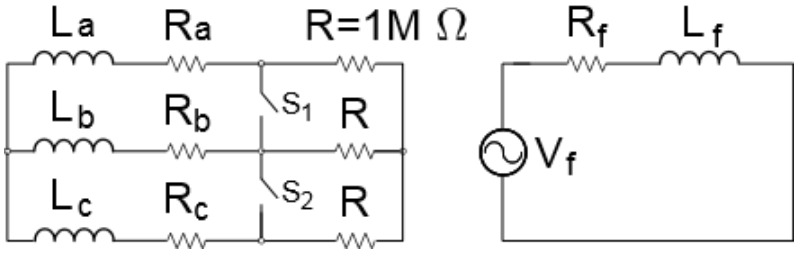


Fig. 87 – Circuits coupled to the FE model for the short-circuit test.

In the test, the simulation was performed by coupling the stator and the rotor external circuits to the FE model, as shown in Fig. 87, where the resistance R is equal to a practical infinite value in order to simulate the no-load condition. These resistances are then short circuited by the switches S1 and S2 at the short circuit time instant. The field winding supply source V_f is such that is able to provide the rated voltage at the no-load operation. This simulation setup was used for both the existing SG and the optimal machine, aiming to show that the unconventionally displaced damper cage topology does not modify the dynamic behaviour of the SG.

A comparison between simulations and experimental results is shown in Fig. 88, where the envelope curves of the short-circuit currents for each phase are shown. A reasonable match between the test and the simulation of the existing machine is achieved. Besides this, a perfect match between the FE envelope curves of the existing and the improved machine can be observed. Therefore, the optimal damper cage topology, in addition to significantly improving the overall efficiency of the machine, does not modify the dynamic performance of the salient-pole 4*MVA* SG considered as proof of concept.

For the sake of completeness and closure of this work, the dynamic parameters of the SG were experimentally evaluated and their values are given in Table 9. These characteristic parameters are usually used to describe the machine's behaviour on sudden short circuit events.

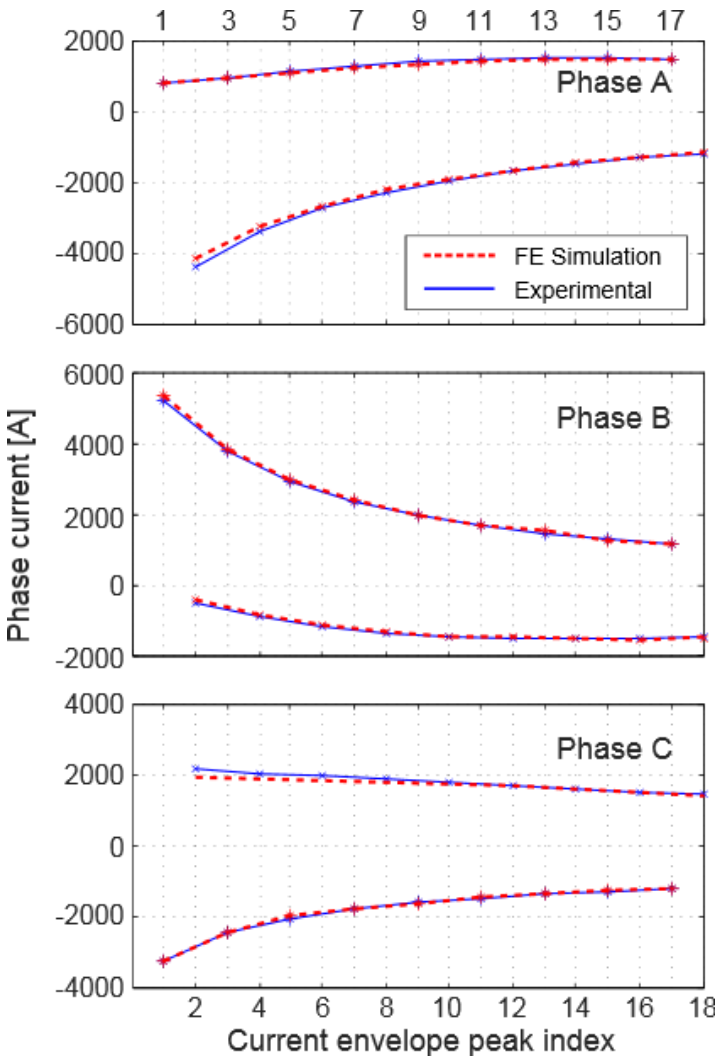


Fig. 88 – Envelope curves resulting from the sudden three-phase short-circuit test: FE results (in red) are relative to the existing and the optimal machine; experimental results (in blue) are relative to the existing machine.

Table 9 – Reactances and time constants of the DIG142 generator.

Dynamic Parameters		
Synchronous reactance	X_d	2.44*p.u.*
Transient reactance	X_d'	0.20*p.u.*
Sub-transient reactance	X_d''	0.16*p.u.*
Transient short-circuit time constant	T_d'	0.268*s*
Sub-transient short-circuit time constant	T_d''	0.0209*s*

6.2.7 Intermediate conclusions

Section 6.2 has dealt with the reduction of the damper cage loss and the output voltage THD in the DIG142 generator. It was shown that the damper cage loss, as well as the THD of the output voltage, is strongly affected by the rotor damping bars geometry.

After a full and detailed validation at several load conditions of the FE model of the considered SGs (see Chapter 4) and a FE sensitivity analysis of the design variables that have a high impact on the damper cage losses and no-load voltage THD (see Chapter 5), an optimal damper cage design for reduced ohmic bar losses and improved output voltage THD was then proposed in Section 6.2. This solution lies in replacing a typical uniformly distributed damper cage with a modulated one, and tailoring the position of each bar to reach the desired objectives. In order to achieve an optimal geometry, a GA-based software has been used to investigate the problem. The optimal solution achieves a loss reduction of about 30% at the no-load condition and 35% at the full-load condition, while maintaining the THD below the critical value of 3%. Also, it has been shown how the improved damper cage topology does not affect the behaviour of the DIG142 in transient conditions.

The results obtained in Section 6.2 have shown how this technique is particularly suited for the type of machine considered, i.e. the DIG142. Nevertheless, it is not limited to this particular SG, as it can also be applied to avoid skewing and, hence, reduce manufacturing cost in smaller alternators.

It is clear that this technique can be further improved and modified according to the specific application which it is intended for. In fact, variants of this technique can include the increase in the number of input variables to be considered. For example, in this work only the bars of one pole were considered, in order to reduce the computational time of the virtual prototyping process. A second iteration might include a consideration of the localized modulation, i.e. not repeated over the poles. This investigation will be the focus of the next section, where the proposed concept will be applied to the HC4 alternator.

6.3 Investigation with modulation – the HC4

In the previous section, the proposed "new" concept (repositioning of the damping bars, according to THD and losses requirements) was investigated. The technique, never used before for such purposes in SGs, may potentially allow for machine efficiency and power density improvements, while meeting stringent power quality requirements. The methodology followed to prove the validity of the proposed technique and the justification for the study relative to the DIG142 alternator has been built on the philosophy highlighted in following steps.

1) Develop an accurate FE model of the 4*MVA* machine.
2) Validate the model against experimental results, carried out on the existing machine.
3) Investigate the proposed technique on the validated FE model, throughout GA-based optimizations.

It is important to note that the optimal machine with the new damper winding shown in Fig. 82 has not been prototyped, as a 4*MVA* generator would need considerable resources and financial effort to prototype. It is also important to note that aim of this work is to prove that the technique is general and is applicable to other power ranges and configurations of SGs. In fact, considering that the conventional displacement of the bars is only a particular case of the "random" displacement, this concept can be generalised and applied to smaller machines, also for other purposes. Related to this, it becomes obvious to apply the modulated concept to the smaller HC4 generator. As explained throughout this thesis, the output voltage of the current product exhibits a THD<3%, however this is achieved with a skewed stator structure. As one of the goals of CGT is that of reducing the manufacturing costs associated to such processes, the proposed modulation is applied to the 400*kVA* SG with the aim of having a THD lower than the critical value of 3% without resorting to the skewing. While the optimizations will be focused on this power quality parameter, the damper cage loss will be also be closely monitored as it was previously shown that the repositioning of the bars affects the inherent losses.

6.3.1 Methodology

In general terms, the concepts, the features and the settings of the optimization procedure discussed above for the DIG142 SG are not modified for the sake of the study relative to the HC4 product. Nevertheless, it is worth to recall the main characteristics and to highlight how the tool has been

slightly modified to adopt the investigation for the 400*kVA* generator. These include the following:

- Interface – ModeFRONTIER of ESTECO is utilised as software for carrying out the GA-based optimizations. This interoperates with Matlab and Magnet during the pre-processing, the solving and the post-processing phases.
- Input parameters – in order to take advantage of the periodicities of the machine and to reduce the computational resources associated with the FE and the GA tools, only 1/4 of the model is considered in first instance, meaning that only the positions of the bars embedded in one salient pole are optimised, while the same positions are then used for the bars over the adjacent (not modelled) poles. Being the number of bars-per-pole equal to 6, this is also the number of the input variables, which are opportunely constrained in such a way that two consecutive bars never interfere with each other.
- Strategy – a DoE based on a random sequence of 50 individuals is used as initial population. A MOGA is used for carrying out a first exploration of the design space. A refinement is then carried out according to the results obtained in the first, preliminary phase (i.e. using the best solutions as initial population for a second round of optimizations).
- Output variables – the objective is that of minimising the damper cage loss and the no-load, line-to-line voltage THD, as for the DIG142 SG. However, there are some slight differences with respect to the study

performed in Section 6.2: main attention is given to the voltage THD rather than the losses minimisation objective. In fact, for the sake of this study, this is by far the most important requirement to achieve in order to avoid the implementation of the stator skewing. On the other hand, it was proven that the damper cage does not represent a significant loss source in the 400kVA SG. Nevertheless, it is essential to maintain this objective below acceptable limits: therefore, as well as for the DIG142, the loss threshold is set at the value lower than the actual no-load damper cage loss found into the benchmark machine (i.e. $\approx 70W$), while the THD threshold value is set at 3%.

Having recalled the features, opportunely adapted for the HC4, of the optimization procedure, the next step is that of showing the relevant results, which are plotted and discussed in the next section.

6.3.2 Preliminary optimization results

As mentioned in Section 6.3.1, six input variables are used for the modulated damper cage optimization, i.e. the positions of the damping bars placed inside one salient pole. This allows for modelling and solving 1/4 of the machine, as shown in Fig. 33 and Fig. 35 of Section 4.1.4, resulting in reduced computational times. It is in fact very important to minimise these computational resources, as all the considered individuals of the various populations correspond to a FE, transient with motion simulation. All these FE evaluations are carried out at no-load and the optimization results are plotted in Fig. 89. Recalling that the THD of the no-load voltage is equal to

5.58% when skewing is not implemented, it is possible to note that improvements with respect to the actual design can be achieved by repositioning the bars over one salient pole. However, the best solution in terms of voltage shape exhibits a THD of ≈4.6% and the losses are also reduced by few watts. This confirms the potential of the proposed concept for a different platform. On the other hand, the achieved THD improvement is not sufficient to avoid the skewing as the power quality standards ask for a THD upper limit of 3%.

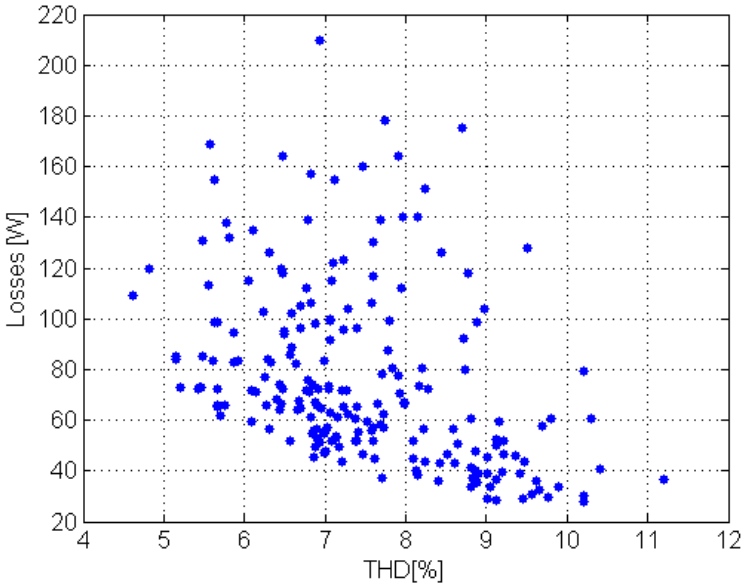


Fig. 89 – No-load damper cage losses vs. THD: preliminary optimizations results (six input parameters).

In order to reach this challenging goal, the modulated damper cage concept with the variant of considering additional input variables is proposed. In particular, a repositioning not repeated over the poles is investigated, meaning that the positions of the bars distributed along two adjacent poles are optimised, resulting in a doubled number (from 6 to 12) of input parameters

being considered for optimization purposes. This variant allows for a significant increase in the number of possible combinations to consider, but comes at the cost of increasing the computational resources. In fact, the minimum angular cross-section to model and solve via FE analysis corresponds in this updated version to 180° (1/2 of the whole machine), as shown for example in Fig. 90. No additional major modifications are necessary for performing this new round of optimizations, meaning that the basic structure of the whole procedure remains that described in Section 6.3.1.

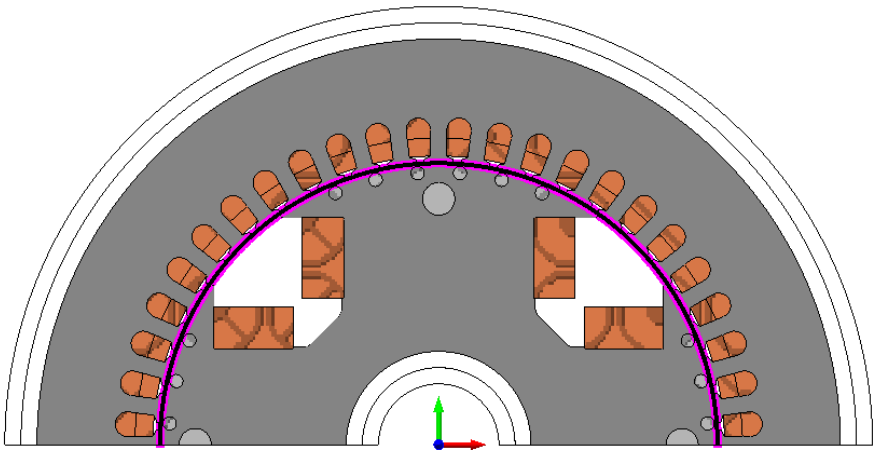


Fig. 90 – Updated FE (half) model of the HC4 used for optimization purposes.

6.3.3 Final optimization results

For this stage of the work (with 12 degrees of freedom used as input variables) all the tests are performed for the no-load operation. The results obtained from the optimization are shown in Fig. 91. Few designs satisfy the objective constraints of 70W and 3%, for the losses and the THD respectively. These achievements are highlighted in the target area in Fig. 91. As in the case of the DIG142, most of these "feasible" solutions have a

damper cage design with a similar geometry and therefore THD and losses are very close to each other.

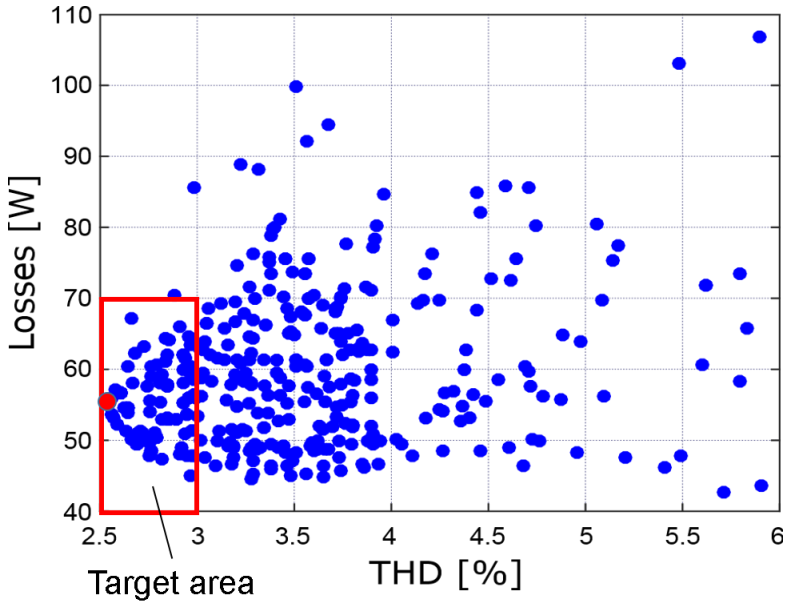


Fig. 91 - No-load damper cage losses vs. THD: optimization solutions with 12 input variables.

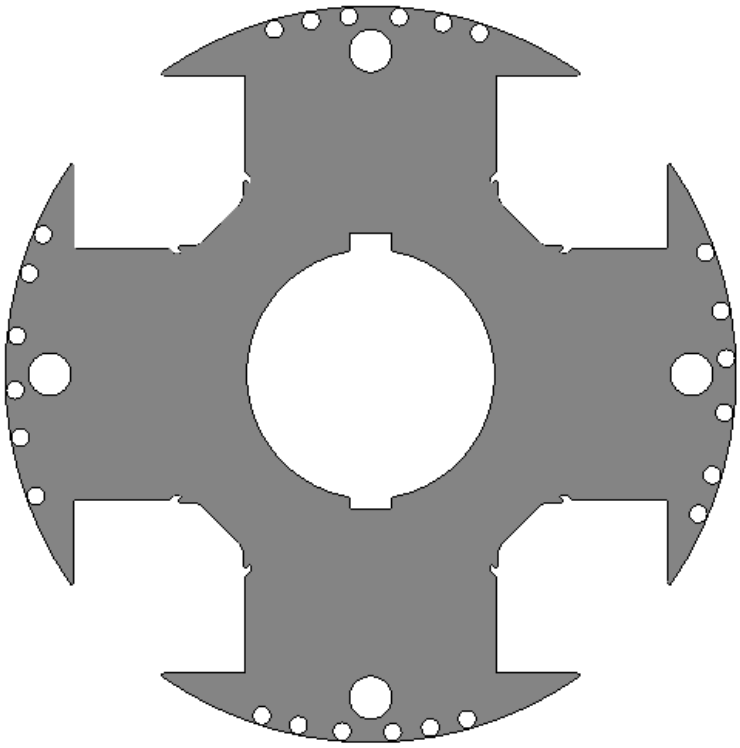


Fig. 92 - Optimal damper cage pattern for reduced losses and THD.

The best solution that combines a minimum THD and an acceptable value of damper cage loss has been selected for the comparison with the actual, benchmark design. The rotor topology of the best machine obtained is highlighted in red (see Fig. 91) and shown in Fig. 92, where the particular pattern of the bar pitch modulation can be observed.

6.3.4 Final proposed solution

The optimal machine, consisting of a skew-less stator and of a rotor equipped with a modulated damper cage, is compared in this section with a) the HC4 with a skew-less stator and a standard rotor (i.e. with bars symmetrically displaced over the poles) and b) the benchmark HC4, consisting of a skewed stator and a standard rotor. For the sake of the clarity of all the figures and tables which will reported in the remaining part of this thesis, these three case studies are termed as follows:

1) Machine A – HC4 with skew-less stator and conventional rotor.
2) Machine B – HC4 with skewed stator and conventional rotor (i.e. the benchmark CGT product).
3) Machine C – HC4 with skew-less stator and modulated rotor (i.e. the optimal, proposed platform).

The comparison of Machine C with Machine A is the fairest one, as both the machines have a skew-less stator and, therefore, it provides the real effectiveness of the proposed concept on the voltage waveform quality. On the other hand, for the sake of completeness, it is worth to show how the optimal machine compares with Machine B.

The comparison between the no-load, line-to-line voltage waveforms of Machine C and A is shown in Fig. 93. The improvements achieved with the modulated damper cage are impressive, resulting in a more than halved THD (from 5.58% to 2.56%) in comparison with Machine A. In Fig. 94, the comparison in terms of amplitude harmonic spectrum is provided, showing that the THD improvement is mainly due to the heavy attenuation of the first group of slotting harmonics, as expected. It can be noticed that also the other slotting harmonic groups are reduced, as highlighted by in green in the same figure, where the amplitudes (on the y-axis) are provided in percent of the fundamental harmonic (not shown in the graph).

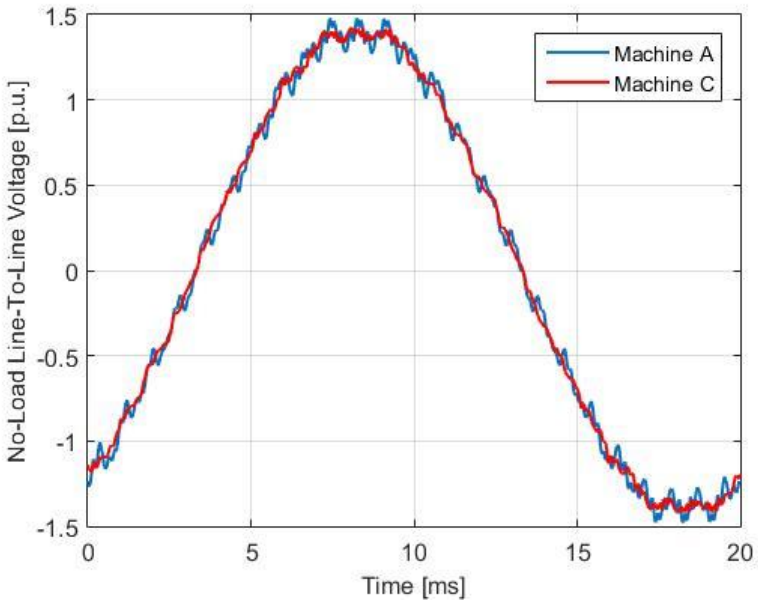


Fig. 93 – Effects of modulation on the voltage waveform: comparison between Machine A and Machine C.

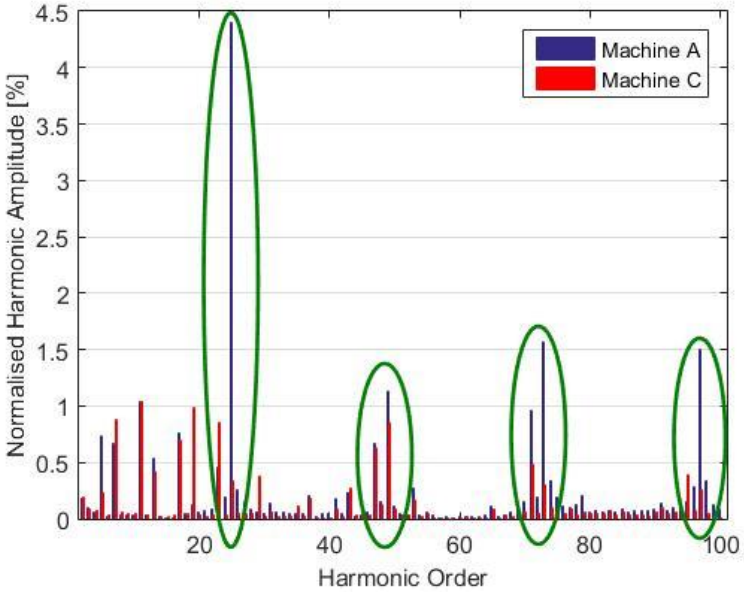


Fig. 94 – No-load line-to-line voltage harmonic amplitude spectra: comparison between Machine A and Machine C.

The same comparison is carried out between the optimal Machine C and the benchmark Machine B. In Fig. 95, it can be observed how Machine B presents a "cleaner" voltage shape than that of Machine C, with a THD=1.26%. This is expected, as the skewing has the effect of almost eliminating the slotting harmonics, as demonstrated and provided in Section 4.4.5. This concept can be also observed in Fig. 96, where the comparison between the respective spectra is shown. This comparative exercise shows that most of the harmonic amplitude values are lower in the current HC4 product than the optimised configuration. However, apart from the 11^{th} harmonic, the optimal machine presents harmonic amplitudes that are lower than the 1% of the fundamental, resulting in an acceptable deformation of the output voltage.

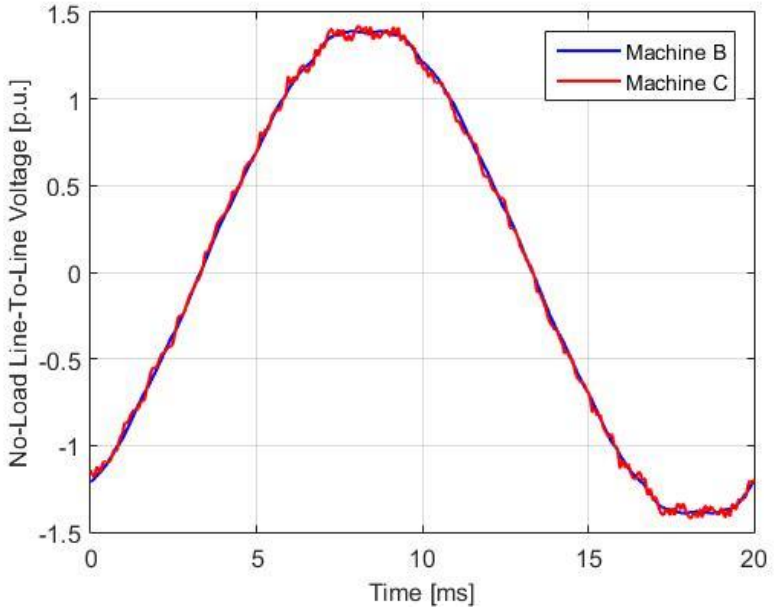


Fig. 95 – No-load line-to-line voltage waveforms: comparison between Machine B and Machine C.

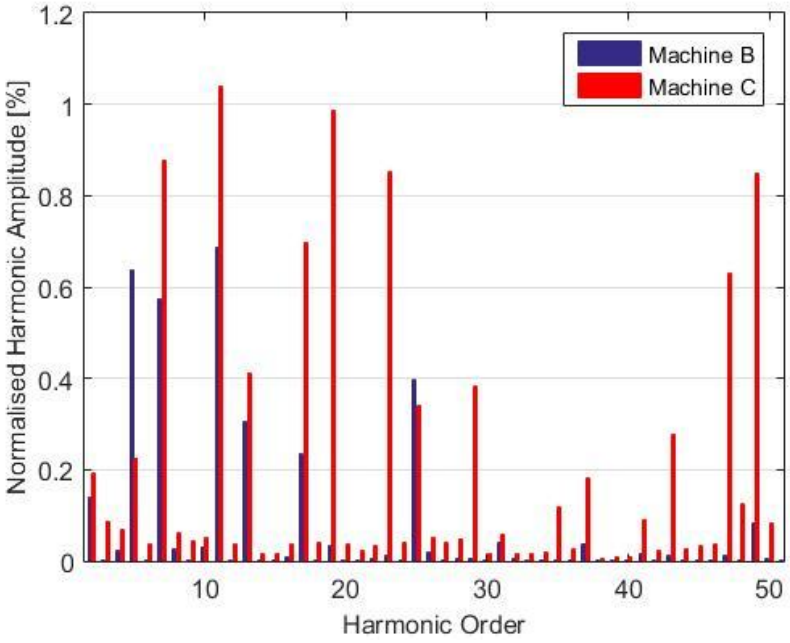


Fig. 96 – No-load line-to-line voltage harmonic amplitude spectra: comparison between Machine B and Machine C.

A summary of the comparison amongst the three topologies is shown in Table 10, where the voltage THD as well as the damper cage loss at no-load operation are compared. Although the benchmark machine (i.e. Machine B) presents a lower THD than that achieved with the optimal HC4 (i.e. Machine C), it is worth to re-underline that this is possible only by implementing the skewing onto the stator. This comes at cost of reduced performance and more elevated manufacturing costs (see Section 2.3). The selected solution, on the other hand, achieves a THD of 2.56% while keeping the stator un-skewed, allowing to meet the stringent requirements relative to this critical parameter. This confirms the validity of the proposed technique, as the machine with a standard rotor and a skew-less stator shows a THD which is more than twice higher than that achieved with the optimal solution. In terms of losses, it can be concluded that the selected machine achieves a reduction of 21.6% and 1.58% at no-load, respectively with respect to Machine A and Machine B, however not significantly influencing the overall efficiency of the machine.

Table 10 – Comparison amongst the three case studies.

Machine Topology	**No-load loss**	**THD**
Machine A	71.3*W*	5.58%
Machine B	56.8*W*	1.26%
Machine C	55.9*W*	2.56%

6.4 Conclusions

This chapter presented improved damper cage topologies aimed at addressing damper cage losses and voltage THD in the considered DIG142 and HC4 salient-pole SGs. This was achieved by repositioning the bars over the salient poles according to the GA-based optimization procedure whose details were discussed throughout the chapter. The main conclusions relative to the work discussed in Chapter 6 can be summarised as follows.

1) An optimal damper cage topology (shown in Fig. 82) was found for the 4*MVA* DIG142 SG, that significantly reduces the inherent loss associated with this winding and keeps the voltage THD at the same value as the baseline machine. Therefore, the proposed, modulated damper cage concept showed high potential for efficiency and power quality improvements in SGs, without modifying the transient performance.
2) In order to confirm the validity of the proposed technique, this was applied to a smaller generator, i.e. the 400*kVA* HC4 SG, for similar purposes. Although a variant of this concept (i.e. the modulation not repeated over the poles) was necessary to achieve a THD lower than 3% without compromising the induced losses, an optimal damper cage topology (see Fig. 92) was found also for this smaller platform, allowing to meet this critical requirement without resorting to disruptive and costly techniques, such as the skewing.

Considering all the above, the next step would consist in validating the FE-GA-based results obtained in this chapter by assessing the proposed modifications onto the studied machines and by performing dedicated experimental measurements. Therefore, considering the drive from CGT towards reducing the manufacturing costs associated with the HC4 skewing, a 400*kVA* generator equipped with a skew-less stator and a rotor with a modulated damper cage was built in order to experimentally prove the proposed technique.

6.5 Contributions to research

The concept proposed in this chapter represents the main novelty of the thesis, as it has never been implemented for addressing damper cage loss and voltage THD in salient-pole SGs. The major benefits deriving from the application of the modulated bar pitch onto salient-pole SGs can be summarised as follows:

- Improvements in terms of efficiency and power quality, without significantly impacting each other.
- No impact on the dynamic performance and associated parameters.
- Ease of manufacturing, resulting in a very low impact on the inherent costs.
- Applicability to platforms of different power range.

The results relative to the DIG142 optimization studies, shown in Section 6.2, have led to one academic publication in a leading journal. The publication name is given below.

- S. Nuzzo, M. Degano, M. Galea, C. Gerada, D. Gerada and N. Brown, “Improved Damper Cage Design for Salient-Pole Synchronous Generators”, *IEEE Transaction on Industrial Electronics*, 2017.

Although the concept of modulating the damper cage has been already published in the journal listed above, the study relative to the HC4 has shown room for updates and variations of the technique. Therefore, more publications are projected in relation to the results reported in Section 6.3.

Chapter 7
Prototype and experimental validation of the proposed concept

This chapter presents the manufacturing of the optimal HC4 rotor configuration proposed for the purposes of this project, as well as the experimental measurements carried out on the prototyped platform for validation purposes.

A brief introduction to the Electrical Discharge Machining (EDM) process is given in Appendix 3, as it represents the selected method for the rotor manufacturing. Some relevant manufacturing details of the HC4 rotor are then discussed in the next section and, in conclusion, the experimental tests are described and the results presented in the form of a comparison exercise with the benchmark machine.

7.1 Manufacturing of the rotor prototype

Considering the description given in Appendix 3, EDM seems to be suitable for the manufacturing of the HC4 rotor equipped with the optimal, unconventionally displaced damping bars. Other manufacturing techniques, such as stamping, laser cutting and water jet cutting, have been considered as potential competitors of EDM in the initial stage of this process. However,

after a trade-off study where the costs and the delivery times of various manufacturing techniques provided by different companies were investigated, EDM was selected as manufacturing method for the job at hand, with an estimated, overall cost of £3700 and a delivery time of about 2 months. Besides these considerations, the key point of this choice was related to logistic advantages, as the workshop of the Department of Electrical and Electronics Engineering of UoN have two EDM machines that were fully available to immediately start the rotor manufacturing. In this section, the high-level steps that led to the completion of the whole rotor stack are discussed.

Square laminations of dimensions 500mm*500*mm* were provided by CGT. In this way, it was possible to use the same ferromagnetic materials that CGT utilises for the rotors and the stators of its own current products. Considering in fact the criticalities related to the internal behaviour of the ferromagnetic materials during the machines' operation, this was an important point to satisfy to allow for a fair comparison between the new prototype and the benchmark HC4. Also, it is important to mention that the stator of the new prototype was produced directly by CGT through conventional stamping, allowing then to use the same lamination materials for both the stator and the rotor. A picture of the skew-less, HC4 stator is shown in Fig. 97.

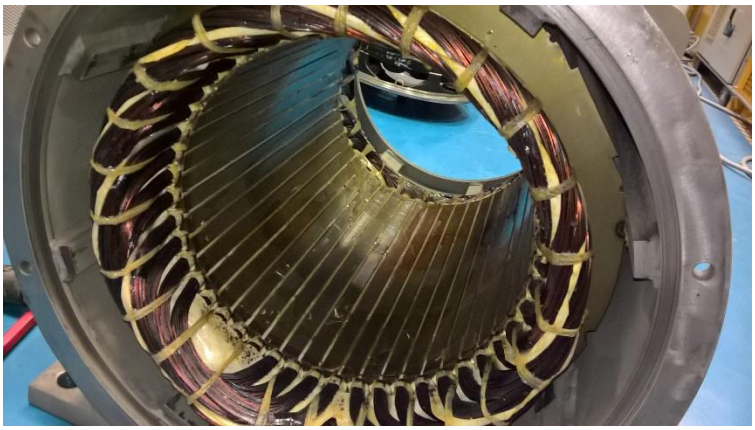


Fig. 97: Photo of the prototyped skew-less HC4 stator.

The detailed dimensions of the rotor lams are not reported in this thesis, due to confidentiality agreements with the company. The general pattern of the optimal HC4 rotor can be observed in Fig. 92, in Section 6.3.3. Due to the limitations in size of the used EMD machines (whose pictures are shown below in Fig. 98), the entire axial length was divided in 4, resulting in four stacks of 125*mm*. The laminations were all preliminary pre-drilled in correspondence of the holes dedicated to the damper bars.



Fig. 98 – EDM machines used for the rotor lams manufacturing.

The new rotor lamination obtained through the described process is shown in Fig. 99, where the particular pattern of the unconventionally displaced damper bars' holes can be observed.

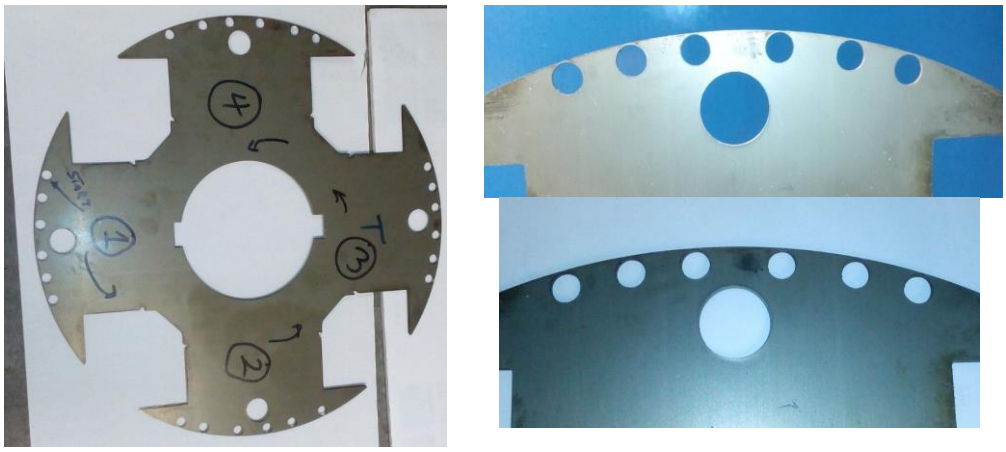


Fig. 99 – Rotor lamination with zoom on the modulated holes for the damper cage.

The rotor laminations were sent to CGT for the assembling of the whole stack and, once this process was completed, the bars were mechanically pushed inside their relevant holes, resulting in the configuration shown below in Fig. 100.

The next step was then that of placing the rotor windings around the salient poles. The active sides of the field winding coils wound around adjacent poles were fixed against each other with plastic clips. Also, a number of thermocouples (bead RTDs sensors, shown in Fig. 101a) were inserted in 2 coils of adjacent poles to take record of the rotor temperatures during test. A number of pictures taken during the winding process of the rotor are illustrated in Fig. 101b and Fig. 101c, while the rotor RTD map is shown in Fig. 102. Here, it can be seen that 10 thermocouples per pole were used, 6 positioned along the axial length and 4 on the end windings. Having completed the rotor windings, the last step consisted in dipping the whole structure for impregnation.

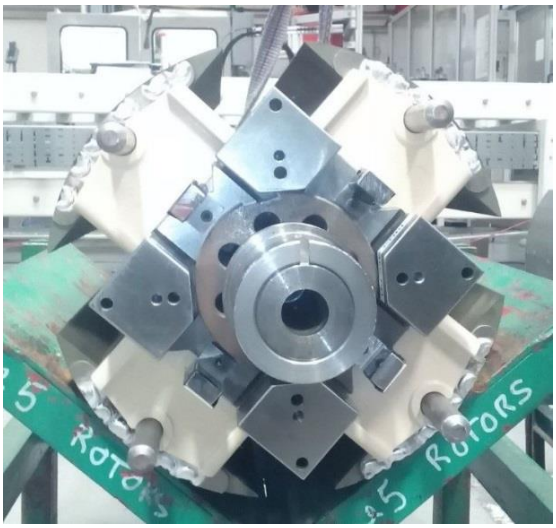
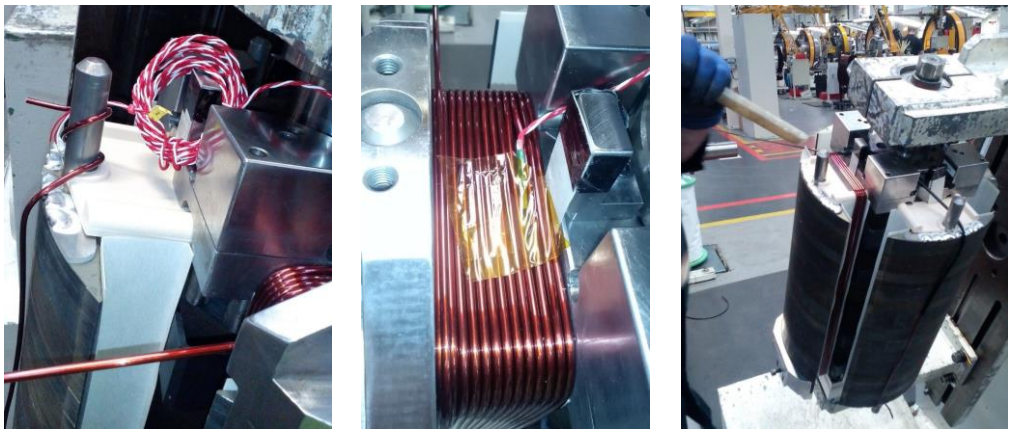


Fig. 100 – Rotor stack, after the insertion of damping bars inside the relative holes.



a) b) c)

Fig. 101 – Rotor winding process: a) bead RTD, b) RTD terminal embedded into the winding layers and c) man at work.

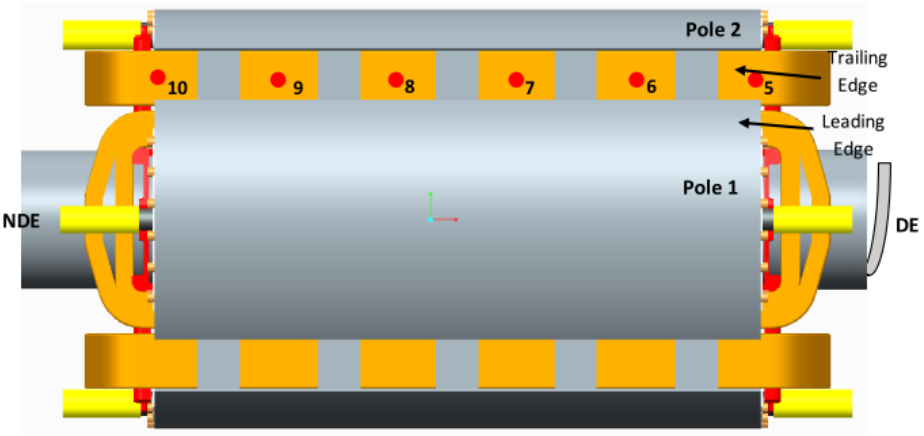
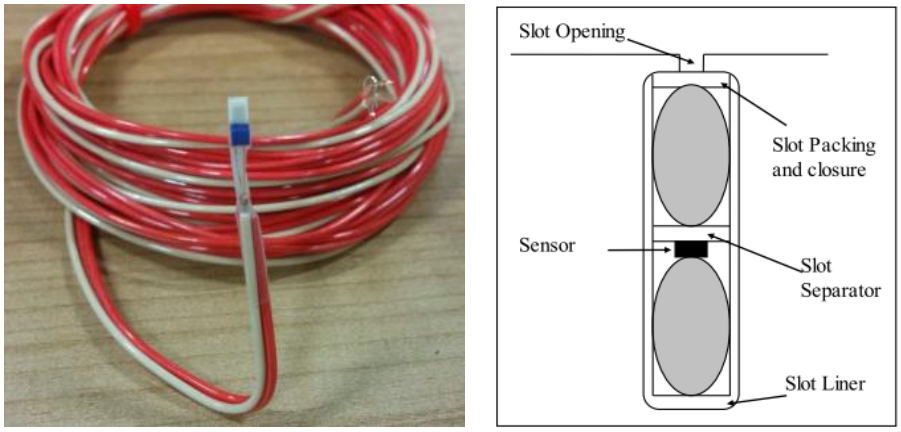


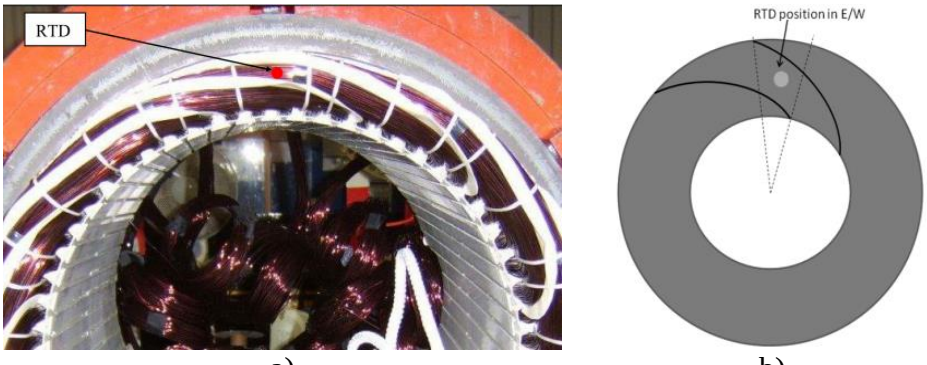
Fig. 102 – Location of rotor winding RTDs.

For the sake of completeness, it is worth to mention that the stator pack was also equipped with 52 thermocouples, with the aim of capturing the axial and circumferential temperature distribution in the slots (using 33 thin-film RTDs, shown in Fig. 103a), the temperature distribution in the end windings (using 12 bead RTDs) and the temperature of the main air streams at various operating conditions (using 7 bead RTDs). The thin-film RTD sensors were located just under the slot separator as detailed in Fig. 103b, while in Fig. 104 it is shown how the bead RTDs are embedded in the end windings.



a) b)

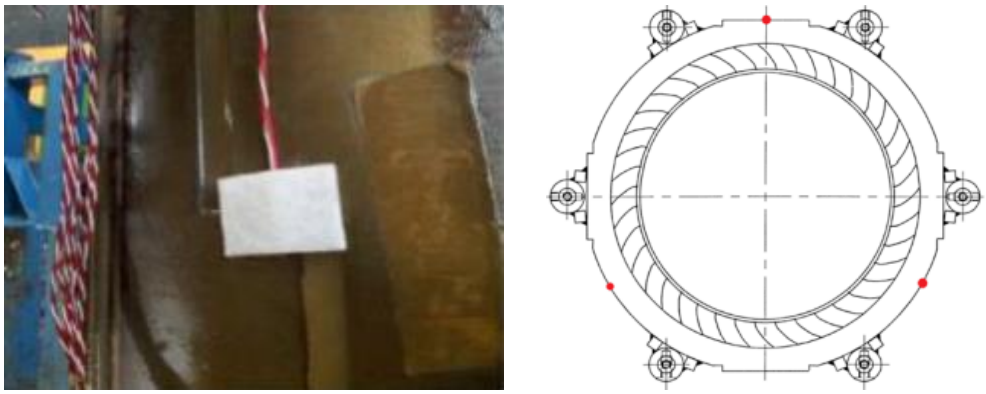
Fig. 103 – Stator winding process: a) thin-film RTD, b) location of RTDs in slots.



a) b)

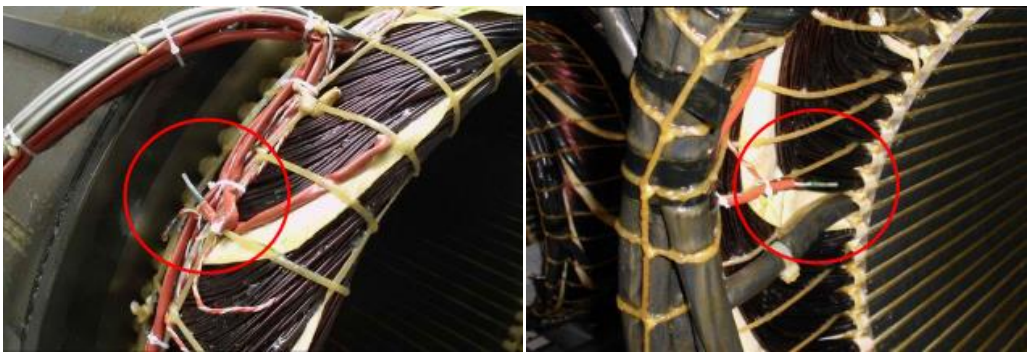
Fig. 104 – Location of RTDs in the end windings: a) photo and b) schematic.

Three RTDs were located on the stator outer surface after impregnation as illustrated in Fig. 105. Finally, bead RTDs were positioned in the air stream attached to the inboard and outboard side of the drive-end and non-drive-end end windings (4 in total, as depicted in Fig. 106).



a) b)

Fig. 105 - Location of RTDs on outer stator surface: a) photo and b) schematic.



a) b)

Fig. 106 – Air temperature sensor in the airstream between a) stator and frame (outboard) and b) rotor and stator (inboard).

Having completed both the stator and the rotor separately, last step was that of completing the assembling process according to standard procedures that CGT applies to the whole range of its products. These include integrating the rotor with the stator, mounting the excitation system (the standard HC4 excitation system was used) onto the same shaft of the main machine,

embedding the system into the case and making the stator terminal box accessible for appropriate connections during testing. A picture of the whole Genset is shown below in Fig. 107.



Fig. 107 – The whole HC4 gen-set prototype.

Following the detailed description of the rotor manufacturing and, in general terms, of the assembling procedure of the whole gen-set described above, the final stage of this project will be that of experimentally validating the proposed concept by carrying out measurements on the built prototype. The relevant results are therefore shown and discussed in the next section.

7.2 Experimental results

The previous section presented the manufacturing process of the optimal rotor topology reported in Fig. 92, in Section 6.3.3. The prototyped 400*kVA* SG is equipped with a skew-less stator. The aim of this configuration is to prove that the alternator is able to achieve a THD lower than 3% without resorting to the skewing, while keeping the efficiency above acceptable

values (i.e. at least maintaining the same efficiency as the baseline HC4). In order to prove the above, experimental measurements were performed on the prototype both in the Tech Centre of CGT and in the High Power Laboratory of UoN.

First, the no-load rated voltage waveform is obtained and post-processed in order to prove the modulated damper cage concept and to confirm the validity of the FE-GA-based optimization results attained and reported in Chapter 6. Then the relevant waveforms and harmonic spectra are presented in a comparative exercise with two machines, previously marked as Machine A and Machine B. Finally, the comparison is carried out between the new prototype (previously marked as Machine C) and the benchmark (Machine B) HC4, with the purposes of showing how the modifications applied to the generator do not deteriorate the overall machine performance, including those during transient conditions.

7.2.1 Waveform analysis

The aim of this test is to confirm the design impact of the unconventionally displaced damper cage on the voltage waveform. This section therefore represents a critical and very important stage of this project, as it is aimed at confirming the validity of the proposed concept by demonstrating that a THD lower than 3%, at no-load operation, is achievable without implementing stator slot skew onto the 400*kVA* SG.

This test was carried out both in CGT and UoN facilities in order to double check the results validity and repeatability. Both the tests achieved the same

results. For the purpose of this thesis, only the test procedures adopted in the HPA of the UoN are reported. A general picture of the test bench is shown in Fig. 108.

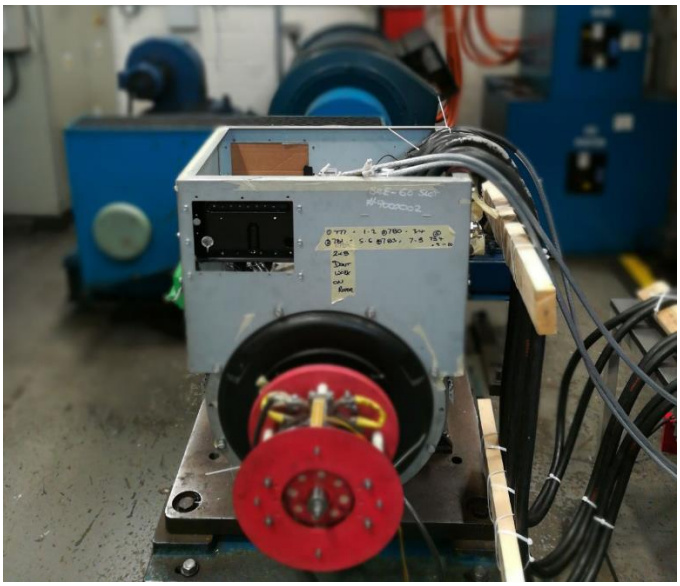


Fig. 108 – HC4 prototype test bench.

The experimental platform is similar to that described in Section 4.4.5.1, consisting of an IM drive, acting as the prime mover, whose speed loop controls the frequency of the SG, which is mounted on the same shaft of the motor. The test can be carried out on a cold or warm machine, as suggested by [118]. However, to be coherent with the corresponding FE evaluation, the evaluation is performed on a cold machine. The alternator was run at rated speed, with the stator windings open-circuited and with the field voltage set in such a way that the rated voltage was available at stator terminals. The AVR was connected to the exciter field winding in order to maintain a constant voltage (i.e. 400*V*) at the armature terminals. The voltage probes (shown in Fig. 109a) were directly connected to these terminals and the

waveforms were observed, recorded and saved on a USB pen drive for post-processing purposes. A picture showing the leads coming out from the stator terminals and used for the voltage measurements is observed in Fig. 109b, while the three-phase, no-load, phase voltages obtained with the skew-less stator, modulated rotor machine can be observed in Fig. 110.



a) b)

Fig. 109 – Voltage measurement: a) LeCroy probe and b) stator terminal box with leads.

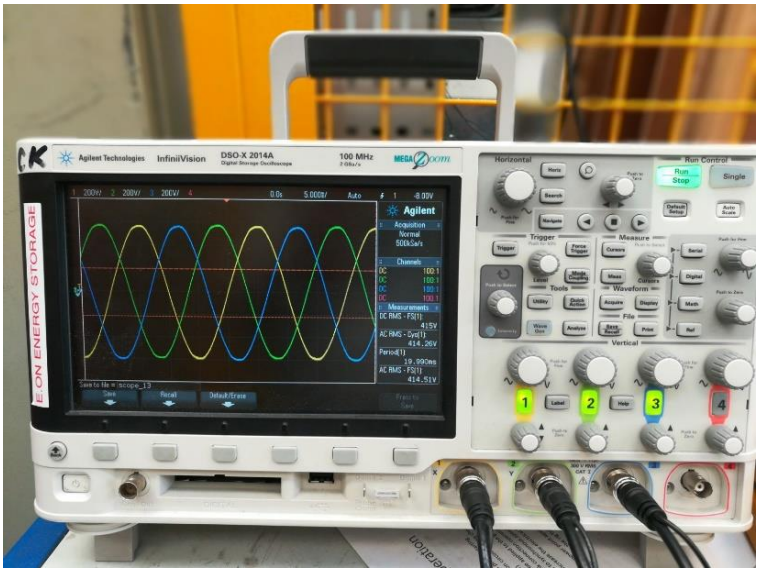


Fig. 110 – Photo of the no-load voltage waveforms available at prototype's stator terminals.

The waveforms shown above in Fig. 110, after post-processing, are compared with the voltage shape obtained through FE analysis for validation purposes. In Fig. 111, the excellent match between numerical and experimental results can be observed. This is also confirmed by the comparison, shown in the same picture, between the THD of such output voltages, where the relevant error is ≈10%. This result finally proves the feasibility of the modulated damper cage concept for power quality improvements. In fact, the study has demonstrated that this design technique is sufficient to guarantee a THD<3%, without resorting to any skewing techniques.

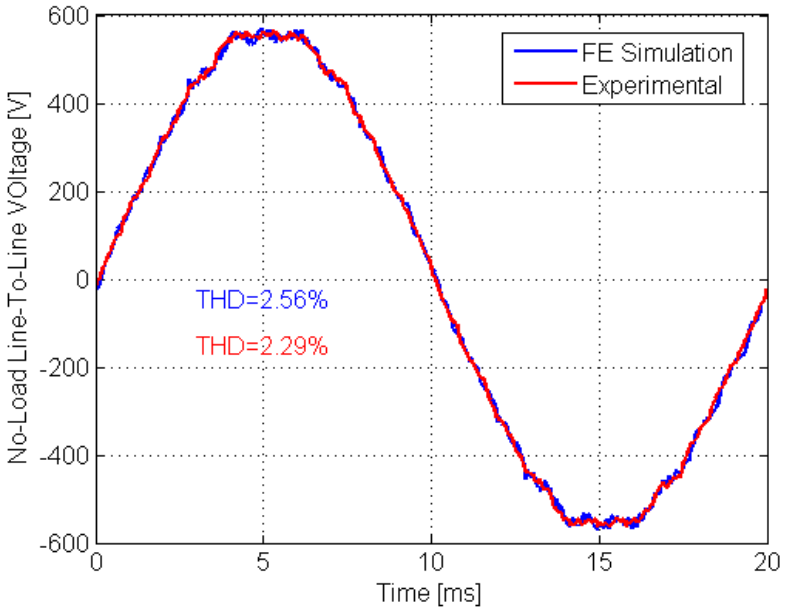


Fig. 111 – No-load line-to-line voltage waveforms: comparison between FE and experimental results.

For the sake of completeness, the measured voltage waveforms are compared with those relative to Machine A (i.e. the HC4 with skew-less stator and conventional rotor) and Machine B (i.e. the HC4 with skewed stator and

conventional rotor). This comparative exercise is shown in Fig. 112. This comparison confirms the results provided in Section 6.3.4, where it was observed that

1) the THD improvement due to the modulated rotor with respect to the normal rotor is mainly due to the heavy attenuation of the first groups of slotting harmonics (see Fig. 94, in Section 6.3.4);
2) the "cleaner" voltage shape of the benchmark machine with respect to the prototyped machine is obtained through the disruptive and costly technique of skewing, which produce almost an elimination of the slotting harmonics.

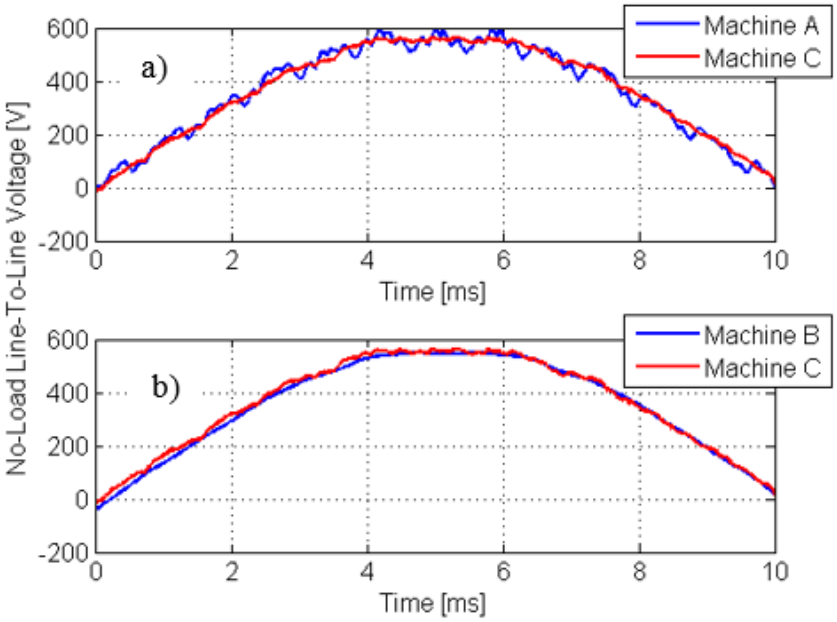


Fig. 112 - No-load line-to-line voltage waveforms: comparison between a) Machine A and Machine C and b) Machine B and Machine C.

It can be concluded that the results presented in this section prove and confirm the validity of the proposed modulation concept in terms of achieving a skew-less machine without compromising voltage quality. These results also show that the GA-FE-based methodology aimed at finding an optimal topology gives excellent results. Having therefore found out that a skew-less configuration can meet very stringent power quality requirements in combination with an optimal damper winding design, the next step consists in proving that the new prototype does not affect the overall, steady-state and transient performance of the benchmark HC4. Hence, in the next sections, a comparison between the performance of the new prototype and the benchmark machine at no-load, short-circuit, full-load and overload operations will be presented and discussed.

7.2.2 No-load characteristic

In general terms, the purposes of this test is to evaluate the saturation within the machine's magnetic circuit, to measure the level of excitation required to magnetise the machine and to verify the capability of the excitation circuit. The no-load characteristic test was performed in the Tech Centre of CGT. The investigation was carried out on a cold machine, with the output terminal open-circuited and with the AVR disconnected, meaning that the excitation system was connected to an external controllable DC supply. The open-circuit test set-up is shown in Fig. 113. The slip rings shown in Fig. 114 were used to record the main field winding voltage and current. A typical power analyser was used for the voltage measurements.

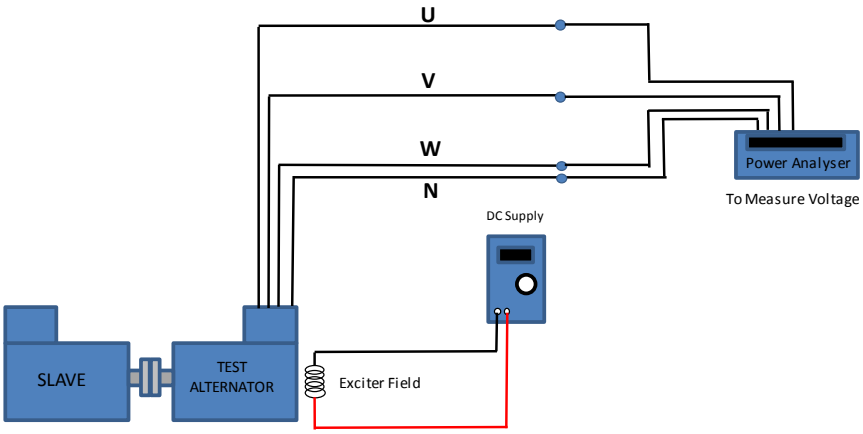


Fig. 113 – Open-circuit characteristic test set-up.

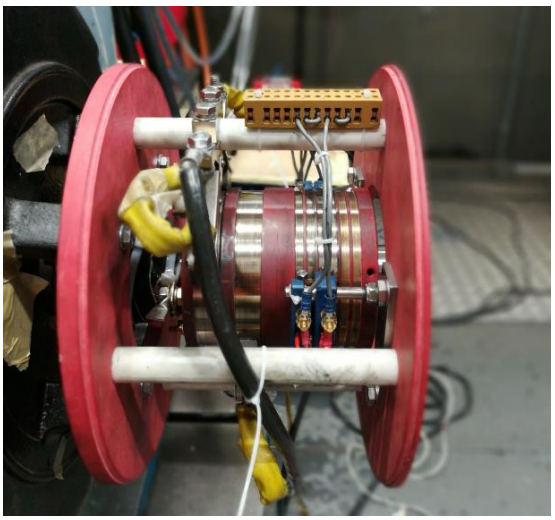


Fig. 114 – Slip rings used for field voltage and current measurements.

In order to eliminate any residual magnetism in the system, a negative DC pulse was applied to the exciter stator winding. The alternator was then run at rated speed and the excitation increased in incremental steps, recording the values of line voltage, exciter voltage and current as well as the main rotor voltage and current (through the slip rings). At the rated voltage, the line-to-line values on each of the three phases were recorded to ensure balance. The excitation was increased until the output volts reached the 130% of the rated voltage. Finally, the line-to-line voltage vs. rotor field current was plotted and

compared in Fig. 115 against the available experimental no-load curve relative to the current HC4. A perfect match between the two curves can be observed and it is found that the new prototype achieves the rated voltage value with a field current reduced by 0.7% in comparison with the original machine. This also confirms the analytical observations carried out in Section 4.3.2, in particular those relative to the fact the skewing does produce a performance deterioration due to the reduced "equivalent" winding factor (see the waveforms of Fig. 40, in Section 4.3.2).

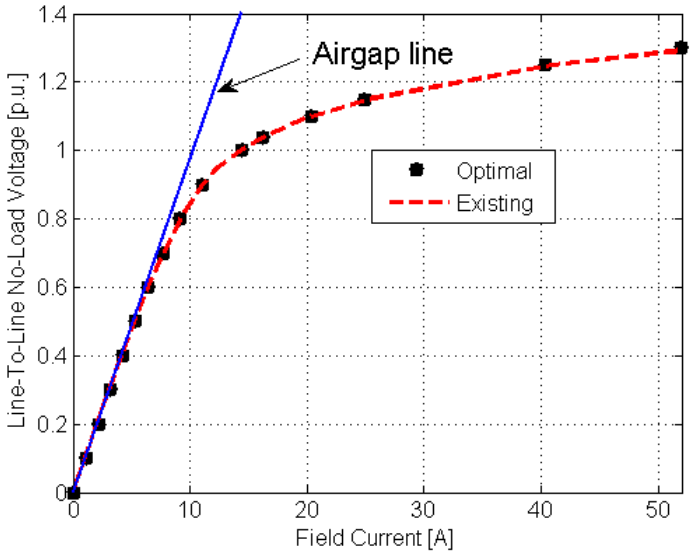


Fig. 115 – No-load characteristic: experimental comparison between optimal and existing HC4.

7.2.3 Short-circuit characteristic

This test aims at determining the excitation requirements and capabilities of the machine under test and at evaluating the unsaturated synchronous reactance. As well as for the no-load characteristic, the short-circuit curves of the new prototype and the benchmark machine are compared to prove that the new design does not affect the performance of this machine. In Fig. 116, the

excellent match between the characteristics can be observed, resulting in a very good match also in respect to the unsaturated synchronous reactance (3.38*p.u.* for the new prototype against 3.35*p.u.* for the existing machine).

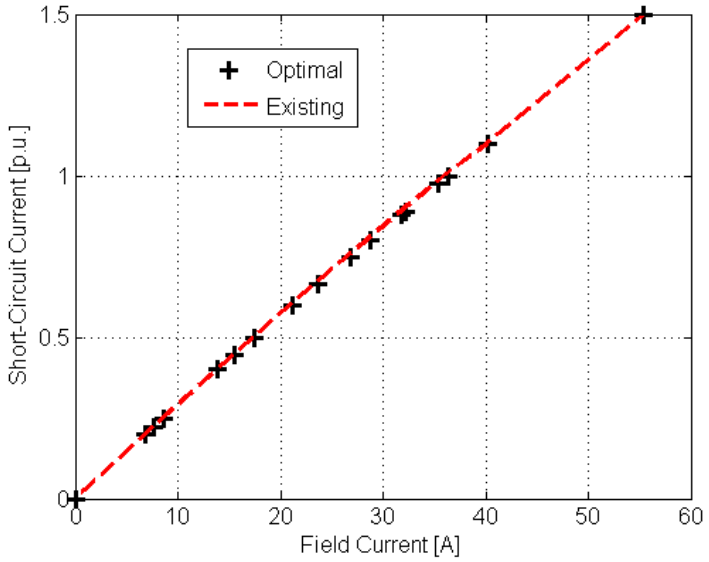


Fig. 116 – Short-circuit characteristic: experimental comparison between optimal and existing HC4.

The investigation is carried out on a cold machine. The test set-up is shown in Fig. 117, while the short circuiting connections are shown in Fig. 118. Current Transformers (CTs), whose full range is very similar to the maximum measured load current of the generator, were used in order to maintain acceptable levels of measurement accuracy. These are shown also in Fig. 118. As well as for the no-load test, the AVR was disconnected and a DC power supply was used to power the excitation system. In order to eliminate any residual magnetism, a negative DC pulse was applied to the exciter stator winding. The generator was run at rated speed and then the excitation was increased in discrete steps until the output current is at least 50% above the rated value. At each step, the values of stator current, exciter

field voltage and current and the generator field voltage and current (through the slip rings) were recorded. It was finally possible to plot the phase current vs. the rotor field current figure shown above in comparison with the one available for the current HC4.

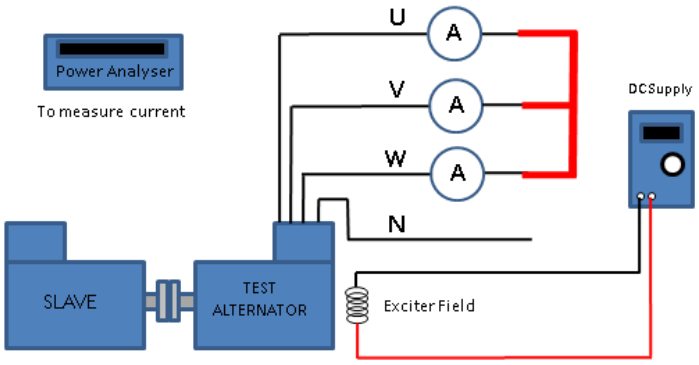


Fig. 117 – Short-circuit test set-up.

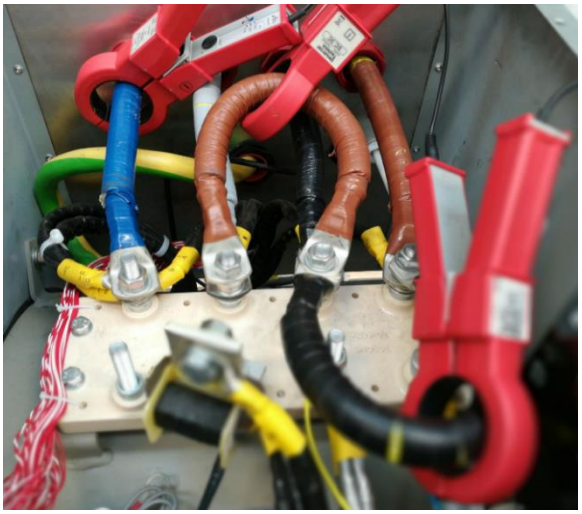


Fig. 118 – Short-circuit test: short-circuiting connections and CTs used for the current measurements.

The last step was that of evaluating the unsaturated synchronous reactance as the ratio of the excitation current required to sustain the rated short-circuit current, to the excitation current required to sustain rated open circuit voltage. This second value is derived from the air gap line extrapolated from the no-

load curve, as shown in Fig. 115, as this line represents the unsaturated excitation requirement.

7.2.4 Power losses and efficiency

The experimental determination of power losses and efficiency in classical SGs represent a well-known and consolidated task, due to the historical experience gained in the field of power generation. In this work, the "summation of losses" method [118] is used for determining the overall machine efficiency. Power losses were partially evaluated through the test described in the previous sections. Other loss contributors mainly present at on-load operation were evaluated through additional tests, according to the procedures discussed below. The power losses to be summed for the efficiency determination include

1) No-load losses, i.e. the mechanical (windage and friction) and the iron losses. The set-up used is that of Fig. 113 of Section 7.2.2, where the machine is driven by a variable speed motor, at constant, rated speed, with a shaft torsionmeter connected between the drive motor and the generator. During the open-circuit test, in addition to the readings required for the no-load characteristic, with slip rings fitted, readings of the torsionmeter and shaft speed are taken for each point on the curve. By using torque and speed values to obtain the shaft power in *kW*, it becomes possible to plot the output voltage against the kilowatts. By extrapolating the voltage curve back to zero volts on the graph, the windage and friction of the machine is where this line

crosses zero volts, while the iron losses are the total losses at rated voltage minus the obtained mechanical losses. The graphs relative to these loss contributors are plotted in Fig. 119 and Fig. 120.

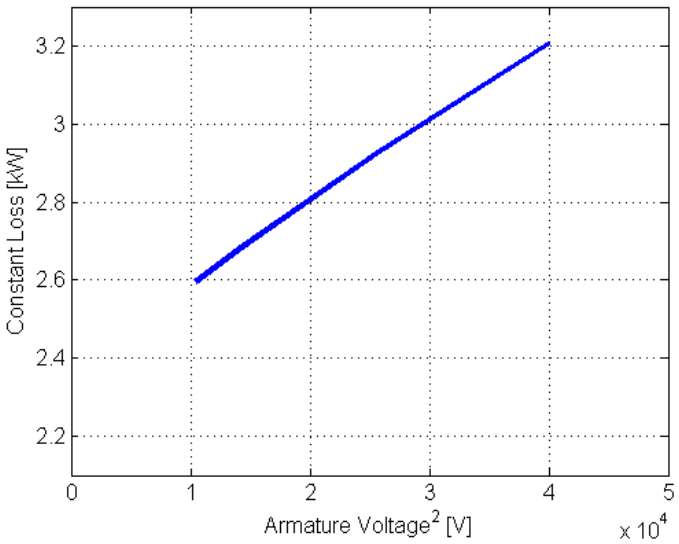


Fig. 119 – Windage and friction loss evaluation.

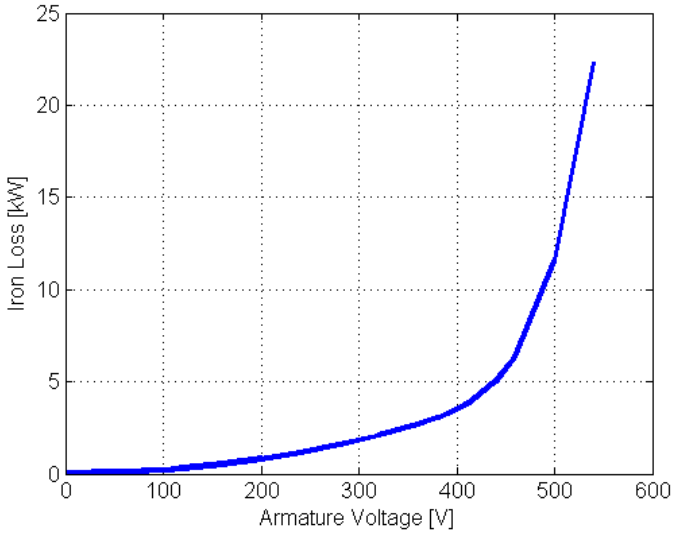


Fig. 120 – Iron loss determination.

2) Full-load losses, i.e. the rotor and the stator copper losses. This test is carried out with the alternator hot, meaning that the machine was run

for a certain number of hours to reach the steady state, at rated load and power factor. This rated condition is achieved by loading the HC4 on resistive and inductive load banks. The load parameters registered during the test were rotor and stator voltages and currents, respectively for the exciter and the main generator, and these are summarised in Table 11.

Table 11 – Electrical load parameters registered during full-load, steady-state operation of the generator prototype.

Load Parameter	**Measured Value**
Armature Voltage	400V
Armature Current	577.4A
Reactive Power	400kVA
Active Power	320kW
Power Factor	0.8
Rotor Current	50.49A
Rotor Voltage	98.9V
Exciter Rotor Voltage	81.6V
Exciter Stator Current	2.342A
Exciter Stator Voltage	45.95V

Through this test, it is also possible to estimate the excitation losses: this contributor is considered equal to the 10% of the main rotor copper loss. This assumption is based on the experience gained by CGT through the testing carried out on the whole range of products that the company produces. Although a detailed characterization of

the excitation system is necessary to properly determine the excitation loss, for the sake of this study (that is aimed at comparing the performance of the new prototype with that of the original machine) the assumption is very well-founded as the excitation system is the same for both the platforms

3) Short-circuit losses, i.e. the additional stray losses. According to [119], this contributor can be defined as additional loss, wherever occurring, caused by the load current due to changes in flux distribution and to eddy currents and, in the case of poly-phase synchronous motors and generators, it shall be deemed to be equal to the values which would be obtained on a short-circuit test, namely the difference between the total measured mechanical input on the short-circuit at the current under consideration, and the sum of the friction, windage, iron, copper and excitation losses. Therefore, in order to experimentally estimate the stray loss, during the short-circuit test, in addition to the readings required for the relative characteristic, readings of the torsionmeter and shaft speed are taken for each point on the curve. By using torque and speed values to obtain the shaft input power in *kW*, it becomes possible to determine this loss as explained above.

Having determined each single loss contributor, it becomes possible to obtain the machine efficiency η by using (37), where P_{out} is the output real power of the machine (i.e. 320kW) and P_{losses} is the sum of losses above determined.

$$\eta = 100 * \left(\frac{P_{out}}{P_{out} + P_{losses}}\right) \quad (37)$$

Table 12 shows the comparison in terms of losses and efficiencies between the new and the existing HC4. Aim of this study is to prove that the design modifications assessed onto the HC4 do not deteriorate the overall performance of the product. This is verified by observing the excellent match between the machines' efficiencies, where it can be noticed that the new prototype does produce a slight improvement (by 0.23%), confirming once again that the bar reposition concept is a very effective technique for improving power quality and efficiency in salient-pole SGs.

Table 12 – Efficiency calculation by loss summation method.

Loss Component	**Optimal Machine**	**Existing Machine**
Windage & Friction	2.387kW	2.141kW
Iron (Fe)	3.933kW	3.884kW
Armature Winding (Cu)	9.599kW	9.593kW
Field Winding (Cu)	4.993kW	5.433kW
Excitation	0.493kW	0.544kW
Additional (Stray)	2.450kW	3.111kW
Total	23.855kW	24.706kW
Efficiency	**93.06%**	**92.83%**

In Table 12, it is interesting to note that the loss reduction achieved by the optimal machine is mainly due to the iron, field winding and stray loss contributors. In particular, due to the negative effects that skewing has on the output voltage (see Section 4.3.2), it can be safely concluded that the skew-less machine requires a field current lower than that needed by the existing machine to achieve the rated voltage, resulting in a reduction of the field winding loss contributor.

7.2.5 Dynamic parameters

One of the most important and critical aspect to consider for a comprehensive study of the new HC4 (equipped with the unconventionally displaced damper cage) is related to the dynamic behaviour of the machine. The aim of this section is therefore that of proving that the new design does not modify the parameters corresponding to the generator short-circuit performance. In order to determine these characteristic values, a suddenly applied three-phase short-circuit test was performed according to the procedure described below.

The test set-up is illustrated in Fig. 121. The alternator under test is coupled to a slave generator by a ring feeder coupling. The coupling bolts require tightening to the correct torque. Adequate size cables are required for the test. Nevertheless, as the instantaneous short circuit only lasts for a fraction of a second, cables able to carry the steady-state current are sufficient for this test.

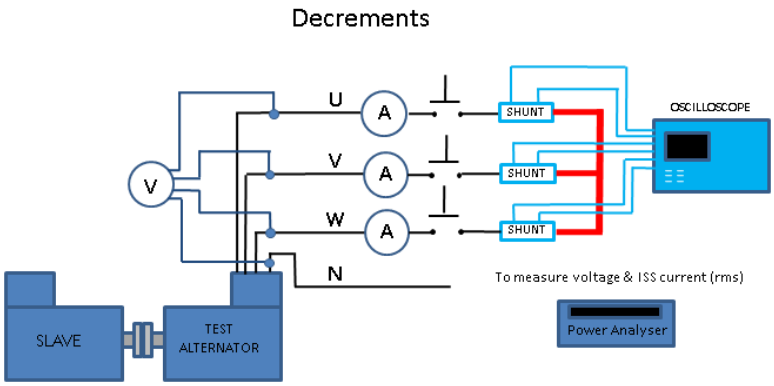
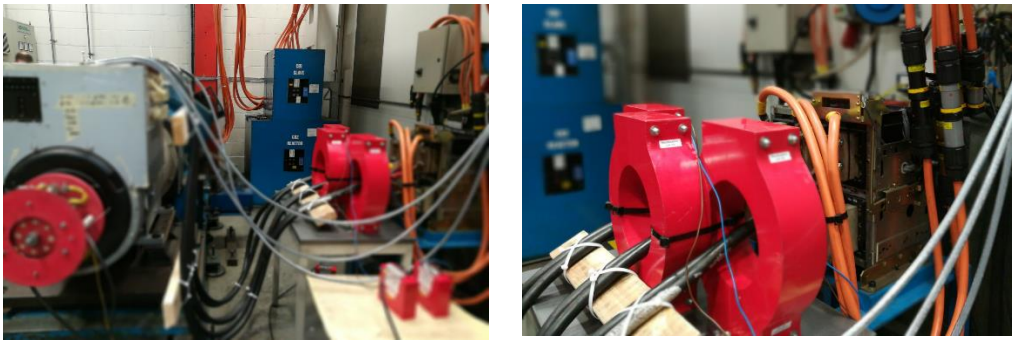


Fig. 121 – Decrement test set-up.

A separate breaker is used to perform the test. The cables are connected from one side of the breaker to the machine under test and to the short on the other side. Suitable sized shunts must be positioned between the shorting bar and the breaker. According to the experience gained in the long history of utilisation of these classical machines, it is estimated that the HC4 under test will carry up to ten times the full-load current in the first instants of the short circuit (i.e. when the breaker is closed). CTs of suitable size are used for the measure of the steady-state current. These are shown in Fig. 122b, while the whole set-up is illustrated in Fig. 122a. Each shunt has a BNC lead connected across its terminals which is linked to the auxiliary panel inside the cell. Another set of BNC leads are then connected from the auxiliary panel outside the test cell to the test equipment used to measure the instantaneous short circuit. A mains key switch is also used in connection with the breaker for its on/off operation (opening and closing). The phases are opportunely insulated from the cables running from the machine to the breaker by using an insulating device. Each phase is cabled to the insulated device for extra support (as shown in the photos of Fig. 122) in order to minimise movement

during the test. A suitable DC power supply is connected to the exciter field winding and, after the generator is run at its rated speed and the output voltage is at its rated value, then it becomes possible to apply the three-phase short-circuit. A Yokogawa oscilloscope is used for recording and saving of the data.



a) b)

Fig. 122 – Decrement test: photo of a) the test cell set-up and b) the CTs.

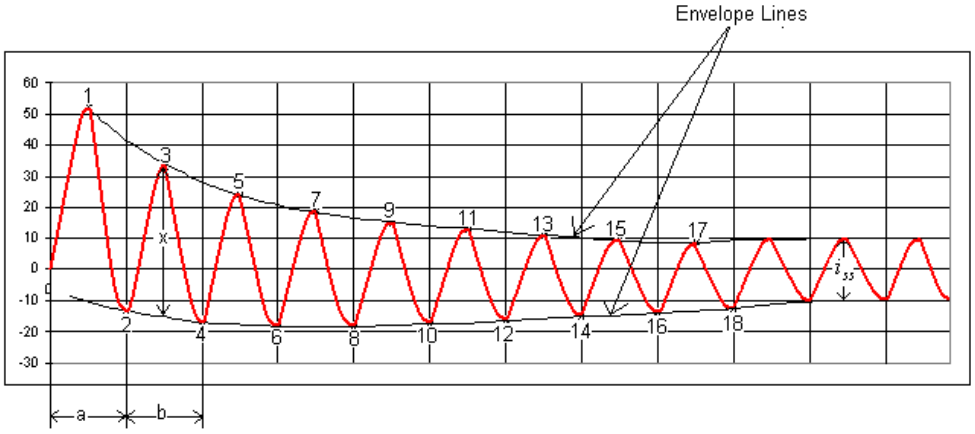


Fig. 123 – Typical current oscillations after a sudden short-circuit.

A classical current oscillation occurring after a sudden three-phase, short-circuit test is illustrated in Fig. 123. The dynamic parameters determination is performed according to the method standardised in [120]. This consists in

several passages and is a simple, “hand” procedure, whose main steps are listed below.

1) Number the peaks and draw the envelope curves (for all the phases), as shown in Fig. 124 for the phase A of the prototype under investigation.

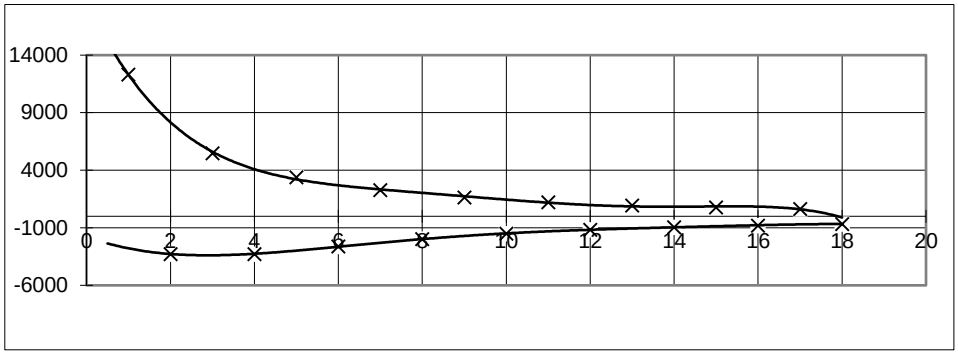


Fig. 124 – Envelope curve for the phase A: numbering of the peaks.

2) On a log-linear graph (x-axis = peak number, y-axis = distance in mm) plot the curves below:
    a. Curve A – The difference between the instantaneous peak-to-peak current and the peak-to-peak steady state current.
    b. Curve B – Extend the straight line portion of Curve A backward to the edge of the paper.
    c. Curve C – The difference between Curve A and Curve B at discrete peak positions.
    d. Curve D – Derived from the mean value of the upper and lower waveform envelope curves (see Fig. 124).
    e. t = 0 – Compute the ratio *a/b* (see Fig. 123). On the log-linear graph, plot a point to the left of peak 2 position which

represents the ratio *a/b* multiplied by the distance between peak 2 and 0. Draw a perpendicular line through this point extending it through Curve B. This represents t = 0.

The curves obtained as described above are shown below in Fig. 125 for the new, optimal HC4.

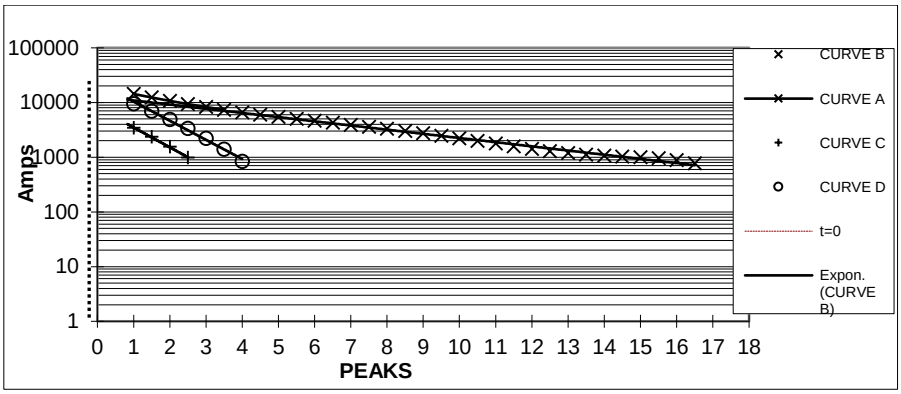


Fig. 125 – Decrement test: curves for the dynamic parameters determination.

3) These curves will then be used to compute the different parameters as described below:

   a. Direct axis transient reactance X_d', whose calculation is given in (38), where I_{rated} is the machine rated current, $i_{t=0}$ the y-axis reading at the point where Curve B intersects the *t=0* line (see Fig. 125), I_{ss} the field current required to produce I_{rated} for a sustained symmetrical short circuit at the generator terminals and, finally, i_{ss} is the steady state current after the fault.

$$X_d' = \frac{I_{rated}}{(i_{t=0} + i_{ss})\frac{I_{ss}}{i_{ss}}} \tag{38}$$

b. Direct axis sub-transient reactance X_d'', calculated as in (39), where $i'_{t=0}$ is the y-axis reading at the point where Curve C intersects the $t=0$ line (see Fig. 125).

$$X_d'' = \frac{I_{rated}}{(i'_{t=0} + i_{t=0} + i_{ss})\frac{I_{ss}}{i_{ss}}} \tag{39}$$

c. Direct axis transient short-circuit time constant T_d'. The use of Curve B, which has a trend line equation in the form $y=A*e^{Bx}$, allows computing T_d' in peaks, by reducing $I_{t=0}$ by $1/e$ and then by transposing the trend line equation, as summarised in (40). Finally, it becomes possible to obtain T_d' in seconds by using (41), where f is the operating frequency and $c=2-(2*(b/a))$.

$$T'_d[in\ peaks] = \frac{\left[\ln\left(\frac{i_{t=0} * \frac{1}{e}}{A}\right)\right]}{B} \tag{40}$$

$$T'_d = \frac{(T'_d[in\ peaks] - 1) + (1 - c)}{2f} \tag{41}$$

4) Direct axis sub-transient short-circuit time constant T_d''. This is computed in a very similar way as for T_d'. Curve C, which has a trend line equation in the form $y=C*e^{Dx}$, is used instead of Curve B to determine T_d'' in peaks by reducing $i'_{t=0}$ by $1/e$ and then by transposing the trend line equation, as summarised in (42). It is then possible to obtain T_d'' in seconds by using (43).

$$T_d''[in\ peaks] = \frac{\left[\ln\left(\frac{i'_{t=0} * \frac{1}{e}}{C}\right)\right]}{D} \tag{42}$$

$$T_d'' = \frac{(T_d''[in\ peaks] - 1) + (1 - c)}{2f} \tag{43}$$

In Table 13, the comparison between the existing and the novel HC4 prototype in terms of dynamic parameters is summarised. This is based around the procedure described above. It can be observed that a very close match between the results exists, thus confirming that, besides the overall performance of the machine (see previous sections), the dynamic behaviour of the generator is insensitive to the modifications applied to the damper winding of the machine.

Table 13 – Dynamic parameters: experimental comparison between optimal and existing topologies.

Dynamic Parameters		**Optimal**	**Existing**
Synchronous reactance	X_d	2.40*p.u.*	2.63*p.u.*
Transient reactance	X_d'	12.17%	12.92%
Sub-transient reactance	X_d''	8.08%	9.14%
Transient SC time constant	T_d'	0.056*s*	0.062*s*
Sub-transient SC time constant	T_d''	0.01226*s*	0.01299*s*

7.3 Conclusions

This chapter presented the manufacturing aspects and the experimental results relative to an innovative, unconventionally displaced, damper cage for improved losses and THD in salient-pole SGs. This new concept was implemented onto the rotor of a 400*kVA* SG, with the aim of showing how tailoring the position of the damping bars allows to achieve a THD lower than 3% without resorting to the stator slot skewing and without compromising the losses associated with such bars.

The EDM technique, whose major features are discussed in Appendix 3, was the selected method for the "in-house" rotor manufacturing. The inherent processes and issues were then discussed as well as the skew-less stator manufacturing and the whole assembling of the gen-set, carried out in CGT. The experimental results of the new prototype were then presented in the form of a comparative exercise with those performed on the HC4 current product, with the aim of proving that the proposed, modulated damper cage does not modify the overall, steady-state and transient performance of the considered platform.

More specifically, in Section 7.2.1, the validity of the proposed concept was proven through the waveform analysis of the rated no-load voltage, which showed a THD equal to 2.29%. This result was very close to the GA-FE-evaluated THD (2.58%), showing also the validity of the proposed optimization strategy. Sections 7.2.2 and 7.2.3 presented the comparison between the no-load and the short-circuit curves evaluated on both the

machines, showing a perfect match between the existing and the new HC4 (Fig. 115 and Fig. 116). In Section 7.2.4, the power loss and efficiency evaluation method was presented and the inherent results were also discussed: in particular, the total losses of the new prototype were reduced by 3.44% with respect to the original machine, resulting in an improved efficiency of 0.23%. Finally, the dynamic performance of the original and the prototyped SGs were compared, showing again an excellent match between the respective characteristic values (see Table 13). All the above confirmed that the new modifications assessed onto the 400*kVA* SG fully meet the power quality requirements related to the no-load voltage THD, while keeping (and even improving) the same steady-state and transient performance of the current product.

7.4 Contributions to research

The work presented in this chapter has shown the validity of the proposed methodology, i.e. the positive effects of having a modulated damper winding have been proven. The experimental results provided in Section 7.2 are being used to develop a journal publication, which is programmed to be submitted to a leading IEEE journal by the end of 2017.

Chapter 8
Conclusion

This work has been developed in such a way as to allow for conclusions, discussions and other aspects to be presented at strategic points of the thesis. Thus in this chapter, only a higher level and more general discussion and conclusions as well as further observations relative to the main achievements and novelties of this project are discussed.

In particular, the general conclusions are first provided in the form of a concise summary of all the chapters of this thesis. Then, more details are given in relation to 1) the implemented hybrid analytical-numerical model, 2) the SS method for modelling skew and 3) the modulated damper cage concept and its effects on the two considered applications. Finally, some ideas for future work are also included.

8.1 General conclusions

This work has shown the critical effect that the damper cage winding has on the operation but also on the manufacturing processes for classical SGs. In this thesis, innovative damper winding schemes, based around asymmetrical, modulated bars were proposed and investigated. It was shown how, through the implementation of this unconventional bar displacement, 1) important gains in terms of losses and THD can be achieved for the 4*MVA* DIG142

prototype, and 2) the historical need for skewing of the stator can be removed for the 400*kVA* HC4 application.

First, a detailed literature survey of the methods most commonly used for achieving the objectives outlined above was discussed in Chapter 2. The most recent advancements in the field of SGs were highlighted, with special focus given to the damper cage and the skewing modelling aspects, as these played the most important role for the sake of the investigation presented in this project. It became thus possible to propose new solutions with respect to the state-of-the-art, in terms of design, analysis and modelling of such already well-consolidated machines.

Advanced analytical, hybrid analytical-numerical and fully numerical (i.e. FE) modelling tools were presented, developed and compared with experimental measurements carried out on the mentioned CGT market products. The results relative to the innovative modelling and analysis techniques proposed in Chapter 3 (relative to the damper cage modelling) and Chapter 4 (the power loss and the skewing modelling) showed an excellent match with the experimental measurements, confirming the validity of such tools.

The studies presented in Chapter 4 were also aimed at investigating the challenges inherent to the power losses (especially for the DIG142) and to the skewing (implemented onto the HC4) effects on the voltage waveforms' quality. Therefore, in Chapter 5, a number of solutions aimed at overcoming the aspects mentioned above were proposed. These investigations, carried out

for both the generators, were presented in the form of in-detail sensitivity analyses of the design variables that have a high impact on the damper cage losses and on the no-load voltage total harmonic distortion. It was concluded that the tangential position over the salient poles of the damping bars can significantly impact (and improve) the losses and THD in both the generators. This "information" was then taken on board and considered for optimization purposes. The symmetrical arrangement of the bars was however abandoned and varied according to the concept of modulation.

An optimal damper cage design for reduced ohmic bar losses and improved voltage THD was then proposed in Chapter 6. This solution lies in replacing a typical, uniformly distributed damper cage with a modulated one, and tailoring the position of each bar to reach the desired objectives. In order to achieve an optimal solution, a GA-based approach has been used to investigate the problem. For the DIG142 alternator, the optimal solution achieves a loss reduction of about 30% at no-load and 35% at full-load, whilst maintaining the THD below the critical value of 3%.

While excellent results were achieved by the optimal DIG142 solution, the more attractive benefits (as perceived by CGT) in renewing the design of the HC4 product led to investigate more deeply the proposed concept on the 400*kVA* SG. In fact, due to the manufacturing costs associated to the skewing, the objective has then become that of meeting the power quality requirements (related to the no-load voltage THD) without resorting to this technique. CGT predicts that without the need for the skewing process, a

single prototype will get off the assembly line, approximately in twenty minutes time less. From preliminary simplified calculations, based on one single prototype, then the improvement resulting from the achievement of this objective is perceived to be of around 3-4% cost saving per machine.

As vessel to investigate the validity of the proposed tools and findings, an optimal damper cage was implemented and built on the 400*kVA* platform, featured with a skew-less stator. The performance of the new prototype was finally experimentally evaluated and compared with the current market product. The new HC4 has shown a THD equal to 2.29%, which is below the set objective of 3%, and an improved efficiency of 0.23%, while keeping the no-load, full-load and transient requirements the same as the existing alternator. The results shown in Chapter 7 have then confirmed the validity of the proposed method and the feasibility of a skew-less generator, potentially improving the HC4's market value.

8.2 Contributions to research

The major contributions to research of this work in terms of academic publications were already mentioned in the final section of every chapter. In summary, the research presented in this thesis has resulted in a number of published works in peer reviewed journals [10, 85, 108] and conference proceedings [24, 38, 78-80, 121, 122].

The major contributions of this research program from a technical point of view can be listed as follows.

1) An accurate, hybrid analytical-numerical model for the electromagnetic analysis of the generators considered in this thesis is developed and implemented. The main novelty is related to how the damper cage modelling has been addressed, resulting in a reduced order of the system of differential equations to be solved. The model has been shown to achieve minimum prediction errors. To the author's knowledge, no similar modelling technique is available in literature. It is the author's belief that this new modelling procedure is better suited in terms of time consumption against accuracy in comparison with other previous works [34, 77], as also confirmed by the summary which will be presented in Section 8.2.1.
2) Accurate, numerical, 2-D FE tools of electromagnetic analysis are developed and built for both the generators. The models have been shown to achieve minimum prediction errors with reasonable time penalties. Thus, increased iteration is possible and feasible during the design processes aimed at achieving optimal design solutions.
3) A fast, FE-based method for modelling skew and its effects in salient-pole SGs is proposed. Although this technique presents some limitations relative to the prediction of the damper cage currents, the advantage gained in terms of computational resources is impressive in comparison with other FE-based techniques. The model has shown an excellent match with the experimental results, especially in terms of

voltage THD, which is an ideal situation for the sake of this study. From an impact perspective, this technique is felt to be a major outcome of this work. The modelling procedure proposed in [108] has excellent potential for the design and development of various machine families.

4) An innovative technique based on bar spacing, i.e. the modulation, is proposed for addressing damper cage loss and voltage THD in SGs. In summary, it is possible to optimally tailor the position of the damping bars in such a way that both bar losses and voltage THD are minimised, without significantly interfering and compromising each other. The technique is applied to the DIG142 and the HC4 platforms, confirming its effectiveness on alternators of different power ranges and designed for different applications. Also in this case, the predicted results have shown excellent match with the measurements (carried out on the 400kVA platform), confirming the validity of the proposed concept. From an impact perspective, this technique is felt to be a major outcome of this work and its excellent potential is also proved by the number of citations that [10] has already gathered in just the first seven months that it has been publicly available.

The technical contributions listed above are discussed in more detail in the next sections, in a sort of comparative exercise with other works and technologies.

8.2.1 The hybrid analytical-numerical model

In Chapter 3, a mixed analytical-numerical model that solves much faster than the classic FE method was implemented with the aim of accurately estimating the no-load voltage waveform in salient-pole SGs, when operating in linear condition.

Firstly, a purely analytical model was presented and described in depth with the final aim of achieving an accurate expression of the inductance matrix, valid for any type of electrical machine. The model, originally proposed by [77], has shown room for updates and variations, resulting from the need of adapting the study to the particular machine considered in this project: the SG. In particular, the application of this powerful analytical tool to a specific electrical machine is missing in the original work. Depending therefore on the specific machine to analyse and on the particular objectives to aim for, the model needs further exploitation and "ad hoc" variations. As in this Ph.D. project the machine under analysis is represented by the SG and the objective is that of predicting its no-load voltage waveform, two major modelling aspects were included and updated with respect to [77]:

1) The slot opening – its effects are of paramount importance on the no-load voltage waveform. While the original work neglects this design feature, the model presented in Chapter 3 does consider the slot openings and the way how these are included in the analytical tool was described in Section 3.6.2.
2) The damper cage – the significant contribution of this short-circuited winding on the voltage waveforms was pointed out throughout the

thesis. The original work does not mention the modelling aspects relative to this winding. Therefore, in Section 3.6.1, an innovative way of modelling this complex rotor winding was presented.

While the above observations highlight differences and updates of the proposed model compared to the original work,

Table 14 compares the damper cage modelling technique presented in this thesis with those classically used by machine designers, if these models were to be applied to the HC4 alternator. These classical ways of modelling the damper windings of SGs still represent today the state-of-the-art in this field.

Table 14 – Major advantages of the proposed model with respect to the classical literature.

Models	**Analysed Portion**	**System order**	**Implications**	**Complexity**
Classical literature	Whole machine	24	Not-null CL mutual inductances	High
	One pole pitch	9	Not null CL mutual inductances	Medium
Proposed work	Whole machine	9	Null CL mutual inductances	Low

In summary, Table 14 highlights the advantages of the proposed technique resulting from the exploitation of the symmetries characterising the machine. The considerations presented in Section 3.6.1 allow to model the entire machine without compromising the order of the system of equations to be solved; on the contrary, just thanks to the fact that the whole machine is

modelled, it becomes possible to obtain null values of all the mutual inductances between the cage loops. This last aspect represents the major further step with respect to the state-of-the-art and allows to achieve a relatively low complexity (and thus high speed) of the overall system.

Finally, the proposed analytical model had to be combined with a numerical approach, due to the induced nature of the damper cage currents, resulting in a highly flexible and fast hybrid technique.

8.2.2 The single-slice technique

Another major technical contribution associated to the research presented in this thesis is related to a fast FE-based method, proposed with the aim of accurately predicting the output voltage and current THD in stator-skewed SGs, at both no-load and on-load operations. As a vessel for studying the proposed SS method, the 400*kVA* HC4 alternator was considered. This innovative tool was compared for validation purposes with the well consolidated AS and MS techniques, at both no-load and full-load conditions, with an excellent match being achieved, indicating the validity of the technique. At this stage, focus was given to the damper cage behaviour, highlighting some limitations of the SS technique in estimating more complex quantities to analyse, such as the currents induced in the bars.

Finally, in order to further validate the SS method, experimental measurements were performed at no-load and at different loadings and power factors, where the voltage THD comparisons showed an excellent similarity. At no-load, the maximum error was 5.97%. The validation however

highlighted a weakness of the technique when going toward the higher loading ratings. This is associated with the machine's armature reaction and the averaging processing philosophy employed by the technique. However, it is also important to note that even with this perceived challenge, the maximum error at full load was 18.9%, again highlighting the adequateness of the modelling technique.

Also, although an increased number of slices (21) is considered for the experimental validation of the SS method, it allows for a reduction of the computational time by 4.5*h* and by 22*h*, in comparison with the AS and the MS techniques respectively, when five slices are used for all of those models. The comparison was carried out using the same desktop computer (32.0*GB* Ram and Intel(R)-Xeon(R) CPU E5-1620 v2 @ 3.70*GHz* Processor) for all the methodologies. It can therefore be safely concluded that the proposed method does achieve the main goal of a fast but accurate technique for modelling skew in SGs.

8.2.3 The modulated damper cage

The modulated damper cage concept, described in Section 6.1, represents the major contribution to research of this project, as its application is unprecedented in the field of wound-field SGs. The concept was first proven on the 4*MVA* DIG142 alternator, where excellent achievements in terms of damping bar losses reduction were registered. During this study, the proposed innovative technique has also shown potential for improvements in terms of voltage THD. Therefore, the modulation was applied to a platform of

different size and power (i.e. the 400*kVA* HC4 SG) in order to achieve the challenging objective of meeting the stringent power quality requirements imposed by grid codes and compliance standards (i.e. THD < 3%), without resorting to the skewing. The experimental measurements carried out on the renewed HC4 confirmed a) the validity of the optimization strategy adopted to achieve the optimal solution and b) the feasibility of a skew-less and, at the same time, power quality compliant SG. The results in terms of damper cage loss and THD improvements, for both the alternators, were extensively detailed in Chapter 6 and Chapter 7, thus they are not reported again in this section. On the other hand, it can be of interest to provide the key THD achievements over the last century and half of different machine topologies, with the aim of highlighting the impressive outcomes deriving from the application of a modulated damper cage on salient-pole SGs. This comparison is given in Table 15. It can be noticed that, besides the topologies which include a modulated damper cage (i.e. the generators renewed in this work), also those which are featured by a "shifted" damper cage (such as the original DIG142) and/or by a skewed stator (such as the existing HC4) are below the THD limit of 3%. However, in this thesis it was demonstrated that the shifted damper cage and the skewing come at the cost of increased damper cage loss, reduced performance and elevated manufacturing cost. The modulated damper cage, therefore, represents the best option to circumvent these challenges and has the potential of marking a significant shift in the market of such classical, often forgotten, wound-field electrical machine. As

mentioned above, based on the number of citations that [10] already has, this technique is already gathering a measure of success.

Table 15 – Harmonic mitigation topologies and applications.

Application	**Year**	**THD**	**Topology**
Early generators [123]	Late 1800s	>12%	Single-layer, full-pitched winding; skew-less
6*MVA* electric generator [124]	Early 1900s	>10% & <12%	Distributed, full-pitched winding; skew-less
Medium-to-large rated SGs [38]	1950s (still produced)	≈5%	Distributed, short-pitched winding; skew-less
Medium-to-large rated SGs [113]	2014	≈2.5%	Distributed, short-pitched winding; skew-less; "shifted" damper cage
Medium-to-large rated SGs (renewed DIG142) [10]	2017	≈2.5%	Distributed, short-pitched winding; skew-less; modulated damper cage
Small-to-medium rated SGs (renewed HC4)	2017	≈2.2%	Distributed, short-pitched winding; skew-less; modulated damper cage
Small-to-medium rated SGs [23]	1980s (still produced)	≈1.5%	Distributed, short-pitched winding; skewed stator

8.3 Future work

The last, conclusive section of this thesis is dedicated to potential future work related to the concepts, models and applications presented in this project. Considering the technical contributions mentioned above in Section 8.2, there are several aspects which have been already targeted as potential areas of future research.

1) The hybrid analytical-numerical model – the limitations highlighted in Chapter 3 can be overcome by revisiting the model and the relevant equations by including the most important non-linearities characterising an electrical machine, which are relevant to the inherently non-linear behaviour of the ferromagnetic materials. Once updated, it can be heavily used for analyses under load conditions. Another area already under investigation is the adaption of the model to the case of modulated damper windings. In fact, an interesting study may be that of running purely analytical optimizations, as one of the main drawbacks of the FE-GA tool described in Chapter 6 is the elevated computation time.
2) The SS, FE technique – the limitations highlighted in Section 8.2.2 relative to the accuracy of the model under load condition can be mitigated by developing and implementing appropriate compensation factors, aimed at overcoming the mentioned inaccuracies. However in order to find appropriate factors, quite some effort is required, including

a. investigating more in depth the optimal number of slices to use;
b. investigating the proposed technique for a number of different platforms, with different power and load ratings.

3) The modulation – due to the significant benefits that this innovative design feature has brought to the DIG142 and the HC4, some interesting areas of investigation may be targeted as follows:

a. investigate the bar modulation all over the 360° of the machine;
b. investigate how the bar modulation affect harmonics lower than the slotting ones, with the aim of considering different stator winding arrangements, e.g. with a decreased (or even null) short pitching;
c. consider the rotor bar modulation in conjunction with several slot number combinations;
d. build an optimization tool that is able to consider all the Cummins SGs power portfolio.

Appendix 1 – Introduction to the FE technique

Numerical methods are based on the determination of the electric and magnetic field distribution through the solution of Maxwell's equations. The FE method is a particular numerical technique that allows to achieve an accurate field solution even when time variable fields are involved and when non-homogeneous, anisotropic and non-linear materials are employed. Today, the FE method represents the most diffused technique for the solution of the vector field problems.

More specifically, the method consists in dividing the whole analysis domain into elementary subdomains, called finite elements, and the field equations are applied to each of them. The study of the electromagnetic field problems allows for a highly accurate local analysis, highlighting dangerous field gradients, localised saturations, etc. In fact, the FE analysis provides an excellent estimation of the machine performance, which would be hardly achievable in applications where classical, analytical methods are difficult to apply. One additional advantage of this technique with respect to the classical methods is that it allows to reduce the number of prototypes, being the relevant analysis very close to the real behaviour of the considered device. However, the FE method has some disadvantages as well. In fact, being a numerical technique, the solution is necessarily approximate. Also, if the method is not correctly applied, it might generate inaccurate or completely

wrong results. The most significant drawback is represented by the relatively high computation time, which grows proportionally to the required accuracy. This is influenced by the dimension of the finite elements, in fact a fine subdivision increases the accuracy but at the same time increases the computation burden. In order to reduce it, one can take advantage of periodicity and symmetry (both geometric and electromagnetic) of the structure under analysis. Thus, by simulating only a portion of the device, the finite elements dimension can be reduced, thus improving the accuracy of the solution without significantly compromising the computation time.

Methodology

According to [93], the typical framework of a FE analysis is organized in the following steps:

1) partition of the domain: in 2-D problems usually each element is a triangle, while in 3-D problems each element is a tetrahedron;
2) choice the interpolating function: these functions are necessary for the resolution of the field problem inside each finite element;
3) formulation of the system of partial differential equations needed to solve the electromagnetic problem: it can be developed through the Galerkin or the Rayleigh-Ritz method [93], indifferently;
4) solution of the problem: the resulting system of equations is solved through common numerical algorithms.

The last step of the FE analysis consists in post-processing the results: once the field solution is obtained in each node, it becomes possible to determine the most significant electromagnetic quantities involved.

2-D modelling

Although electrical machines are inherently 3-D structures, a full 3-D analysis requires heavy processing and significant computational resources. An appreciable reduction in the computation time can be achieved by taking advantage of the machine symmetry and therefore by analysing the device in a 2-D environment.

In rotating machines, the planar symmetry can be adopted: it is assumed that the magnetic phenomena are identical in each plane (*x*, *y*) perpendicular to the rotational axis *z*. In 2-D analyses with planar symmetry, the study can be simplified as follows: 1) the current density vector $\bar{J}$ has only the *z*-component and, consequently, 2) the potential vector $\bar{A}$ (that is parallel to $\bar{J}$) has only the *z*-component; 3) the flux density vector $\bar{B}$ has components only on the plane (*x*, *y*) as $rot\bar{A} = \bar{B} = \left[\frac{\delta A_z}{\delta y}, -\frac{\delta A_z}{\delta x}, 0\right]$ and, finally, 4) if the permeability μ is constant, the field problem is described by the Poisson's equation given in (44).

$$\frac{\delta^2 A_z}{\delta x^2} + \frac{\delta^2 A_z}{\delta y^2} = -\mu J_z \tag{44}$$

Considering the above, it is clear that a 2-D analysis significantly simplifies the field solution. On the other hand, it is also true and obvious that some

inherently 3-D phenomena (such as the effects due to the end parts of the machine) are omitted in 2-D analyses. However, the applications of appropriate correction factors could allow to take such phenomena partially or totally into account, if they are not negligible.

Boundary conditions

One way to overcome the issues related to the computational limitations associated to the FE method is that of exploiting the symmetries of an electrical machine. The boundary conditions assignment therefore assumes a paramount importance in the resolution of the field problem.

There are 3 types of boundary conditions: 1) the Dirichlet's condition, 2) the Neumann's condition and 3) the periodic boundary conditions. Major features of these conditions are given below.

1) The imposition of the Dirichlet's boundary condition consists in assigning a given value (typically constant) to the magnetic vector potential A_z on a given part of the boundary. In the analysis of electrical machines, the homogeneous Dirichlet's condition (i.e. $A_z = 0$) is usually adopted, meaning that the flux lines are tangential to the boundary and that they do not cross the boundary itself; such condition is equivalent to consider an external material with a magnetic permeability equal to 0.
2) The Neumann's boundary condition corresponds to imposing a given value to the derivative of A_z normal to the boundary, so that the flux

lines have a given incidence angle with the boundary. When the homogeneous Neumann's condition (i.e. $\frac{d\boldsymbol{A}}{dn} = 0$, where n is the unity vector normal to the boundary line) is imposed to the analysis, the flux lines and, therefore, the components of $\bar{B}$ are constrained to be normal to the boundary. This condition is equivalent to have an infinite permeability material just outside the domain.

3) A periodic boundary condition assigns a correspondence between the values of the magnetic vector potential along two or more boundary lines. In general terms, 2 boundary lines are chosen: a principal line is selected and the magnetic vector potential of the other line is expressed as a function of the magnetic potential of the principal line. This kind of boundary conditions is really useful in structures that exhibit a repetition of the electromagnetic field. The application of such conditions allows again to reduce the domain of analysis and, more specifically, permits to model portions of the machine, while the neglected (i.e. not modelled) parts are considered as mirrored images.

Considering all the above, it is clear that an appropriate choice of the boundary conditions can potentially reduce the computation burden associated to the analysis of electrical machines and, at the same time, increase the accuracy of the solution. Also salient-pole SGs exhibit inherent periodicities and symmetries which have been heavily used in this thesis to reduce the domain of electromagnetic analysis of the corresponding FE models.

Appendix 2 – Introduction to GAs

General introduction

GAs were invented with the goal to create a computer algorithm that would mimic some functions of natural evolution. The idea is based on the following concept: starting from a randomly created population, the nature, over a long term, produces a new population with individuals that are more suitable to the environment than the previous random one; thus, this feature could be reflected upon an algorithm in order to solve very complex problems.

In nature, the evolution is based on the principle that chromosomes which decode into more successful individuals reproduce more often. Processes of mutation and recombination (crossover) occur, allowing to produce new chromosomes from the genes of the parent's ones. Throughout this process, evolution does not keep track of the success rate of the generation and thus it has no memory. Also, the evolution process does not consider the type of environment it is dealing with. The only information that is available to biologic evolution is contained in the chromosomes of the current population. GAs simulate the mechanism of the biological evolution. The algorithm is not aware of the problem that it is trying to solve. The only information that is provided to it is how the chromosomes are decoded into functional individuals of the population and how successful each individual is in adopting to the environment.

In general terms, a GA is initialised by a set of individuals (represented by the chromosomes) called the population. Solutions from one population are taken and used to form a new, "better" one. The individuals of the new population are selected according to their "fitness" into the environment. The fitness parameter is an index of how successful an individual is, while the environment is represented by the objective function when the GA is applied to an optimization problem.

The main steps of a basic GA can be summarised as follows:

1) Generate a random population of *N* chromosomes (i.e. individuals).
2) Evaluate the fitness function of each chromosomes in the population.
3) Create a new population according to the following steps:
    a. select two parent chromosomes from a population according to their fitness value;
    b. with a crossover probability, mate the parents to form a new offspring (if no crossover is performed, the offspring is an exact copy of the parents);
    c. with a mutation probability, mutate randomly one part of the chromosome.
4) Use the new generated population for further run (go to step 2) of algorithm until one of the end conditions is satisfied.

The structure of a basic GA is however very general and flexible, therefore there are many aspects that can be implemented differently in various problems. In fact, depending on the application and the type of problem to be

solved, the encoding method to be adopted for creating chromosomes, the selection process of parents for crossover and the mutation operation can be implemented in different ways. Always in general terms, the general guidelines for selection of crossover and mutation are provided below:

- A practical problem is how to select parents for crossover; the main idea is that of selecting the best parents, according to the Darwin's evolution theory that they will produce better offspring. There are many methods of how to select the best chromosomes, for example Roulette wheel selection [125], rank selection [126] and some others. Once the best chromosomes have been selected, the crossover operator can be applied to form new offspring.
- After a crossover is performed, the mutation operator can be used. It consists in randomly changing the new offspring. The mutation provides the genetic diversity of the offspring in order to enlarge the search space and to avoid any loss of useful genetic information.

When a new population is created through crossover and mutation operators, one potential risk is that the best chromosomes from the last population could be lost. In order to circumvent this issue, the so-called strategy of *elitism* can be adopted. It consists in copying, with no modifications, at least one of the best chromosomes into the new population. Associated to the concepts of crossover and mutation are also their inherent probability parameters. The crossover probability informs one on how often the crossover will be performed. If the crossover probability is 100% then all offspring is

generated by crossover, while if it is equal to 0%, the entire new generation is made from exact copies of chromosomes belonging to the previous population. The mutation probability, on the other hand, informs on how often the mutation occurs. If the mutation probability is 0% the offspring is taken after crossover without any change, while if it is equal to 100%, the whole chromosome is mutated. Hence, the following considerations can be drawn:

- A low crossover probability causes a contracted search that can be ineffective because similar individuals invade the population, while a very high value introduces too many new chromosomes into the new generation, which can lead to lose the best individuals of the previous round.
- A too low value of the mutation probability inhibits the search towards new zones, however a low value is usually adopted for this parameter to allow for an effective search; on the other side, a high value produces many mutated chromosomes in the new population which can alter the selection process of the algorithm and it can compromise the convergence of the procedure. It is clear from the above that mutation is necessary to prevent that the GAs fall into local optimum.

Considering this, in general terms, very typical values of crossover and mutation probabilities are 80-90% and 1-2%, respectively.

Another parameter that plays a very important role in the setting procedure of a GA-based optimisation is the population size *N*, i.e. the number of individuals of one population. A low number of chromosomes can prevent the GA from performing crossover and, therefore, only a small part of the search space is explored. On the other hand, if the population is made of too many individuals, GA can be very computational. It is clear from the above that the setting of the GA's parameters significantly depends on the optimisation problem under study and that no general theory exists for the setting procedure relative to the GA's parameters.

One of the main advantages of GAs is in their parallelism, meaning that the GA acts in a search space with more individuals, so they are less likely to get stuck in a local optimum than other methods. In addition, the GAs do not require a good initial point to start the optimization, as they can evolve from poor initial points in a game of survival of the fittest. On the other hand, the main disadvantage of GAs is in their required computational time.

The last, general aspect to mention is related to how and when the algorithm stops. Theoretically, the algorithm can continue indefinitely even if it has converged to the global optimum of the objective function. Therefore a stopping rule is necessary to inform the algorithm when it must stop. Also in this case, this can be achieved in several ways and depends on the optimisation problem. Some of the possible methods include

a) to fix the maximum number of generations and to use the best individual of all generations as the optimum result;

b) to fix the time elapsed and to select the optimum similarly to the previous point;
c) to let the algorithm converge to an average fitness value with some error margin.

In this section, the high-level concepts and the general rules of GA-based optimisation have been introduced. While these can be applied straight forward to single-objective optimization problems, further observations are needed for the sake of study, as the optimisation process relative to this project consists of two objectives to be minimised, namely the damper cage loss and voltage THD. Considering this, the concepts behind the multi-objective optimisation problems are reported in the next section.

Multi-objective optimization problems

In the majority of the cases, the design of electrical machines represents an optimization process of multiple objectives. In a multi-objective optimization problem, there are two general approaches that can be adopted in order to achieve an optimal solution. The first approach consists in combining the individual objective functions into a single composite function or separately treating all the objective functions by assigning a set of constraints. In the former case, the determination of a single objective function is possible with methods such as utility theory, weighted sum method, etc. However, the main limitation is strictly related to the selection of weights or utility functions, which can be a very difficult task even for well-known problems; also, small perturbations in the weights can sometimes lead to inaccurate and different

solutions. In the latter case, a constraining value must be assigned to each objective. In both cases, an optimization method would return a single solution rather than a set of solutions that can be examined for trade-offs.

In order to overcome these issues, the second general approach is that of determining an entire Pareto optimal solution set or a representative subset. A Pareto optimal set consists of a set of solutions that are non-dominated with respect to each other. More specifically, a solution belongs to the Pareto optimal set if it is not dominated by any other solution, meaning that a Pareto optimal solution cannot be improved with respect to any objective without worsening at least one other objective. The set of all feasible, non-dominated solutions is referred to as the Pareto optimal set, and the corresponding objective function values in the objective space are called the Pareto front. These Pareto optimal sets are often preferred to single solutions because they are useful when real-life problems are considered, since the final solution of the decision maker is always a trade-off. One negative aspect of this approach is that, due to its size, it becomes impossible in practice to identify the entire Pareto optimal set. Therefore a practical approach is that of investigating the set of solutions that represents as close as possible the Pareto optimal set. This is called the best-known Pareto front. Considering the above, a multi-objective optimization algorithm should achieve the following three conflicting goals:

1) The best-known Pareto front should be as close as possible to the true Pareto front. Ideally the best-known Pareto set should be a subset of the Pareto optimal set.
2) The solutions in the best-known Pareto set should be uniformly distributed and diverse over the Pareto front in order to provide the decision maker a true picture of the available trade-offs.
3) The best-known Pareto front should capture the whole spectrum of the Pareto front. This requires to investigate solutions at the extreme ends of the objective function space.

For a given computational time limit, the first goal is best served by focusing the search on a particular region of the Pareto front. On the contrary, the second goal demands the search effort to be uniformly distributed over the Pareto front. The third goal aims at extending the Pareto front at both ends, exploring new extreme solutions.

There are a lot of different ways to implement a multi-objective GA, and generally they differ based on their fitness assignment, elitism, or diversification approaches. With respect to the fitness assignment, there are three main approaches to solve it:

1) The weighted sum approach, where each solution in the population uses different weights in the calculation of the summed objective function and the weights can be embedded within the chromosomes. Therefore multiple solutions can be simultaneously searched in a single run; in addition, the weights can be adjusted to promote

diversity of the population. The main advantage of this method is the straightforward implementation, while its main disadvantage is the difficulty in finding solutions uniformly distributed when the true Pareto front is non-convex.

2) The alternating objective functions method, where the population is randomly divided into *K* equal sized sub-populations, where *K* is the number of objectives; then a fitness value is assigned to each solution in the sub-population, based on the corresponding objective function. The sub-population solution are chosen through a proportional selection for crossover and mutation. These are performed on the new population in the same way as for a single objective GA. The main advantage of the alternating objectives approach is that it is easy to implement and computationally as efficient as a single objective GA. Its major drawback is that the population tends to converge to solutions which are superior in one objective, but poor at others.

3) The Pareto-ranking approach, where the population is ranked according to a dominance rule, and then to each solution is assigned a fitness value based on its rank in the population and not on its actual objective function value. There are different ranking approaches to assign fitness values to individual solutions, and they are usually combined with various fitness sharing techniques aimed at achieving a uniform Pareto front. In fact, without taking preventive measures, the population tends to form relatively few cluster in multi-objective

GAs. This phenomenon is called genetic drift, and several approaches have been devised to prevent it.

One of the most important aspect to consider in multi-objective optimization systems is related to the implementation of elitism, whose general features have been introduced in the previous section. In multi-objective GAs, the whole set of non-dominated solutions are potentially eligible as elitist solutions. However, the implementation of elitism in multi-objective optimization is not straightforward as in a single-objective GA, due to the large number of possible elitist solutions. Therefore, it is typical to set the maximum number of solutions to include in the elite set and, then, either keep them within the population or store them in an external secondary list to be reintroduced into the population in a second instance.

Another aspect related to most real-word optimization problems is how handle the constraints that must be satisfied. A single-objective GA may use one of four different constraint handling strategies: 1) discarding unfeasible solutions (the "death penalty"), 2) reducing the fitness of unfeasible solutions by using a penalty function, 3) crafting genetic operators to always produce feasible solutions, 4) transforming unfeasible solutions to be feasible ("repair"). While the constraint handling strategies 1, 3 and 4 are directly applicable to the multi-objective case, the implementation of the penalty function strategy is not a simple task in multi-objective GAs, due to the fact that the fitness assignment is based on the non-dominance rank of a solution and not on its objective function values.

Appendix 3 – Introduction to EDM

The EDM [127], also known as spark machining, spark eroding, burning, die sinking, wire burning or wire erosion, is a manufacturing process whereby a desired shape is obtained by using electrical discharges. Material is removed from the workpiece by a series of rapidly recurring current discharges between two electrodes, separated by a dielectric liquid and subject to an electric voltage. One of the electrodes is called the tool-electrode, while the other is called the workpiece-electrode. The process depends upon the tool and workpiece not making actual contact.

When the voltage between the two electrodes is increased, the intensity of the electric field in the volume between the electrodes becomes greater than the strength of the dielectric, which breaks down, allowing current to flow between the two electrodes. This phenomenon is the same as the breakdown of a capacitor. As a result, the material is removed from the electrodes. Once the current stops (or is stopped), new liquid dielectric is usually conveyed into the inter-electrode volume (commonly referred to as "flushing"), enabling the solid particles to be carried away and the insulating properties of the dielectric to be restored. Also, after a current flow, the difference of potential between the electrodes is restored to the same value as before the breakdown, so that a new liquid dielectric breakdown can occur.

To obtain a specific geometry, the EDM tool is guided along the desired path very close to the work; ideally it should not touch the workpiece, although in

reality this may happen due to the performance of the specific motion control in use. In this way, a large number of current discharges (colloquially also called sparks) happen, each contributing to the removal of material from both tool and workpiece, where small craters are formed. The size of the craters is a function of the technological parameters set for the specific job at hand. They can be with typical dimensions ranging from the nanoscale (in micro-EDM operations) to some hundreds of micro-meters in roughing conditions.

EDM is often included in the "non-conventional" group of machining methods, together with processes such as electrochemical machining, water jet cutting, laser cutting, and opposite to the "conventional" group, such as turning, milling, grinding, drilling and any other process whose material removal mechanism is essentially based on mechanical forces) [128].

To conclude up this section, the major advantages and disadvantages of EDM techniques are listed below. The positive aspects include machining of:

- Complex shapes that would otherwise be difficult to produce with conventional cutting tools.
- Extremely hard material to very close tolerances.
- Very small workpieces where conventional cutting tools may damage the part from excess cutting tool pressure.
- There is no direct contact between tool and workpiece. Therefore, delicate sections and weak materials can be machined without perceivable distortion.

- A good surface finish can be obtained; a very good surface may be obtained by redundant finishing paths.
- Very fine holes can be attained and tapered holes may be produced.

EMD techniques have also some negative aspects which include:

- The slow rate of material removal.
- The additional time and cost used for creating electrodes for ram/sinker EDM.
- Reproducing sharp corners on the workpiece is difficult due to electrode wear.
- Specific power and power consumption is very high.
- Excessive tool wear occurs during machining.
- Electrically non-conductive materials can be machined only with specific set-up of the process.

Considering the above, EDM seems to be suitable for the manufacturing of the HC4 rotor equipped with the optimal, unconventionally displaced damping bars. Other manufacturing techniques, such as stamping, laser cutting and water jet cutting, have been considered as potential competitors of EDM in the initial stage of this process. However, after a trade-off study where the costs and the delivery times of various manufacturing techniques provided by different companies were investigated, EDM was selected as manufacturing method for the job at hand.

References

[1] G. Neidhöfer, "The evolution of the synchronous machine," *Engineering Science and Education Journal*, vol. 1, pp. 239-248, 1992.

[2] "IEEE Recommended Practices and Requirements for Harmonic Control in Electrical Power Systems," ed: IEEE, 1992, pp. 1-112.

[3] "IEEE Guide for Identifying and Improving Voltage Quality in Power Systems," in *2011*, ed: IEEE, pp. 1-70.

[4] M. H. J. Bollen, *Understanding Power Quality Problems*. New York: IEEE Press, 2000.

[5] R. C. Dugan, *Electrical Power Systems Quality*. New York: McGraw-Hill Professional, 2002.

[6] *The Dranetz Field Handbook for Power Quality Analysis*. Edison, NJ: Dranetz Technologies, Inc., 1991.

[7] W. Yi, D. M. Ionel, and D. Staton, "Ultrafast Steady-State Multiphysics Model for PM and Synchronous Reluctance Machines," *IEEE Trans. Ind. Appl.*, vol. 51, pp. 3639-3646, Sep./Oct. 2015.

[8] K. S. Jiji, N. H. Jayadas, and C. A. Babu, "FEM-based Virtual Prototyping and Design of Third Harmonic Excitation System for Low-Voltage Salient-Pole Synchronous Generators," *IEEE Trans. Ind. Appl.*, vol. 50, May/Jun. 2014.

[9] M. P. Kostenko and L. M. Piotrovskiĭ, *Electrical Machines*: Creset, 1968.

[10] S. Nuzzo, M. Degano, M. Galea, C. Gerada, N. Brown, and D. Gerada, "Improved Damper Cage Design for Salient-Pole Synchronous Generators," *IEEE Trans. Ind. Electron.*, vol. 64, pp. 1958-1970, 2017.

[11] D. A. Kocabas, "Novel winding and core design for maximum reduction of harmonic magnetomotive force in AC motors," *Ieee Trans. Magn.*, vol. 45, pp. 735-745, Feb. 2009.

[12] B. Standards, vol. BS EN60034-1, ed, 2010.

[13] "IEEE Guide for Insulation Maintenance of Electric Machines," ed: IEEE, 2016, pp. 1-86.

[14] P. H. Connor, S. J. Pickering, C. Gerada, C. N. Eastwick, C. Micallef, and C. Tighe, "Computational fluyd dynamics of an entire synchronous generator for improved thermal management," *IET Electr. Power Appl.*, vol. 7, pp. 231-236, Mar. 2013.

[15] P. H. Connor, S. J. Pickering, C. Gerada, C. N. Eastwick, and C. Micallef, "CFD modelling of an entire synchronous generator for improved thermal management," presented at the 6th IET Interantional Conference on Power Electronics, Machines and Drives (PEMD 2012), 2012.

[16] G. Traxler-Samek, T. Zickermann, and A. Schwery, "Cooling airflow, losses and temperatures in large air-cooled synchronous machines," *IEEE Trans. Ind. Electron.*, vol. 57, pp. 172-180, Jan. 2010.

[17] J. Pyrhonen, T. Jokinen, and V. Hrabovcova, *Design of rotating electrical machines*. Somerset, GB: Wiley, 2013.

[18] M. A. Kabir and I. Husain, "New multilayer winding configuration for distributed MMF in AC machines with shorter end-turn length,," presented at the IEEE Power and Energy Society General Meeting (PESGM), 2016.

[19] S. Jordan, C. Manolopoulos, and J. M. Apsley, "Winding configurations for five-phase synchronous generators with diode rectifier," *IEEE Trans. Ind. Electron.*, vol. 63, pp. 517-525, 2016 Jan.

[20] J. Bache-Wiig, "Application of fractional pitch windings to alternating-current generators," *Proc. Instr. Electr. Eng.*, vol. 27, pp. 657-665, 1908.

[21] C. A. Adams, "Electromotive force wave-shape in alternators," *Proc. Instr. Electr. Eng.*, vol. 28, pp. 791-814, 1909.

[22] A. Al-Timimy, M. Degano, P. Giangrande, G. Lo Calzo, Z. Xu, M. Galea, *et al.*, "Design and optimization of a high power density machine for flooded industrial pump," presented at the 2016 XXII International Conference on Electrical Machines (ICEM), 2016.

[23] A. Spargo, S. Ilie, and J. Chan, "Salient-pole rotor optimisations for synchronous generators using FEA software," presented at the 2017 IEEE Workshop on Electrical Machines Design, Control and Diagnosis (WEMDCD), Nottingham, UK, 2017.

[24] Y. Wang, G. Vakil, S. Nuzzo, M. Degano, M. Galea, C. Gerada, *et al.*, "Sensitivity analysis for performance and power density," in *IEEE Workshop on Electrical Machines Design, Control and Diagnosis (WEMDCD)*, 2017.

[25] C. Concordia, *Synchronous Machines - Theory and Performance*: Chapman and Hall, Ltd., 1952.

[26] I. Boldea, *The Electric Generators Handbook - Synchronous Generators*. Boca Raton, FL: CRC Press, Taylor & Francis Group, 2006.

[27] E. Kimbark, *Power System Stability-Volume 1*: Wiley-IEEE Press, Chapter XIV, 1995.

[28] G. Traxler-Samek, T. Lugand, and A. Schwery, "Additional losses in the damper winding of large hydrogenerators at open-circuit and load conditions," *IEEE Trans. Ind. Electron.*, vol. 57, pp. 154-160, Jan. 2010.

[29] M. M. Liwshitz, "Harmonics of the salient pole synchronous machine and their effects part III. Differential leakage of the damper winding with respect to the main wave. Current distribution in the damper bars," *Trans. Amer. Instr. Elect. Eng. Power App. Syst.*, vol. 77, pp. 462-469, Apr. 1958.

[30] I. M. Canay, "Calculation of negative-sequence losses and negative-sequence resistance of turbogenerators," *IEEE Trans. Power App. Syst.*, vol. PAS-94, pp. 764-773, May 1975.

[31] H. Karmaker and A. M. Knight, "Investigation and simulation of fields in large salient-pole synchronous machines with skewed stator slots," *IEEE Trans. Energy Convers.*, vol. 20, pp. 604-610, Sep. 2005.

[32] A. M. Knight, H. Karmaker, and K. Weeber, "Use of a permeance model to predict force harmonic components and damper winding effects in salient-pole synchronous machines," *IEEE Trans. Energy Convers.*, vol. 17, pp. 709-716, Dec. 2002.

[33] E. Wallin, M. Ranlof, and U. Lundin, "Design and construction of a synchronous generator test set-up " presented at the International Conference on Electrical Machines (ICEM), Rome, Italy, Sep. 2010.

[34] A. Tessarolo, C. Bassi, and D. Giulivo, "Time-stepping finite-element analysis of a 14-MVA salient-pole shipboard alternator for different damper winding design solution," *IEEE Trans. Ind. Electron.*, vol. 59, pp. 2524-2535, Jun. 2012.

[35] A. Schwery, G. Traxler-Samek, and E. Schmidt, "Application of a transient finite element analysis with coupled circuits to calculate the voltage shape of a synchronous generator," in *CEFC*, 2002.

[36] D. w. Zhang, Y. j. Peng, and Z. n. Fan, "No-load voltage waveform optimization and rotor heat reduction of tubolar hydro-generator," presented at the Intern. Conf. Electrical Machines and Systems (ICEMS), Beijing, China, Aug. 2011.

[37] P. A. Hargreaves, M. B. C., and R. Hall, "Open circuit voltage distortion in salient pole synchronous generators with damper windings," presented at the 5th Intern. Conf. on Power Electronics, Machines and Drives (PEMD), 2010.

[38] S. Nuzzo, M. Galea, C. Gerada, D. Gerada, A. Mebarki, and N. Brown, "Damper cage loss reduction and no-load voltage THD improvements in salient-pole synchronous generators," presented at the 8th IET International Conference on Power Electronics, Machines and Drives (PEMD 2016), 2016.

[39] C. I. McClay and S. Williamson, "Influence of rotor skew on cage motor losses," *IEE Proc. on Electr. Power Appl.*, vol. 154, pp. 414-422, Sep. 1998.

[40] A. Tenhunen and A. Arkkio, "Modelling of induction machines with skewed rotor slots," *IEE Proc. on Electr. Power Appl.*, vol. 148, pp. 45-50, 2001.

[41] D. G. Dorrell, P. J. Holik, and C. B. Rasmussen, "Analysis and effects of inter-bar current and skew on a long skewed-rotor induction motor for pump applications," *IEEE Trans. Magn.*, vol. 43, pp. 2534-2536, Jun. 2007.

[42] K. J. Binns, R. Hindmarsh, and B. P. Short, "Effect of skewing slots on flux distribution in induction machines," *Proc. Instr. Electr. Eng.*, vol. 118, pp. 543-549, Mar./Apr. 1971.

[43] L. Wang, X. Bao, C. Di, and J. Li, "Effects of novel skewed rotor in squirrel-cage induction motor on electromagnetic force," *IEEE Trans. Magn.*, vol. 41, Nov. 2015.

[44] S. L. Ho, S. Niu, and W. N. Fu, "A novel solid-rotor induction motor with skewed slits in radial and axial directions and its performance analysis using finite element method," *IEEE Trans. Appl. Supercond.*, vol. 20, pp. 1089-1092, Jun. 2010.

[45] P. Handgruber, A. Stermecki, O. Biro, A. Belahcen, and D. E., "3-D eddy current analysis in steel laminations of electrical machines as a contribution for improved iron loss modeling," presented at the 2012 XXth International Conference on Electrical Machines, Marseille, France, 2012.

[46] Z. Q. Zhu and D. Howe, "Influence of design parameters on cogging torque in permanent magnet machines," *IEEE Trans. Energy Convers.*, vol. 15, pp. 407-412, Dec. 2000.

[47] S. M. Hwang, J. B. Eom, Y. H. Jung, D. W. Lee, and B. S. Kang, "Various design techniques to reduce cogging torque by controlling energy variation in permanent magnet motors," *IEEE Trans. Magn.*, vol. 37, pp. 2806-2809, Jul. 2001.

[48] W. Q. Chu and Z. Q. Zhu, "Investigation of torque ripples in permanent magnet synchronous machines with skewing," *IEEE Trans. Magn.*, vol. 49, pp. 1211-1220, 2013.

[49] A. B. Letelier, D. A. Gonzales, J. A. Tapia, R. Wallace, and A. M. Valenzuela, "Cogging torque reduction in an axial flux PM machine via stator slot displacement and skewing," *IEEE Trans. Ind. Appl.*, vol. 43, pp. 685-693, May/jun. 2007.

[50] W. Fei and Z. Q. Zhu, "Comparison of cogging torque reduction in permanent magnet brushless machines by conventional and herringbone skewing techniques," *IEEE Trans. Energy Convers.*, vol. 28, pp. 664-674, Sep. 2013.

[51] R. Lateb, N. Takorabet, and F. Meibody-Tabar, "Effect of magnet segmentation on the cogging torque in surface-mounted permanent-magnet motors," *IEEE Trans. Magn.*, vol. 42, pp. 442-445, Mar. 2006.

[52] T. Raminosoa, C. Gerada, and M. Galea, "Design considerations for a fault-tolerant flux-switching permanent-magnet machine," *IEEE Trans. Ind. Electron.*, vol. 58, pp. 2818-2825, Jul. 2011.

[53] R. Islam and I. Husain, "Permanent-magnet synchronous motor magnet designs with skewing for torque ripple and cogging torque reduction," *IEEE Trans. Ind. Appl.*, vol. 45, pp. 152-160, 2009.

[54] W. Zhao, T. A. Lipo, and B. I. Kwo, "Torque pulsation minimization in spoke-type interior permanent magnet motors with skewing and sinusoidal permanent magnet configurations," *IEEE Trans. Magn.*, vol. 51, Nov. 2015.

[55] H. Xie, Y. Wei, Y. Liu, Y. Feng, Y. Zhang, X. Yang, *et al.*, "Research of asymmetrical bidirectional magnet skewing technique in modular multi-stage axial flux permanent magnet " *IEEE Trans. Magn.*, vol. 51, Mar. 2015.

[56] M. Aydin and M. Gulec, "Reduction of cogging torque in double-rotor axial-flux permanent-magnet disk motors: a review of cost-effective magnet-skewing techniques with experimental verification," *IEEE Trans. Ind. Electron.*, vol. 61, pp. 5025-5034, 2014.

[57] A. Vagati, M. Pastorelli, G. Franceschini, and S. C. Petrache, "Design of low-torque-ripple synchronous reluctance motors," *IEEE Trans. Ind. Appl.*, vol. 34, pp. 758-765, Jul./Aug. 1998.

[58] N. Bianchi, S. Bolognani, D. Bon, and M. Dai Pre, "Rotor flux-barrier design for torque ripple reduction in synchronous reluctance and PM-assisted synchronous reluctance motors," *IEEE Trans. Energy Convers.*, vol. 45, pp. 921-928, 2009.

[59] X. B. Bomela and M. J. Kamper, "Effect of stator chording and rotor skewing on performance of reluctance synchronous machine," *IEEE Trans. Ind. Appl.*, vol. 38, Jan./Feb. 2002.

[60] E. Howard, M. J. Kamper, and S. Gerber, "Asymmetric flux barrier and skew design optimization of reluctance synchronous machines," *IEEE Trans. Ind. Appl.*, vol. 51, pp. 3751-3760, Sep./Oct. 2015.

[61] P. Lazari, J. Wang, and B. Sen, "3-D effects of rotor step-skews in permanent magnet-assisted synchronous reluctance machines," *IEEE Trans. Magn.*, vol. 51, Nov. 2015.

[62] Z. n. Fan, Y. Liao, L. Han, and L. d. Xie, "No-load voltage waveform optimization and damper bars heat reduction of tubular hydrogenerator by

different degree of adjusting damper bar picth and skewing stator slot," *IEEE Trans. Energy Convers.*, vol. 28, pp. 461-469, Sep. 2013.

[63] A. M. Knight, S. Troitskaia, N. Stranges, and A. Merkhouf, "Analysis of large synchronous machines with axial skew, part 1: flux density and open-circuit voltage harmonics," *IET Electr. Power Appl.*, vol. 3, pp. 389-397, Sep. 2009.

[64] A. M. Knight, S. Troitskaia, N. Stranges, and A. Merkhouf, "Analysis of large synchronous machines with axial skew, part 2: inter-bar resistance, skew and losses," *IET Electr. Power Appl.*, vol. 3, pp. 398-406, Sep. 2009.

[65] V. Ostovic, *Dynamics of saturated electrical machines*. New York, NY, USA: Springer-Verlag, 1989.

[66] J. M. Gojko, D. D. Momir, and O. B. Aleksandar, "Skew and linear rise of mmf across slot modeling - winding function approach," *IEEE Trans. Energy Convers.*, vol. 14, pp. 315-320, Sep. 2009.

[67] C. Xia, Z. Zhang, and Q. Geng, "Analytical modelling and analysis of surface mounted permanent magnet machines with skewed slots," *IEEE Trans. Magn.*, vol. 51, May 2015.

[68] M. Galea, L. Papini, H. Zhang, C. Gerada, and T. Hamiti, "Demagnetization analysis for halbach array configurations in electrical machines," *IEEE Trans. Magn.*, vol. 51, Sep. 2015.

[69] Y. S. Chen and Z. Q. Zhu, "Calculation of d- and q-axis inductances of PM brushless ac machines accounting for skew," *IEEE Trans. Magn.*, vol. 41, pp. 3940-3942, Oct. 2005.

[70] S. A. Afsari, H. Heydari, and B. Dianati, "Cogging torque mitigation in axial flux magnetic gear system based on skew effects using an improved quasi 3-D analytical method," *IEEE Trans. Magn.*, vol. 51, Sep./Oct. 2015.

[71] P. Dziwniel, B. B., F. Piriou, J. P. Ducreux, and P. Thomas, "Comparison between two approaches to model induction machines with skewed slots," *IEEE Trans. Magn.*, vol. 36, pp. 1453-1457, Jul. 2000.

[72] J. Gyselinck, L. Vandevelde, and J. Melkebeek, "Multi-slice modeling of electrical machines with skewed slots -the skew discretization error," *IEEE Trans. Magn.*, vol. 37, pp. 3233-3237, Sep. 2002.

[73] S. Williamson, T. J. Flack, and A. F. Volshenk, "Representation of skew in time-stepped two-dimensional finite-element models of electrical machines," *IEEE Trans. Ind. Appl.*, vol. 31, pp. 1009-1015, May 1995.

[74] R. Wang, S. Pekarek, P. O'Regan, A. Larson, R. Van Maaren, and "Incorporating skew in a magnetic equivalent circuit model of synchronous machines," *IEEE Trans. Energy Convers.*, vol. 30, Jun. 2015.

[75] D. Novotny and T. A. Lipo, *Vector control and dynamics of AC drives*: Oxford University Press, 2001.

[76] P. Krause and O. Wasynczuk, *Analysis of electric machinery*: IEEE Press, 1995.

[77] P. Bolognesi, "A mid-complexity analysis of long-drum-type electrical machines suitable for circuital modelling," presented at the ICEM 2008 Conf., 2008.

[78] S. Nuzzo, P. Bolognesi, M. Galea, and C. Gerada, "An hybrid analytical-numerical approach for the analysis of salient-pole synchronous generators

with a symmetrical damper cage," in *IEEE International Electric Machines and Drives Conference (IEMDC)*, Miami, FL, USA, 2017.

[79] S. Nuzzo, M. Galea, C. Gerada, and N. Brown, "Prediction of the voltage drop due to the diode commutation process in the excitation system of salient-pole synchronous generators," presented at the 19th International Conference on Electrical Machines and Drives (ICEMS), 2016.

[80] S. Nuzzo, M. Galea, C. Gerada, and N. Brown, "An analytical and genetic-algorithm-based design tool for brushless excitation systems of low-medium rated synchronous generators," presented at the 2016 19th International Conference on Electrical Machines and Systems, 2016.

[81] M. Bortolozzi, A. Tessarolo, and C. Bruzzese, "Analytical computation of end-coil leakage inductance of round-rotor synchronous machines field winding," *Ieee Trans. Magn.*, vol. 52, 2016.

[82] A. Tessarolo, "Analytical determination of slot leakage field and inductances of electrical machines with double-layer windings and semiclosed slots," *IEEE Trans. Energy Convers.*, vol. 30, pp. 1528-1536, 2015.

[83] A. Tessarolo, S. Mohamadian, and M. Bortolozzi, "A new method for determining the leakage inductances of a nine-phase synchronous machine from no-load and short-circuit tests," *IEEE Trans. Energy Convers.*, vol. 30, pp. 1515-1527, 2015.

[84] B. Prieto, M. Martinez-Iturralde, L. Fontan, and I. Elosegui, "Analytical calculation of the slot leakage inductance in fractional-slot concentrated-winding machines," *IEEE Trans. Ind. Electron.*, vol. 62, pp. 2742-2752, 2015.

[85] S. Nuzzo, C. Gerada, N. Brown, and M. Galea, "Analysis, Modelling and Design Considerations for the Excitation Systems of Synchronous Generators," *IEEE Trans. Ind. Electron.*, vol. PP, pp. 1-1, 2017.

[86] T. A. Lipo, *Analysis of synchronous machines*: CRC Press Taylor & Francis Group, 2012.

[87] P. P. Teodorescu, N. Stanescu, and N. Pandrea, *Integration of Ordinary Differential Equations and of Systems of Ordinary Differential Equations* 1ed.: Wiley-IEEE Press, 2013.

[88] H. C. Martin and G. F. Carey, *Introduction to Finite Element Analysis: Theory and Applications*. New York: McGraw-Hill, 1973.

[89] R. D. Cook, *Concepts and Applications of Finite Element Analysis*. New York: Wiley, 1981.

[90] P. P. Silvester and R. L. Ferrari, *Finite Element Analysis and Design of Electromagnetic Devices*. Cambridge, England: Cambridge University Press, 1983.

[91] J. M. Jin, *The Finite Element Method in Electromagnetism*. New York: John Wiley & Sons, 1992.

[92] N. Ida and J. P. A. Bastos, *Electromagnetism and Calculation of Fields*. New York: Springer-Verlag, 1992.

[93] N. Bianchi, *Electrical Machine Analysis Using Finite Elements*. Boca Raton, FL, USA: CRC Press, 2005.

[94] J. D. Edwards and E. M. Freeman, *MagNet 5.1 User Guide*: Infolytica Corporation, 1995.

[95] "Magnetic materials – Part 2: Methods of measurement of the magnetic properties of electrical steel strip and sheet by means of an Epstein frame " vol. IEC 60404-2, ed: IEC, 2008.

[96] D. N. Dyck and J. P. Webb, "Solenoidal Current Flows for Filamentary Conductors," *IEEE Trans. Magn.*, vol. 40, 2004.

[97] S. A. Swann and J. W. Salmon, "Effective resistance and reactance of a rectangular conductor placed in semi-closed slot," in *Institution of Electrical Engineering*, 1963, pp. 1656-1662.

[98] D. K. Cheng, *Field and Wave Electromagnetism*. Reading, MA, USA: Addison-Wesley, 1989.

[99] P. P. Teodorescu, N. Stanescu, and N. Pandrea, *Solution of Systems of Nonlinear Equations*, 1 ed.: Wiley-IEEE Press, 2013.

[100] C. P. Steinmetz, "On the law of hysteresis: Part I," *Trans. Amer. Instr. Elect. Eng.*, vol. 9, pp. 3-51, 1892.

[101] C. P. Steinmetz, "On the law of hysteresis: Part II," *Trans. Amer. Instr. Elect. Eng.*, vol. 9, pp. 621-724, 1892.

[102] G. Bertotti, *Hysteresis in magnetism*. San Diego: Academic Press, 1998.

[103] G. Bertotti, "Space-time correlation properties of the magnetization process and eddy current losses: Theory," *Journal of Applied Physics*, vol. 54, 1983.

[104] P. Pillay, "Improved Design of Motors for Increased Efficiency in Residential and Commercial Buildings," Ph.D., Clarkson University, New York, 13699.

[105] Y. Chen and P. Pillay, "An improved formula for lamination core loss calculations in machines operating with high frequency and high flux density excitation," presented at the IEEE 37th IAS Annual Meeting, 2002.

[106] A. Boglietti, A. Cavagnino, D. M. Ionel, M. Popescu, D. Staton, and S. Vaschetto, "A general model to predict the iron losses in PWM inverter-fed induction motor," *IEEE Trans. Ind. Appl.*, vol. 46, pp. 1882-1890, 2017.

[107] G. Y. Sizov, P. Zhang, D. M. Ionel, N. A. O. Demerdash, I. P. Brown, A. O. Smith, *et al.*, "Modeling and analysis of effects of skew on torque ripple and stator tooth forces in permanent magnet ac machines," presented at the IEEE Energy Conversion Congress and Exposition (ECCE), 2012.

[108] S. Nuzzo, M. Galea, C. Gerada, and N. Brown, "A fast method for modelling skew and its effects in salient-pole synchronous generators," *IEEE Trans. Ind. Electron.*, vol. 64, pp. 7679-7688, 2017.

[109] B. Marcusson and U. Lundin, "Axial magnetic fields at the ends of a synchronous generator at different points of operation," *IEEE Trans. Magn.*, vol. 51, 2015.

[110] B. Marcusson and U. Lundin, "Finite-element calculation of 3-D transientelectromagnetic field in end region and eddy-current loss decrease in stator end clamping plate of large hydrogenerator," *IEEE Trans. Ind. Electron.*, vol. 62, pp. 7331-7338, 2015.

[111] S. Wang, Z. Zhao, L. Yuan, and B. Wang, "Investigation and analysis of the influence of magnetic wedges on high voltage motors performance," presented at the IEEE Vehicle Power Propulsion Conference, 2008.

[112] P. M. Lindh, D. Vinnikov, J. Pyrhonen, and P. Ponomarev, "Influence of wedge material on losses of a traction motor with tooth coil windings,"

presented at the IEEE Annual Conference Ind. Electron. Soc. , Vienna, Austria, 2013.

[113] A. Biebighauser and A. Ghita, "Rotor for a rotating electrical machine," UK Patent, 2014.

[114] M. M. Rahimian and K. Butler-Purry, "Modeling of synchronous machines with damper windings for condition monitoring," in *IEEE Int. Electr. Mach. Drives Conf.*, Miami, FL, USA, May 2009, pp. 577-584.

[115] M. A. Khan, I. Husain, R. Islam, and J. T. Klass, "Design of experiments to address manufacturing tolerances and process variations influencing cogging torque and back EMF in the mass production of the permanent-magnet synchronous motors," *IEEE Trans. Ind. Appl.*, vol. 50, pp. 346-355, 2014.

[116] M. Cong and Q. Liyan, "Multiobjective optimization of switched reluctance motors based on design of experiments and particle swarm optimization," *IEEE Trans. Energy Convers.*, vol. 30, pp. 1144-1153, 2015.

[117] S. Poles, "MOGA-II. An improved multi-objective genetic algorithm," Esteco, Trieste, Italy2003.

[118] "British Standards " vol. BS EN60034-2, ed, 2007.

[119] P. Richardson, "Stray losses in synchronous electrical machinery," *Journal of the Institution of Electrical Engineers - Part II: Power Engineering* vol. 92, pp. 291-301, August 1945.

[120] "Guide for Test Procedures for Synchronous Machines Part I - Acceptance and Performance Testing Part II-Test Procedures and Parameter Determination for Dynamic Analysis," vol. 115-2009, ed: IEEE, 2009.

[121] C. Spagnolo, S. Nuzzo, G. Serra, C. Gerada, and M. Galea, "Analysis of single-phase synchronous generators operating in single-phase condition," in *Workshop on Electrical Machines Design, Control and Diagnosis*, Nottingham, UK, 2017.

[122] D. Fallows, S. Nuzzo, A. Costabeber, and M. Galea, "Field modulation for generator harmonic mitigation," in *Workshop on Electrical Machines Desing, Control and Diagnosis*, Nottingham, UK, 2017.

[123] S. P. Thompson, *Poliphase electric currents and alternate-currents motors*: Spon & Chamberlain, 1900.

[124] W. J. Foster, "Potential waves of alternating-current generators," *Trans. Amer. Instr. Elect. Eng.*, vol. XXXII, pp. 749-764, 1913.

[125] L. Zhang, H. Chang, and R. Xu, "Equal-width partitioning roulette wheel selection in genetic algorithm," presented at the Conference on Technologies and Applications of Artificial Intelligence, 2012.

[126] A. Morales, E. Boman, and S. J. Ko, "An efficient algorithm to calculate sample and rank selection probabilities for weighted median filters," *IEEE Signal Procecessing Letters*, vol. 9, pp. 148-150, 2002.

[127] E. C. Jameson, *Electrical Discharge Machining*, 2001.

[128] W. J. McCarthy and J. A. McGeough, *Machine tool*: Encyclopædia Britannica.